PERFORMANCE AND DESIGN OF COMPOSITE BEAMS WITH WEB OPENINGS

by

Rex C. Donahey

David Darwin

A Report on Research Sponsored by

THE AMERICAN INSTITUTE OF STEEL CONSTRUCTION

Research Project

21.82

UNIVERSITY OF KANSAS

LAWRENCE, KANSAS

April 1986

50272-101

REPORT DOCUMENTATION PAGE	1. REPORT NO.	2.	3. Recipient's Accession No.

4. Title and Subtitle

Performance and Design of Composite Beams with Web Openings

5. Report Date

April 1986

6.

7. Author(s)

Rex C. Donahey and David Darwin

8. Performing Organization Rept. No.

SM Report No. 18

9. Performing Organization Name and Address

Structural Engineering and Materials Laboratory
University of Kansas Center for Research, Inc.
2291 Irving Hill Drive, West Campus
Lawrence, Kansas 66045

10. Project/Task/Work Unit No.

11. Contract(C) or Grant(G) No.

(C)

(G) 21.82

12. Sponsoring Organization Name and Address

American Institute of Steel Construction
400 North Michigan Avenue
Chicago, Illinois 60611-4185

13. Type of Report & Period Covered

14.

15. Supplementary Notes

16. Abstract (Limit: 200 words)

Fifteen tests to failure were carried out on full scale composite beams with web openings. All beams had ribbed slabs using formed steel deck. Ribs were perpendicular to or parallel to the steel section. The effects of moment-shear ratio, partial composite construction, deck rib orientation, slab thickness, opening shape, opening eccentricity, and modification of the deck over the opening are studied. A strength model and three versions of a practical design technique are developed. The model and the design techniques are compared with all experimental work on composite beams with web openings. Serviceability criteria are developed.

The peak loads attained by composite beams with ribbed slabs at web openings are governed by the failure of the slab. Rib failure occurs in slabs with transverse ribs, while longitudinal shear failure occurs in slabs with longitudinal ribs. As the number of shear connectors above the opening and between the opening and the support increases, the failure load increases. The failure of composite beams with ribbed slabs is, in general, ductile. First yield in the steel around the opening does not give an accurate indication of the section capacity. The strength model and the design techniques accurately predict the strength of composite beams at web openings for beams with solid or ribbed slabs.

17. Document Analysis a. Descriptors

beams (supports), buildings, composite structures, concrete, deflections, formed steel deck, load factors, openings, resistance factors, ribbed slabs, steel, structural analysis, structural engineering, ultimate strength, web beams

b. Identifiers/Open-Ended Terms

c. COSATI Field/Group

18. Availability Statement	19. Security Class (This Report)	21. No. of Pages
Release Unlimited	Unclassified	
	20. Security Class (This Page) Unclassified	22. Price

ACKNOWLEDGEMENTS

This report is based on a thesis submitted by Rex C. Donahey to the Department of Civil Engineering of the University of Kansas in partial fulfillment of the requirements for the Ph.D. degree.

The research was supported by the American Institute of Steel Construction under Research Project 21.82.

Stud welding equipment and shear studs were provided by the Nelson Stud Welding Division of TRW. Steel decking was provided by United Steel Deck, Inc. Reinforcing steel was provided by ARMCO INC. and Sheffield Steel. Numerical calculations were performed at the University of Kansas Computer Aided Engineering Laboratory.

TABLE OF CONTENTS

TABLE OF CONTENTS (continued)

TABLE OF CONTENTS (continued)

LIST OF TABLES

LIST OF TABLES (continued)

LIST OF FIGURES (continued)

increased above a predetermined value, the bottom tee is also assigned increasing increments of shear. In a comparison with the experimental results of Granade, the model greatly underestimates the shear strength of composite beams with web openings (Fig. 1.1). The model does, however, illustrate the significant increase in moment capacity provided by the concrete.

Swartz and Eliufoo (40) developed an elastic analysis technique for web openings in composite beams using the Vierendeel method. Their technique is based on full composite action and considers a transformed, cracked section. Their method compares reasonably well with finite element solutions. Although Swartz and Eliufoo did not make a comparison with experimental results, their test case uses the same section and loading as Beam 2 in an experimental study by Clawson and Darwin (9, 11). Comparison of Swartz and Eliufoos' predictions with the experimental results indicates that the most significant deviation is in the prediction of concrete stresses. This deviation is probably due to their assumption of zero slip at the concrete-steel interface.

Clawson and Darwin (9, 10, 11) conducted an experimental investigation of composite beams with web openings and developed a strength model to predict the behavior of the beams. Six openings were tested with heights and lengths of 60 and 120 percent of the steel section depth, respectively. All beams were constructed with solid slabs.

They found that, although the peak loads were governed by failure of the concrete slab, failure was generally ductile. They also found that the compressive strains in the concrete generally remained low, well after the steel had begun to yield. Prior to failure, large slips occurred between the concrete and steel.

Clawson and Darwin observed that the moment to shear ratio (M/V) at the opening had a prominent effect on the failure mode. For openings under high bending stress and low shear, failure tended to be governed by crushing of the concrete, while beams under moderate or high shear exhibited Vierendeel action, with large differential deformation through the opening. They also found that the point of inflection in the portion of the beam above the opening, or top tee, was not at the centerline of the opening, but was displaced towards the low moment end.

Clawson and Darwin (10, 11) proposed a model in which the slab contributes to both the moment and shear capacity at a web opening. Shear forces are assigned both to the concrete slab and to the steel tees. Concrete forces are assumed to exist only at the high moment end of the opening, while the reinforcing steel is considered to be yielding in tension at the low moment end of the opening.

The model developed by Clawson and Darwin accounts for combined shear and normal stress in the concrete. A failure criterion for the concrete was developed by transforming principal stress data (23) to a state of combined shear and compression. Shear stresses in the concrete are assumed to be effective over a width of the slab equal

to three times the slab thickness. The concrete force is limited by the material model or by normal force equilibrium. Interaction diagrams are generated by assigning increasing amounts of shear to both the top and bottom tees. Clawson and Darwin show that the model is conservative for beams with solid slab construction.

A simplified version of the model (11) was developed for use in design. Maximum moment capacity and maximum shear capacity are calculated for the beam at the opening, the values are plotted on a moment-shear interaction diagram, and the points are connected with an ellipse. The simplified version shows good agreement with the detailed model (Fig. 1.2).

Cho (8) largely duplicated the work of Clawson and Darwin using small sections relative to the concrete slab. He arrived at essentially the same conclusions.

More recently, Redwood and Wong (34, 46) conducted an experimental and analytical study of composite beams with web openings. They tested 6 rectangular openings with heights and lengths of 60 and 120 percent of the steel section depth, respectively. All beams had ribbed slab construction with the ribs transverse to the steel section.

Their work confirmed that the failure mode of composite beams with web openings is largely a function of the M/V ratio. Beams with high and medium M/V ratios had compressive failures of the concrete slab, while beams with low M/V ratios had diagonal cracking above the

opening accompanied by rib splitting and separation of the steel and slab.

The analysis procedure developed by Redwood and Wong (34) obtains the maximum bending and shear strengths. The maximum moment that can be sustained at the maximum shear is also calculated, generating a vertical line on the right side of the interaction curve. The curve is closed with an ellipse.

The procedure developed by Redwood and Wong is based on the formation of four hinges, one at each corner of the opening. No stress is allowed in the concrete at the low moment end, while the concrete force at the high moment end of the opening is limited by the shear capacity of the stud connectors above the opening. The procedure is very conservative for high shear cases. Redwood and Wong felt that it was important to model the compressive stresses in the slab at the low moment end, brought about by slip of the concrete deck, and that consideration of this should result in higher predicted strengths.

Redwood and Wong expressed concern about concrete cracking at working loads at the low moment end of openings subjected to high shears (low M/V ratios). They did observe, however, that deflections at working loads satisfied live load deflection criteria normally used.

More recently, Redwood and Poumbouras (30, 32) tested three additional openings. The tests were designed to study the influence of the amount of shear connection above the opening and the effect of

construction loads acting on the steel section before composite action is effective. The openings were subjected to high shears and had a relatively low number of shear connectors between the opening and the point of zero moment.

Redwood and Poumbouras concluded that limited shear connection above the opening will significantly reduce the strength of openings with low M/V ratios. They also concluded that construction loads up to 60 percent of the non-composite beam strength at the opening have only a small effect on the strength of the composite section.

Poumbouras (30) has proposed a strength model for composite beams with ribbed slabs. Compressive forces are assumed in the slab at both the low moment and high moment ends of the opening. The concrete force at the low moment end is assumed to be at the top of the slab at zero shear; however, it is allowed to move to the bottom of the slab as the shear at the opening is increased. The concrete force at the high moment end is selected such that moment equilibrium is satisfied at the opening. The model is not conservative for openings with high shear and a low number of shear connectors above the opening and between the opening and the support.

Redwood and Poumbouras developed an analysis procedure that includes the compressive force in the concrete at the low moment end of the opening (33). This force is set equal to the total shear connector capacity between the opening and the point of zero moment. The shape of their interaction curve (Fig. 1.3) is similar to that of Redwood and Wong (33). Their procedure provides a good match with

their tests (30, 32) and those of Redwood and Wong (34, 46). They do, however, express some concern about applying the theory to openings with a heavy steel section and a thin slab.

Momeni (28) modified the model developed by Clawson and Darwin to include web reinforcement in the analysis. His model allows the cracked portion of the slab at the high moment end of the opening to carry shear. A concrete material model described by a single function is used in place of a two-function relationship used by Clawson and Darwin (10, 11). The top tee is allowed to carry all of the shear at the opening, up to the maximum shear capacity of the top tee. The model produces unconservative results for beams using shallow steel sections with openings with low M/V ratios.

Donoghue (15) proposed a design procedure that neglects the shear contribution of the slab to strength. His procedure includes consideration of web reinforcement at the opening.

The design procedure proposed by Redwood and Wong has been incorporated in a design aid published by U.S. Steel (44). A series of tables of non-dimensional parameters are presented to allow the rapid construction of interaction diagrams for composite beams with web openings.

In a 1984 state-of-the-art paper, Darwin described the behavior and failure modes of composite beams with web openings (14) and summarized current analysis techniques.

Tests of prototype beams with reinforced openings were recently conducted in Illinois (37) and in Australia (41). The former test

was conducted on a 21 in. deep beam with a large (15 x 39 in.) opening at the midspan. Failure occurred in the slab near the support. The latter test was conducted on a 530 mm (20.9 in.) deep beam with a large [300 x 715 mm (11.8 x 28.1 in.)] opening and a small [300 x 515 mm (11.8 x 20.3 in.)] opening at approximately the quarter points in the span. The test was not continued to failure. The Australian design was based in part on the Clawson and Darwin (10, 11) model and on an elastic finite element analysis.

1.3 OBJECT AND SCOPE

This study consists of laboratory tests and detailed analyses leading to a comprehensive design procedure for composite beams with web openings.

Fifteen tests to failure were carried out on composite beams with web openings. All specimens were full scale composite beams with ribbed slabs using formed steel deck. Slabs had ribs oriented either perpendicular to or parallel to the steel section. Parameters investigated included moment-shear ratio, partial composite behavior, deck rib orientation, slab thickness, opening shape, opening eccentricity, and modification of the deck over the opening.

A strength model is developed which shows good agreement with all experimental work on composite beams with web openings. Three versions of a practical strength design technique are presented. A comprehensive design procedure, including both strength and serviceability criteria is developed.

CHAPTER 2

EXPERIMENTAL WORK

2.1 GENERAL

A number of experimental investigations of composite beams with rectangular web openings have been conducted (8, 9, 11, 19, 32, 34, 37, 41). Granade (19), Clawson and Darwin (9, 11), and Cho (8) tested composite beams with solid, or flat-soffit slab construction. Redwood and others at McGill University (32, 34, 46) tested composite beams with ribbed slab construction with the ribs oriented transverse to the steel section. Prototype tests were conducted in Illinois (37) and Australia (41). The test configurations used in previous investigations are summarized in Appendix B. This information is used in Chapters 4 and 5 as input for strength calculations.

The current experimental study is designed both to investigate parameters not included in earlier studies and to confirm trends indicated in those studies.

2.2 TEST SPECIMENS

Nine test beams with a total of 15 rectangular web openings were tested (Fig. 2.1 - 2.10). One W10 x 15 and eight W21 x 44 sections were used. All beams had ribbed slab construction; the ribs were oriented transversely on 8 beams and longitudinally on 1 beam. All slabs were made using normal weight concrete. The concrete slab dimensions, shear stud quantities and locations, and opening sizes and locations were varied.

The moment-shear (M/V) ratio at the web opening has been shown to have a significant effect on the behavior of composite beams with web openings (9, 11). Tests 1 through 3 and and Test 6a were used to provide additional information on the effect of the M/V ratio. Test 1 (Fig. 2.1) had a low M/V ratio (3.5 ft.), Test 2 (Fig. 2.2) had a medium M/V ratio (6.5 ft.), and Test 3 (Fig. 2.3) had a high M/V ratio (45.1 ft.). For Test 6A (Fig. 2.5), the opening was placed at a point of contraflexure (M/V = 0 ft.).

Tests 2, 4A, 4B, and 5A (Fig. 2.2 and 2.4), which had medium M/V ratios (6.5 ft.), and Test 6B (Fig. 2.6), which had a low M/V ratio (3.5 ft.) were used to investigate the effect of the quantity of shear connectors above the web opening and between the opening and the support. Tests 2 and 4B had a large number of shear connectors between the web opening and the support, while Tests 4A and 5A had a low number of shear connectors between the opening and the support. Tests 2 and 5A had 4 and 2 shear connectors, respectively, above the opening, while Tests 4A and 4B had none. The steel deck in Tests 4A and 4B was attached to the steel beam at each rib above the opening using puddle welds.

Test 6B (Fig. 2.6) was used to test a possible reinforcement procedure for composite beams with web openings. 22 gage steel pans were fabricated to match the deck profile (Fig. 2.11 and 2.12). The pans were placed on the top flange of the steel beam between the ribs of the deck from the high moment end of the opening to the support. 4 x 6 in. rectangular holes were cut in the deck above the pans and 2

shear connectors were welded through each pan to the steel beam. During concrete placement, the concrete around the pans was well consolidated to ensure that any voids were removed.

Most of the test openings were concentric (top and bottom steel tees were of equal depth), had depths equal to 60 percent of the beam depth (0.60d), and had lengths equal to 120 percent of the beam depth (1.20d). There were, however, exceptions. Test 5B (M/V = 6.5 ft., Fig. 2.4) had an opening with a 1 in. negative (downward) eccentricity and an opening shape of 0.67d x 1.20d. Test 8B (M/V = 2.46 ft., Fig. 2.9) had a 0.15 in. negative eccentricity and an opening shape of 0.63d x 1.84d. Test 9A (M/V = 3.5 ft., Fig. 2.10) had a concentric opening and an opening shape of 0.71d x 1.20d. Test 9B (M/V = 3.0 ft., Fig. 2.10) had a 0.13 in. negative eccentricity and an opening shape of 0.71d x 0.71d.

Tests 7A (M/V = 3.5 ft.) and 7B (M/V = 6.5 ft.) (Fig. 2.7) were used to study the effect of deck orientation on composite beams with web openings and used steel deck with the ribs placed parallel to the beam.

Tests 8A (M/V = 3.28 ft.), 8B, 9A, and 9B (Fig. 2.8 - 2.10) were used to evaluate the effect of the relative thickness of the slab on opening behavior. Tests 1 through 7B had relatively thin slabs compared to the depth of the beam, while Tests 8A through 9B had relatively thick slabs. The ratio of the slab thickness above the ribs, t_s, to steel beam depth, d, for Tests 1 through 7B was

approximately 0.1. The ratios for Beams 8 and 9 were 0.25 and 0.19, respectively.

2.3 BEAM DESIGN

The composite beams were designed following the AISC Steel Construction Manual (2). All beams were designed to be fully composite and were designed to fail at the web opening.

The slab reinforcement for Beams 1 to 6, 8 and 9 was designed following the ACI Building Code (1). Transverse and longitudinal reinforcement were selected to meet ACI temperature steel requirements based on the gross slab thickness. Reinforcement consisted of #3 bars on nominal 12 in. centers in both directions and provided a nominal slab reinforcement ratio of 0.0018. The longitudinal reinforcement rested on the formed steel deck, and the transverse reinforcement was tied to the longitudinal reinforcement at the centerlines of the deck ribs. Beam 7 reinforcement was selected based on Steel Deck Institute recommendations for minimum temperature steel (36). The minimum recommended reinforcing ratio is 0.00075 based on the slab thickness above the deck flutes. 6 x 6-W1.4 x W1.4 welded wire fabric was placed at the top of the steel decking.

The metal decking was selected to minimize the decking stiffness and to minimize the net concrete above the deck. 22 gage decking with 3 in. deep ribs on 12 in. centers was selected.

2.4 MATERIALS

Beams 1 through 6 were fabricated using A572 Grade 50 W21 x 44 sections. Beams 7 and 9 were fabricated using A36 W21 x 44 sections. Beam 8 used an A36 W10 x 15 section. The yield strength, static yield strength and tensile strength of the rolled sections were measured using standard test coupons from both the web and the flanges in a screw-type test machine. Specimens were loaded through the yield plateau at a relative head speed of 0.5 mm/min. At a minimum of two points on the yield plateau, the displacement was stopped so that the static yield load could be determined. When the load stabilized (at the static yield load), displacement was resumed. When strain hardening was observed, the relative head speed was increased to 5 mm/min. and loading was continued to failure. The average steel properties are summarized in Table 2.1.

The deformed reinforcing steel was Grade 60 with a yield stress of 70.9 ksi. The yield stress of the welded wire fabric was measured as 90.9 ksi using the 0.2% offset method.

All shear studs were supplied by the Nelson Stud Welding Division of TRW. Beams 1 through 7 had 3/4 in. diameter studs with a tensile strength of 67.9 ksi. Beam 8 had 5/8 in. diameter studs with a tensile strength of 63.2 ksi, and Beam 9 had 3/4 in. diameter studs with a tensile strength of 68.8 ksi. The 3/4 in. diameter studs were Nelson Type S3L, and the 5/8 in. diameter studs were Nelson Type H4L, modified for through-deck welding.

The steel decking was 22 gage Lok-Floor decking with 3 inch ribs supplied by United Steel Deck, Inc. The deck profile is shown in Fig. 2.12. The yield and tensile strengths of the decking were 40.7 ksi and 53.1 ksi, respectively.

The concrete was normal weight, Portland cement concrete supplied by a local ready-mix company. Coarse aggregate was crushed limestone, and fine aggregate was Kansas River sand. All mixes were ordered with entrained air. Concrete slump and air content were measured at the time of placement. Concrete strengths were measured using standard 6 by 12 in. test cylinders. Concrete properties are summarized in Table 2.2.

2.5 BEAM FABRICATION

The initial step in beam fabrication was the preparation of the web opening. The opening location was marked and 3/4 in. diameter holes were drilled at the corners to reduce stress concentrations. The opening was flame cut using an oxy-acetylene torch. Strain gage locations were ground with an abrasive wheel.

Stiffeners were either welded or bolted to the beam web at load points and supports on Beams 2 through 9. No stiffeners were used on Beam 1. Bearing plates for the beam supports were bolted in place.

The steel section was supported at each end, and shoring was installed to support the deck. Metal decking was positioned on the section and attached to the shoring with nails to prevent deck movement during stud welding. Shear studs were welded though the deck

using a Nelson Stud Welding unit. With the exception of Beam 4, studs were welded in each rib. The ribs over the openings in Beam 4 were attached to the wide flange section using 3/4 in. puddle welds.

After the shear studs were welded in place, the deck was scraped and brushed to remove welding debris. The nails holding the decking to the shoring were removed and the form sides were installed. All joints between the steel decking and concrete forms were caulked, and the reinforcing steel was installed.

The concrete was delivered by truck and placed using a 1 cubic yard bucket. After the forms were filled, the concrete was consolidated using a 1-1/2 in. electric vibrator inserted on 1 ft. centers. The concrete was screeded using a metal-edged screed and finished using a magnesium bull-float.

Slump and air tests were performed and test cylinders were cast as the beam was cast. After the concrete had begun to set, the slab and the test cylinders were covered with polyethylene sheets. All test cylinders were stored near the slab. The beam and the cylinders were kept continuously moist until a strength of 3000 psi was reached. The concrete was then allowed to dry.

Two openings were tested on Beams 4 through 9. After the first opening was tested, a second opening was cut in the steel section at the opposite end of the beam. A plate was welded in the first opening. The damaged concrete above the first opening was repaired using gypsum cement grout or high strength concrete.

On Tests 4B, 5B, and 6B, transverse cracks formed in the slabs above the openings when the openings were cut. On Tests 4B and 6B, the cracks formed at the low moment edge of the rib peak at the low moment end of the opening, while on Test 5B, the crack formed at the high moment edge of the rib peak at the high moment end of the opening. All of the cracks extended completely across the top of the slab and extended approximately 1 in. down the side of the slab.

The opening locations, load configurations, and span lengths are shown in Fig. 2.1 through 2.10. Section and opening dimensions are summarized in Table 2.3. Stud quantities and rib dimensions are summarized in Table 2.4.

2.6 INSTRUMENTATION

The beams were instrumented with electrical resistance strain gages and DC linear variable differential transformers (LVDT's). Strain gages were placed on both the steel and the concrete around the opening. Steel gages were located along a line 1-1/2 in. from the vertical edges of the opening to reduce the effect of stress concentrations at the opening corners. Concrete gages were placed on the top of the slab for all tests. In most cases, concrete gages were also placed on the bottom of the slab. 1 by 4 in. slots were cut in the steel decking and closed with duct tape before concrete placement. The tape was supported from below. Before the beam was tested, the support and tape were removed to expose the bottom of the slab.

Micromeasurements 120 ohm foil strain gages with a 0.240 in. gage length were applied to the steel following the gage manufacturer's recommended procedures. Precision Measurements 120 ohm paper-backed strain gages with 2.4 in. gage lengths were bonded to the concrete using Duco cement. All gages were wired with shielded cables. For Tests 1 through 3, the strain gages were read using Vishay Model P-350A strain indicators and a Hewlett-Packard 3052A data acquisition system with Diego Systems Model 113 strain gage conditioners. For Tests 4A through 9B, strain gages were read using a Hewlett-Packard Model 3054A data acquisition system. For all beams, the data acquisition system was controlled using a Hewlett-Packard 9825T Computer.

LVDT's were installed at the point of maximum moment and at the ends of the opening to monitor beam deflection. LVDT's were also installed at the ends of the concrete slab to monitor slip between the slab and the steel section.

Some of the openings had LVDT's installed at the ends of the opening to monitor the relative movement of the slab and the steel section. For these beams, steel bars were embedded in the slab to allow the measurement of horizontal slip. Holes were also cut in the steel decking to allow the vertical separation to be monitored. All LVDT's were read using the Hewlett-Packard data acquisition systems.

White wash was applied to the steel beam around the web opening to act as brittle coating. Diluted latex paint was applied to the concrete slab so that cracks could be seen.

2.7 LOAD SYSTEM

When the concrete reached the desired strength, the deck shoring was removed, and the beam was placed on pin and roller supports. Bearing plates were grouted to the concrete at the load points. On beams with transverse deck ribs, additional bearing plates were grouted between the steel beam and the steel deck (load was applied at the rib peak). The loading system was installed (Fig. 2.13).

The loading system applied load at one or two load points on each beam. At each load point, two tension rods transferred load through rockers to the top of a transverse load beam in contact with the test specimen. All load systems, with the exception of the load system for Test 8B, had 1-1/2 in. diameter hot-rolled tension rods. The load system for Test 8B had 1 in. diameter cold-rolled tension rods. The tension rods extended through openings in the load beam, the concrete slab, and the lab structural floor. Below the structural floor, the rods passed through hollow core Enerpac jacks which applied the load (Fig. 2.13). Hydraulic pressure was applied using an Amsler pendulum dynamometer. A manifold with flow control valves was used to control the individual jacks to prevent twisting of the test beam.

The tension rods were instrumented as load cells using two longitudinal and two transverse gages in a full-bridge circuit and were calibrated using a Tinius-Olsen column tester. The tension rods were monitored using a Hewlett-Packard data acquisition system and

computer. During a test, the load and deflection were monitored at two second intervals.

For Beams 1 through 6, Test 8A, and Beam 9, the total weight of the load system was 0.6 kips per load point. For Beam 7, which did not require bearing plates between the steel beam and the steel deck, the weight was 0.55 kips per load point. For Test 8B, which had 1 in. diameter tension rods, the weight was 0.44 kips per load point.

2.8 LOADING PROCEDURE

Each beam was cycled 13 times to low maximum loads to relieve residual stresses, to seat the loading system, and to test the instrumentation.

The tests to failure were run using the following procedure. Initial readings were taken at zero hydraulic system pressure and with the jacks hanging freely from the load rods. The first and second load increments were equal to the peak load of the pre-test cycles. The remaining load increments varied according to beam behavior. Preselected increments of load were used until the load-deflection curve indicated the beam was softening (the load-deflection curve became nonlinear). Load increments were then selected to produce increments of deflection for the remainder of the test. Load and deflection were plotted continuously. Concrete cracks were marked at each load step using felt pens. Prior to softening, the load was maintained while the instrumentation was read

and cracks were marked. Once the load deflection curve became non-linear, the deflection was maintained while readings were taken and cracks were marked. After failure, all additional cracks were marked and photographs were taken.

Two of the 15 tests deviated from the standard loading procedure. During Tests 1 and 3, after the specimens had been loaded well above their initial yield, the specimens had to be unloaded and then reloaded to failure. For Test 1, significant twisting of the beam was noted at 70 percent of the ultimate applied load. The beam was unloaded and the load system was adjusted to compensate for the twisting. For Test 3, large deflections at 98 percent of the ultimate applied load caused large rotations in the load beams, resulting in bending of the load rods. The beam was unloaded and the load system was adjusted to compensate for the rotation of the load beams. After the beam was reloaded to 98 percent of ultimate, the beam had to be unloaded a second time for further adjustments prior to the final application of load.

The results of the tests are described in the next chapter.

CHAPTER 3

EXPERIMENTAL RESULTS

3.1 GENERAL

Previous experimental work has shown that the deformation and failure mode of composite beams with web openings is largely a function of the moment-shear (M/V) ratio at the opening (8, 9, 11, 19, 32, 34, 36).

For openings with high M/V ratios, the openings tend to have small relative deformations across the opening and to fail in a flexural mode. At failure, the bottom tee completely yields in tension, and the concrete crushes at the high moment end of the opening.

As the M/V ratio decreases, the Vierendeel effect becomes more pronounced, as the shear at the opening induces secondary bending moments in the tees. Differential deflections across the opening increase. The concrete tends to crack at the top of the slab at the low moment end of the opening, and the bottom tee has compressive, as well as tensile strains. At failure, the concrete slab tends to separate from the steel section at the high moment end of the opening. Beams with solid slabs display a diagonal tension failure in the slab (9, 11), while beams with ribbed slabs display rib separation cracking (34, 46).

The results of the tests from the current study are presented and evaluated in the following sections.

3.2 BEHAVIOR UNDER LOAD

Most of the tests in the current study had relatively low M/V ratios (Tests 1, 2, 4A-9B). For these tests, the behavior under load was dominated by the effects of secondary bending. Large differential deformations across the opening were observed as the beams were loaded (Fig. 3.1). One test (Test 3) had a high M/V ratio. The behavior of this opening was dominated by the primary moment at the opening. Relatively small differential deformations across the opening were observed (Fig. 3.2).

Load-deflection diagrams for the 15 tests in this study are presented in Fig. 3.3 to 3.17. Strain distributions at the opening are presented in Fig. 3.18 to 3.32 for 4 stages of applied load (elastic, first yield, late yield, and collapse).

As a general rule, the failure of the beams was quite ductile. The peak loads were preceeded by major cracking in the concrete, yielding of the steel, and large deflections in the member (Fig. 3.3 - 3.17).

In all cases, yielding in the steel tees was observed at relatively low levels of loading (Fig. 3.18-3.32). As the tests progressed, transverse and longitudinal cracking occurred in the slabs. As the tests approached ultimate, the concrete around the shear studs above the opening failed, and the slab lifted from the steel beam at the high moment end of the opening.

The applied load at first yield and the applied load at the first occurrence of transverse, longitudinal, and diagonal cracking

near the opening are presented in Table 3.1. These loads are expressed as percentages of the applied (total - dead) load at failure.

First yielding was noted in tension in the top or the bottom tee. For Tests 1-6A, and 7A-8A, first yielding occurred in tension at the top of the low moment end of the bottom tee. For Tests 6B, 8B, 9A, and 9B, first yielding occurred in tension at the bottom of the high moment end of the top tee. First yielding occurred at applied loads as low as 19 percent, and as high as 52 percent of ultimate, with an average of 33 percent (Table 3.1). As concluded for beams with solid slabs (9, 10), the first yield does not give an accurate measure of section capacity.

Transverse, diagonal, and longitudinal cracks were noted in the slabs as the loads increased. Transverse cracks formed in the top of the slab at the low moment end of the openings (Fig. 3.33). The cracks occurred at applied loads as low as 25 percent, and as high 96 percent of ultimate (Table 3.1). For Tests 4B, 5B, and 6B, transverse cracks occurred when the opening was being cut. However, these cracks appeared to have no effect on the behavior of the opening under load. As the loading increased, all transverse cracks increased in width and in depth, eventually propagating to within approximately 1/2 in. of the bottom of the slab.

All tests with transverse ribs displayed diagonal cracking. Diagonal cracking occurred at an average applied load of 63 percent of ultimate. Diagonal cracks started at the high moment end of the opening at the low moment end of a rib and propagated toward the load

point as the load was increased. For Tests 7A and 7B, which had longitudinal ribs, no diagonal cracks were observed.

Longitudinal cracking (Fig. 3.33) occurred at an average applied load of 80 percent of ultimate. Longitudinal cracks started at the top of the slab at the low moment end of the opening directly above the steel section and propagated toward the load point and the support as the load increased.

Failure at openings was preceeded by failure of the concrete around the studs above the opening and between the opening and the support. For the tests with longitudinal ribs, a longitudinal shear failure occurred between the rib and the surrounding deck (Fig. 3.34), and a slight slab uplift was noted. For the tests with transverse ribs, the concrete failed in a shearing mode in the rib (Fig. 3.35). The rib pulled away from the concrete around the stud group, leaving a wedge-shaped block. For high shear tests on beams with ribs transverse to the steel section (Tests 1, 2, 4A-6A, and 8A-9B), rib failure was followed by slab uplift, resulting in bridging of the slab over the opening (Fig. 3.36). For the high moment test (Test 3), only a minor slab uplift was noted (Fig. 3.2). For tests 6B, 8A, and 8B, the diagonal cracks in the slab propagated to the top surface of the slab near the load point. All tests exhibited a large amount of slip between the concrete and steel.

At all stages of loading, strains at the opening indicate a lack of strain compatibility between the tees and between the top tee steel and the slab (Fig. 3.18-3.32). The strain data show that, with

the exception of Test 3 (high M/V) (Fig. 3.20), strains were quite low in the concrete slab at failure.

The moments and shears at ultimate and the modes of failure for the current test series are presented in Table 3.2. The failure loads include the weight of the beam and load system, as well as the applied loads.

3.3 DISCUSSION OF BEHAVIOR

The tests in the current study confirm that the behavior of composite beams with web openings is largely controlled by the M/V ratio at the opening. Deformation, cracking in the slab, and the failure load are all functions of the M/V ratio.

In general, the deflection across a web opening, δ_o, increases as the M/V ratio decreases. It is useful to normalize δ_o with respect to the deflection at the point of maximum moment at failure, δ_m, to obtain a normalized opening deflection, $\overline{\delta} = \delta_o/\delta_m$. δ_o, δ_m, and $\overline{\delta}$ are summarized in Table 3.3.

For tests with low to intermediate M/V ratios, $\overline{\delta}$ is high. As the M/V ratio increases, $\overline{\delta}$ decreases. Tests 1 through 6B had similar sections. $\overline{\delta}$ was 2.27 for Test 6A (M/V = 0), an average of 1.06 for Tests 1 and 6B (M/V = 3.5 ft), an average of 1.03 for Tests 2, 4A, 4B, 5A, and 5B (M/V = 6.5 ft), and 0.03 for Test 3 (M/V = 45.2 ft).

Transverse cracking of the concrete slab at the low moment end of the opening is also strongly affected by the M/V ratio. As the M/V ratio decreases, transverse cracks tend to appear at lower loads.

Cracking occurred at only 21 percent of the maximum applied load for Test 6A (M/V = 0), an average of 42 percent for Tests 1 and 7A (M/V = 3.5 ft), an average of 65 percent for Tests 2, 4A, 5A, and 7B (M/V = 6.5 ft), and 96 percent of the maximum load for Test 3 (M/V = 45.2 ft) (Table 3.1).

Longitudinal and diagonal cracking of the slab appear not to be functions of the M/V ratio (Table 3.1). Longitudinal cracking occurred at 70 percent of the maximum applied load for Test 6A (M/V = 0), an average of 86 percent for Tests 1 and 7A (M/V = 3.5 ft), an average of 84 percent for Tests 2, 4A, 5A, and 7B (M/V = 6.5 ft), and 76 percent for Test 3 (M/V = 45.2 ft). Diagonal cracking occurred at 70 percent of the maximum applied load for Test 6A, an average of 67 percent for Tests 1 and 7A, an average of 81 percent for Tests 2, 4A, 5A, and 7B, and 76 percent for Test 3.

The failure loads were affected by the quantity of shear connectors above the opening and between the opening and the support. As the quantity of connectors increased, the failure load tended to increase. Tests 2, 4A, 4B and 5A had M/V ratios of 6.5 ft, had the same section and opening dimensions, and had approximately the same material strengths. Test 2 had a high number of studs over the opening and between the opening and the support (H-H), Test 4A had no studs over the opening and a low number of studs between the opening and the support (N-L), Test 4B had no studs over the opening and a high number of studs between the opening and the support (N-H), and Test 5A had a low number of studs above the opening and a low number

of studs between the opening and the support (L-L). The shears at failure for Tests 2 (H-H), 4B (N-H), 5A (L-L), and 4A (N-L) were 39.0, 39.0, 34.6, and 32.7, respectively (Table 3.2).

Test 4B (N-H) and Test 2 (H-H) failed at the same maximum shear, even though the quantities of shear connectors were not the same. This is probably due to the fact that the puddle welds in the ribs above the opening effectively transferred shear between the steel tee and the concrete. The shear transfer was calculated to be 11.4 kips for Test 4B and 25.9 kips for Test 2 using the elastic strain distributions for the two tests. Very large deflections were required in order to mobilize the shear strength of the puddle welds (Table 3.3).

Test 6B was used to evaluate a possible reinforcement procedure for composite beams with web openings (Section 2.2). Test 6B and Test 1 had M/V ratios of 3.5 ft and had approximately the same material strengths. Test 6B had additional studs over the opening and between the opening and the support. Test 1 failed at a shear of 37.8 kips, while Test 6B failed at a shear of 48.9 kips. The additional studs provided a significant increase in shear capacity. The failure mode of Test 6B was also affected by the additional studs (Table 3.2). For Test 1, diagonal cracking in the slab occurred at 67 percent of ultimate, while for Test 6B, diagonal cracking occurred at 94 percent of ultimate. While rib failure occurred for both tests, the rib failure in Test 6B was followed by a diagonal tension

failure near the load point similar to that observed in beams with solid slabs (9, 11).

As the shear at a web opening increases, the moment capacity at the opening decreases. An interesting way to illustrate this compares the normalized failure moment with a generalized measure of the M/V ratio as follows: The moments at failure, M_n(test) for the current test series (Table 3.2) along with those for previous tests (Table B.4), are normalized by dividing by the calculated "pure" moment capacity at the opening, M_m. M_m is obtained using the Slutter and Driscoll procedure (35) for the flexural capacity of the net section at the opening and considering partial composite action. M_n(test)/M_m is compared to the M/V ratio normalized to the depth of the steel section, d. The M/Vd ratio is equivalent to a "shear-span to depth ratio". M_n(test)/M_m is plotted versus ln(M/Vd) in Fig. 3.37. Test 6A (M/Vd = 0) and Tests 4A and 4B (puddle welds over the opening) are excluded from the plot.

A positive trend exists between M_n(test)/M_m and ln(M/Vd), indicating that the moment at failure is strongly dependent on the (M/Vd) ratio at the opening. The correlation coefficient, r, obtained from a linear regression analysis of the data in Fig. 3.37 is 0.944.

3.4 SUMMARY

The location of the opening (as indicated by the M/V or M/Vd ratios) has a major effect on the opening behavior and on the

capacity at the opening. As the M/V ratio decreases, deflections across the opening increase and transverse cracking occurs at lower loads.

First yield of the steel around an opening is not a good measure of the section capacity.

The failure of the beams in the current study was, in general, quite ductile.

The amount of shear transfer between the concrete and the steel above the opening and between the opening and the support has a major effect on the strength of beams with web openings. Increased shear transfer allows the concrete slab to contribute more to the strength.

CHAPTER 4

STRENGTH MODEL

4.1 GENERAL

A number of strength models for composite beams with web openings have been proposed (10, 11, 28, 30, 42). All of the models are based on the static theorem of plasticity (21) and are used to generate moment-shear interaction diagrams representing the strength of beams at web openings. For each combination of moment and shear, moment equilibrium is enforced. The steel tees are assumed to yield in either tension or compression, and the interaction of shear and normal stress is accounted for based on the von Mises yield criterion.

Three of the models pertain to composite beams with solid slabs (10, 11, 28, 42), while one of the models was developed specifically for composite beams with ribbed slabs (30). One of the models (28) includes the effects of reinforcement around the opening.

In addition to the strength models, a number of simplified design techniques have been developed (11, 15, 33, 34).

The existing strength models are limited in application, while the simplified design techniques do not provide detailed information on the behavior or strength at an opening, over the full range of moments and shears. This chapter presents a comprehensive strength model which is applicable to any slab configuration and includes provisions for web reinforcement. The model is relatively complex and is formulated primarily as a research tool. Chapter 5 presents

accurate, practical design techniques that were developed based on the lessons learned with the model.

The model is described in five major sections. The basic assumptions are discussed in Section 4.2, along with a general discussion of the procedure used to develop moment-shear interaction diagrams. The interaction between shear and compressive stresses in the steel and in the concrete are considered in Section 4.3. Equilibrium equations relating the moments, shears, and axial forces in the bottom and top tees are developed in Sections 4.4 and 4.5, respectively. Details of the interaction procedure are presented in Section 4.6.

In the final section, the model is used to predict the strength of tests. Ratios of test to calculated strength are presented and discussed.

4.2 OVERVIEW OF THE MODEL

The model presented here represents a modification and major extension of the model developed by Clawson and Darwin (10, 11). The modifications are based on the improved understanding obtained from the 29 additional tests that have been completed since Clawson and Darwin completed their work, along with the experience gained from other models and design procedures (15, 28, 33, 34, 42).

The model is based on the static theorem of plasticity (21). Therefore, failure mechanisms must be assumed. The mechanisms are functions of the moment and shear acting at the opening.

For pure bending (V = 0), the entire opening is assumed to form a plastic hinge. The bottom tee yields in tension, while the concrete crushes (Fig. 4.1).

When both shear and bending act at the opening, the shear induces secondary bending moments in the top and bottom tees at both ends of the opening. Plastic hinges are assumed at both ends of the bottom tee and at the high moment end of the top tee. In addition, the concrete is assumed to fail under combined compression and shear at the high moment end of the opening (Fig. 4.2).

The forces acting at a web opening are shown in Fig. 4.3. The maximum shear capacity at the opening is calculated by assuming zero axial force in the bottom and top tees ($P_b = P_t = 0$). Plastic hinges form at both ends of the bottom tee. Two failure modes, a "mechanism" failure and a "shear" failure, are considered for the top tee. A "mechanism" failure occurs with plastic hinges forming at both ends of the top tee. The concrete is assumed to fail under combined compression and shear at both ends of the opening. At the high moment end, the failure occurs at the top of the slab, while at the low moment end, the failure occurs at the bottom of the slab (Fig. 4.4). A "shear" failure occurs when the pure shear capacity of both the concrete and the steel is exceeded in the top tee (Fig. 4.5). The strength of the top tee in pure shear, $V_t(max)$, is the lower of the strengths found for the two failure modes. The shear strength of the beam at the web opening is the sum of the top and the bottom tee shear strengths.

Moment-shear interaction diagrams are developed by calculating the primary moment capacity, $M_{primary}$, at the opening centerline as the shear is increased from zero to the maximum shear capacity. A predetermined portion of the shear is assigned to the bottom and top tees (V_b and V_t, respectively) (Fig. 4.3). Using V_b, an axial force, P_b, and secondary bending moments, M_{bl} and M_{bh}, are calculated. P_t and V_t are applied to the top tee ($P_t = P_b$ and is applied in the opposite direction). The secondary moment capacity of the high moment end of the top tee, M_{th}, is then calculated. Finally, $M_{primary}$ is calculated using the secondary moment capacities and the axial force.

$$M_{primary} = Pz + M_{th} + M_{bh} - 0.5a_o V_{total} \qquad (4.1)$$

in which z = the distance between the axial forces, $P = P_b = P_t$, a_o = the opening length, and $V_{total} = V_b + V_t$.

The following simplifying assumptions are used:

1) The steel will yield in tension or compression.
2) Shear forces can be carried in the steel and concrete at both ends of the opening.
3) Shear forces in the steel are carried only in the webs.
4) Shear stresses in the steel webs are uniformly distributed over the full depth of the steel tees.
5) The normal forces in the concrete are applied over an area defined by the equivalent stress block (1).

6) The compressive forces in the concrete are limited by the crushing capacity of the slab, normal force equilibrium, and the shear capacity of the shear studs between the ends of the opening and between the opening and the supports.

The model includes provisions for web reinforcement at the opening. In addition, the model includes provisions for solid slabs and ribbed slabs with either transverse or longitudinal ribs.

It must be noted that, while the model is an extension of the Clawson and Darwin model, there are significant differences. In the Clawson and Darwin model, concrete force exists only at the high moment end of the opening, the slab is fully composite, and reinforcing steel in the slab is considered. Shear forces in the steel can be carried in the flanges, as well as in the webs of the tees. In addition, the Clawson and Darwin model does not include provisions for web reinforcement and applies only to solid slab construction.

4.3 MATERIALS

Both concrete and steel are assumed to be in a state of plane stress. The models for these materials are described below.

4.3.1 Steel

The structural steel is represented as a rigid, perfectly plastic material. The maximum yield strength, σ_o, is the yield stress obtained from a uniaxial tension test. No strain hardening is considered.

The steel yield criterion is the von Mises yield hypothesis. For a state of plane stress, this reduces to

$$\sigma_o^2 = \sigma_x^2 + 3\tau_{xy}^2 \qquad (4.2a)$$

in which σ_x = normal stress and τ_{xy} = shearing stress. For a web under combined tension and shear, the reduced longitudinal yield strength due to shear, F_{ywr}, is

$$F_{ywr} = (F_{yw}^2 - 3\tau_{xy}^2)^{1/2} \qquad (4.2b)$$

in which F_{yw} = yield strength of the web in uniaxial tension.

4.3.2 Concrete

The strength model for concrete is based on the biaxial tests of Kupfer, Hilsdorf, and Rüsch (23) for combined tension and compression (Fig. 4.6). Clawson and Darwin (10, 11) transform the principal stress data for concrete with a nominal compressive strength of 4450 psi (23) to a state of combined shear stress, τ, and normal stress, f. τ and f, normalized with respect to the concrete strength, f'_c, are presented in Fig. 4.7. The maximum shear stress, $0.21f'_c$, is obtained at a normal stress of $0.73f'_c$.

Clawson and Darwin (10, 11) fit the data with two parabolic curves. The right-hand and left-hand curves are, respectively,

$$\tau = \left[-2.9\left(\frac{f}{f'_c}\right)^2 + 4.2\left(\frac{f}{f'_c}\right) - 1.3\right]f'_c \qquad (4.3a)$$

and

$$\tau = \left[-0.32\left(\frac{f}{f'_c}\right)^2 + 0.46\left(\frac{f}{f'_c}\right) - 0.042\right]f'_c \qquad (4.3b)$$

Both equations are used in the failure model.

The concrete is assumed to be in compression and shear at both ends of the opening. The concrete compressive strength is limited to 0.85f, with f given by either Eq. (4.3a) or (4.3b). The normal stress is applied over the effective width of the slab, b_e (defined in Section 4.5), while the shear stress is applied over a width equal to 3 times the gross slab thickness, T_s. The nominal shear strength of the concrete is limited to $3.5\sqrt{f'_c}$ (10,11).

4.4 BOTTOM TEE

The forces in the bottom tee under a positive primary moment are shown in Fig. 4.3. These forces consist of a shear force, an axial force, and secondary moments. Equilibrium for the bottom tee requires that

$$P_b = P_{bl} = P_{bh} \qquad (4.4a)$$

$$V_b = V_{bl} = V_{bh} \qquad (4.4b)$$

$$M_{bl} + M_{bh} = V_b a_o \qquad (4.4c)$$

in which P_{bl} = the low moment end axial force, P_{bh} = the high moment end axial force, V_{bl} = the low moment end shear force, and V_{bh} = the high moment end shear force.

The web stub is assumed to extend through the flange and stiffener. The shear stress in the web, τ_b, is

$$\tau_b = V_b/(s_b t_w) \tag{4.5}$$

in which s_b = the web stub depth, and t_w = the web thickness (Fig. 4.8). F_{ywr} and τ_b are related by Eq. (4.2b) with $\tau_b = \tau_{xy}$.

Plastic hinges are assumed to form at each end of the tee. The equilibrium relationships (Eq. (4.4)) and the von Mises criterion (Eq. (4.2b)) are used to express P_b as a function of V_b.

4.4.1 Low Moment End

When a positive primary moment is applied to the web opening, the low moment end of the bottom tee is subjected to a tensile force and a negative secondary moment. The top of the tee is in tension, while the bottom of the tee is in compression.

The neutral axis is assumed to be in either the web or the flange, at a distance g, from the top of the tee (Fig. 4.9). The neutral axis will always be below the stiffener, if the area of the stiffener is no larger than the area of the flange.

The minimum value for g is attained when $P_b = 0$. As the axial force increases with increasing primary moment, the neutral axis

shifts downward. The maximum axial force, P_u, is obtained when V_b = 0. The neutral axis is, therefore, at the bottom of the flange, and $g = s_b$. P_u is given by

$$P_u = F_{yf}(b_f - t_w)t_f + F_{yw}s_b t_w + F_{ys}(b_s - t_w)t_s \qquad (4.6)$$

in which F_{ys} = the yield strength of the stiffener, t_s = the stiffener thickness, b_s = the total stiffener width, including the web thickness, F_{yf} = the yield strength of the flange, t_f = the flange thickness, and b_f = the flange width (Fig. 4.8). P_u is often referred to as the squash load (21). For a specific stress distribution, P_b is less than or equal to P_u. The squash load ratio, n, is defined (21) as

$$n = P_b/P_u;\ 0 \leq n \leq 1 \qquad (4.7)$$

Equations of equilibrium can be written for any stress distribution with a neutral axis location, g. When the neutral axis is in the flange (Fig. 4.9a), normal force equilibrium results in

$$P_b = F_{ywr}t_w(2g - s_b) + F_{ys}t_s(b_s - t_w) + F_{yf}(b_f - t_w)(2g - 2s_b + t_f) \qquad (4.8)$$

Using $A_w = s_b t_w$ and $A_s = t_s(b_s - t_w)$ and solving for g gives

$$g = \frac{P_b - F_{ys}A_s + F_{yf}(b_f - t_w)(2s_b - t_f) + F_{ywr}A_w}{2(F_{ywr}t_w + F_{yf}(b_f - t_w))} \qquad (4.9)$$

Moment equilibrium requires that

$$M_{bl} = F_{ywr}t_w(\frac{s_b^2}{2} - g^2) - F_{ys}A_s y_s + F_{yf}(b_f - t_w)(s_b^2 + \frac{t_f^2}{2} - s_b t_f - \frac{g^2}{2}) \qquad (4.10)$$

Combining Eq. (4.6), (4.7), (4.9), and (4.10) gives M_{bl} in terms of n.

$$M_{bl} = C_{f1}^2 C_{f3} n^2 + 2C_{f1}C_{f2}C_{f3}n + C_{f2}^2 C_{f3} + C_{f4} \qquad (4.11a)$$

in which $$C_{f1} = \frac{(A_f F_{yf} + A_w F_{yw} + A_s F_{ys})}{2(F_{ywr}t_w + F_{yf}(b_f \not{+} t_w))} \qquad (4.11b)$$

$$C_{f2} = \frac{F_{ywr}A_w - F_{ys}A_s + F_{yf}(b_f - t_w)(2s_b - t_f)}{2(F_{ywr}t_w + F_{yfr}(b_f - t_w))} \qquad (4.11c)$$

$$C_{f3} = - F_{ywr}t_w - F_{yf}(b_f - t_w) \qquad (4.11d)$$

and $$C_{f4} = F_{ywr}A_w \frac{s_b}{2} - F_{ys}A_s y_s + \frac{F_{yf}(b_f - t_w)}{2}(s_b^2 + (t_f - s_b)^2) \qquad (4.11e)$$

When the neutral axis is in the web (Fig. 4.9b), normal force equilibrium gives

$$P_b = F_{ywr}t_w(2g - s_b) + F_{ys}t_s(b_s - t_w) - F_{yf}t_f(b_f - t_w) \tag{4.12}$$

Using $A_f = t_f(b_f - t_w)$ and solving for g gives

$$g = \frac{P_b - F_{ys}A_s + F_{ywr}A_w + F_{yf}A_f}{2F_{ywr}t_w} \tag{4.13}$$

Moment equilibrium requires that

$$M_{bl} = F_{ywr}t_w(\frac{s_b^2}{2} - g^2) - F_{ys}A_s y_s + F_{yf}A_f(s_b - \frac{t_f}{2}) \tag{4.14}$$

Combining Eq. (4.6), (4.7), (4.13), and (4.14) gives M_{bl} in terms of n.

$$M_{bl} = C_{w1}^2 C_{w3} n^2 + 2C_{w1}C_{w2}C_{w3}n + C_{w2}^2 C_{w3} + C_{w4} \tag{4.15a}$$

in which $$C_{w1} = \frac{A_f F_{yf} + A_w F_{yw} + A_s F_{ys}}{2(F_{ywr}t_w)} \tag{4.15b}$$

$$C_{w2} = \frac{F_{ywr}A_w - F_{ys}A_s + F_{yt}A_f}{2(F_{ywr}t_w)} \tag{4.15c}$$

$$C_{w3} = - F_{ywr} t_w \qquad (4.15d)$$

and $$C_{w4} = F_{ywr} A_w \frac{s_b}{2} - F_{ys} A_s y_s + F_{yf} A_f (s_b - t_f/2) \qquad (4.15e)$$

Eq. (4.11a) and (4.15a) are quadratic equations in n. For any value of M_{b1}, therefore, the corresponding axial force, $P_b = nP_u$, can be found.

The neutral axis crosses over from the flange to the web when when $g = s_b - t_f$. Substituting for g in Eq (4.12) gives

$$P_b = F_{ywr} t_w (s_b - 2t_f) + F_{ys} (b_s - t_w) t_s - F_{yf} (b_f - t_w) t_f \qquad (4.16)$$

Substituting for P_b in Eq. (4.7) and consolidating terms gives

$$n^f_{x1} = \frac{F_{ywr} t_w (s_b - 2t_f) - F_{yf} A_f + F_{ys} A_s}{(F_{yf} A_f + F_{ywr} A_w + F_{ys} A_s)} \qquad (4.17)$$

in which n^f_{x1} = the flange to web crossover ratio at the low moment end of the bottom tee.

4.4.2 High Moment End

When the opening is subjected to a positive primary moment, the high moment end of the bottom tee is subjected to a tensile force and

positive secondary moment. Therefore, the top of the tee will be in compression, and the bottom of the tee will be in tension.

The neutral axis is located a distance g from the top of the tee. Unlike the low moment end, the neutral axis can be located anywhere within the stub depth (Fig. 4.10).

The maximum value for g is attained when $P_b = 0$. As the tension force is increased under increasing primary moment, the neutral axis shifts upward. Based on normal force and moment equilibrium, equations giving M_{bh} in terms of n are developed.

When the neutral axis is in the web above the stiffener (Fig. 4.10a), normal force equilibrium requires that

$$P_b = F_{ywr}t_w(s_b - 2g) + F_{ys}(b_s - t_w)t_s + F_{yf}(b_f - t_w)t_f \qquad (4.18)$$

Moment equilibrium requires that

$$M_{bh} = C_{a1}^2 C_{a3} n^2 - 2C_{a1}C_{a2}C_{a3}n + C_{a2}^2 C_{a3} + C_{a4} \qquad (4.19a)$$

in which $$C_{a1} = \frac{(A_f F_{yf} + A_w F_{yw} + A_s F_{ys})}{2(F_{ywr} t)} \qquad (4.19b)$$

$$C_{a2} = \frac{F_{ywr}A_w + F_{ys}A_s + F_{yt}A_f}{2(F_{ywr}t_w)} \qquad (4.19c)$$

$$C_{a3} = - F_{ywr}t_w \tag{4.19d}$$

and $$C_{a4} = F_{ywr}A_w \frac{s_b}{2} - F_{ys}A_s y_s + F_{yf}A_f(s_b - t_f/2) \tag{4.19e}$$

When the neutral axis is in the stiffener (Fig. 4.10b), normal force equilibrium requires that

$$P_b = F_{ywr}t_w(s_b - 2g) + 2F_{ys}(b_s - t_w)(y_s - g) + F_{yf}(b_f - t_w)t_f \tag{4.20}$$

Moment equilibrium requires that

$$M_{bh} = C_{s1}^2 C_{s3} n^2 - 2C_{s1}C_{s2}C_{s3}n + C_{s2}^2 C_{s3} + C_{s4} \tag{4.21a}$$

in which $$C_{s1} = \frac{(A_f F_{yf} + A_w F_{yw} + A_s F_{ys})}{2(F_{ywr}t_w + F_{ys}(b_s - t_w))} \tag{4.21b}$$

$$C_{s2} = \frac{A_f F_{yf} + A_w F_{ywr} + 2F_{ys}(b_s - t_w)y_s}{2(F_{ywr}t_w + F_{ys}(b_s - t_w))} \tag{4.21c}$$

$$C_{s3} = - F_{ywr}t_w - F_{ys}(b_s - t_w) \tag{4.21d}$$

and $$C_{s4} = F_{yf}A_f(s_b - t_f/2) + F_{ywr}A_w \frac{s_b}{2} + \frac{F_{ys}(b_s - t_w)}{2}\left[(y_s + t_s/2)^2 + (y_s - t_s/2)^2\right] \tag{4.21e}$$

The neutral axis crosses over from the web above the stiffener to the stiffener when $g = y_s - t_s/2$. Substituting for g in Eq. (4.18) gives

$$P_b = F_{ywr}t_w(s_b - 2y_s + t_s) + F_{ys}(b_s - t_w)t_s + F_{yf}(b_f - t_w)t_f \qquad (4.22)$$

Substituting for P_b in Eq. (4.7) and consolidating terms gives

$$n^s_{xh} = \frac{F_{ywr}t_w(s_b - 2y_s + t_s) + F_{yf}A_f + F_{ys}A_s}{(F_{yf}A_f + F_{yw}A_w + F_{ys}A_s)} \qquad (4.23)$$

in which n^s_{xh} = the squash load ratio at crossover from the web above the stiffener to the stiffener at the high moment end of the tee.

If the neutral axis is in the web below the stiffener (Fig. 4.10c), the moment-axial force equation for the high moment end is

$$M_{bh} = C^2_{w1}C_{w3}n^2 - 2C_{w1}C_{w2}C_{w3}n + C^2_{w2}C_{w3} + C_{w4} \qquad (4.24)$$

in which the coefficients are given by Eq. (4.15b) - (4.15e). The neutral axis crossover from the stiffener to the web below the stiffener occurs when $g = y_s + t_s/2$. Therefore, the squash load ratio at crossover, n^w_{xh}, is

$$n^w_{xh} = \frac{F_{ywr}t_w(s_b - 2y_s - t_s) + F_{yf}A_f - F_{ys}A_s}{(F_{yf}A_f + F_{yw}A_w + F_{ys}A_s)} \qquad (4.25)$$

If the neutral axis is in the flange (Fig. 4.10d), the moment-axial force equation for the high moment end is

$$M_{bh} = C_{f1}^2 C_{f3} n^2 - 2C_{f1}C_{f2}C_{f3}n + C_{f2}^2 C_{f3} + C_{f4} \qquad (4.26)$$

in which the coefficients are given by Eq. (4.11b) - (4.11e). The web-flange crossover occurs when $g = s_b - t_f$. Therefore, the squash load ratio at crossover, n_{xh}^f, is

$$n_{xh}^f = \frac{F_{ywr} t_w (2t_f - s_b) + F_{yf} A_f - F_{ys} A_s}{(F_{yf} A_f + F_{yw} A_w + F_{ys} A_s)} \qquad (4.27)$$

Eq. (4.19a), (4.21a), (4.24) and (4.26) are quadratic equations in n. For any value of M_{bh}, the corresponding axial force, $P_b = nP_u$ can be found.

4.4.3 Total Capacity

Moment-axial force equations are developed by substituting Eq. (4.11a) or (4.15a) for M_{bl} and Eq. (4.19a), (4.21a), (4.24), or (4.26) for M_{bh} in Eq. (4.4c). The neutral axis may be located within one of two regions at the low moment end (Fig. 4.9a and 4.9b), while the neutral axis may be located within one of four regions at the high moment end (Fig. 4.10a-4.10d). Thus, a total of eight possible moment equilibrium relationships exist. The correct neutral axis locations at the low and high moment ends must be found by trial.

The procedure for establishing the neutral axis locations is described in Appendix C.

Once the neutral axis locations are established, a moment-axial force equation (selected from Eq. (C.1)-(C.7)) is obtained. n is determined by solving the equation, which is a quadratic in terms of n. M_{bl} is then calculated using Eq. (4.11a) or (4.15a) and M_{bh} is calculated using Eq. (4.19a), (4.21a), (4.24), or (4.26). Finally, P_b is calculated using Eq. (4.7).

4.5 TOP TEE

The forces and moments acting in the top tee under a positive moment are shown in Fig. 4.3. As with the bottom tee, these include a shear force, an axial force, and secondary moments.

Equilibrium for the top tee requires that

$$P_t = P_{tl} = P_{th} \tag{4.28a}$$

$$V_t = V_{tl} = V_{th} \tag{4.28b}$$

$$M_{tl} + M_{th} = V_t a_o \tag{4.28c}$$

in which P_{tl} = the low moment end axial force, P_{th} = the high moment end axial force, V_{tl} = the low moment end shear force, and V_{th} = the high moment end shear force.

Shear can be carried by both the steel tee and the slab.

$$V_t = V_c + V_s \tag{4.29}$$

in which V_c = the portion of the top tee shear carried by the concrete and V_s = the portion of the top tee shear carried by the web of the steel tee.

The shear stress in the steel web, τ_s, is

$$\tau_s = V_s/(s_t t_w) \qquad (4.30)$$

in which s_t = the web stub depth (Fig. 4.11). F_{ywr} for the top tee web and τ_s are related by Eq. (4.2b) with $\tau_s = \tau_{xy}$.

The concrete can carry shear in the compression zone at both ends of the opening. The concrete is assumed to be in compression at the bottom of the slab at the low moment end and at the top of the slab at the high moment end. As with Clawson and Darwin's model, the shear is carried in a width equal to 3 times the gross slab thickness (10, 11). The shear stress in the concrete is

$$\tau_c = \frac{V_c}{3T_s c} \qquad (4.31)$$

in which T_s = the total (gross) slab thickness, and c = the distance from the neutral axis to the extreme compressive fiber in the concrete. The compressive stress in the concrete is carried over width b_e (2).

$$b_e \leq \text{Span}/4$$

$$\leq \text{Beam spacing} \qquad (4.32)$$

$$\leq 16T_s + b_f$$

$$\leq \text{Slab width}$$

c is selected such that for given shear and normal forces, the concrete stresses comply with Eq. (4.3a) or (4.3b). It should be noted that, in general, c will not be the same at both ends of the opening.

In the top tee, all of the shear is assumed to be applied to the steel web, if the applied shear is less than or equal to the plastic shear capacity of the web, V_{pt}. The concrete carries any shear in excess of V_{pt}. For the top tee,

$$V_{pt} = s_t t_w F_y/\sqrt{3} \qquad (4.33a)$$

The upper bound of the shear that can be applied to the top tee is the "pure shear" capacity for the top tee, $V_t(sh)$.

$$V_t(sh) = \frac{3.5\sqrt{f'_c}\, A_{cv}}{1000} + V_{pt}\ , \text{ kips} \qquad (4.33b)$$

in which $A_{cv} = 3T_s t_e$ and t_e = the effective slab thickness. t_e is dependent on the type of slab. For ribbed slabs with the ribs perpendicular to the beam,

$$t_e = t_s = \text{the minimum slab thickness} \qquad (4.34a)$$

For ribbed slabs with the ribs parallel to the beam,

$$t_e = \frac{T_s + t_s}{2} \qquad (4.34b)$$

$$= \text{the average of the maximum and minimum slab thicknesses}$$

For solid slabs,

$$t_e = T_s = \text{the slab thickness} \qquad (4.34c)$$

Normal forces exist in the steel tee and in the slab. Equilibrium requires that

$$P_t = P_{cl} + P_{sl} \qquad (4.35a)$$

$$= P_{ch} + P_{sh} \qquad (4.35b)$$

in which P_{cl} = the low moment end concrete force, P_{ch} = the high moment end concrete force, P_{sl} = the low moment end steel force, and P_{sh} = the high moment end steel force. P_{ch} is given by

$$P_{ch} \leq NRQ_n \tag{4.36a}$$

$$\leq P_c \tag{4.36b}$$

$$\leq P_t - P_{smax} \tag{4.36c}$$

in which N = the number of studs between the high moment end of the opening and the support, R = the reduction factor for studs in ribbed slabs, Q_n = the nominal strength of one stud shear connector embedded in a solid slab (3, 29), P_c = the crushing capacity of the slab (reduced for V_c), and P_{smax} = the maximum capacity of the top tee steel (reduced for V_s). P_{cl} is given by

$$P_{cl} = P_{ch} - N_o RQ_n \geq 0 \tag{4.37}$$

in which N_o = the number of shear connectors above the opening.

For slabs with transverse ribs, R is (2, 3, 20)

$$R = \frac{.85}{\sqrt{N_r}}\left(\frac{w_r}{h_r}\right)\left(\frac{H_s}{h_r} - 1.0\right) \leq 1.0 \tag{4.38}$$

in which h_r = the nominal rib height in inches, H_s = the length of the stud connector after welding in inches, N_r = the number of stud connectors in one rib, and w_r = the average width of the concrete rib.

For slabs with ribs parallel to the steel beam, the reduction factor is (2, 3, 20)

compression. The top of the steel tee is in tension, while the bottom of the tee is in compression.

From Eq. (4.35a), the force in the steel at the low moment end, P_{sl}, is given by

$$P_{sl} = P_t - P_{cl} \tag{4.46}$$

The neutral axis in the steel tee is located at a distance g from the bottom of the tee (Fig. 4.13). The neutral axis can be located anywhere within the steel tee at the low moment end.

When the neutral axis is in the web below the stiffener (Fig. 4.13a), normal force equilibrium requires that

$$P_{sl} = -F_{yf}A_f - F_{ywr}t_w(s_t - 2g) - F_{ys}A_s \tag{4.47}$$

The neutral axis crosses over from the web below the stiffener to the stiffener when $g = y_s - \frac{t_s}{2}$. The force in the steel at crossover, P^s_{xl}, is

$$P^s_{xl} = -F_{yf}A_f - F_{ywr}t_w(s_t - 2y_s + t_s) - F_{ys}A_s \tag{4.48}$$

If $P_{sl} < P^s_{xl}$, the neutral axis is in the web below the stiffener and

Moment equilibrium requires that

$$M_{tl} = F_{yf}A_f(s_t - t_f/2) + \frac{F_{ywr}t_w}{2}(s_t^2 - 2g^2) - F_{ys}A_s y_s - P_{cl}y_{cl} \qquad (4.58)$$

If $P_{sl} > P_{xl}^f$, the neutral axis is in the flange (Fig. 4.13d) and

$$g = \frac{P_{sl} + F_{yf}(b_f - t_w)(2s_t - t_f) + F_{ywr}A_w - F_{ys}A_s}{2(F_{yf}(b_f - t_w) + F_{ywr}t_w)} \qquad (4.59)$$

Moment equilibrium requires that

$$M_{tl} = \frac{F_{yf}(b_f - t_f)}{2}(2s_t^2 - 2t_f s_t + t_f^2 - 2g^2) + \frac{F_{ywr}t_w}{2}(s_t^2 - 2g^2) - F_{ys}A_s y_s - P_{cl}y_{cl} \qquad (4.60)$$

4.4.1.2 High moment end

When the opening is subjected to a positive primary moment, the high moment end of the top tee is subjected to a compressive force and a positive secondary moment. At the maximum "mechanism" shear load, the top tee is subjected only to a positive secondary moment. In either case, the top of the concrete slab is in compression.

Also, the top of the steel tee is in compression while the bottom of the tee is in tension.

From Eq. (4.35b), the force in the steel at the high moment end, P_{sh}, is

$$P_{sh} = P_t - P_{ch} \tag{4.61}$$

The neutral axis is located a distance g from the bottom of the tee (Fig. 4.14). Unlike the low moment end, the neutral axis is assumed to be above the stiffener in one of only two regions. This is always true, if the area of the stiffener is no larger than the area of the flange.

When the neutral axis is in the web (Fig. 4.14a), normal force equilibrium requires that

$$P_{sh} = F_{yf}A_f + F_{ywr}t_w(s_t - 2g) - F_{ys}A_s \tag{4.62}$$

The web-flange crossover occurs when $g = s_t - t_f$. The force in the steel at crossover, P^f_{xh}, is

$$P^f_{xh} = F_{yf}A_f - F_{ywr}t_w\,(s_t - 2t_f) - F_{ys}A_s \tag{4.63}$$

If $P_{sh} > P^f_{xh}$, the neutral axis is in the web at the high moment end (Fig. 4.14a). Therefore,

$$g = \frac{-P_{sh} + F_{yf}A_f + F_{ywr}A_w - F_{ys}A_s}{2F_{ywr}t_w} \qquad (4.64a)$$

If $F_{ywr} = 0$, then

$$g = s_t - t_f \qquad (4.64b)$$

Moment equilibrium requires that

$$M_{th} = F_{yf}A_f(s_t - t_f/2) + \frac{F_{ywr}t_w}{2}(s_t^2 - 2g^2)$$
$$+ F_{ys}A_s y_s + P_{ch}y_{ch} \qquad (4.65)$$

If $P_{sh} < P_{xh}^f$, the neutral axis is in the flange at the high moment end (Fig. 4.14b). The neutral axis location is given by

$$g = \frac{-P_{sh} + F_{yf}(b_f - t_w)(2s_t - t_f) + F_{ywr}A_w - F_{ys}A_s}{2(F_{yf}(b_f - t_w) + F_{ywr}t_w)} \qquad (4.66)$$

and the high moment end secondary moment is

$$M_{th} = \frac{F_{yf}(b_f - t_w)}{2}(2s_t^2 - 2t_f s_f + t_f^2 - 2g^2)$$
$$+ \frac{F_{ywr}t_w}{2}(s_t^2 - 2g^2) - F_{ys}A_s y_s + P_{ch}y_{ch} \qquad (4.67)$$

4.6 DETAILS OF INTERACTION PROCEDURE

The initial step in developing an interaction diagram is to find the shear capacities of the bottom and top tees.

The bottom tee shear strength, $V_b(max)$, is calculated by varying the shear force in the tee (using bisection) until zero normal force exists in the tee.

The top tee shear strength, V_{tm}, is the minimum of the "mechanism" strength, $V_t(max)$, and the "pure shear" strength, $V_t(sh)$. The "mechanism" strength is calculated by varying the shear force in the tee (using bisection) until moment equilibrium, Eq. (4.28c) is satisfied for the tee. Shear is applied to the slab only if the total shear required to satisfy moment equilibrium is greater than V_{pt}. If the concrete forces are too high for moment equilibrium to be satisfied, the high moment end concrete force is incrementally reduced until Eq. (4.28c) is satisfied (The difference between P_{ch} and P_{cl} is maintained using Eq. (4.37)). The "shear" strength is found using Eq. (4.33b).

The total shear strength, V_m, is the sum of $V_b(max)$ and V_{tm}. The interaction diagram is developed by assigning to the opening incrementally larger values of shear from 0 to V_m. As the shear is increased from 0 to 90 percent of V_{tm}, all of the shear is assigned to the top tee (Fig. 4.15). The top tee shear, V_t, is then varied linearly from 90 to 100 percent of V_{tm} [$V_t = qV_{tm}$ $(0.9 \leq q \leq 1.0)$] as the bottom tee shear, V_b, is increased quadratically from 0 to 10 percent of $V_b(max)$.

$$V_b = 0.10V_b(max)(1 - \sqrt{1 - q'}) \qquad (4.68a)$$

in which

$$q' = 100(q - 0.9)^2 \qquad (4.68b)$$

Additional shear is assigned to the bottom tee only (Fig. 4.15). This procedure was selected to provide a good match with test results, as well as a reasonable shape for the interaction diagram. Since the overall method is an equilibrium procedure, the interaction diagrams represent lower bound solutions.

The axial force in the top and bottom tees is governed by the bottom tee. At an assigned value of bottom tee shear, an axial force and secondary bending moments are calculated. An axial force of equal magnitude but opposite direction is applied to the top tee. The top tee shear force is applied, and the high moment end secondary moment is calculated.

The low moment end secondary moment is not calculated at top tee shears lower than V_{tm}. At these shears, the low moment end will not be completely plastic at the maximum high-moment-end secondary moment.

The primary moment at the opening centerline (Eq. (4.1) and Fig. 4.3) is

$$M_{primary} = Pz + M_{th} + M_{bh} - 0.5a_oV_{total} \qquad (4.69)$$

using $z = h_o$.

The shear capacities of the top and bottom tees are calculated at zero axial force. The point of contraflexure in the top tee, however, will not be at the opening centerline. Therefore, $M_{primary}$ will be greater than zero. In order to complete the interaction diagram, a value of total shear must be calculated for zero primary moment. This is done using the procedure used by Clawson and Darwin (10, 11). The top tee shear is held constant at V_{tm}, while the bottom tee shear is decreased slightly. A compressive axial force is then applied to the bottom tee, and a tensile axial force is applied to the top tee such that

$$Ph_o = - M_{th} - M_{bh} + 0.5a_o V_{total} \qquad (4.70)$$

4.7 COMPARISON WITH TEST RESULTS

The model is used to predict the strength of the 15 tests in the current study along with the 22 prior tests. Ratios of test to calculated strength are tabulated in Table 4.1. Interaction curves for the model are compared with the test data from the current tests in Figs. 4.16 to 4.30.

The interaction curves are calculated using the material strengths, beam geometries, and shear stud quantities summarized in Chapter 2 and Appendix B. The experimental web, flange, and stiffener yield strengths are used in the calculations.

For the beams with solid slabs tested by Clawson and Darwin (9, 11), the calculations indicate that the stud capacities are limited

by the tensile strength of the shear connectors (Eq. (4.41)). For these calculations, a strength of 60 ksi (a typical industry minimum) is used, since the actual strengths are not known. It is important to note that no stud failures were observed in any of the tests.

In addition to the individual comparisons, Table 4.1 includes the means and standard deviations of the test/theory ratios for each test series, for each slab type (ribbed or solid), and for all of the tests. The ratios for Tests 4A and 4B for the current series are not included in these calculations. These tests had no shear connectors above the opening, but did have puddle welds in each rib. It was found that the puddle welds in the ribs above the openings transferred significant shear between the top tee steel and the slab. Since the tabulated ratios for Tests 4A and 4B are based on zero shear transfer above the openings, they do not provide a fair measure of model accuracy.

The interaction diagrams emphasize a point that has been made before (9, 10, 14); that is, the interaction between moment and shear capacity at a web opening is rather weak. The moment capacity at a web opening is largely unaffected by shear until the shear reaches the maximum shear capacity.

The strength model provides exceptionally good agreement with the experimental results. For beams with ribbed slabs, the mean and standard deviation are 1.023 and 0.070, respectively. For beams with solid slabs, the mean and standard deviation are 1.074 and 0.060,

respectively. The overall mean and standard deviation for the model are 1.042 and 0.071.

The lowest individual test/theory ratio is 0.904 (Test R0). In addition to Test R0, Test 1 has a particularly low test/theory ratio (0.919). For both tests, the deviation may be the result of the load history of the tests. Both tests were loaded above initial yield, unloaded, and then reloaded to failure. In the initial cycle, significant twisting of the beams was noted. In the model, however, cyclic effects and out of plane bending are not considered.

Tests 8A, 8B, and 9A also have relatively low test/theory ratios. These tests had relatively stiff slabs and had a low number of studs over the opening. The stiff slabs tended to pull away from the steel tees, resulting in bridging of the slab. As a result of the bridging, the failure point in the concrete slab was close to the to the load point, while the model assumes failure at the high moment end of the opening. Also, the studs over the opening may have failed primarily in tension, rather than in shear. The model does not include provisions for interaction between tension and shear in the studs above the opening.

In general, tests with solid slabs have high test/theory ratios. In the tests conducted by Clawson and Darwin (9, 11), no stud failures were noted. The stud forces used in the model, however, are limited by the assumed tensile capacities of the studs. It is likely that the studs had higher tensile capacities than the assumed capacities.

Tests 3, R3, R4, and C3 had high M/V ratios. Three of these tests, R3, R4, and C3 failed at relatively high test/theory ratios. This is probably the result of the representation of the steel in the tees. In tests with high M/V ratios, the steel sections were subjected to high tensile strains (well over 2 percent). The steel was, therefore, in the strain hardening range. The model, however, has no provisions for strain hardening. The effect of strain hardening in high shear tests will be lower, because of the high strain gradients in the steel tees. Test 3 had a relatively low test/theory ratio when compared with the other tests with high M/V ratios. This may be the result of cyclic loading during the test. Test 3 was loaded above initial yield, unloaded, and reloaded to failure (The initial cycle was terminated to allow adjustment of the load system).

The following chapter presents practical design techniques that were developed based on lessons learned with the model. The model results are compared with the results obtained with the practical design techniques, as well as with the Redwood and Poumbouras (33) analysis procedure.

CHAPTER 5

STRENGTH DESIGN PROCEDURES

5.1 GENERAL

While the strength model presented in Chapter 4 provides good agreement with test results, it is not well suited for design. The "mechanism" shear capacity must be found by iteration, and the interaction diagram is calculated "point by point". Therefore, the model requires the use of a computer. A useful design procedure should require no more than a programmable calculator.

A number of design procedures for composite beams with unreinforced openings have been proposed (11, 33, 34). In all cases, the maximum moment capacity is found using the standard strength procedures developed by Slutter and Driscoll (35). The procedures differ in the methods used to find the maximum shear capacity at the opening and the methods used to construct moment-shear interaction curves.

The methods used to establish the maximum shear capacity are based on local moment equilibrium (11, 33, 34). A four hinge mechanism is assumed at the opening, and moment equilibrium is enforced for the bottom and top tees. The methods differ in the simplifying assumptions used to reduce the complexity of the calculations and in the forces assumed in the concrete slab. The methods also differ in the limiting shear at the opening corresponding to a "pure" shear failure.

Clawson and Darwin (11) have proposed a design procedure which enforces local equilibrium but which requires iteration. In the top tee, the concrete is assumed to crush at the high moment end and to be fully cracked at the low moment end. The shear capacity is limited by the pure shear capacities of the webs and the concrete. The moment-shear interaction diagram is obtained by connecting the maximum shear and moment capacities with an ellipse. Clawson and Darwin (11) show that the design procedure provides reasonable agreement with the results of tests of composite beams with solid slabs. Redwood and Wong (34) show that the procedure also gives reasonable agreement with the results of tests on composite beams with ribbed slabs. Because the procedure requires iteration, however, any practical application to design requires the use of a computer.

Redwood and Wong (34) have proposed a procedure which does not enforce local equilibrium. The flange thicknesses are assumed to be small relative to the depths of the tee section webs above and below the opening. Equilibrium of normal forces in the tees is not enforced. The concrete force at the high moment end is limited by the shear capacity of the stud connectors above the opening. Zero force is assumed in the concrete at the low moment end. A closed form solution is obtained. The shear capacity is limited by the pure shear capacity of the top tee and bottom tee webs.

The maximum shear and the maximum moment that can be sustained at the maximum shear are calculated, generating a vertical line on the right side of the interaction curve. The curve is closed with an

ellipse between the maximum moment at zero shear (found considering partial composite action) and the maximum moment at the maximum shear. Because the interaction curve is not continuous, calculation of the capacity for a given M/V ratio is somewhat cumbersome. The procedure is very conservative for openings with low M/V ratios in beams with either solid or ribbed slabs. The Redwood and Wong procedure has been used by U.S. Steel (44) as the basis of a design aid.

Redwood and Poumbouras (33) have proposed a modification of Redwood and Wong's procedure which provides a good match with test results on composite beams with ribbed slabs. The method includes provision for a compressive force in the concrete at the low moment end of the opening, which is set equal to the total shear connector capacity between the opening and the support.

The interaction curve is similar to the curve used by Redwood and Wong. The maximum shear and the maximum moment that can be sustained at the maximum shear are calculated, generating a vertical line on the right side of the interaction curve. The curve is closed with an ellipse between the maximum moment at zero shear (assuming full composite action) and the maximum moment at the maximum shear. The maximum moment at zero shear (considering partial composite action) is calculated, generating a horizontal line between zero shear and the interaction curve. The calculation of the capacity for a given M/V ratio is, therefore, even more cumbersome than for the Redwood and Wong procedure.

The Redwood and Poumbouras procedure is the most accurate of the three existing procedures for beams with ribbed slabs. However, it is very conservative at high shears for beams with solid slabs.

The existing design procedures have limitations. While the Clawson and Darwin procedure can produce good agreement with test results for beams with solid or ribbed slabs, it requires the use of a computer. The procedures proposed by Redwood and others are easier to apply, but they are very conservative when applied to solid slab construction. There is, therefore, a need for comprehensive design procedures which give consistent agreement with test results and are easily applied.

5.2 OVERVIEW OF DESIGN PROCEDURES

Three design procedures are presented which allow the rapid construction of moment-shear interaction diagrams for composite beams. The proposed methods require the calculation of the maximum moment capacity, M_m, and the maximum shear capacity, V_m, at a web opening in a composite beam. The calculation of these points and the application of an interaction equation are discussed in the following sections.

The procedures are based on the following assumptions:

1) The steel will yield in tension or compression.
2) Shear forces can be carried in the steel and concrete at both ends of the opening.
3) Shear forces in the steel are carried only in the webs.

4) Shear stresses are uniformly distributed over the stub depth.

5) The normal forces in the concrete are applied over an area defined by the equivalent stress block (1).

Fig. 5.1 illustrates openings in composite beams with a solid slab, a ribbed slab with the ribs transverse to the beam, and a ribbed slab with the ribs parallel to the beam. The openings are of length a_o and depth h_o and may have an eccentricity e (positive upward) with respect to the centerline of the steel section. The slab thicknesses, T_s and t_s, effective slab width, b_e, and steel section dimensions, d, b_f, t_f, t_w, s_t, and s_b, are as shown.

5.3 INTERACTION CURVE

Once M_m and V_m have been obtained, intermediate values of shear and moment are obtained using an interaction curve of the form

$$\left(\frac{M_n}{M_m}\right)^3 + \left(\frac{V_n}{V_m}\right)^3 = 1 \qquad (5.1)$$

in which V_n = the nominal shear capacity and M_n = the nominal moment capacity at a web opening in a composite beam (Fig. 5.2). The nominal capacities can be determined for a given ratio of moment to shear, M/V, as follows. From Eq. (5.1),

$$\left(\frac{M_n}{M_m}\right)^3 \left(\frac{V_m}{V_n}\right)^3 + 1 = \left(\frac{V_m}{V_n}\right)^3 \qquad (5.2)$$

Letting $M_n/V_n = M/V$ and solving for V_n yields

$$V_n = V_m \left[\frac{(\frac{M}{V})^3}{(\frac{M_m}{V_m})^3} + 1 \right]^{-1/3} \tag{5.3}$$

and

$$M_n = V_n(\frac{M}{V}) \tag{5.4}$$

$$= M_m \left[\frac{(\frac{M_m}{V_m})^3}{(\frac{M}{V})^3} + 1 \right]^{-1/3} \tag{5.5}$$

The complete interaction curve is described by a single function. This is conceptually sound since the interaction between moment and shear should be continuous. It also allows a single equation to be used to calculate the nominal shear capacity at a given M/V ratio. Thus, the application of the procedure is simple. As will be shown, Eq. (5.1) provides good agreement with test results.

5.4 MAXIMUM MOMENT CAPACITY

The maximum moment capacity, M_m, of a composite beam at a web opening is obtained using the strength procedures developed by Slutter and Driscoll (35). Fig. 5.3 illustrates stress diagrams for sections in pure bending. The steel section is assumed to be fully plastic in both tension and compression, while the compressive force

in the concrete, P_{ch}, is limited by 1) the crushing capacity of the slab, P_c, 2) the shear capacity of the stud connectors between the high moment end of the opening and the support, P_{studs}, and 3) the yield capacity of the net steel section, T'.

$$P_{ch} \leq P_c \tag{5.6a}$$

$$\leq P_{studs} \tag{5.6b}$$

$$\leq T' \tag{5.6c}$$

The concrete stress is assumed to be at $0.85f'_c$ over the depth of the equivalent stress block.

The crushing capacity of the slab is

$$P_c = 0.85f'_c b_e t_e \tag{5.7}$$

in which f'_c = the compressive strength of the concrete in ksi, b_e = the effective slab width (2), and t_e = the effective slab thickness. t_e is dependent on the type of slab. For ribbed slabs with the ribs perpendicular to the beam,

$$t_e = t_s = \text{the minimum slab thickness} \tag{5.8a}$$

For ribbed slabs with the ribs parallel to the beam,

$$t_e = \frac{T_s + t_s}{2} \qquad (5.8b)$$

= the average of the maximum and minimum slab thicknesses.

For solid slabs,

$$t_e = T_s = \text{the slab thickness.} \qquad (5.8c)$$

The shear capacity of the stud connectors is

$$P_{studs} = NRQ_n \qquad (5.9)$$

in which N = the number of studs between the high moment end of the opening and the support, R = the reduction factor for studs in ribbed slabs, and Q_n = the nominal strength of one stud shear connector embedded in a solid slab (3, 29).

For slabs with transverse ribs, R is (2, 3, 20)

$$R = \frac{.85}{\sqrt{N_r}}\left(\frac{w_r}{h_r}\right)\left(\frac{H_s}{h_r} - 1.0\right) \leq 1.0 \qquad (5.10a)$$

in which h_r = the nominal rib height in inches, H_s = the length of the stud connector after welding in inches, N_r = the number of stud

connectors in one rib, and w_r = the average width of the concrete rib.

For slabs with ribs parallel to the steel beam, the reduction factor is (2, 3, 20)

$$R = .6\left(\frac{w_r}{h_r}\right)\left(\frac{H_s}{h_r} - 1.0\right) \leq 1.0 \qquad (5.10b)$$

For solid slab construction, R = 1.0.

Q_n is given by

$$Q_n = 0.5A_{sc}\sqrt{f'_c E_c} \qquad (5.11a)$$

in which A_{sc} = the cross-sectional area of a stud shear connector, f'_c = the compressive strength of the concrete in ksi, E_c = the modulus of elasticity of the concrete in ksi and is given by

$$E_c = 57\sqrt{f'_c} \quad ; \; f'_c \text{ in psi} \qquad (5.11b)$$

The product RQ_n is limited such that

$$RQ_n \leq A_{sc}F_u \qquad (5.12)$$

in which F_u = the minimum tensile strength of a stud in ksi (2, 3, 29).

Under pure bending, the shear is zero; therefore, the web yield strength is not reduced. The yield capacity of the net steel section is

$$T' = F_y\left(2(b_f - t_w)t_f + s_t t_w + s_b t_w\right) \tag{5.13}$$

in which F_y = the yield strength of the section, b_f = the flange width, t_w = the web thickness, t_f = the flange thickness, s_t = the top tee stub depth, and s_b = the bottom tee stub depth (Fig. 5.1).

For solid slabs or for ribbed slabs with transverse ribs, the depth of the stress block is

$$\bar{a} = \frac{P_{ch}}{0.85f'_c b_e} \tag{5.14}$$

P_{ch} acts at a distance d_h from the top of the flange.

$$d_h = T_s - \bar{a}/2 \tag{5.15}$$

For ribbed slabs with longitudinal ribs, Eq. (5.15) will hold if $\bar{a} \leq t_s$. If $\bar{a} > t_s$, d_h must be calculated by considering the concrete below the top of the steel deck.

The expression used to calculate M_m depends on which of the inequalities in Eq. (5.6) governs. If $P_{ch} = T'$ (Eq. (5.6c) and Fig. 5.3(a)), the maximum moment capacity is

$$M_m = P_{ch}d_h + F_y(b_f - t_w)t_f d + F_y t_w \left(\frac{s_t^2 - s_b^2}{2} + s_b d\right) \quad (5.16)$$

If $P_{ch} < T'$ (Eq. (5.6a) and (5.6b)), the neutral axis will be in the steel tee. The compressive force in the steel is

$$C' = \frac{T' - P_{ch}}{2} \quad (5.17)$$

The neutral axis location in the top tee, x, is measured from the top of the steel section. If $C' \leq F_y b_f t_f$ (Fig. 5.3(b)), $x < t_f$ and is given by

$$x = \frac{C'}{F_y b_f} \quad (5.18)$$

and

$$M_m = P_{ch}d_h + F_y(b_f - t_w)(t_f d - x^2) + F_y t_w\left(\frac{s_t^2 - s_b^2}{2} + s_b d - x^2\right) \quad (5.19)$$

If $C' > F_y b_f t_f$ (Fig. 5.3(c)), $x > t_f$ and is given by

$$x = \frac{C'}{F_y t_w} - \frac{(b_f - t_w)t_f}{t_w} \quad (5.20)$$

and

$$M_m = P_{ch} d_h + F_y(b_f - t_w)(t_f d - t_f^2)$$

$$+ F_y t_w\left(\frac{s_t^2 - s_b^2}{2} + s_b d - x^2\right) \qquad (5.21)$$

5.5 MAXIMUM SHEAR CAPACITY

All current strength procedures for composite beams with web openings use a "mechanism" failure mode as one of the limits for the shear capacity (11, 33, 34). The "mechanism" mode is based on the formation of plastic hinges at both ends of the top and the bottom tees. Shear and normal stresses in the steel are limited by the von Mises yield criterion. Normal stresses in the concrete are limited to $0.85f'_c$.

A closed-form solution for the maximum shear capacity at a web opening requires the use of one or more simplifying assumptions. Some of these simplifications are:

1) Using simplified versions of more detailed material models,
2) Limiting the neutral axes locations in the steel tees to a specified range, and
3) Ignoring local equilibrium within the tees.

Three procedures for estimating the maximum shear capacity are presented in the following sections. Each procedure uses one or more simplifications. The three procedures share a common basis.

V_m is found by assuming that

$$P_t = P_b = P = 0 \qquad (5.22)$$

in which P_t = the top tee force and P_b = the bottom tee force at the opening (Fig. 5.4). This approximates zero moment at the centerline of the opening. The moment is not exactly zero because the secondary bending moments in the top tee, M_{th} and M_{tl}, are not equal. Therefore, while the primary moment (= Pz) is zero, the total moment at the centerline of the opening has a small but finite value.

The normal forces in the concrete at the ends of the opening, P_{ch} and P_{cl}, are limited by the shear stud capacities between the ends and the nearest support. The high moment end force, P_{ch}, is located near the top of the slab, and the low moment end concrete force, P_{cl}, is located near the bottom of the slab (Fig. 5.5). This assumption is also used by Redwood and Poumbouras (33). It agrees with test observations and, for given values of P_{ch} and P_{cl}, maximizes the calculated shear at a web opening. Normal stresses in the concrete are fixed at $0.85f'_c$, and are represented using the equivalent stress block. The effect of shear stress on the normal stresses in the concrete is ignored.

The maximum force in the concrete at the high moment end of the opening is

$$P_{ch} \leq P_c \qquad (5.23a)$$

$$\leq P_{studs} \qquad (5.23b)$$

in which P_c and P_{studs} are given by Eq. (5.7) and Eq. (5.9), respectively.

The force in the concrete at the low moment end of the opening is

$$P_{cl} = P_{ch} - N_o R Q_n \geq 0 \tag{5.24}$$

in which N_o = the number of shear studs over the opening. R and Q_n are given in Eq. (5.9)-(5.12).

P_{ch} acts at a distance d_h from the top of the flange. d_h is given by Eq. (5.14). P_{cl} acts at a distance d_l from the top of the flange. For slabs with transverse ribs, d_l is given by

$$d_l = T_s - t_s + \frac{0.5P_{cl}}{0.85f'_c\, b_e} \tag{5.25a}$$

For solid slabs, d_l is given by

$$d_l = \frac{0.5P_{cl}}{0.85f'_c\, b_e} \tag{5.25b}$$

For slabs with longitudinal ribs, d_l is the distance to the centroid of the concrete force in the trapezoidal ribs within b_e (Fig. 5.1).

In the top tee, all of the shear is assumed to be applied to the web if the applied shear is less than or equal to the plastic shear capacity of the web, V_{pt}. The concrete carries any shear in excess of V_{pt}. For the top tee,

$$V_{pt} = s_t t_w F_y/\sqrt{3} \tag{5.26}$$

The upper bound of the shear that can be applied to the top tee is the "pure shear" capacity for the top tee, $V_t(sh)$.

$$V_t(sh) = \frac{3.5\sqrt{f'_c}\, A_{cv}}{1000} + V_{pt} \text{ , kips} \qquad (5.27)$$

in which $A_{cv} = 3T_s t_e$ and t_e is given by Eq. (5.8).

In the bottom tee all of the shear is assumed to be carried by the web.

5.5.1 Maximum Shear Capacity - Method I

Fig. 5.5 illustrates the stress distributions at the opening for a mechanism failure. The steel section is assumed to be fully plastic in both tension and compression. In both the top and bottom steel tees, the neutral axis is assumed to be in the flange. The flange yield strength, F_{yf}, is not reduced for shear, since the shear is assumed to be carried by the web. The web yield strength, F_{ywr}, is reduced for shear. F_{ywr} is obtained using a linear approximation of the von Mises criterion (Fig. 5.6). Normal force equilibrium is enforced in the top tee steel, but equilibrium is not necessarily enforced at the concrete-steel interface.

The von Mises criterion (Eq. (4.2)) is

$$\sigma_x^2 + 3\tau_{xy}^2 = \sigma_o^2 \qquad (5.28a)$$

A dimensionless form of the von Mises surface, $f(x)$, $x = \sigma_x/\sigma_o$, is given by

$$f(x) = \left(\frac{\tau_{xy}}{\sigma_o}\right) = \frac{1}{\sqrt{3}} \left(1 - \left(\frac{\sigma_x}{\sigma_o}\right)^2\right)^{1/2} \tag{5.28b}$$

$f(x)$ is quadratic. Several methods can be used to approximate $f(x)$ with a straight line, including least squares, near minimax, and minimax approximations (12). The minimax approximation (also known as the best uniform approximation) provides a line, $p(x)$, that is the same distance from $f(x)$ at three locations for $0 \leq x \leq 1$. The distance has alternate changes of sign in this interval (Fig. 5.6). $p(x)$ minimizes the norm, $||f - p||_\infty$, given by

$$||f - p||_\infty = \max_{0 \leq x \leq 1} |f(x) - p(x)| \tag{5.29}$$

In this case, $p(x)$ is given by

$$p(x) = \left(\frac{\tau_{xy}}{\sigma_o}\right) = .69692 - \frac{1}{\sqrt{3}} \left(\frac{\sigma_x}{\sigma_o}\right) \tag{5.30}$$

for which the norm on the interval $0 \leq x \leq 1$ is

$$||f - p||_\infty = 0.11957 \tag{5.31}$$

f(x) and p(x) are illustrated in Fig. 5.6. Eq. (5.30) can also be expressed as

$$\sigma_x = \lambda\sigma_o = \sqrt{3}\tau_{xy} \tag{5.32a}$$

in which $\lambda = 1.207$.

Therefore, the reduced yield strength for the web due to shear, F_{ywr}, is

$$F_{ywr} = \lambda F_{yw} - \sqrt{3}\tau_{xy} \tag{5.32b}$$

in which F_{yw} = the yield strength of the web in uniaxial tension.

Eq. (5.28) limits τ_{xy} such that

$$\tau_{xy} \leq \sigma_o/\sqrt{3} = 0.58\sigma_o \tag{5.33}$$

compared to a maximum of $0.70\sigma_o$ in Eq. (5.32). Eq. (5.33) is used as an upper bound on the application of Eq. (5.32), at the limit $F_{ywr} = 0$ (Fig. 5.6).

Since V_m is found by assuming that $P_t = 0$, normal force equilibrium between the steel tee and the slab requires that, in addition to the restrictions placed on P_{ch} by Eq. (5.23),

$$P_{ch} \leq P_{smax} \tag{5.34a}$$

in which P_{smax} = the tensile capacity of the top tee.

$$P_{smax} = F_y t_f (b_f - t_w) + F_y t_w s_t \tag{5.34b}$$

It should be noted that the effect of shear stress on the normal stress in the web is not included in P_{smax}.

5.5.1.1 Bottom Tee

The shear capacity of the bottom tee is obtained by finding the plastic moment and shear force that satisfy moment equilibrium for the bottom tee (Eq. (4.4c)).

$$V_b a_o = M_{bl} + M_{bh} \tag{5.35}$$

in which V_b = the bottom tee shear, M_{bl} = the secondary moment at the low moment end of the opening, and M_{bh} = the secondary moment at the high moment end of the opening. When $P_b = 0$,

$$M_{bl} = M_{bh} = M_b \tag{5.36}$$

and

$$V_b a_o = 2M_b \tag{5.37}$$

in which M_b = the secondary moment at each end of the opening.

The neutral axis location is assumed to be in the flange, at a distance, g, from the bottom of the flange (Fig. 5.5). Normal force equilibrium ($P_b = 0$) results in

$$g = \frac{F_{yf}(b_f - t_w)t_f + F_{ywr}t_w s_b}{2(F_{yf}(b_f - t_w) + F_{ywr}t_w)} \tag{5.38}$$

in which F_{yf} = the yield strength of the flange, b_f = the flange width, t_w = the web thickness, s_b = the bottom tee stub depth, and t_f = the flange thickness. Moment equilibrium requires that

$$V_b a_o = 2F_{yf}(b_f - t_w)(\frac{t_f^2}{2} - g^2) + 2F_{ywr}t_w(\frac{s_b^2}{2} - g^2) \tag{5.39}$$

Substituting for g in Eq. (5.39) gives

$$F_{yf}^2(b_f - t_w)^2 t_f^2 + 2F_{yf}F_{ywr}t_w(b_f - t_w)(s_b^2 - s_b t_f + t_f^2) + F_{ywr}^2 t_w^2 s_b^2 = 2V_b a_o(F_{yf}(b_f - t_w) + F_{ywr}t_w) \tag{5.40}$$

For design purposes, $F_{yf} = F_{yw} = F_y$, the specified yield strength of the section. Using $\tau_{xy} = V_b/(s_b t_w)$ and substituting Eq. (5.33) for F_{ywr} in Eq. (5.40) gives

$$V_b(max) = F_y\left(\frac{\beta - \sqrt{\beta^2 - 4\alpha\gamma}}{2\alpha}\right) \qquad (5.41)$$

in which $\alpha = 3 + 2\sqrt{3}\,\frac{a_o}{s_b}$

$$\beta = 2\sqrt{3}\,\frac{(b_f - t_w)}{s_b}\,(s_b^2 - s_b t_f + t_f^2) + 2\sqrt{3}\lambda t_w s_b + 2a_o\left((b_f - t_w) + \lambda t_w\right)$$

$$\gamma = (b_f - t_w)^2 t_f^2 + \lambda^2 t_w^2 s_b^2 + 2\lambda t_w (b_f - t_w)(s_b^2 - s_b t_f + t_f^2)$$

and $\lambda = 1.207.$

5.5.1.2 Top Tee

The shear capacity of the top tee is governed by the smaller of the "shear" and "mechanism" failure loads.

The "mechanism" capacity of the top tee is found by satisfying moment equilibrium for the top tee (Eq. (4.28c)).

$$V_t a_o = M_{th} + M_{tl} \qquad (5.42)$$

in which V_t = the top tee shear (Fig. 5.5).

The neutral axes in the steel tees are assumed to be in the flange at both ends of the opening. An analysis of the openings in Chapter 4 shows that this is by far the most common case. Because force is transferred from the concrete to the steel by the studs over

the opening, the neutral axes locations in the steel are not necessarily the same at both ends of the opening (Fig. 5.5).

The neutral axis locations, g_h at the high moment end and g_l at the low moment end, are measured from the top of the flange (Fig. 5.5). Based on normal force equilibrium,

$$g_h = \frac{-P_{ch} + F_{yf}(b_f - t_w)t_f + F_{ywr}t_w s_t}{2(F_{yf}(b_f - t_w) + F_{ywr}t_w)} \qquad (5.43a)$$

and

$$g_l = \frac{P_{cl} + F_{yf}(b_f - t_w)t_f + F_{ywr}t_w s_t}{2(F_{yf}(b_f - t_w) + F_{ywr}t_w)} \qquad (5.44b)$$

Moment equilibrium requires that

$$\begin{aligned} V_t a_o = {} & P_{ch}d_h - P_{cl}d_l - F_{yf}(b_f - t_w)\left(\frac{g_h^2 + g_l^2}{2}\right) \\ & - F_{ywr}t_w\left(\frac{g_h^2 + g_l^2}{2}\right) + F_{yf}(b_f - t_w)(t_f - g_h)\left(g_h + \frac{t_f - g_h}{2}\right) \\ & + F_{yf}(b_f - t_w)(t_f - g_l)\left(g_l + \frac{t_f - g_l}{2}\right) \\ & + F_{ywr}t_w(s_t - g_h)\left(g_h + \frac{s_t - g_h}{2}\right) \\ & + F_{ywr}t_w(s_t - g_l)\left(g_l - \frac{s_t - g_l}{2}\right) \end{aligned} \qquad (5.45)$$

in which V_t = the total top tee shear.

Substitution for g_h and g_l and consolidation of terms gives

$$4F_{yf}(b_f - t_w)(P_{ch}d_h - P_{cl}d_l) + F_{ywr}(4t_w(P_{ch}d_h - P_{cl}d_l))$$
$$- P_{ch}^2 - P_{cl}^2 + 2F_{yf}(b_f - t_w)t_f(P_{ch} - P_{cl})$$
$$+ F_{ywr}(2t_w s_t(P_{ch} - P_{cl})) - 4F_{ywr}F_{yf}(b_f - t_w)t_f t_w s_t$$
$$+ 2F_{yf}^2(b_f - t_w)^2 t_f^2 + F_{ywr}^2(2t_w^2 s_t^2)$$
$$+ 4F_{ywr}F_{yf}(b_f - t_w)t_w(s_t^2 + t_f^2)$$
$$= 4V_t a_o(F_{yf}(b_f - t_w) + F_{ywr}t_w) \qquad (5.46)$$

Again, for design purposes, $F_y = F_{yf} = F_{yw}$.

The top tee steel is assumed to carry all of V_t unless the top tee capacity exceeds V_{pt} (Eq. 5.26). Using $\tau_{xy} = V_t/(s_t t_w)$, substituting Eq. (5.32b) for F_{ywr}, and using $V_t(\max) = V_t$:

$$V_t(\max) = F_y\left(\frac{\beta - \sqrt{\beta^2 - 4\alpha\gamma}}{2\alpha}\right) \qquad (5.47)$$

in which $\alpha = 3 + 2\sqrt{3}\,\frac{a_o}{s_t}$

$$\beta = 2\sqrt{3}\,\frac{(b_f - t_w)}{s_t}(s_t^2 - s_t t_f + t_f^2) + 2\sqrt{3}\,\lambda t_w s_t$$
$$+ 2a_o\left((b_f - t_w) + \lambda t_w\right) + \frac{2\sqrt{3}}{s_t F_y}(P_{ch}d_h - P_{cl}d_l)$$

$$+ \frac{\sqrt{3}}{F_y}(P_{ch} - P_{cl})$$

$$\Upsilon = (b_f - t_w)^2 t_f^2 + \lambda^2 t_w^2 s_t^2$$

$$+ 2\lambda(b_f - t_w)t_w(s_t^2 - s_t t_f + t_f^2)$$

$$+ \frac{2((b_f - t_w) + \lambda t_w)}{F_y}(P_{ch}d_h - P_{cl}d_l)$$

$$- \frac{(P_{ch}^2 + P_{cl}^2)}{2F_y^2} + \frac{((b_f - t_w)t_f + \lambda t_w s_t)}{F_y}(P_{ch} - P_{cl})$$

and $\lambda = 1.207.$

If $V_t(max) \geq V_{pt}$, then F_{ywr} reduces to zero in Eq. (5.46). Thus, the normal force in the web reduces to zero. Normal force equilibrium requires that

$$P_{ch} \leq F_y t_f (b_f - t_w) \tag{5.48}$$

If Eq. (5.48) controls, instead of Eq. (5.23), a new value of P_{cl} must be calculated using Eq. (5.24). For $F_{ywr} = 0$, $V_t(max)$ is given by

$$V_t(max) = \frac{(P_{ch}d_h - P_{cl}d_l)}{a_o} + \frac{t_f(P_{ch} - P_{cl})}{2a_o}$$

$$+ \frac{F_{yf}t_f^2(b_f - t_w)}{4a_o} - \frac{(P_{ch}^2 + P_{cl}^2)}{4a_o F_{yf}(b_f - t_w)} \geq V_{pt} \tag{5.49}$$

5.5.1.3 Total Shear Capacity

The total shear capacity, V_m, is found by adding the bottom tee shear strength, $V_b(max)$, and the smaller of the top tee strengths, $V_t(sh)$ or $V_t(max)$.

5.5.2 Maximum Shear Capacity - Method II

This procedure recognizes that the flange thicknesses in the top and bottom tees are small relative to the stub depths. Thus, the contribution of the normal stresses in the flanges to the secondary moments will be small if the moments are calculated about the extreme fibers of the flanges. Flange stresses are, therefore, not used to calculate the secondary moments, and the normal and shear stresses in the web are assumed to be uniform, to extend through the stub depth (Fig. 5.7), and to be limited using the von Mises yield criterion (Eq. (5.28a)).

It should be noted that P_{ch} is not limited by Eq. (5.34), as with Method I. Application of Eq (5.34) to Method II is inconsistent with the simplified representation used for the steel tees and produces unconservative results.

Although the approach used here is different from that used by Redwood and Poumbouras, the bottom and top tee "mechanism" capacities are identical to the capacities obtained by Redwood and Poumbouras (33) for cases in which $V_t(max) < V_{pt}$.

5.5.2.1 Bottom Tee Shear Capacity

The normal stress distributions in the bottom tee are shown in Fig. 5.7. The reduced yield strength in the web, F_{ywr}, and the shear stress in the web, τ_b, are related by the von Mises yield criterion (Eq. (5.28a)).

$$F_{ywr}^2 + 3\tau_{xy}^2 = F_{yw}^2 \tag{5.50}$$

with $\tau_b = \tau_{xy}$.

The normal force in the bottom tee web is

$$P_{wb} = s_b t_w F_{ywr} \tag{5.51}$$

The shear force in the bottom tee web is

$$V_b = s_b t_w \tau_b \tag{5.52}$$

From Eq. (5.50), the maximum shear stress in the bottom tee is

$$\tau_{pb} = F_{yw}/\sqrt{3} \tag{5.53}$$

Substituting τ_{pb} for τ_{xy} in Eq. (5.50), the plastic shear capacity of the bottom tee, V_{pb}, is obtained

$$V_{pb} = s_b t_w F_{yw}/\sqrt{3} \tag{5.54}$$

Expressing F_{ywr}, τ_b, and F_{yw} in Eq. (5.54) in terms of P_{wb}, V_b, and V_{pb} allows the normal force in the web to be expressed as follows.

$$P_{wb} = \sqrt{3V_{pb}^2 + 3V_b^2} \tag{5.55}$$

P_{wb} acts at a distance $s_b/2$ from the bottom of the tee at each end of the opening. Therefore, taking moments about the bottom of the flange, moment equilibrium of the bottom tee will require that

$$V_b a_o = P_{wb}(s_b/2) + P_{wb}(s_b/2) \tag{5.56}$$

The bottom tee shear capacity in terms of the normal force is

$$V_b = \frac{P_{wb}\, s_b}{a_o} \tag{5.57}$$

Substituting Eq. (5.55) into Eq. (5.57) gives

$$V_b^2 = \frac{(3V_{pb}^2 - 3V_b^2)}{a_o^2}\, s_b^2 \tag{5.58}$$

The maximum shear capacity of the bottom tee is found by solving Eq. (5.58) for V_b.

$$V_b(max) = V_{pb}\sqrt{\alpha_b/(1 + \alpha_b)} \tag{5.59}$$

in which $\alpha_b = 3(s_b^2/a_o^2)$. Eq. (5.59) is identical to the expression for the bottom tee capacity developed by Redwood and Wong (34) and Redwood and Poumbouras (33).

5.5.2.2 Top Tee Shear Capacity

The top tee capacity is found in much the same manner as the bottom tee capacity. The forces in the concrete, P_{ch} and P_{cl}, only slightly complicate the derivation.

The normal stress distributions for the top tee are shown in Fig. 5.7. The reduced yield strength in the web, F_{ywr}, and the shear stress in the web, τ_t, are related by Eq. (5.50) with $\tau_t = \tau_{xy}$.

The normal force in the top tee web is

$$P_{wt} = s_t t_w F_{ywr} \tag{5.60}$$

The shear force in the top tee is

$$V_t = s_t t_w \tau_t \tag{5.61}$$

maximum top tee shear that can be calculated using Eq. (5.68) is $V_t(max) = V_{pt}$, when $\mu = \nu$. Therefore, when $\mu > \nu$, the steel is fully yielding in shear and $P_{wt} = 0$. In this case, $V_t(max)$ is given by

$$V_t(max) = \frac{(P_{ch}d_h - P_{cl}d_l)}{a_o} \geq V_{pt} \qquad (5.70)$$

Normal force equilibrium may require that P_{ch}, P_{cl}, d_h, and d_l be recalculated using Eq. (5.48), (5.24), (5.14), and (5.25), respectively, before applying Eq. (5.70).

It is of interest to note that Eq. (5.70) is equivalent to the first term of Eq. (5.49) in Method I.

5.5.2.3 Total Shear Capacity

The total shear capacity, V_m, is found by adding the bottom tee shear strength, $V_b(max)$, and the smaller of the top tee strengths, $V_t(sh)$ or $V_t(max)$.

5.5.3 Maximum Shear Capacity - Method III

This procedure follows the derivation for Method II, but uses the linear approximation to the von Mises yield surface of Method I (Eq. (5.32)) in place of Eq. (5.50). This procedure allows linear equations for the bottom and top tee shear capacities to be developed.

5.5.3.1 Bottom Tee Capacity

Using the linear approximation to the von Mises surface, the reduced yield strength for the bottom tee web, F_{ywr}, is given by

$$F_{ywr} = \lambda F_{yw} - \sqrt{3}\tau_{xy} \tag{5.32b}$$

with $\tau_b = \tau_{xy}$. Substituting for F_{ywr}, τ_b, and F_{yw} in terms of P_{wb} (Eq. (5.51)), V_{pb} (Eq. (5.54)), and V_b (Eq. (5.52)), the following expression is obtained

$$P_{wb} = \lambda\sqrt{3}V_{pb} - \sqrt{3}V_b \tag{5.71}$$

Based on moment equilibrium (Eq. (5.56)), the bottom shear tee capacity in terms of P_{wb} is

$$V_b = \frac{P_{wb}s_b}{a_o} \tag{5.57}$$

Substituting Eq. (5.57) into Eq. (5.71) and solving for V_b gives

$$V_b(\max) = \frac{\lambda\sqrt{3}V_{pb}}{(a_o/s_b + \sqrt{3})} \tag{5.72}$$

5.5.3.2 Top Tee Capacity

Using the linear approximation to the von Mises criterion, the normal force in the top tee web, P_{wt}, can be expressed as

$$P_{wt} = \lambda\sqrt{3}V_{pt} - \sqrt{3}V_t \tag{5.73}$$

From moment equilibrium (Eq. (5.42)), the top tee shear capacity is expressed in terms of P_{wt} (using the same notation as Method II) as

$$V_t = \frac{P_{wt}}{\nu} + \frac{\mu V_{pt}}{\nu} \tag{5.66}$$

μ and ν are given in Eq. (5.64) and Eq. (5.65).

$V_t(\max)$ is obtained by substituting Eq. (5.73) into Eq. (5.66) and solving for V_t.

$$V_t(\max) = V_{pt}\left(\frac{(\mu + \lambda\sqrt{3})}{(\nu + \sqrt{3})}\right) \tag{5.74}$$

If $V_t(\max) > V_{pt}$, then the quadratic von Mises criterion will give $F_{ywr} = 0$. Therefore, $P_{wt} = 0$ and as with Method II,

$$V_t(\max) = \frac{(P_{ch}d_h - P_{cl}d_l)}{a_o} \geq V_{pt} \tag{5.70}$$

Normal force equilibrium may require that P_{ch}, P_{cl}, d_h, and d_l be recalculated using Eq. (5.48), (5.24), (5.14), and (5.25), respectively, before applying Eq. (5.70).

5.5.3.3 Total Shear Capacity

The total shear capacity, V_m, is found by adding the bottom tee shear strength, $V_b(max)$, and the smaller of the top tee strengths, $V_t(sh)$ or $V_t(max)$.

5.6 COMPARISON WITH TEST RESULTS

Test strength to calculated strength ratios are tabulated in Table 5.1 for the Redwood and Poumbouras (33) design procedure, the strength model from Chapter 4, and the three design procedures (Methods I, II, and III). The interaction curves for the three design procedures are compared with test data in Figs. 5.8 to 5.10. The data points are found by calculating $V_n(test)/V_m$ and $M_n(test)/M_m$ for each opening.

V_m and M_m are calculated for the model and all design procedures using the material strengths, beam geometries, and shear stud quantities summarized in Chapter 2 (Tables 2.1-2.4) and Appendix B. The web, flange, and (where applicable) stiffener yield strengths are used in all calculations for the strength model and for all moment calculations in the design procedures, including the Redwood and Poumbouras procedure. Only the web yield strengths are used in the shear calculations for the Redwood and Poumbouras design procedure, design Method II, and design Method III, while both the web and

flange yield values are used for design Method I. The expressions for the shear capacity in Method I that include both the web and flange yield strengths are presented in Appendix D.

For the comparisons, the shear stud capacities are calculated using Eq. (5.11) and (5.12) in the strength model and in design Methods I, II, and III. Redwood and Poumbouras do not discuss stud capacity calculations (33), but Redwood and Wong (34) recommend that Eq. (5.11a) be used, with the modulus of elasticity for the concrete given by

$$E_c = 5000\sqrt{f'_c} \quad \text{MPa} \tag{5.71}$$

Eq. (5.71) is therefore used in place of Eq. (5.11b) in Eq. (5.11a) to obtain Q_n, the nominal strength of a shear connector, in the Redwood and Poumbouras procedure. Eq. (5.71) results in stud capacities that are approximately 3 percent greater than those obtained using Eq. (5.11b).

The test/theory ratios shown in Table 5.1 for the McGill University tests differ from those published by Redwood and Poumbouras (33). Redwood and Poumbouras did not publish the stud capacities used in their calculations. Stud capacities based on pushout test results were, however, published elsewhere (32, 34). Using the pushout capacities, the test/theory ratios for the McGill series more closely match, but do not coincide with, the ratios

published by Redwood and Poumbouras (33). The three sets of ratios are compared in Table 5.2.

For the beams with solid slabs tested by Clawson and Darwin (9, 11), the calculations indicate that the stud capacities are limited by the tensile strength of the shear connectors (Eq. (5.12)). For these calculations, a tensile strength of 60 ksi is used, since the actual strengths are not known. This is a typical industry minimum. It is important to note that no stud failures where observed in any of the tests.

Means and standard deviations of test/theory ratios are presented in Table 5.1 for each test series, for each slab type (ribbed or solid), and for all of the tests. The ratios for Tests 4A and 4B are not included in these calculations. These tests had no shear connectors above the opening, but did have puddle welds in each rib. It was found that the puddle welds in the ribs above openings transferred significant shear between the top tee steel and the slab. Since the tabulated ratios for Tests 4A and 4B are based on zero shear transfer above the openings, they do not provide a fair measure of model or design procedure accuracy.

Comparing the results, the strength model provides the best agreement with experimental results. For ribbed slabs and for solid slabs, the strength model has the best (closest to 1.0) mean and the lowest standard deviation of the five procedures considered. For beams with ribbed slabs, the mean and standard deviation are 1.023 and 0.070, respectively. For beams with solid slabs, the mean and

standard deviation are 1.074 and 0.060. The model also has the best overall mean and standard deviation, 1.042 and 0.071.

Of the design procedures, Method I provides the best agreement with test results. Overall, the mean and the standard for the 35 tests is 1.065 and 0.082, respectively. These values compare to the respective values of 1.223 and 0.423 for the Redwood and Poumbouras Method, 1.076 and 0.102 for Method II, and 1.095 and 0.106 for Method III.

On the average, the strength calculated using Method I is greater than the strength calculated using Method II, and the strength calculated using Method II is greater than the strength calculated using Method III. However, this is not the case for deep beams with thin slabs. For Tests 1-7B, (d = 20.63 in. and t_s = 2.0 in.), the strength calculated using Method II is greater than the strength calculated using Method I, while Methods I and III provide roughly equivalent results.

The results of the analyses indicate that, in general, the accuracy of the procedure is a function of the refinement of the assumptions. The most refined procedure is the strength model, with moment and normal force equilibrium enforced for each point on the interaction curve. The strength model provides the best agreement with test results. All of the design procedures are less refined and use empirical interaction curves. The design procedures provide somewhat poorer agreement with the test results than does the model. The most refined of the design procedures is Method I, which enforces

normal force equilibrium in the steel tees. Method I provides better agreement with test results than Method II, Method III, or the Redwood and Poumbouras procedure, which ignore normal force equilibrium in the steel tees.

Design Method II and the Redwood and Poumbouras procedure are similar. They do not, however, produce the same results. In terms of strength, the stud capacities used in the Redwood and Poumbouras procedure are approximately 3 percent higher than the stud capacities used in Method II. This difference has little affect on the results. Of much greater importance, Method II provides a higher upper bound for the shear that can be applied to the top tee by allowing the upper limit to include a concrete component. The shape of the interaction curves used in the two procedures is also different. Design Method II (as with Methods I and III) uses a cubic equation and is easily applied for a given M/V ratio. The Redwood and Poumbouras procedure, however, uses an interaction curve defined by three functions and is somewhat cumbersome to apply.

The results obtained for solid slabs show the largest difference between Method II and the Redwood and Poumbouras procedure. The difference is primarily the result of the higher upper bound for the top tee shear capacity that can be obtained with Method II. Method II has a mean of 1.129 and a standard deviation of 0.102 for solid slabs. The Redwood and Poumbouras procedure has a mean of 1.499 and a standard deviation of 0.596.

5.7 RECOMMENDATIONS

Methods I, II, and III provide reasonable agreement with test results and can be applied using a calculator.

Comparing the first two methods, Method I provides a better agreement with test results, while Method II is slightly simpler to implement. Both methods are recommended for design. The selection of one method over the other will depend on the availability of a computer or a micro-computer. Method I is recommended for design offices which have access to a computer. Method II is recommended only for design offices which do not have access to a computer.

A comparison of Methods II and III favors Method II on accuracy and Method III (slightly) on ease of application. Since Method II is only slightly more complex than Method III, the greater accuracy of Method II makes it the more preferable of the two for design.

CHAPTER 6

DESIGN OF COMPOSITE BEAMS WITH WEB OPENINGS

6.1 GENERAL

The design procedures presented in Chapter 5 provide good agreement with test results. For a given location, opening size, and beam geometry, the nominal shear and moment capacities of a composite beam at a web opening are easily determined. In the following sections, Design Methods I and II are summarized, and recommendations are made for applying the methods. Detailing recommendations are made.

The deflection analysis of composite beams with web openings is also discussed in the following sections. Deflections are calculated using the stiffness method of matrix analysis, incorporating modeling assumptions verified by test data (Appendix E).

6.2 STRENGTH DESIGN

6.2.1 Summary of the Strength Design Procedures

The strength methods presented in Chapter 5 allow the calculation of the nominal capacity of a composite beam at a web opening. The methods use identical procedures to calculate the maximum moment capacity, M_m, and have a common basis for the calculation of the maximum shear capacity, V_m. The procedures differ only in the simplifying assumptions used to a obtain closed-form solution for V_m.

6.2.2 Load and Resistance Factors

The proposed Load and Resistance Factor Design (LRFD) Specification for Structural Steel Buildings (3) defines the design flexural strength as

$$\text{Design Moment} = \phi_b M_n \tag{6.2}$$

where ϕ_b = the resistance factor for bending. For compact composite sections, $\phi_b = 0.85$. The design shear strength is defined as

$$\text{Design Shear} = \phi_v V_n \tag{6.3}$$

where ϕ_v = the resistance factor for shear. The LRFD Specification specifies $\phi_v = 0.90$ for composite design. This value is, however, based on the assumption that shear is carried only in the web of the steel section. For Design Methods I and II, V_n is dependent on composite behavior at the opening. It is recommended, therefore, that the designer use $\phi_v = \phi_b = 0.85$.

The required strength of a composite beam with a web opening is found using the critical combination of factored loads (3). Normally, the critical combination for a composite beam with a web opening is given by

$$\text{Factored Load} = 1.2D + 1.6L \tag{6.4}$$

in which D = the dead load due to the self-weight of the structural elements and the permanent features on the structure and L = the live load due to occupancy and moveable equipment. The factored load is used to calculate M_u and V_u.

6.3 DETAILING

The strength and performance of a composite beam with a web opening can be enhanced through detailing practice. A number of recommendations can be made, based on the available data.

The tests conducted by Redwood and Poumbouras (30, 32) and the current tests (Chapter 3) indicate that the strength at an opening is highly dependent upon the shear connector capacity above the opening and between the opening and the support. Thus, increasing the number of shear connectors and using the maximum possible length of shear studs in ribbed slabs will increase the strength at an opening. The design procedures reflect this.

All tests indicate that the slab carries a significant portion of the shear at the opening. For ribbed slabs, this tends to result in bridging in the slabs (Chapter 3). An increased density of shear connectors adjacent to the high moment end of the opening is warranted to resist the bridging effect. It would be good practice to use at least two studs per foot for a distance equal to the depth of the section, d, or the length of the opening, a_o, whichever is greater from the high moment end of the opening toward the direction of increasing moment.

The tendency of the slabs to crack both transversely and longitudinally suggests the need to increase the reinforcing steel in the slab over the opening. The increased reinforcing steel will not prevent the cracks from forming, but will limit the crack widths. Transverse and longitudinal reinforcement ratios of 0.0025, based on the gross area of the slab, in the vicinity of the opening (that is, within a distance $d \geq a_o$) are suggested.

Beams with longitudinal ribs tend to fail due to a shear failure between the rib and the surrounding deck (Chapter 3). This type of failure has been noted in the current study, as well as in tests of stub girders (4, 6, 22). The nature of the failure suggests that transverse reinforcing steel that crosses the crack surface will improve the post-crack performance. Additional transverse reinforcement, with a shape that drops down into the rib over the beam, will intersect the crack plane at about 90 degrees and limit slip along the plane. While this type of reinforcement is not considered in American codes, it is in British standards (5, 47).

6.4 DEFLECTION

The stiffness method of matrix analysis is routinely applied to deflection analysis using general purpose structural analysis programs. It is particularly attractive for the analysis of beams with web openings since it can automatically enforce compatibility of displacement and rotation at the ends of an opening.

A composite beam with a web opening is illustrated in Fig. 6.1a. The beam can be modeled using uniform beam elements and rigid links (Fig. 6.1b). The uniform beam elements representing the composite section away from the opening (elements 1, 4, and 5) are modeled using the effective moment of inertia, I_{eff}, and the effective area for shear stress, A_y. I_{eff} (Eq. (E.7)) is given by

$$I_{eff} = I_s + \sqrt{V'_h/V_h}(I_{tr} - I_s) \leq I_{tr} \tag{6.5a}$$

$$V'_h \leq V_h \tag{6.5b}$$

in which I_s = the moment of inertia of the steel beam, I_{tr} = the moment of inertia of the transformed composite section, V'_h = the sum of the shear stud capacities between the point of maximum moment and the nearest point of zero moment, and V_h is the minimum of the tensile yield capacity of the gross steel section or the crushing strength of the concrete slab. A_y (Eq. (E.8)) is given by

$$A_y = dt_w \tag{6.6}$$

in which t_w = the web thickness of the steel section. The uniform beam elements representing the top and bottom tees at the opening (elements 2 and 3, respectively) are connected to beam elements 1 and 4 using 4 rigid links. The top and bottom tees are modeled using

moments of intertia, I_t and I_b; effective areas for shear stress, A_{yt} and A_{yb}; and effective areas for axial stress, A_t and A_b.

I_t and I_b are calculated using the web and flange for each steel tee (the concrete is not considered for I_t). A_{yt} and A_{yb} (Eq. (E.9)) are given by

$$A_{yt} = s_t t_w \tag{6.7a}$$

and

$$A_{yb} = s_b t_w \tag{6.7b}$$

in which s_t = the top tee stub depth and s_b = the bottom tee stub depth. A_t is the transformed area of the top tee, and A_b is the area of the bottom tee. The application of the stiffness method to composite beams with web openings is discussed in greater detail in Appendix E.

6.5 DESIGN EXAMPLE

The AISC Manual of Steel Construction (2) provides 3 examples of composite beam design. The beam from Example 2 is used in this section to illustrate the design of composite beams with web openings.

6.5.1 Problem Statement

A simply-supported composite beam is part of a floor system of an office building. The center-to-center beam spacing is 8 ft. (Fig. 6.2). The beam span is 36 ft. An 11 x 22 in. opening is required at the span quarter point. The slab is 4 in. thick and will be placed on metal decking with 2 in. ribs on 6 in. centers. The concrete is normal weight, with a nominal compressive strength of 3000 psi. A36 steel will be used.

Limit deflection during construction to 1-1/2 in. and during service to L/360.

The loads are specified as follows:

Live load = 100 psf

Partition load = 20 psf

Ceiling load = 8 psf

4 in. slab = 41 psf

Steel (assumed)= 7 psf

A W21 x 44 steel section is selected in the AISC example.

6.5.2 Solution

Section Properties:

For the W21 x 44 steel section with an 11 x 22 in. concentric opening, the section properties are

$b_f = 6.50$ $\quad$ $s_t = 4.83$

$t_f = 0.45$ $\quad$ $s_b = 4.83$

$t_w = 0.35$ $\quad$ $T_s = 4$

$d = 20.66$ $\quad$ $t_s = 2$

in which b_f = the flange width, T_s = the gross slab thickness and t_s = the slab thickness above the ribs.

The effective slab width, b_e, is given by

$b_e \leq$ Span/4 = 1/4(36)(12) = 108 in.

$\leq$ Beam spacing = 8(12) = 96 in.

$\leq 16T_s + b_f$ = 16(4) + 6.5 = 70.5 in. <== Controls

The cross-section at the web opening is shown in Fig. 6.3.

Design Loads:

The factored load (Eq.(6.4)) is given by

$$\text{Factored Load} = 1.2D + 1.6L$$
$$= 1.2(0.020 + 0.008 + 0.041 + 0.007) + 1.6(0.100)$$
$$= 0.091 + 0.160 = 0.251 \text{ ksf}$$

Therefore, the uniform load on the section, w, is

$$w = 0.251(8) = 2.008 \text{ kips/ft}$$

At the opening centerline, the factored shear and moment are

$$V_u = \frac{wl}{4} = \frac{2.008(36)}{4} = 18.07 \text{ kips}$$

and

$$M_u = \frac{3wl^2}{32}$$
$$= \frac{3}{32}(2.008)(36)^2$$
$$= 244.0 \text{ ft-kips} = 2928 \text{ in.-kips}$$

Stud Parameters:

Try 3/4 x 3-1/2 in. studs (Note: The maximum allowable height is used to obtain the maximum capacity per stud). The parameters for the shear capacity of the studs are obtained using Eq. (5.10a), (5.11a), and (5.11b).

$$A_{sc} = (0.75)^2\pi/4 = 0.44 \text{ in.}^2$$

$$E_c = 57\sqrt{f'_c}$$
$$= 57\sqrt{3000} = 3122 \text{ ksi}$$

$$Q_n = 0.5A_{sc}\sqrt{f'_c E_c}$$
$$= 0.5(0.44)\sqrt{3(3122)} = 21.3 \text{ kips}$$

Assume 1 stud per rib ($N_r = 1$) and a rib width, w_r, of 2.5 in.

$$R = \frac{.85}{\sqrt{N_r}}\left(\frac{w_r}{h_r}\right)\left(\frac{H_s}{h_r} - 1.0\right) \leq 1.0$$

$$= \frac{.85}{\sqrt{1}}\left(\frac{2.5}{2}\right)\left(\frac{3.5}{2} - 1.0\right) = 0.797$$

Maximum Moment Capacity:

The crushing capacity of the slab (Eq. (5.7)) is given by

$$P_c = 0.85\, f'_c b_e t_e$$
$$= 0.85(3)(70.5)(2) = 360 \text{ kips}$$

The opening is to be located 9'-0" from the support. A minimum of 19 studs will be located between the high moment end of the opening and the support. Therefore, the shear stud capacity between the high moment end of the opening and the support (Eq. (5.9)) is

$$P_{studs} = NRQ_n$$
$$= 19(.797)(21.3) = 323 \text{ kips}$$

The yield capacity of the net steel section (Eq. (5.13)) is

$$T' = F_y\left(2(b_f - t_w)t_f + s_t t_w + s_b t_w\right)$$
$$= 36\left(2(6.50 - 0.35)(0.45) + 4.83(0.35) + 4.83(0.35)\right)$$
$$= 321 \text{ kips}$$

Finally, the compressive force in the concrete is given by Eq. (5.6).

$$P_{ch} \leq P_c = 360$$
$$\leq P_{studs} = 323$$
$$\leq T' = 321 \quad \text{<== Controls}$$

P_{ch} acts at a distance, d_h, from the top of the flange. d_h is obtained using Eq. (5.14) and (5.15).

$$\bar{a} = \frac{P_{ch}}{0.85f'_c b_e}$$

$$= \frac{321}{0.85(3)(70.5)} = 1.79 \text{ in.}$$

$$d_h = T_s - \bar{a}/2$$

$$= 4 - 1.79/2 = 3.10 \text{ in.}$$

Since $P_{ch} = T'$, the moment capacity (Eq. (5.16)) is

$$M_m = P_{ch}d_h + F_y(b_f - t_w)t_f d + F_y t_w \left(\frac{s_t^2 - s_b^2}{2} + s_b d\right)$$

$$= 321(3.10) + 36(6.5 - 0.35)(0.45)(20.66) + 36(0.35)\left(\frac{4.83^2 - 4.83^2}{2} + 4.83(20.66)\right)$$

$$= 995 + 2058 + 1257 = 4310 \text{ in.-kips}$$

Maximum Shear Capacity:

The "pure shear" capacities at the web opening are found using Eq. (5.54), (5.26), and (5.27).

$$V_{pb} = s_b t_w F_y/\sqrt{3}$$

$$= 4.83(0.35)(36)/\sqrt{3} = 35.1 \text{ kips}$$

$$V_{pt} = s_t t_w F_y/\sqrt{3}$$
$$= 4.83(0.35)(36)/\sqrt{3} = 35.1 \text{ kips}$$

$$A_{cv} = 3T_s t_e$$
$$= 3(4)(2) = 24 \text{ in}^2$$

$$V_t(sh) = \frac{3.5\sqrt{f'_c}\, A_{cv}}{1000} + V_{pt}$$
$$= \frac{3.5\sqrt{3000}(24)}{1000} + 35.1 = 39.7 \text{ kips}$$

Bottom Tee Shear Capacity:

Method I

For Method I, the bottom tee shear capacity is given by Eq. (5.41).

$$\alpha = 3 + 2\sqrt{3}\,\frac{a_o}{s_b}$$
$$= 3 + 2\sqrt{3}\,\frac{(22)}{4.83} = 18.8$$

$$\beta = 2\sqrt{3}\,\frac{(b_f - t_w)}{s_b}\,(s_b^2 - s_b t_f + t_f^2)$$
$$+ 2\sqrt{3}\lambda t_w s_b + 2a_o\big((b_f - t_w) + \lambda t_w\big)$$
$$= 2\sqrt{3}\,\frac{(6.5 - 0.35)}{4.83}\,(4.83^2 - 4.83(0.45) + 0.45^2)$$
$$+ 2\sqrt{3}(1.207)(0.35)(4.83)$$
$$+ 2(22)\big((6.5 - 0.35) + 1.207(0.35)\big)$$
$$= 94.2 + 7.0 + 289.2 = 390.4$$

$$\gamma = (b_f - t_w)^2 t_f^2 + \lambda^2 t_w^2 s_b^2$$
$$+ 2\lambda t_w (b_f - t_w)(s_b^2 - s_b t_f + t_f^2)$$
$$= (6.5 - 0.35)^2 (0.45)^2 + 1.207^2 (0.35^2)(4.83^2)$$
$$+ 2(1.207)(0.35)(6.5 - 0.35)(4.83^2$$
$$- 4.83(0.45) + 0.45^2)$$
$$= 7.7 + 4.1 + 111.0 = 122.8$$

$$V_b(\max) = F_y\left(\frac{\beta - \sqrt{\beta^2 - 4\alpha\gamma}}{2\alpha}\right)$$
$$= 36\left(\frac{390.4 - \sqrt{390.4^2 - 4(18.8)(122.8)}}{2(18.8)}\right) = 11.5$$

Method II

For Method II, the shear capacity of the bottom tee is given by Eq. (5.59).

$$\alpha_b = 3\left(\frac{s_b}{a_o}\right)^2$$
$$= 3\left(\frac{4.83}{22}\right)^2 = 0.145$$

$$V_b(\max) = V_{pb}\sqrt{\alpha_b/(1 + \alpha_b)}$$
$$= 35.1\sqrt{0.145/1.145} = 12.5 \text{ kips}$$

Top Tee Shear Capacity:

Method I

For Method I, the top tee shear capacity is given by (Eq. (5.47). Using Eq. (5.34b), the concrete force at the high moment end is limited to the tensile capacity of the top tee.

$$P_{smax} = F_y t_f (b_f - t_w) + F_y t_w s_t$$
$$= 36(0.45)(6.5 - 0.35) + 36(0.35)(4.83)$$
$$= 100 + 61 = 161 \text{ kips}$$

$$P_{ch} \leq P_c = 360$$
$$\leq P_{studs} = 323$$
$$\leq P_{smax} = 161 \quad \text{<== Controls}$$

$$\bar{a} = \frac{161}{0.85(3)(70.5)} = .90$$

$$d_h = 4 - \frac{.90}{2} = 3.55 \text{ in.}$$

The deck ribs are on 6 in. centers. With a 22 in. opening, a minimum of 3 ribs will be above the opening. The concrete force and location at the low moment end are obtained using Eq. (5.24) and (5.25a).

$$P_{cl} = P_{ch} - N_o R Q_n$$
$$= 161 - 3(.797)(21.3) = 110 \text{ kips}$$

$$d_1 = T_s - t_s + \frac{0.5P_{cl}}{0.85f'_c\, b_e}$$

$$= 4 - 2 + \frac{0.5(110)}{0.85(3)(70.5)} = 2.30 \text{ in.}$$

The top tee "mechanism" capacity is given by Eq (5.47).

$$\alpha = 3 + 2\sqrt{3}\,\frac{a_o}{s_t}$$

$$= 3 + 2\sqrt{3}\,\left(\frac{22}{4.83}\right) = 18.8$$

$$\beta = 2\sqrt{3}\,\frac{(b_f - t_w)}{s_t}\,(s_t^2 - s_t t_f + t_f^2) + 2\sqrt{3}\,\lambda t_w s_t$$

$$+ 2a_o\left((b_f - t_w) + \lambda t_w\right) + \frac{2\sqrt{3}}{s_t F_y}\,(P_{ch}d_h - P_{cl}d_1)$$

$$+ \frac{\sqrt{3}}{F_y}\,(P_{ch} - P_{cl})$$

$$= 2\sqrt{3}\,\left(\frac{6.5 - 0.35}{4.83}\right)(4.83^2 - 4.83(0.45) + 0.45^2)$$

$$+ 2\sqrt{3}\,(1.207)(0.35)(4.83)$$

$$+ 2(22)\left((6.5 - 0.35) + 1.207(0.35)\right)$$

$$+ \frac{2\sqrt{3}}{4.83(36)}\,\left(161(3.55) - 110(2.30)\right)$$

$$+ \frac{\sqrt{3}}{36}\,(161 - 110)$$

$$= 94.2 + 7.1 + 289.2 + 6.3 + 2.5 = 399.3$$

$$\gamma = (b_f - t_w)^2 t_f^2 + \lambda^2 t_w^2 s_t^2$$

$$+ 2\lambda(b_f - t_w)t_w(s_t^2 - s_t t_f + t_f^2)$$

$$+ \frac{2\left((b_f - t_w) + \lambda t_w\right)}{F_y}\,(P_{ch}d_h - P_{cl}d_1)$$

$$- \frac{(P_{ch}^2 + P_{cl}^2)}{2F_y^2} + \frac{\left((b_f - t_w)t_f + \lambda t_w s_t\right)}{F_y}(P_{ch} - P_{cl})$$

$$= (6.5 - 0.35)^2(0.45)^2 + 1.207^2(0.35)^2(4.83^2)$$

$$+ 2(1.207)(6.5 - 0.35)(0.35)(4.83^2)$$

$$- 4.83(0.45) + 0.45^2)$$

$$+ \frac{2\left((6.5 - 0.35) + 1.207(0.35)\right)}{36}(161(3.55) - 110(2.30))$$

$$- \frac{(161^2 + 110^2)}{2(36)^2}$$

$$+ \frac{\left((6.5 - 0.35)(0.45) + 1.207(0.35)(4.83)\right)}{36}(161 - 110)$$

$$= 7.7 + 4.2 + 111.0 + 116.3 - 14.7 + 6.8 = 231.3$$

$$V_t(max) = F_y\left(\frac{\beta - \sqrt{\beta^2 - 4\alpha\gamma}}{2\alpha}\right)$$

$$= 36\left(\frac{399.3 - \sqrt{399.3^2 - 4(18.8)(231.3)}}{2(18.8)}\right)$$

$$= 21.5 \text{ kips} < V_{pt}$$

Method II

For Method II, P_{ch} is limited only by Eq. (5.23).

$$P_{ch} \leq P_c = 360$$

$$\leq P_{studs} = 323 \text{ <== Controls}$$

$$\bar{a} = \frac{323}{0.85(3)(70.5)} = 1.80$$

$$d_h = 4 - \frac{1.80}{2} = 3.10 \text{ in.}$$

$$P_{cl} = 323 - 3(.797)(21.3) = 272$$

$$d_1 = 4 - 2 + \frac{0.5(272)}{0.85(3)(70.5)}$$

$$= 2.76 \text{ in.}$$

The maximum shear capacity is found using Eq. (5.64), (5.65), and (5.68).

$$\mu = \frac{(P_{ch}d_h - P_{cl}d_1)}{s_t V_{pt}}$$

$$= \frac{(323(3.10) - 272(2.76))}{4.83(35.1)} = 1.48$$

$$\nu = \frac{a_o}{s_t}$$

$$= \frac{22}{4.83} = 4.55$$

$$V_t(\max) = V_{pt}\left(\frac{2\mu\nu + \sqrt{12\nu^2 - 12\mu^2 + 36}}{2(3 + \nu^2)}\right)$$

$$= 35.1\left(\frac{2(1.48)(4.55) + \sqrt{12(4.55^2) - 12(1.48^2) + 36}}{2(3 + 4.55^2)}\right)$$

$$= 21.9 \text{ kips} < V_{pt}$$

Total Capacity:

Method I

$$V_m = V_b(\max) + V_t(\max)$$

$$= 11.5 + 21.5$$

$$= 33.0 \text{ kips}$$

Method II

$$V_m = V_b(max) + V_t(max)$$
$$= 12.5 + 21.9$$
$$= 34.4 \text{ kips}$$

Strength Check:

The M/V ratio is

$$\frac{M}{V} = \frac{2928}{18.07} = 162 \text{ in.}$$

Method I

The nominal capacity is given by Eq. (6.1).

$$V_n = V_m \left[\frac{(\frac{M}{V})^3}{(\frac{M_m}{V_m})^3} + 1 \right]^{-1/3}$$
$$= 33.0 \left[\frac{(162^3)}{(\frac{4310}{33.0})^3} + 1 \right]^{-1/3}$$
$$= 23.1 \text{ kips}$$

$$M_n = V_n(\frac{M}{V})$$
$$= 23.2(162) = 3745 \text{ in.-kips}$$

Using Eq. (6.3) and (6.2), the shear and moment capacities at the web opening are found.

Shear Capacity = $\phi_v V_n$

= 0.85(23.1)

= 19.6 > V_u = 18.1 ok

Moment Capacity = $\phi_b M_n$

= 0.85(3745)

= 3183 > M_u = 2928 ok

Method II

Shear Capacity = 19.9 ok

Moment Capacity = 3227 ok

The selected section has adequate strength with an 11 x 22 in. web opening at the span quarter point. In the event that a section is not adequate with the required opening, several alternatives are available to the designer. The material strengths can be increased, the section weight or depth can be increased, or the deck configuration may be changed. Although an increase in section depth will increase the height of a story, the total depth will normally be less than the depth obtained if utilities are routed below, rather than through the section.

Deflections:

The beam deflections are calculated for construction and service loads considering shear deformations throughout the span. The beam is modeled as shown in Fig. 6.1b.

Before the concrete has hardened, the loads will consist of the weight of the slab and the weight of the steel section. The load, therefore, is

$$\text{Construction load} = 0.041 + 0.007$$
$$= 0.048 \text{ ksf}$$

and the uniform load on the beam, w, is

$$w = 0.048(8) = 0.384 \text{ kips/ft}$$

At this stage, the beam is modeled using the properties of the steel section only. Elements 1, 4, and 5 (Fig. 6.1b) are modeled using $I_s = 843$ in.^{4} and $A_y = 7.23$ in.^{2}. The top tee (element 2) is modeled using $I_t = 8.32$ in.^{4}, $A_t = 4.46$ in.^{2}, and $A_{yt} = 1.69$ in.^{2}, while the bottom tee (element 3) is modeled using $I_b = 8.32$ in.^{4}, $A_b = 1.69$ in.^{2}, and $A_{yt} = 1.69$ in.^{2}. The eccentricities for the top and bottom tees are 9.27 in. and -9.27 in., respectively.

After the concrete has hardened, additional loads will include the live load, the partition load, and the ceiling load. The additional load is

Service load = 0.100 + 0.020 + 0.008 = 0.128 ksf

and the uniform load is

$$w = 0.128(8) = 1.024 \text{ kips/ft}$$

The beam is now modeled using the composite properties. Elements 1, 4, and 5 are modeled using I_{eff} = 2044 in.^{4} and A_y = 7.23 in.^{2}. The top tee is modeled using I_t = 8.32 in.^{4}, A_t = 18.56 in.^{2}, and A_{yt} = 1.69 in.^{2}. The bottom tee is modeled using I_b = 8.82 in.^{4}, A_b = 4.46 in.^{2}, and A_{yb} = 1.69 in.^{2}. The eccentricities for elements 2 and 3 are 2.32 in. and -16.23 in., respectively.

The deflections are obtained using the general purpose finite element program POLO-FINITE (24).

The respective increments in deflection at the point of maximum moment are 0.614 and 0.703 in. under construction and service loads, while the respective deflections across the opening are 0.086 and 0.095.

Comparing the deflections to the specified limits:

0.614 < 1-1/2 in. ok

0.703 < L/360 = 36(12)/360 = 1.20 in. ok

It is worthwhile to compare these deflections with those obtained using a more traditional approach. Considering only flexural deformations in the beam and ignoring the web opening, the respective increments in deflection at the point of maximum moment are 0.59 and 0.65 in. under construction and service loads. The deflections are close because the beam used in this example has a long span and a short opening relative to its length. The effects of shear deformation and of the web opening on the overall deflections are, therefore, relatively small.

Detailing:

In addition to the studs required over the opening and between the opening and the support, studs should be placed in the four ribs adjacent to the high moment end of the opening (d = 21 in., a_o = 22 in., use 22 in.).

The slab above the opening requires additional reinforcing.

$$A_r = 0.0025(12)T_s$$
$$= 0.0025(12)(4) = 0.12 \text{ in.}^2/\text{ft}$$

Use #3 bars on 10 in. centers in both directions. Since $a_o > d$, the transverse reinforcement should extend 22 in. on each side of the section, and the longitudinal reinforcement should extend 22 in. on each end of the opening.

6.6 SUMMARY

Design Methods I and II allow rapid calculation of the nominal shear and moment capacities of a composite beam with a web opening. The nominal capacities are applied to design using LRFD procedures. It is recommended that the designer increase the number and the length of shear connectors, if possible, to take advantage of the increased capacity at the opening afforded by increased shear connector capacity. Additional shear connectors near the high moment end of the opening and additional reinforcing steel in the slab are also recommended. The stiffness method of matrix analysis is recommended for estimating the deflections of composite beams with web openings. A design example is provided.

CHAPTER 7

SUMMARY AND CONCLUSIONS

7.1 SUMMARY

This study consists of laboratory tests and detailed analyses leading to a comprehensive design procedure for composite beams with web openings.

Fifteen tests to failure were carried out on composite beams with web openings. All specimens were full scale beams with ribbed slabs using formed steel deck. The ribs were oriented either perpendicular to or parallel to the steel section. The key parameters of the study included moment-shear ratio at the opening, partial composite behavior, deck rib orientation, slab thickness, opening shape, opening eccentricity, and modification of the deck over the opening.

A strength model is developed for both unreinforced and reinforced openings and members with either solid or ribbed slabs. Three versions of a practical strength design technique for unreinforced openings are also presented. The strength model and the design techniques are compared with all experimental work on composite beams with web openings. A comprehensive design procedure, including both strength and serviceability criteria is developed.

7.2 CONCLUSIONS

Based on the study presented in this report, the following conclusions can be made:

1) The peak loads attained by composite beams with ribbed slabs at web openings are governed by the failure of the concrete slab. For slabs with transverse ribs, rib failure around the shear connectors occurs. For slabs with longitudinal ribs, a longitudinal shear failure occurs.

2) As the number of shear connectors above the opening and between the opening and the support increases, the failure load increases.

3) As the ratio of moment to shear at an opening decreases, deflections across the opening increase and transverse cracking occurs at lower loads.

4) The failure of composite beams with ribbed slabs at web openings is, in general, quite ductile. Failure is preceded by major cracking in the slab, yielding of the steel, and large deflections in the member.

5) First yield in the steel around an opening does not give an accurate measure of the section capacity.

6) The strength of composite beams with web openings can be calculated with reasonable accuracy using equilibrium methods. The strength model provides an accurate prediction of the test results from this study and from previous investigations.

7) Relatively simple strength design procedures, based on equilibrium methods, also give a good prediction of test results.

8) The analyses using the strength model and the strength design procedures clearly indicate the importance of considering

partial composite action in determining the strength of composite beams with web openings.

9) Beam deflections can be estimated, with reasonable accuracy, using the stiffness method of matrix analysis. The opening is modeled as two uniform beam elements, each connected to the beam by two rigid links. The most accurate estimates are obtained using a model which considers shear deflections (model V). Similar results can, however, be obtained by multiplying the deflections obtained with model V by a correction factor.

10) The effect of a web opening on beam deflection increases as both the shear at the opening and the relative size of the opening increase.

7.3 FUTURE WORK

Only two composite beams with reinforced openings have been tested (8). Additional testing, particularly of partially reinforced openings (openings with reinforcement at only one tee), is required. The test results can be used to confirm the accuracy of the strength model, which accounts for reinforcement at the opening.

An extension of the current simplified design procedures which accounts for reinforcement at the opening is required.

Stability considerations were outside the scope of this project. While elastic buckling was not observed in any of the reported tests of composite beams with web openings, no stability criterion have been developed for composite beams with web openings.

An investigation of buckling at web openings in composite beams is required.

The contribution of the slab to the strength of composite beams at web openings is well documented. Additional work is required, however, to investigate modifications of the slab that will provide inexpensive reinforcement at the opening.

To date, no tests of adjacent openings in composite beams have been conducted. An investigation of the interaction between adjacent openings in composite beams is, therefore, highly desirable.

The deflection analysis of composite beams with web openings can be simplified by the development of design aids which allow the designer to apply factors, based on opening size and location, to the bending deflection of a beam without an opening.

1. ACI, Building Code Requirements For Reinforced Concrete (ACI 318-83), American Concrete Institute, Detroit, MI, 1983, 111 pp.

2. AISC, Manual Of Steel Construction, Eighth Edition, American Institute of Steel Construction, Inc., Chicago, IL, 1980.

3. AISC, Proposed Load And Resistance Factor Design Specification for Structural Steel Buildings, American Institute of Steel Construction, Inc., Chicago, IL, 1983, 166 pp.

4. Bjorhovde, R., and Zimmerman, T. J., "Some Aspects of Stub-Girder Design," Engineering Journal, AISC, Vol. 17, No. 3, 3rd Quarter, 1980, pp. 54-69.

5. British Standards Institution, BS 5400, Steel, Concrete and Composite Bridges, Part 5: Code of Practice for Design of Composite Bridges, BSI, London, 1979.

6. Buckner C. D., Deville, D. J., and McKee D. C., "Shear Strength of Slabs in Stub Girders," Journal of the Structural Division, ASCE, Vol. 107, No. ST2, Feb. 1981, pp. 273-280.

7. Canadian Standards Association, Steel Structures for Buildings--Limit States Design, Standard No. CAN3-S16.1-M78, CSA, Rexdale, Ontario, Dec. 1978.

8. Cho Soon Ho, "An Investigation On The Strength Of Composite Beams With Web Openings," Thesis presented to Hanyong University, Seoul, Korea, Dec. 1982, in partial fulfillment of the requirements for the degree of M.S. Arch. Eng., 270 pp.

9. Clawson, W. C., and Darwin, D., "Tests Of Composite Beams With Web Openings," Journal of the Structural Division, ASCE, Vol. 108, No. ST1, Jan. 1982, pp. 145-162.

10. Clawson, W. C., and Darwin, D., "Strength Of Composite Beams With Web Openings," Journal of the Structural Division, ASCE, Vol. 108, No. ST3, Mar. 1982, pp. 623-641.

11. Clawson, W. C., and Darwin, D., "Composite Beams With Web Openings," Structural Engineering and Engineering Materials SM Report No. 4, University of Kansas Center for Research, Inc., Lawrence, Kansas, Oct. 1980, 209 pp.

12. Conte, S. D., and de Boor, C., Elementary Numerical Analysis: An Algorithmic Approach, 3rd Edition, McGraw-Hill, Inc., 1980, 432 pp.

13. Cook, R. D., Concepts and Applications Of Finite Element Analysis, 2nd Edition, John Wiley and Sons, New York, 1981, 537 pp.

14. Darwin, D., "Composite Beams With Web Openings,"Proceedings, National Engineering Conference, American Institute of Steel Construction, Chicago, IL, March 1984, 17 pp. Also, Journal of the Boston Society of Civil Engineers Section, ASCE, Vol. 71, No. 1 & 2, 1985, pp. 67-83.

15. Donoghue, C. M., "Composite Beams With Web Openings: Design," Journal of the Structural Division, ASCE, Vol. 108, No. ST12, Dec. 1982, pp. 2652-2667.

16. Dougherty, B. K., "The Effects Of Rectangular Web Holes On The Behavior Of Steel Beams," thesis presented to the University of Natal, Durban, South Africa, in 1978, in partial fulfillment of the requirements for the degree of Doctor of Philosophy in Engineering.

17. Dougherty, B. K., "Elastic Deformation Of Beams With Web Openings," Journal of the Structural Division, ASCE, Vol. 106, No. ST1, Jan. 1980, pp. 301-312.

18. Fenves, S. J., Logcher, R. D., and Mauch, S.P., STRESS: A Reference Manual, A Problem-Oriented Computer Language for Structural Engineering, The Department of Civil Engineering, Massachusetts Institute of Technology, Cambridge, 1965.

19. Granade, C. J., "An Investigation Of Composite Beams Having Large Rectangular Openings In Their Webs," thesis presented to the University of Alabama, at University, Alabama, in 1968, in partial fulfillment of the requirements for the degree of Master of Science.

20. Grant, J. A., Jr., Fisher, J. W., and Slutter, R. G., "Composite Beams with Formed Steel Deck," AISC Engineering Journal, Vol. 14, No.1, First Quarter, 1977, pp 24-43.

21. Horne, M. R. Plastic Theory of Structures, The M.I.T. Press, Cambridge, Massachusetts, 1971, 173 pp.

22. Kullman, R. B., Hosain, M. U., "Shear Capacity of Stub-girders: Full Scale Tests," Journal of Structural Engineering, Vol. 111, No. 1, January, 1985, pp. 56-75.

23. Kupfer, H., Hilsdorf, H. K., and Rüsch, H., "Behavior Of Concrete Under Biaxial Stress," ACI Journal, Proceedings, Vol. 66., No. 8, Aug. 1969, pp. 656-666.

24. Lopez, L. A., Dodds, R. H., Jr., Rehak, D. R., and Urzua, J., Polo-Finite: A Structural Mechanics System For Linear And Nonlinear Analysis, Issued as a technical report by: Civil Engineering Laboratory, University of Illinois at Urbana-Champaign and Department of Civil Engineering, University of Kansas, Lawrence, KS, 1980.

25. Logcher, R. D., et. al., ICES STRUDL-I, The Structural Design Language, Department of Civil Engineering, M.I.T., Cambridge, 1967.

26. McCormick, M. M., Open Web Beams -- Behavior, Analysis And Design, BHP Melbourne Research Laboratories Report MRL 17/18, Melbourne Research Laboratories, The Broken Hill Proprietary Company Limited, Clayton, Vic., Australia, Feb. 1972, 195 pp.

27. McCormick, M. M., Discussion of "Suggested Design Guides For Beams With Web Holes," Journal of the Structural Division, ASCE, Vol. 98, No. ST12, Dec. 1972, pp. 2814-2816.

28. Momeni, Ali M., "Strength Of Composite Beams With Eccentric, Reinforced, Rectangular Web Openings," thesis presented to Kansas State University, Manhattan, Kansas, in 1983, in partial fulfillment of the requirements for the degree of Doctor of Philosophy.

29. Ollgaard, J. G., Slutter, R. G., and Fisher, J. W., "Shear Strength of Stud Connectors in Lightweight and Normal-Weight Concrete," AISC Engineering Journal, Vol. 8, No. 2, April, 1971, pp 55-64.

30. Poumbouras, G., "Modification Of A Theory Predicting The Shear Strength Of Composite Beams With Large Web Openings," Project Report, No. U83-20, Department of Civil Engineering and Applied Mechanics, McGill University, Montreal, Quebec, Canada, April 1983, 109 pp.

31. Redwood, R. G., "Plastic Behavior and Design of Beams with Web Openings," Proceedings, First Canadian Structural Engineering Conference, Toronto, Canadian Steel Industries Construction Council, Toronto, Canada, Feb. 1968, pp. 127-138.

32. Redwood, R. G., and Poumbouras, G., "Tests Of Composite Beams With Web Holes," Canadian Journal of Civil Engineering, Vol. 10, No. 4, 1983, pp. 713-721.

33. Redwood, R. G., and Poumbouras, G., "Analysis Of Composite Beams With Web Openings," Journal of the Structural Engineering, ASCE, Vol. 110, No. ST9, Sept. 1984, pp. 1949-1958.

34. Redwood, R. G., and Wong, P. K., "Web Holes In Composite Beams With Steel Deck," Proceedings, Eighth Canadian Structural Engineering Conference, Canadian Steel Construction Council, Willowdale, Ont., Canada, Feb. 1982, 41 pp.

35. Slutter, R. G., and Driscoll, G. C., Jr., "Flexural Strength Of Steel-Composite Beams," Journal of the Structural Division, ASCE, Vol. 91, No. ST2, Apr. 1965, pp. 71-99.

36. Steel Deck Institute, Design Manual for Floor Decks and Roof Decks, 1978.

37. Structural Investigation Of A Typical Floor Beam At The 200 West Adams Building, Chicago, Illinois, WJE No. 840795, Wiss Janney, Elstner Associates, Inc., Northbrook, IL, Aug. 1984, 21 pp.

38. "Suggested Design Guides For Beams With Web Holes," by the Subcommittee on Beams with Web Openings of the Task Committee on Flexural Members of the Structural Division, John E. Bower, Chmn., Journal of the Structural Division, ASCE, Vol. 97, No. ST11, Nov. 1971, pp. 2702-2728.

39. "Suggested Design Guides For Beams With Web Holes," Closure by the Subcommittee on Beams with Web Openings of the Task Committee on Flexural Members of the Structural Division, John E. Bower, Chmn., Journal of the Structural Division, ASCE, Vol. 99, No. ST6, June 1973, pp. 1312-1315.

40. Swartz, S. E., and Eliufoo, K. S., "Composite Beams With Web Openings," Journal of the Structural Division, ASCE, Vol. 106, No. ST5, May 1980, pp. 1203-1208.

41. Thompson, P. J., and Ainsworth, I., "Composite Beams With Web Penetrations: Grosvenor Place, Sydney, Third Conference on Steel Developments, Australian Institute of Steel Construction, Melbourne, Australia, May, 1985, 18 pp.

42. Todd, D.M., and Cooper, P. B., "Strength Of Composite Beams With Web Openings," Journal of the Structural Division, ASCE, Vol. 106, No. ST2, Feb. 1980, pp. 431-444.

43. Uniform Building Code, International Conference of Building Officials, Whittier, 1985, 819 pp.

44. U.S. Steel Corp., Rectangular, Concentric And Eccentric Unreinforced Web Penetrations In Composite Steel Beams - A Design Aid, ADUSS 27-8532-01, Pittsburgh, Pa., Oct. 1984, 27 pp.

45. U.S. Steel Corp., Rectangular Concentric and Eccentric Unreinforced Web Penetrations in Steel Beams - A Design Aid, ADUSS 27-7108-01, Pittsburgh, Pa., June 1981, 28 pp.

46. Wong, P. P. U., and Redwood, R. G., "Pilot Test Of A Hollow Composite Beam Containing A Web Opening," Structural Engineering Report, No. 80-6, McGill University, Montreal, Quebec, Canada, Dec. 1980, 40 pp.

47. Yam, Lloyd C. P., Design Of Composite Steel-Concrete Structures, Surrey University Press, London, 1981, 168 pp.

Table 2.1 Steel Strength, ksi.

	TOP FLANGE			BOTTOM FLANGE		
Beam	Yield	Static Yield	Tensile	Yield	Static Yield	Tensile
1	54.6	50.6	71.9	52.3	50.7	71.9
2	52.3	49.2	71.2	51.2	48.8	71.4
3	52.6	50.6	71.6	51.7	49.6	71.5
4	52.6	50.0	71.9	53.6	50.2	71.8
5	53.1	50.4	72.4	54.7	49.5	72.2
6	53.6	50.8	71.7	52.7	49.7	72.4
7	40.6	38.4	68.6	41.1	38.5	68.7
8	47.6	45.0	69.4	47.7	45.1	69.9
9	41.1	38.5	68.7	40.6	38.4	68.6

	WEB (HORIZ.)			WEB (VERT.)		
Beam	Yield	Static Yield	Tensile	Yield	Static Yield	Tensile
1	55.4	51.8	72.8	55.9	53.0	73.4
2	53.1	50.7	73.5	55.5	53.2	74.2
3	52.5	50.4	73.4	54.9	53.3	74.1
4	53.7	50.7	74.1	56.1	53.4	74.4
5	52.7	50.0	72.0	55.9	52.9	73.2
6	52.7	50.2	73.9	57.0	54.7	75.9
7	41.2	38.8	70.1	42.4	39.7	68.7
8	50.8	47.7	72.1	----	----	----
9	41.2	38.8	70.1	42.4	39.7	68.7

Table 2.2 Concrete Properties.

Test	Slump in.	Cement Factor sacks/yd^3	Age at Test (days)	% Air	f'_c psi
1	3-3/4	6	8	2	4470
2	1-1/4	5	7	4	4850
3	3/4	5	7	2-3/4	5400
4A	2-3/4	5	18	3	4740
4B			33		5280
5A	2-3/4	5	12	1-1/2	4740
5B			21		5090
6A	4	5	12	5-1/2	4020
6B			23		4300
7A	3-1/2	5	47	6-1/2	4190
7B			66		4300
8A	4-1/4	5	15	N.A.	3940
8B			120		4990
9A	4-1/4	5	41	6-1/2	4170
9B			48		4360

Table 2.3 Section and Opening Dimensions, in.

Test	Section	d	b_f(Top)	t_f(Top)	t_w	s_t^+	s_b
1	W21 x 44	20.63	6.51	0.440	0.358	4.178	4.101
2			6.50	0.427	0.357	4.094	4.094
3			6.57	0.423	0.358	4.105	4.097
4A			6.50	0.435	0.357	4.100	4.100
4B			6.50	0.435	0.357	4.125	4.125
5A			6.51	0.440	0.358	4.168	4.110
5B			6.57	0.440	0.358	4.110	2.123
6A			6.58	0.440	0.357	4.120	4.115
6B			6.58	0.440	0.357	4.120	4.115
7A			6.66	0.409	0.360	4.025	4.150
7B			6.66	0.409	0.360	4.075	4.188
8A	W10 x 15	10.13	3.98	0.268	0.231	2.090	2.090
8B			3.98	0.268	0.231	2.025	1.725
9A	W21 x 44	20.63	6.67	0.425	0.365	2.960	2.960
9B			6.67	0.427	0.369	3.075	2.812

Test	b_f(Bot)	t_f(Bot)	b_{conc}	b_e*	t_s	T_s	Opening Size
1	6.50	0.430	48.0	48.0	2.0	5.0	12.38 x 24.75
2	6.51	0.448	48.0	48.0	2.0	5.0	12.38 x 24.75
3	6.56	0.435	48.0	48.0	2.0	5.0	12.38 x 24.75
4A	6.57	0.440	48.0	48.0	2.0	5.0	12.38 x 24.75
4B	6.57	0.440	48.0	48.0	2.0	5.0	12.38 x 24.75
5A	6.50	0.430	48.0	48.0	2.0	5.0	12.38 x 24.75
5B	6.45	0.430	48.0	48.0	2.0	5.0	14.39 x 24.75
6A	6.57	0.432	48.0	48.0	2.0	5.0	12.38 x 24.75
6B	6.57	0.432	48.0	48.0	2.0	5.0	12.38 x 24.75
7A	6.59	0.412	48.0	48.0	2.0	5.0	12.38 x 24.75
7B	6.59	0.412	48.0	48.0	2.0	5.0	12.38 x 24.75
8A	4.02	0.280	39.4	36.0	2.5	5.5	5.95 x 11.82
8B	4.02	0.280	39.4	36.0	2.5	5.5	6.38 x 18.63
9A	6.61	0.429	48.0	48.0	4.0	7.0	14.75 x 24.75
9B	6.61	0.427	48.0	48.0	4.0	7.0	14.75 x 14.75

+ Opening eccentricity = e
  e = 0 for Tests 1 through 5A, 6A through 8A, and 9A
  e = -1.00 in. for Test 5B
  e = -0.15 in. for Test 8B
  e = -0.13 in. for Test 9B

* b_e = effective slab width

Table 2.4 Stud and Rib Properties.

Test	Stud Diameter in.	H_s [+] in.	h_r [t] in.	w_r [tt] in.	N_o [*]	N [**]
1	3/4	4.5	3.0	6.0	2*2	5*2
2					2*2	5*2 + 3*4
3					2*2	10*2
4A					0*2	5*1
4B					0*2	5*2 + 3*4
5A					2*1	7*1
5B					2*2	8*2
6A					2*2	6*2
6B					8	20
7A					10	22
7B					6	22
8A	5/8	5.0			1*2	4*2
8B					1*2	3*2
9A	3/4	5.5			2*2	5*2
9B					1*2	4*2

[+] H_s = stud height after welding

[t] h_r = rib height

[tt] w_r = average rib width

[*] N_o = no. of studs over opening -- For transverse ribs = no. of ribs * no. of studs/rib

[**] N = no. of studs between high moment end of the opening and the support -- For transverse ribs = no. of ribs * no. of studs/rib

Table 3.1 Test Behavior.

Test	$\frac{M}{V}^{+}$ (ft)	First Yield % Ult^{+}	Appearance of First Crack: Transverse % Ult^{+}	Longitudinal % Ult^{+}	Diagonal % Ult^{+}
1	3.50	36	44	92	67
2	6.50	32	65	80	80
3	45.20	44	96	76	81
4A	6.50	32	69	95	69
4B	6.50	19	0*	88	51
5A	6.50	31	58	93	93
5B	6.50	30	0*	47	70
6A	0.00	36	21	70	70
6B	3.50	34	0*	65	94
7A	3.50	35	40	80	N.A.
7B	6.50	25	66	66	N.A.
8A	3.30	25	93	93	93
8B	2.50	52	42	87	71
9A	3.50	27	25	91	53
9B	3.00	38	38	70	70

+ Applied Load
* Crack appeared when opening was cut

Table 3.2 Test Results.

Test	Applied Load $\frac{M}{V}$ at Opening (ft)	Total Load $\frac{M}{V}$ at opening (ft)	Total Load $\frac{M}{Vd}$ at opening	Maximum Total Load at Opening M (in.-kips)	Maximum Total Load at Opening V (kips)	Failure Mode
1	3.50	3.54	2.06	1606	47.8	Rib Failure
2	6.50	6.61	3.85	3095	39.0	Rib Failure
3	45.20	44.80	26.07	6075	11.3	Crushing at Failure
4A	6.50	6.63	3.86	2603	32.7	Rib Failure
4B	6.50	6.62	3.85	3096	39.0	Rib Failure
5A	6.50	6.67	3.88	2768	34.6	Rib Failure
5B	6.50	6.65	3.87	2568	32.2	Rib Failure
6A	0.00	0.00	0.00	0.0	41.0	Rib Failure
6B	3.50	3.53	2.05	2070	48.9	Rib Failure-Diag. Tension
7A	3.50	3.53	2.05	1845	43.5	Long. Shear
7B	6.50	6.61	3.85	3379	42.6	Long. Shear
8A	3.28	3.32	3.93	774	19.4	Rib Failure-Diag. Tension
8B	2.45	2.49	2.95	427	14.3	Rib Failure-Diag. Tension
9A	3.50	3.56	2.07	1474	34.5	Rib Failure
9B	3.00	3.13	1.82	1775	47.3	Rib Failure

Table 3.3 Relative Deflection at Failure.

Test	Applied $\frac{M}{V}$ (ft)	δ_m^* (in.)	δ_o^+ (in.)	$\bar{\delta}^t$
1	3.50	0.72	0.77	1.07
2	6.50	0.74	0.60	0.81
3	45.20	4.00	0.10	0.03
4A	6.50	0.58	0.71	1.22
4B	6.50	1.31	1.27	0.97
5A	6.50	1.95	1.88	0.96
5B	6.50	1.04	1.26	1.21
6A	0.00	1.05	2.38	2.27
6B	3.50	1.36	1.43	1.05
7A	3.50	0.88	0.82	0.93
7B	6.50	0.99	0.51	0.52
8A	3.30	0.61	0.42	0.69
8B	2.50	0.55	0.70	1.27
9A	3.50	0.96	1.61	1.68
9B	3.00	0.98	1.27	1.30

* δ_m = Deflection at point of maximum moment.

\+ δ_o = Deflection across web opening.

t $\bar{\delta} = \delta_o/\delta_m$

Table 4.1 Ratios of Test to Calculated Strength for the Strength Model.

Test[t]	Test: Shear kips	Test: Moment in.-kips	Test/Theory Ratio
1	37.8	1606.0	0.919
2	39.0	3095.0	0.993
3	11.3	6075.0	1.060
4A	32.7	2603.0	1.128
4B	39.0	3096.0	1.314
5A	34.6	2768.0	0.949
5B	32.2	2568.0	0.995
6A	41.0	0.0	1.118
6B	48.9	2070.0	1.027
7A	43.5	1845.0	1.092
7B	42.6	3379.0	1.128
8A	19.4	774.0	0.942
8B	14.3	427.0	0.947
9A	34.5	1474.0	0.962
9B	47.3	1755.0	1.006
Mean*			1.011
Std. Dev.*			0.070
R0	18.2	752.0	0.904
R1	26.0	978.0	1.059
R2	28.7	2904.0	1.089
R3	16.4	3993.0	1.135
R4	13.1	3212.0	1.102
R5	27.6	1038.0	0.995
R6	21.2	786.0	1.076
R7	30.5	1134.0	1.001
R8	28.9	1075.0	1.001
Mean			1.040
Std. Dev.			0.071

Ribbed slab summary:

Mean*	1.023
Std. Dev.*	0.070

Test[t]	Test: Shear kips	Test: Moment in.-kips	Test/Theory Ratio
C1	33.4	2886.0	1.095
C2	36.8	4107.0	1.114
C3	14.0	5468.0	1.118
C4	47.6	1723.0	1.093
C5	48.1	3511.0	1.129
C6	40.4	1471.0	1.079
G1	32.7	791.0	1.164
G2	26.5	1296.0	1.018
Mean			1.101
Std. Dev.			0.043
CHO3	35.7	634.0	1.126
CHO4	46.7	1477.0	0.999
CHO5	17.9	2319.0	1.013
CHO6	40.6	721.0	1.064
CHO7	20.6	2664.0	0.960
Mean			1.032
Std. Dev.			0.064

Solid slab summary:

Mean	1.074
Std. Dev.	0.060

Overall summary:

Mean*	1.042
Std. Dev.*	0.071

t G - Granade (19)
C - Clawson and Darwin (9, 11)
CHO - Cho (8)
R - McGill Tests (32, 34)

* Tests 4A and 4B excluded from calculations.

Table 5.1 Ratios of Test to Calculated Strength for the Redwood and Poumbouras (33) Procedure, the Strength Model (Chapter 4), and Strength Design Methods I, II, and III.

Test #	Test Shear kips	Test Moment in.-kips	Test/Theory Ratio: Redwood-Poumbouras Procedure	Model	Design Method I	Design Method II	Design Method III
1	37.8	1606.0	0.895	0.919	0.968	0.913	0.967
2	39.0	3095.0	0.986	0.993	1.053	1.026	1.080
3	11.3	6075.0	1.014	1.060	1.027	1.027	1.028
4A	32.7	2603.0	1.046	1.128	1.157	1.083	1.132
4B	39.0	3096.0	1.212	1.314	1.360	1.238	1.298
5A	34.6	2768.0	0.919	0.949	1.009	0.960	1.009
5B	32.2	2568.0	0.977	0.995	1.058	1.020	1.074
6A	41.0	0.0	1.137	1.118	1.135	1.132	1.199
6B	48.9	2070.0	1.016	1.027	1.080	1.044	1.093
7A	43.5	1845.0	0.984	1.092	1.035	1.000	1.005
7B	42.6	3379.0	1.030	1.128	1.093	1.087	1.097
8A	19.4	774.0	1.081	0.942	0.971	0.985	0.990
8B	14.3	427.0	0.918	0.947	0.926	0.934	0.928
9A	34.5	1474.0	1.116	0.962	0.937	0.976	0.973
9B	47.3	1755.0	1.362	1.006	0.987	1.011	1.018
Mean*			1.033	1.011	1.021	1.009	1.035
Std. Dev.*			0.123	0.070	0.063	0.059	0.072
R0	18.2	752.0	0.976	0.904	0.941	0.950	0.955
R1	26.0	978.0	1.090	1.059	1.100	1.114	1.163
R2	28.7	2904.0	1.234	1.089	1.191	1.326	1.384
R3	16.4	3993.0	1.126	1.135	1.080	1.084	1.084
R4	13.1	3212.0	1.068	1.102	1.118	1.113	1.118
R5	27.6	1038.0	1.171	0.995	1.031	1.040	1.081
R6	21.2	786.0	1.111	1.076	1.127	1.124	1.191
R7	30.5	1134.0	1.017	1.001	1.022	1.043	1.040
R8	28.9	1075.0	1.091	1.001	1.015	1.092	1.098
Mean			1.098	1.040	1.069	1.098	1.124
Std. Dev.			0.077	0.071	0.075	0.101	0.119
Ribbed slab summary:							
Mean*			1.060	1.023	1.041	1.045	1.072
Std. Dev.*			0.109	0.070	0.070	0.089	0.102

*Tests 4A and 4B excluded from calculations.

Table 5.1 Continued.

Test #	Test Shear kips	Test Moment in.-kips	Test/Theory Ratio: Redwood-Poumbouras Procedure	Test/Theory Ratio: Model	Test/Theory Ratio: Design Method I	Test/Theory Ratio: Design Method II	Test/Theory Ratio: Design Method III
C1	33.4	2886.0	1.417	1.095	1.143	1.187	1.192
C2	36.8	4107.0	1.115	1.114	1.138	1.123	1.128
C3	14.0	5468.0	1.156	1.118	1.139	1.139	1.139
C4	47.6	1723.0	1.037	1.093	1.056	1.051	1.056
C5	48.1	3511.0	1.087	1.129	1.127	1.128	1.134
C6	40.4	1471.0	1.294	1.079	1.055	1.122	1.128
G1	32.7	791.0	1.865	1.164	1.198	1.284	1.300
G2	26.5	1296.0	1.511	1.018	1.087	1.143	1.153
Mean			1.310	1.101	1.118	1.147	1.154
Std. Dev.			0.279	0.043	0.049	0.067	0.070
CHO3	35.7	634.0	2.573	1.126	1.160	1.191	1.199
CHO4	46.7	1477.0	1.513	0.999	1.064	1.061	1.071
CHO5	17.9	2319.0	1.019	1.013	0.978	0.978	0.979
CHO6	40.6	721.0	2.856	1.064	1.276	1.311	1.320
CHO7	20.6	2664.0	1.046	0.960	0.954	0.958	0.959
Mean			1.801	1.032	1.086	1.100	1.106
Std. Dev.			0.862	0.064	0.133	0.149	0.153
Solid slab summary:							
Mean			1.499	1.074	1.105	1.129	1.135
Std. Dev.			0.596	0.060	0.087	0.103	0.106
Overall summary:							
Mean*			1.223	1.042	1.065	1.076	1.095
Std. Dev.*			0.423	0.071	0.082	0.102	0.106

* Tests 4A and 4B excluded from calculations.

Table 5.2 Ratios of Test to Calculated Strength for the Redwood and Poumbouras (33) Procedure.

Test	Published Ratios (33)	Calculated Ratios*	Calculated Ratios**
R0	0.995	0.976	0.976
R1	1.129	1.131	1.090
R2	1.163	1.158	1.234
R3	1.126	1.126	1.126
R4	1.108	1.095	1.068
R5	1.169	1.171	1.171
R6	1.116	1.112	1.111
R7	1.017	1.014	1.017
R8	1.098	1.091	1.091
Mean	1.102	1.097	1.098
Std. Dev.	0.060	0.064	0.077

* Based on stud capacities from pushout tests (30, 32, 34, 46).
** Based on stud capacities calculated using $E_c = 5000\sqrt{f'_c}$ MPa.

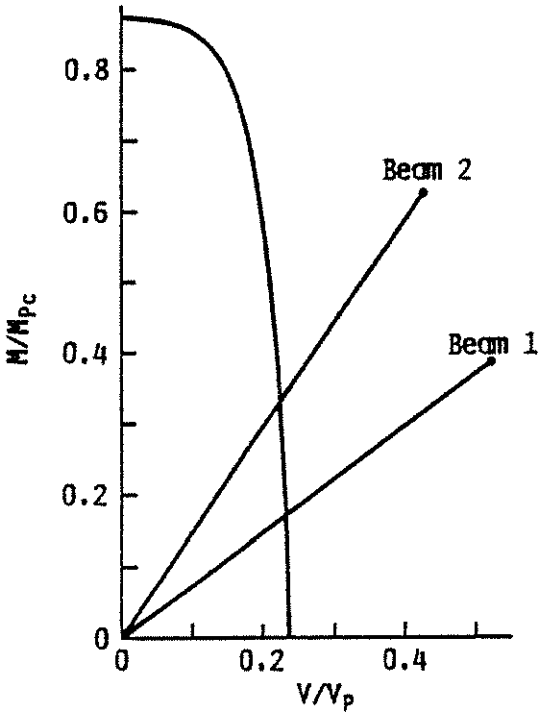

Fig. 1.1 Comparison of Todd-Cooper Model with Granade's Beams (42).

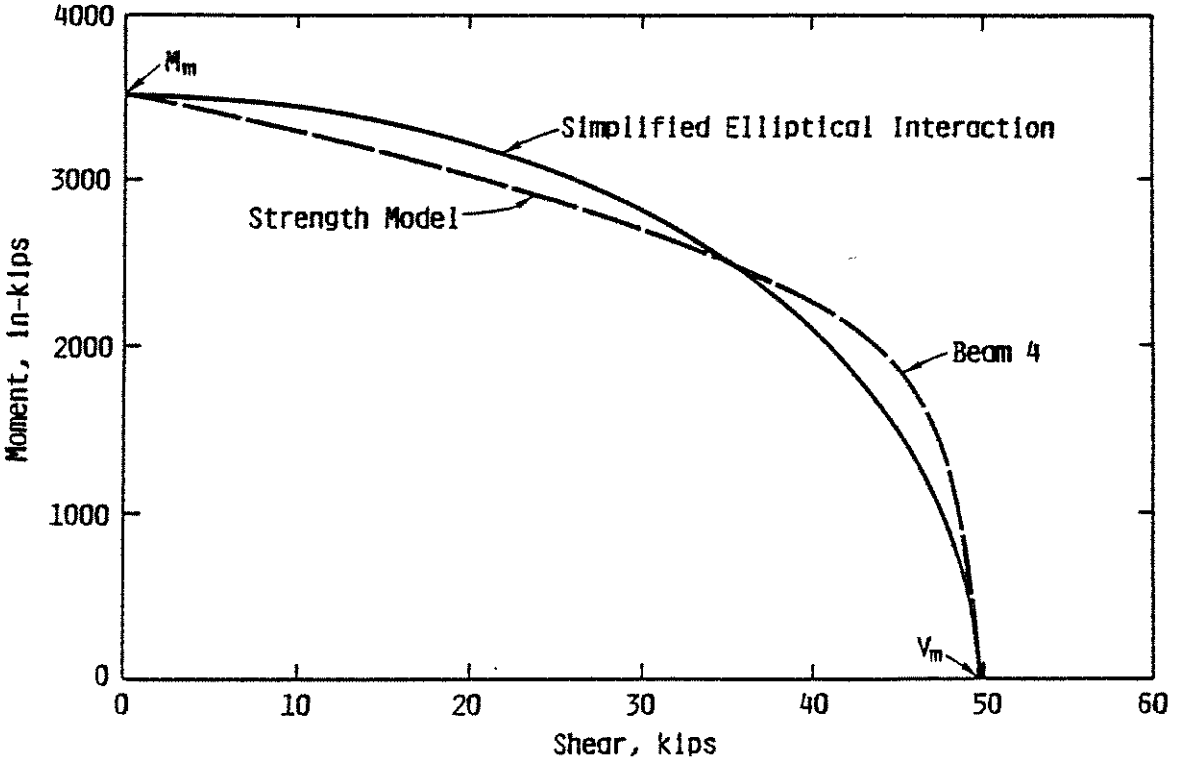

Fig. 1.2 Full Strength Model and Simplified Moment-Shear Interaction Diagrams for Clawson and Darwin (10, 11).

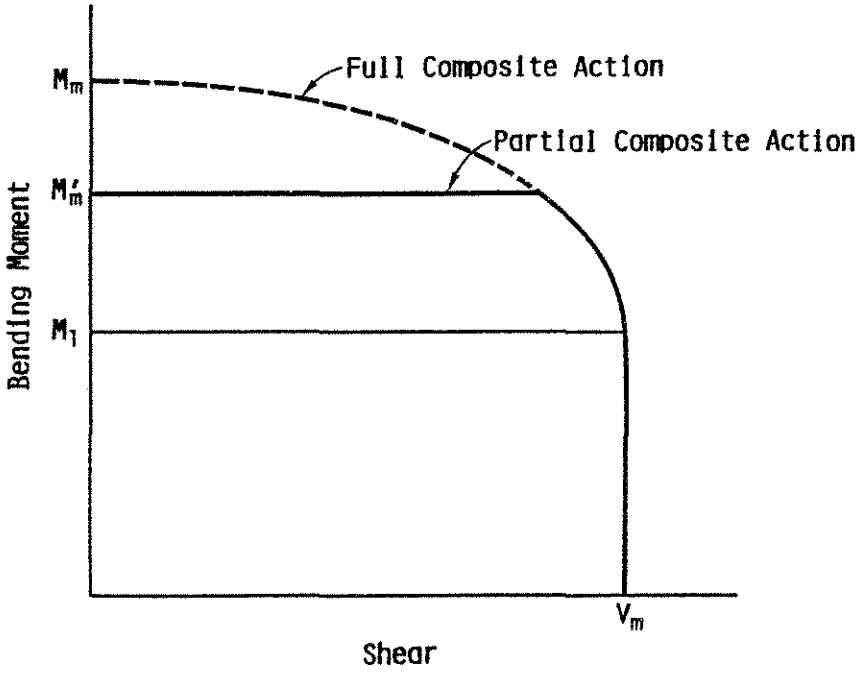

Fig. 1.3 Moment-Shear Interaction Diagram for Redwood and Poumbouras (33).

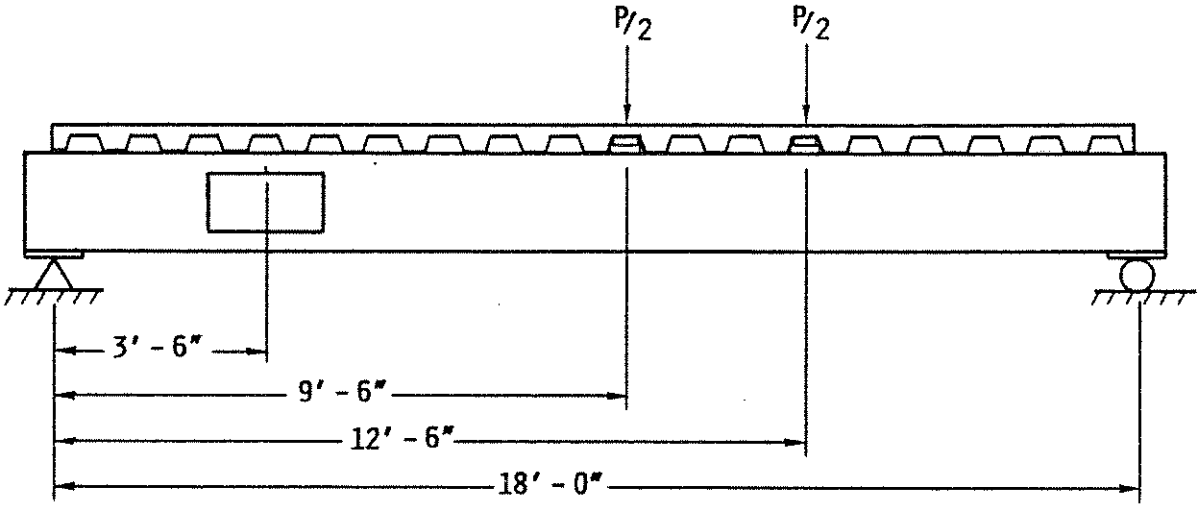

Fig. 2.1 Layout for Test 1.

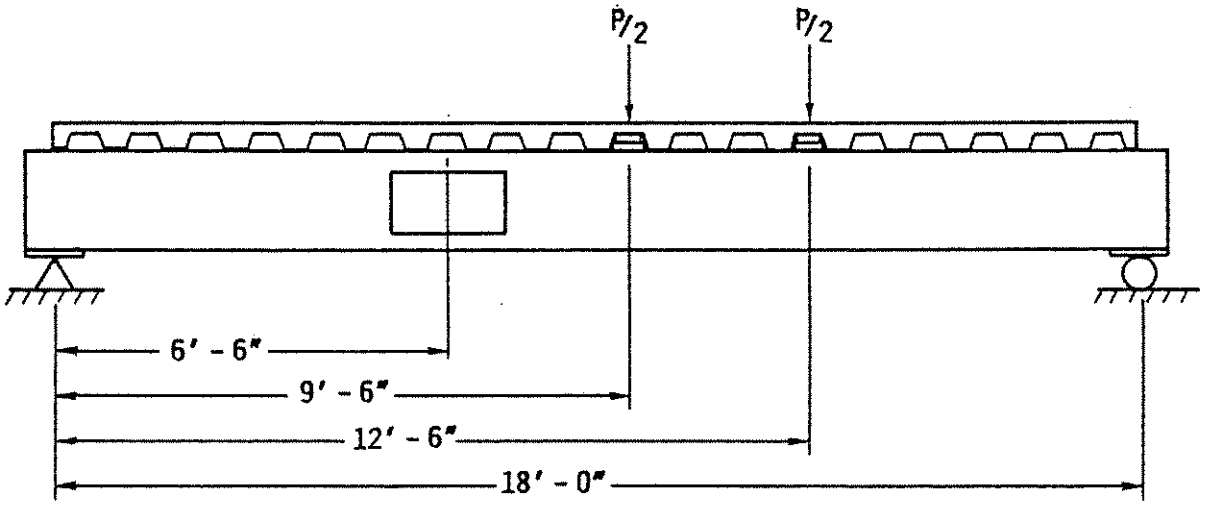

Fig. 2.2 Layout for Test 2.

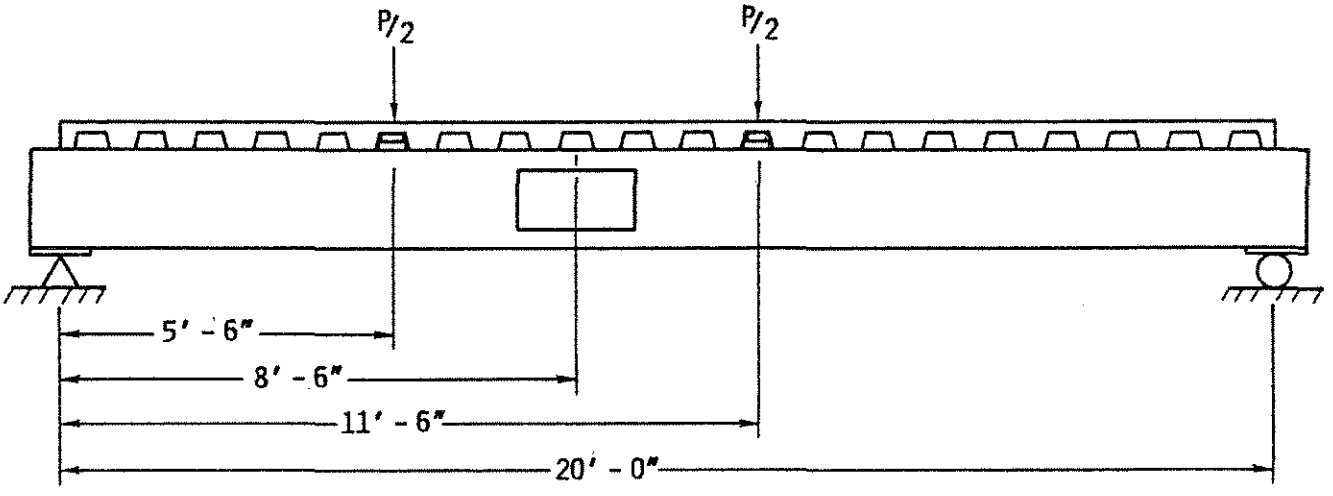

Fig. 2.3 Layout for Test 3.

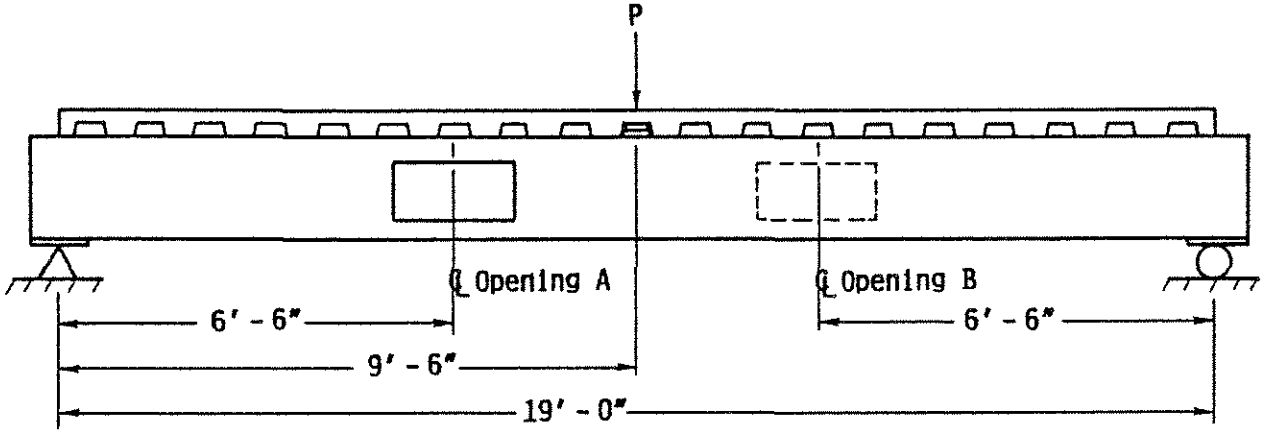

Fig. 2.4 Layout for Tests 4A, 4B, 5A, and 5B.

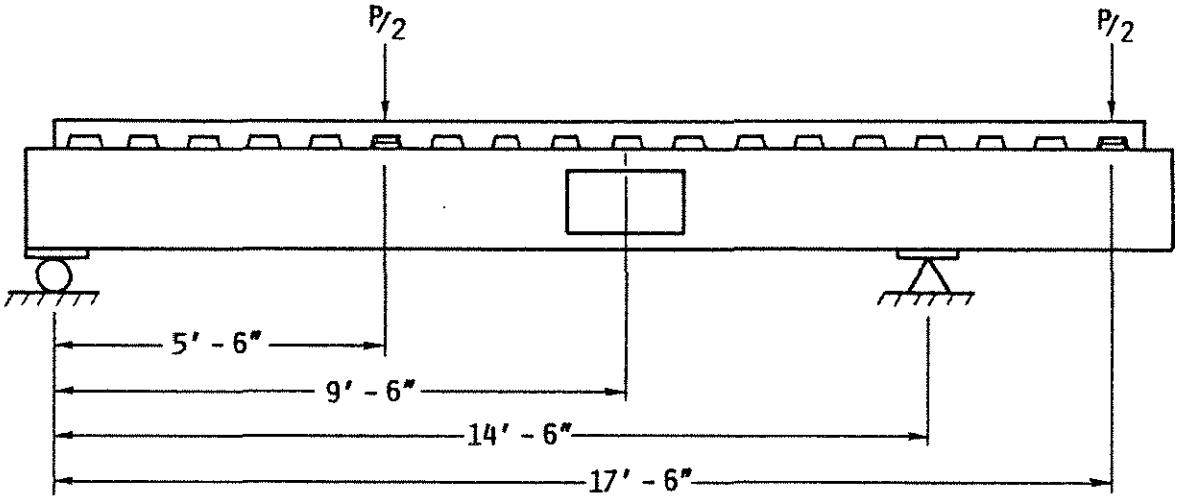

Fig. 2.5 Layout for Test 6A.

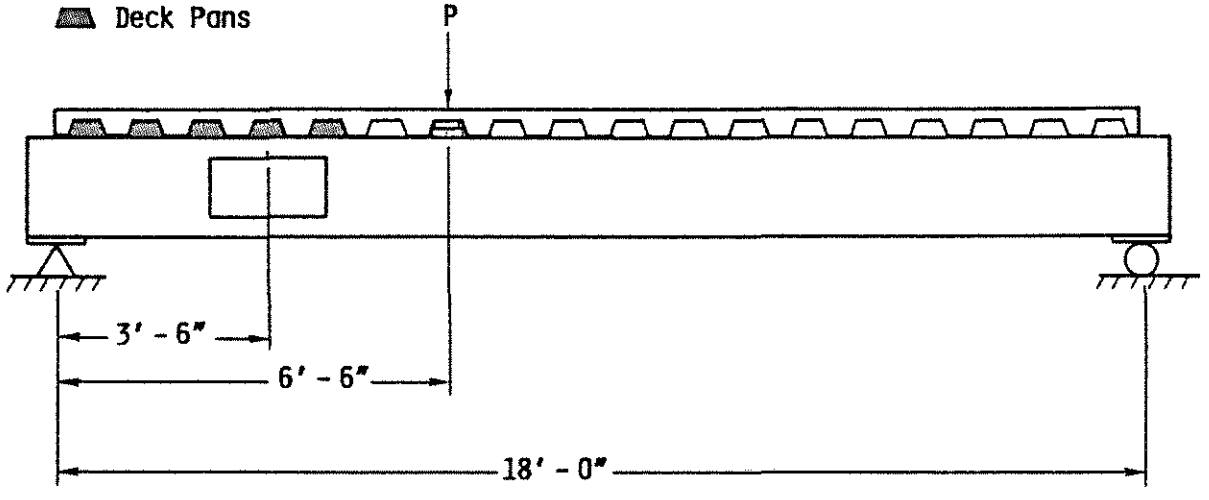

Fig. 2.6 Layout for Test 6B.

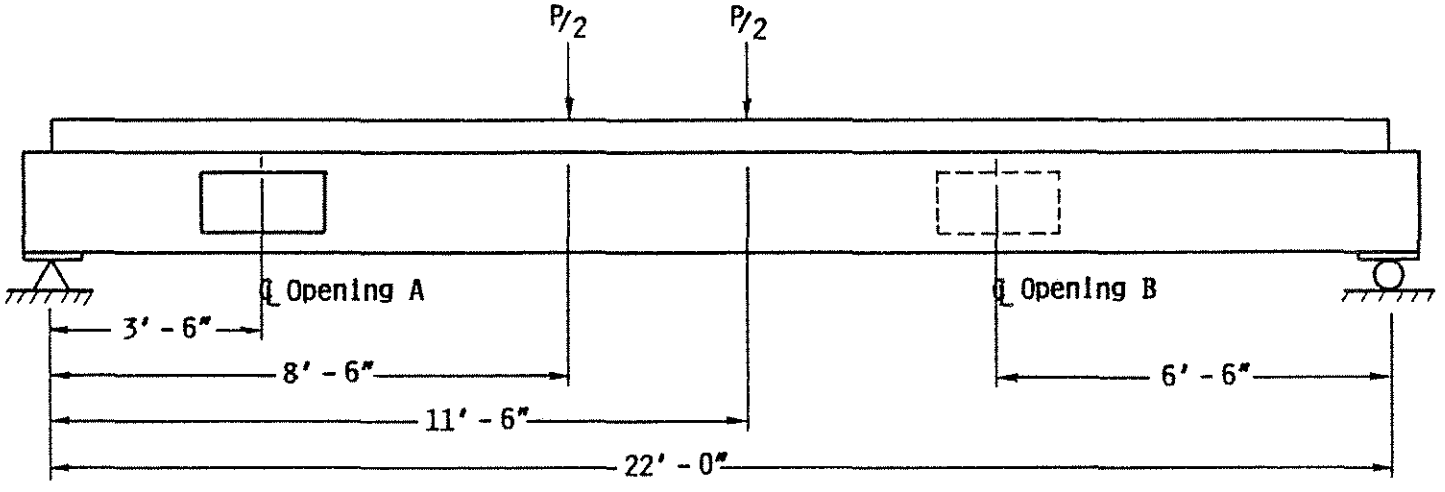

Fig. 2.7 Layout for Test 7A and 7B.

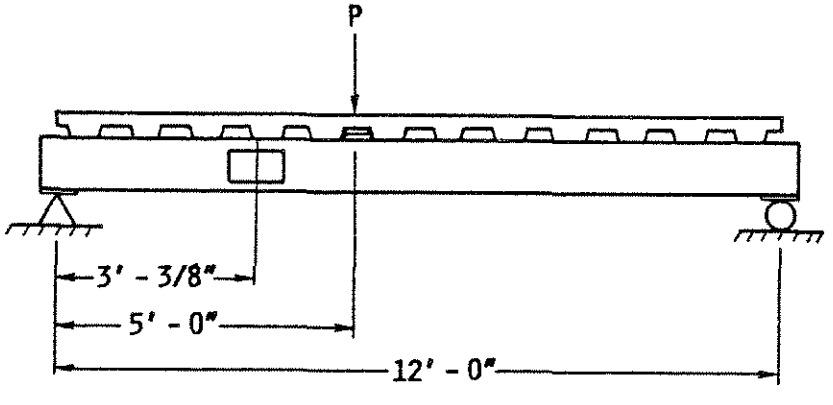

Fig. 2.8 Layout for Test 8A.

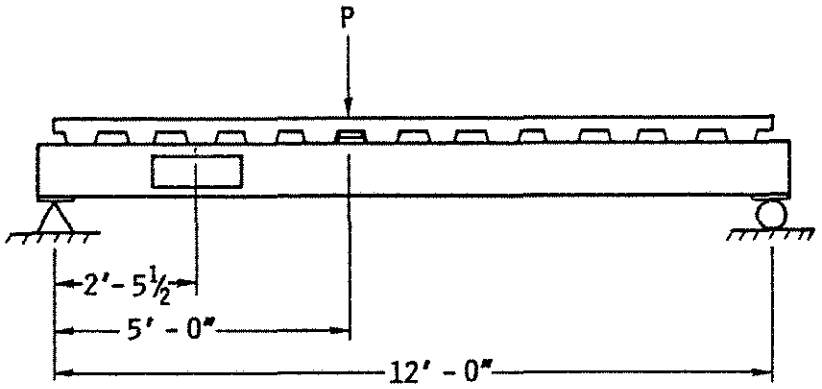

Fig. 2.9 Layout for Test 8B.

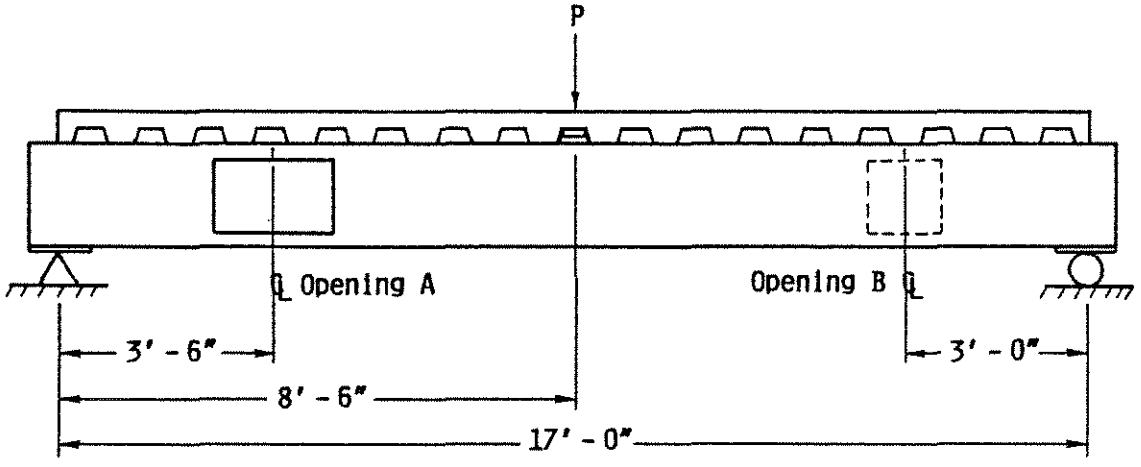

Fig. 2.10 Layout for Tests 9A and 9B.

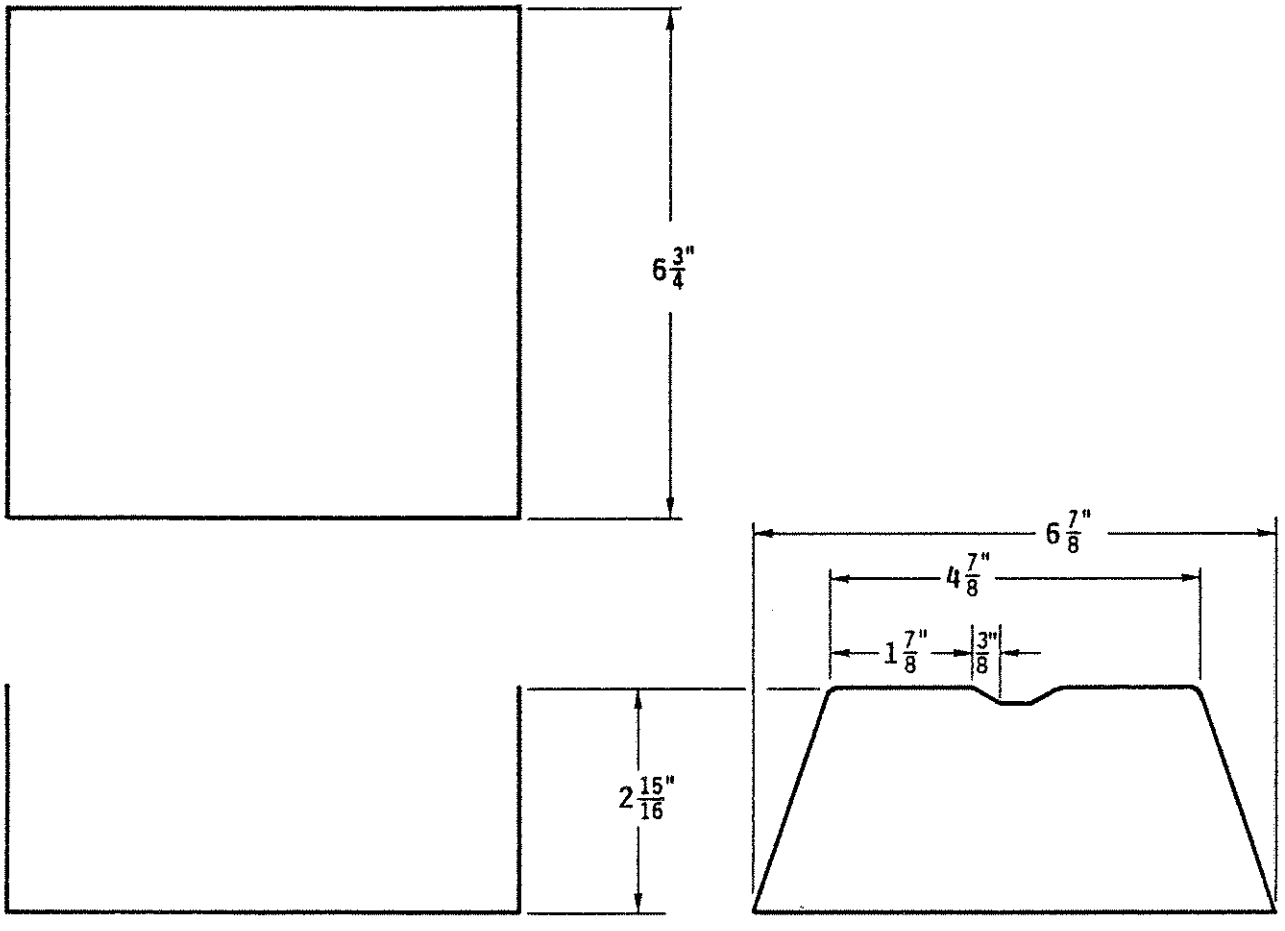

Fig. 2.11 Deck Inserts.

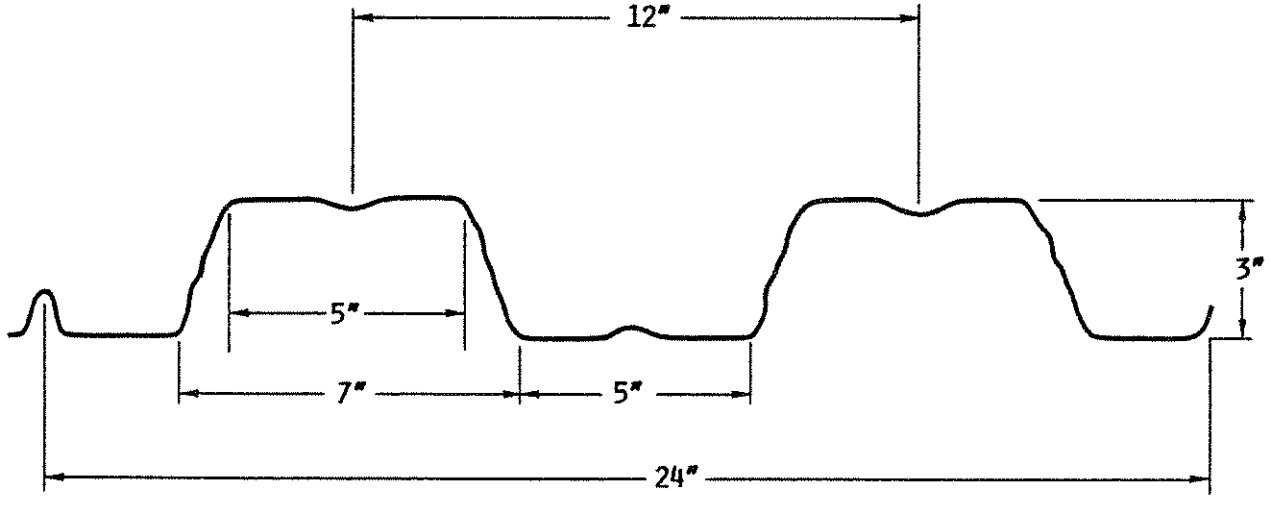

Fig. 2.12 Deck Profile (United Steel Deck).

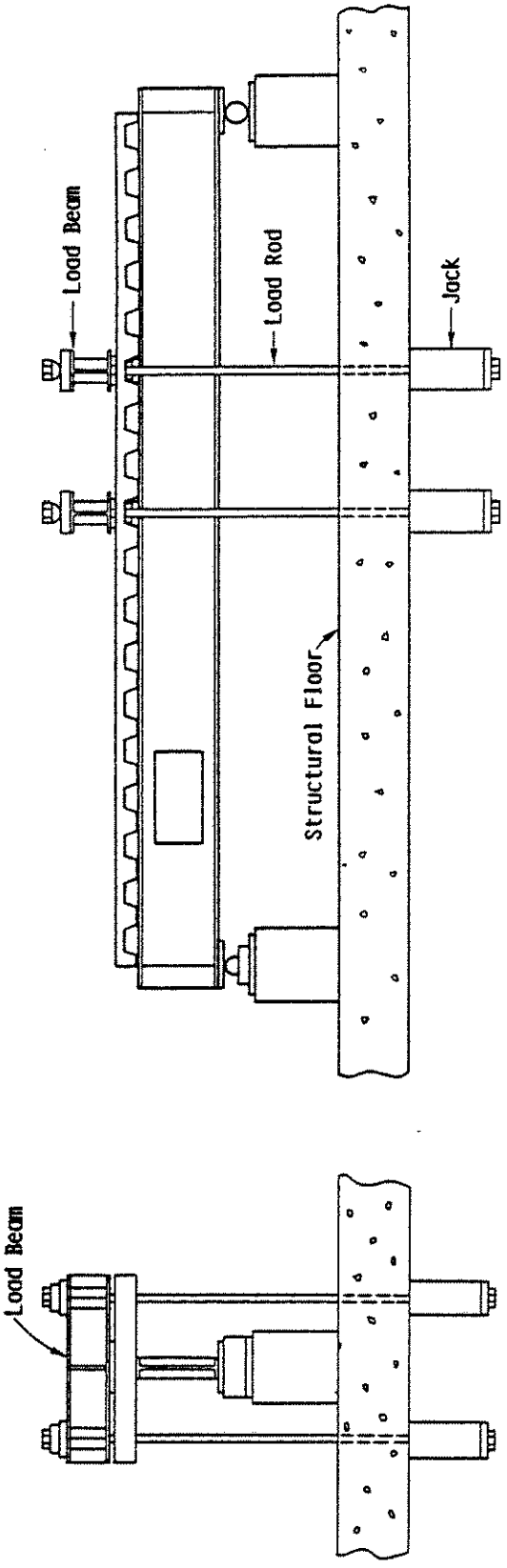

Fig. 2.13 Loading System.

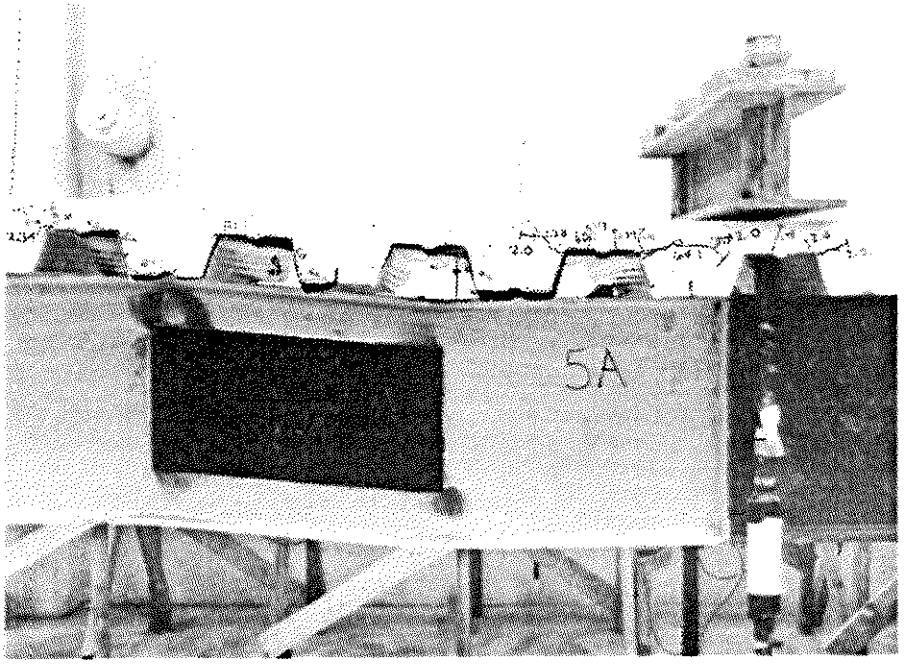

Fig. 3.1 Failure at Web Opening with Low M/V Ratio.

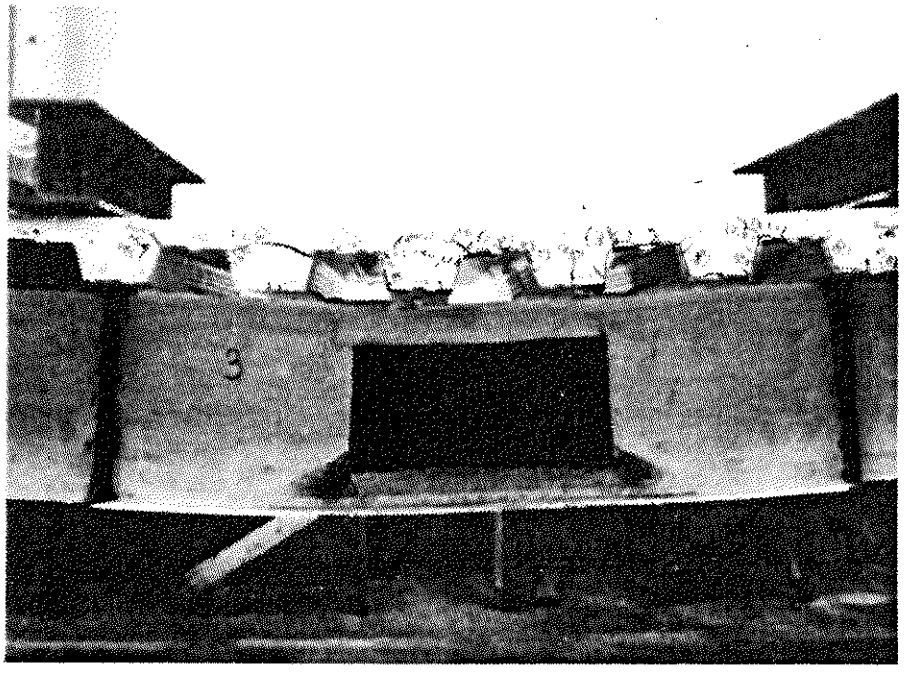

Fig. 3.2 Failure at Web Opening with High M/V Ratio.

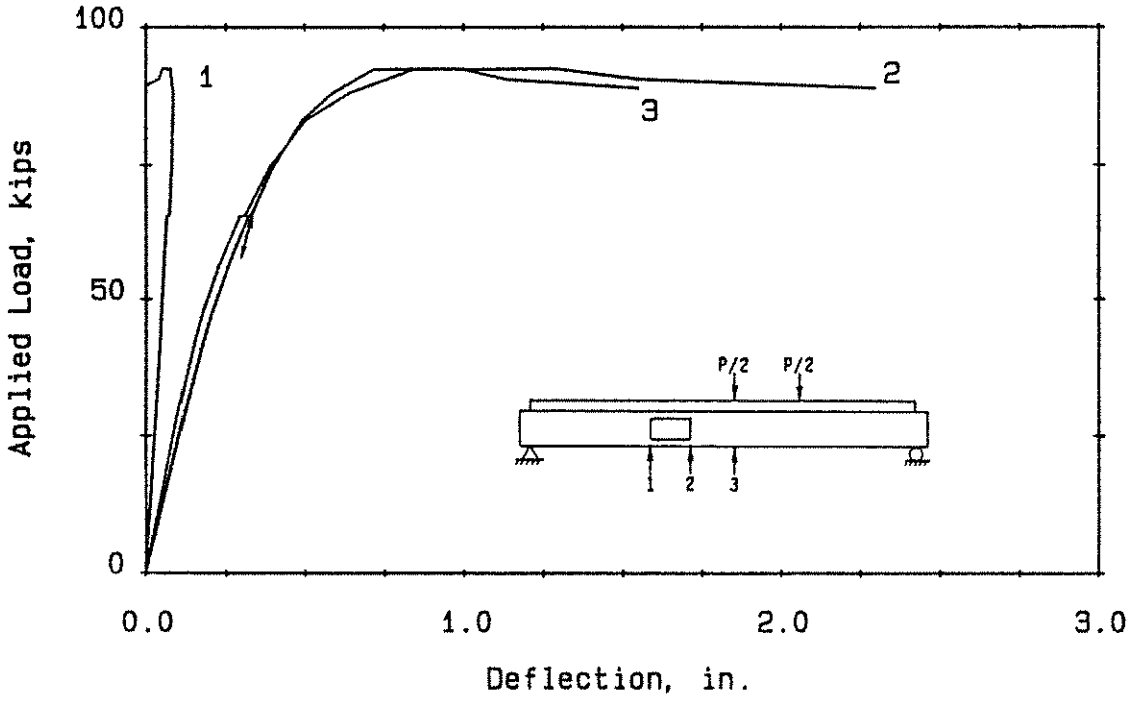

Fig. 3.3 Load-Deflection Curves for Test 1.

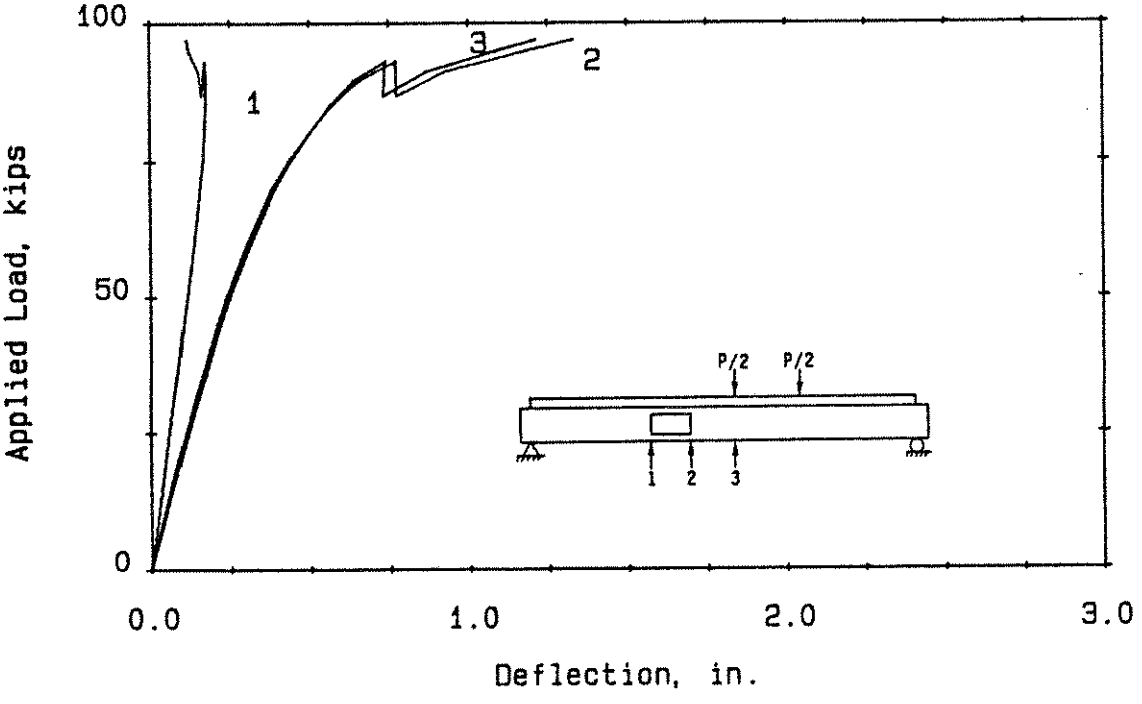

Fig. 3.4 Load-Deflection Curves for Test 2.

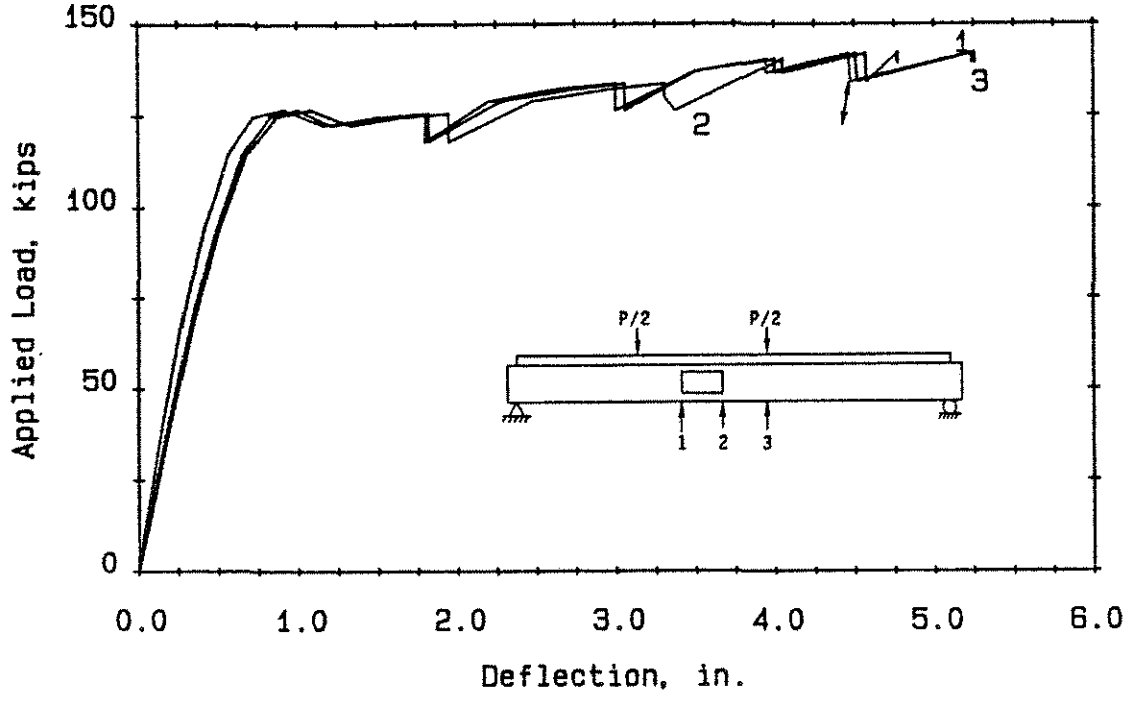

Fig. 3.5 Load-Deflection Curves for Test 3.

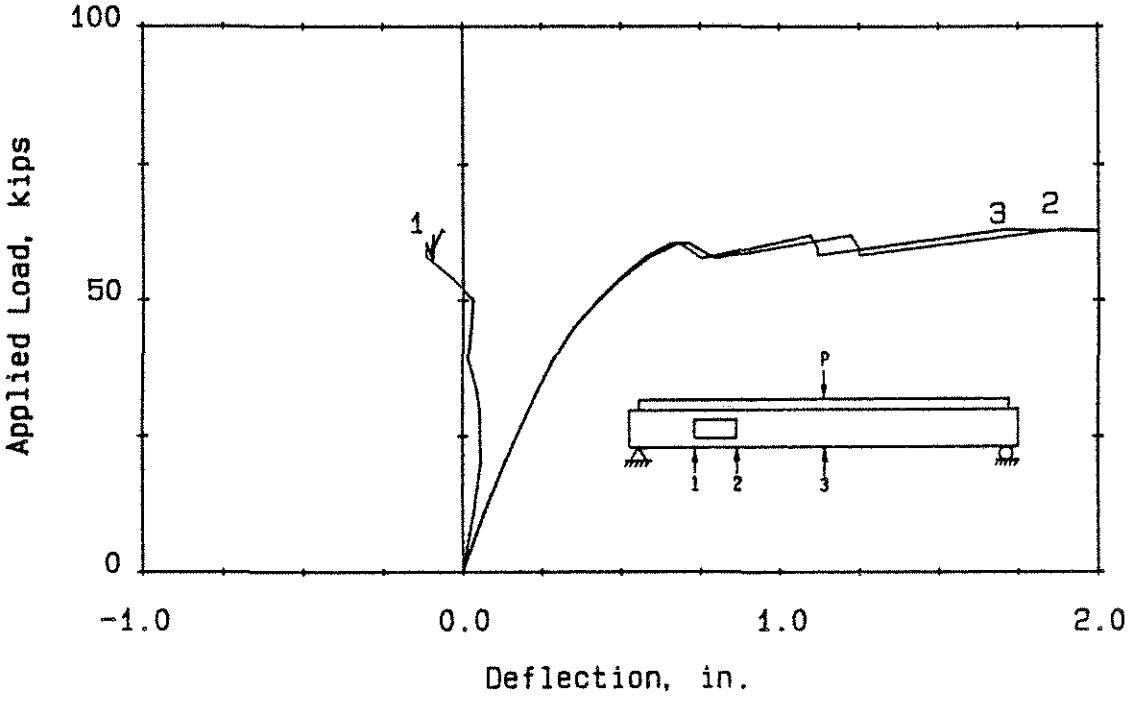

Fig. 3.6 Load-Deflection Curves for Test 4A.

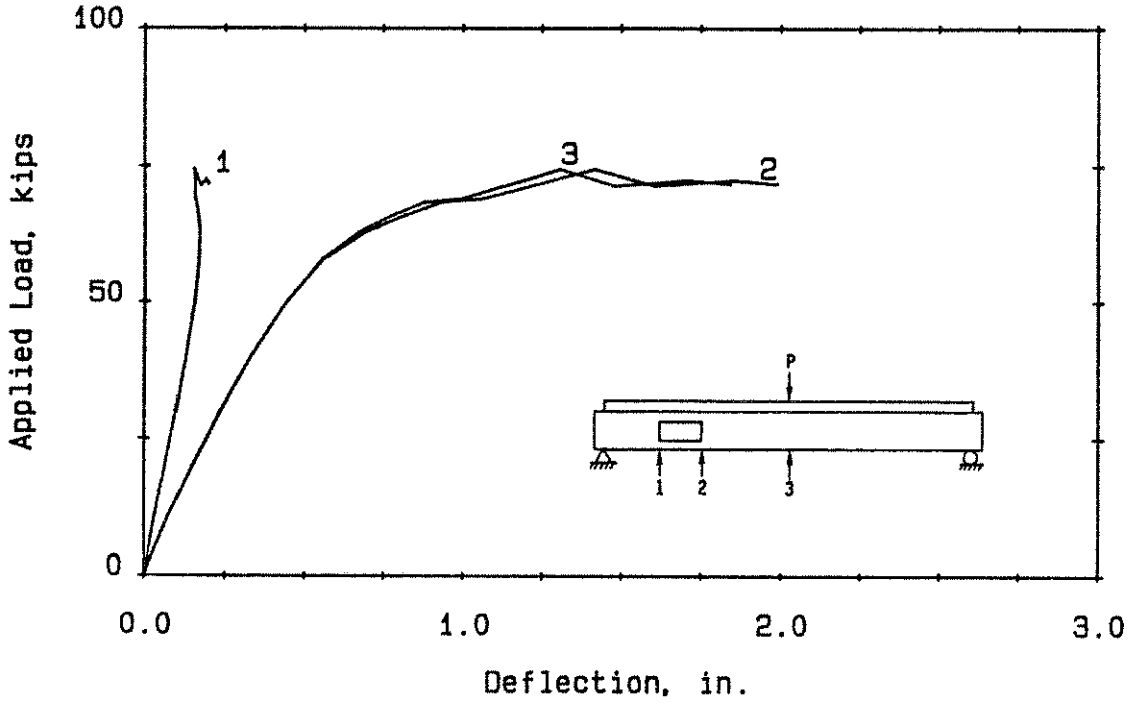

Fig. 3.7 Load-Deflection Curves for Test 4B.

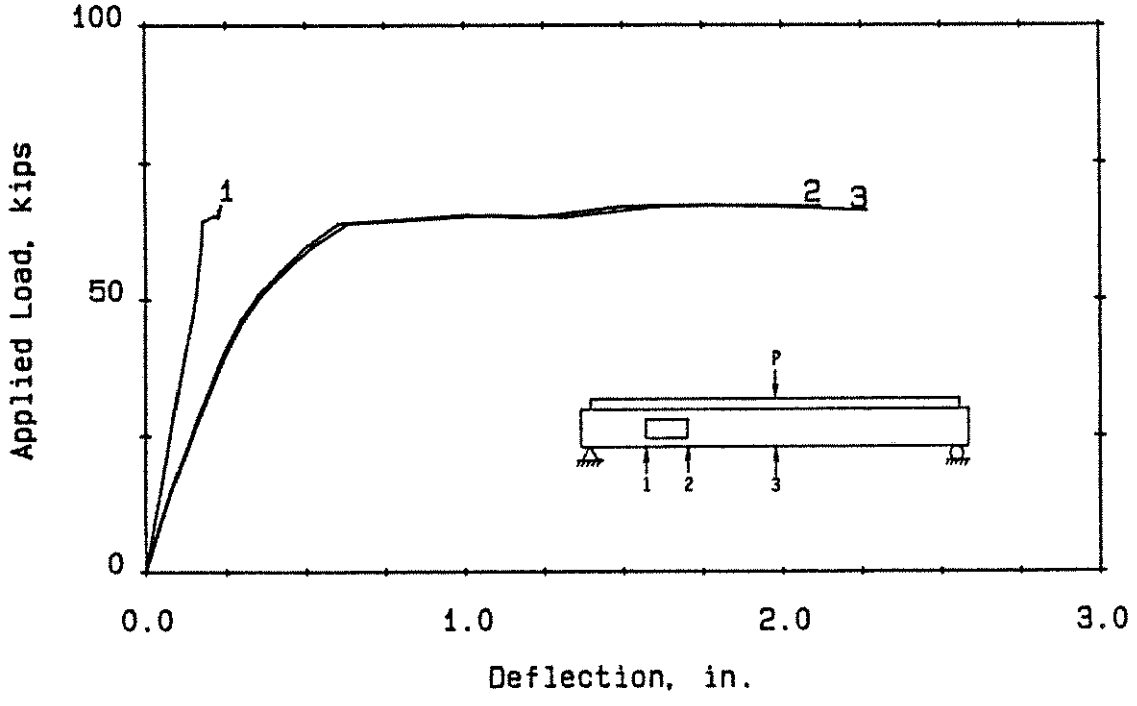

Fig. 3.8 Load-Deflection Curves for Test 5A.

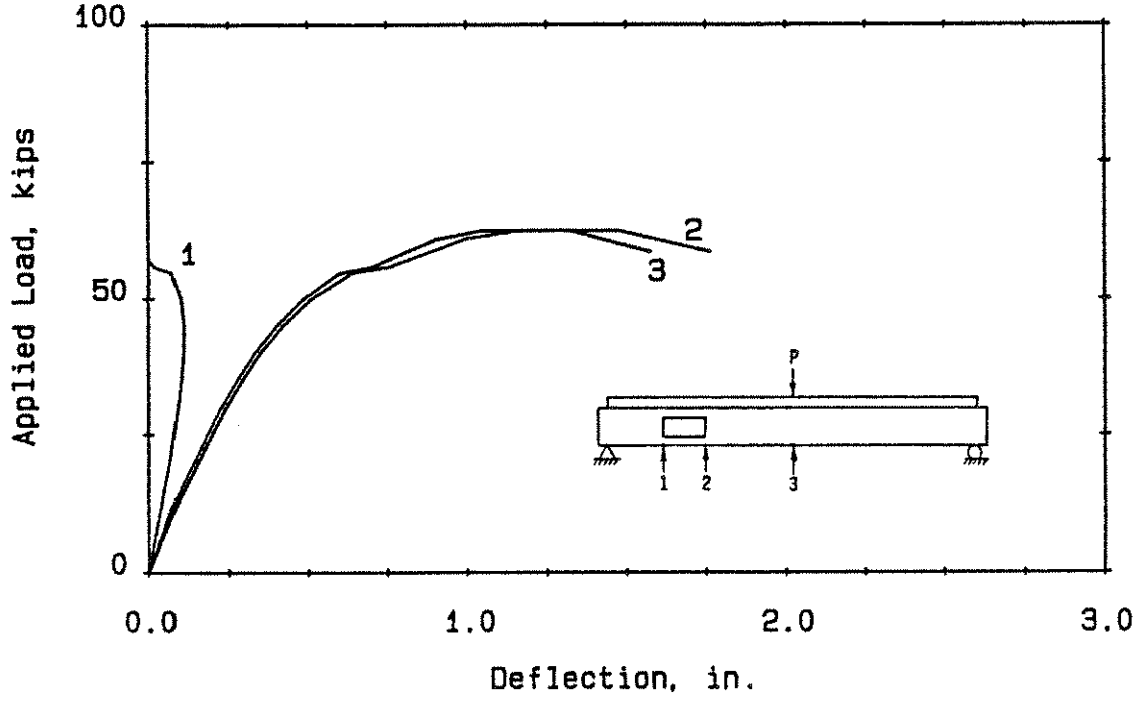

Fig. 3.9 Load-Deflection Curves for Test 5B.

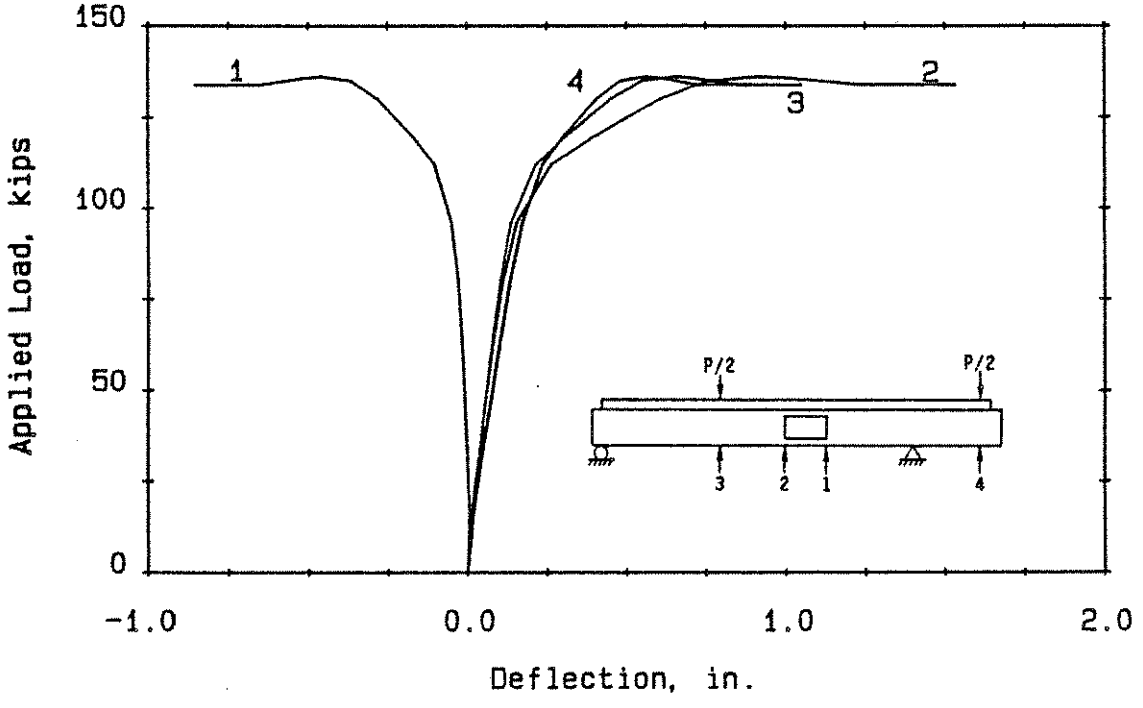

Fig. 3.10 Load-Deflection Curves for Test 6A.

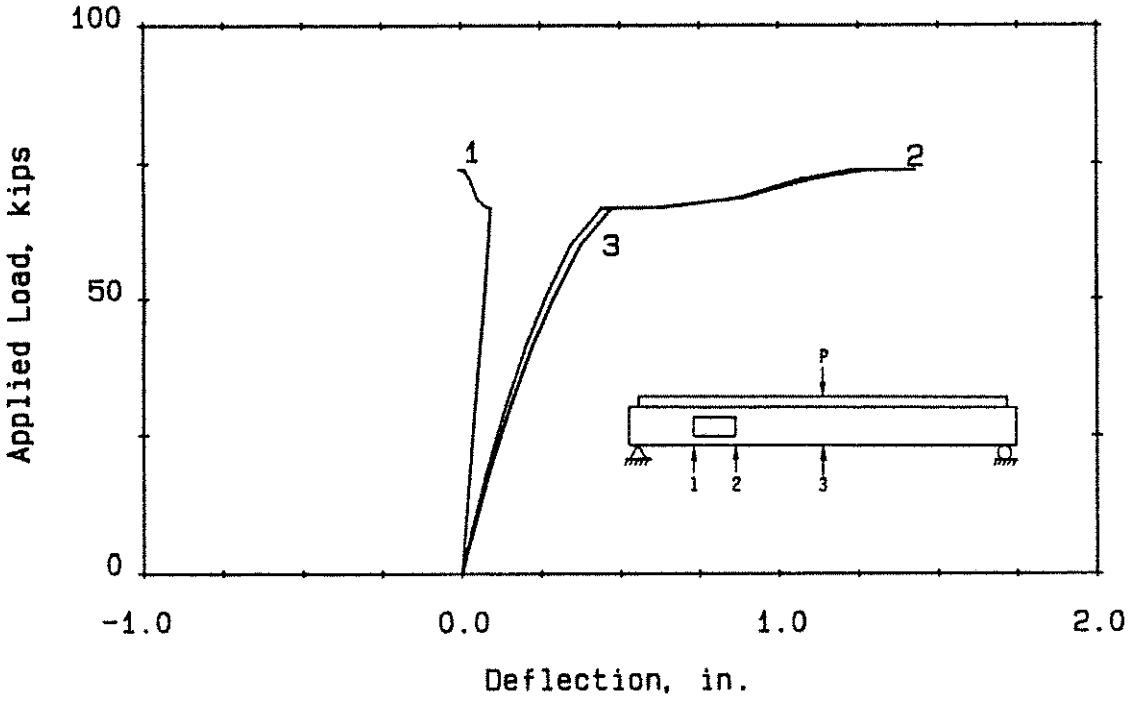

Fig. 3.11 Load-Deflection Curves for Test 6B.

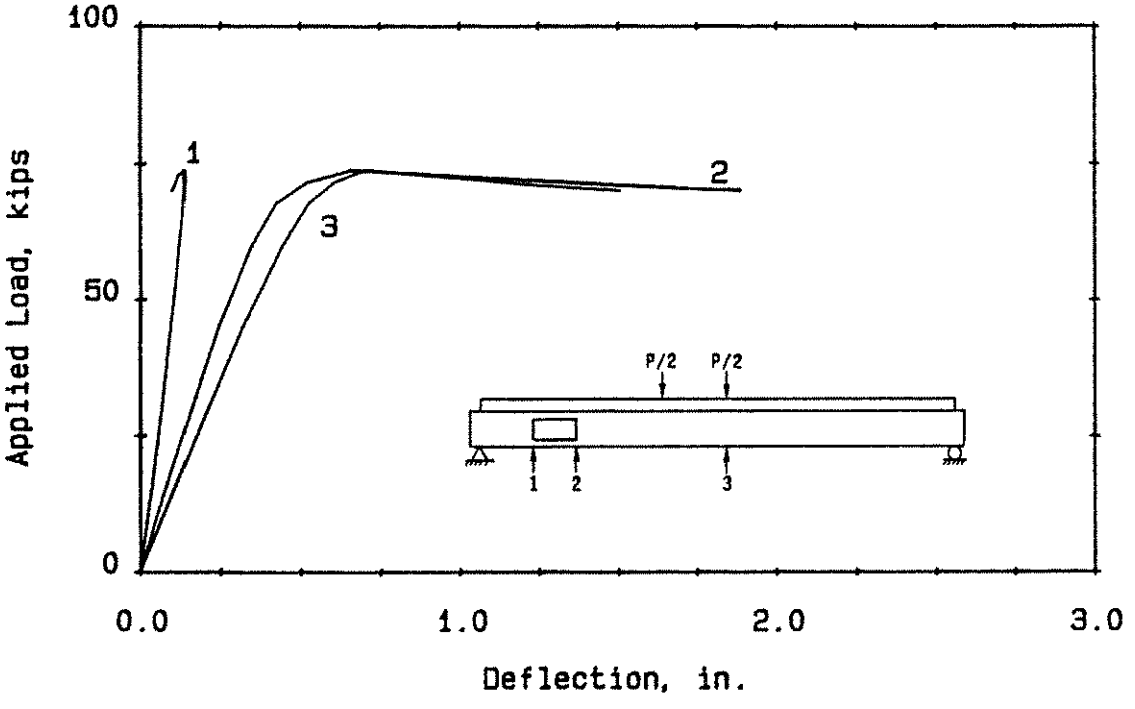

Fig. 3.12 Load-Deflection Curves for Test 7A.

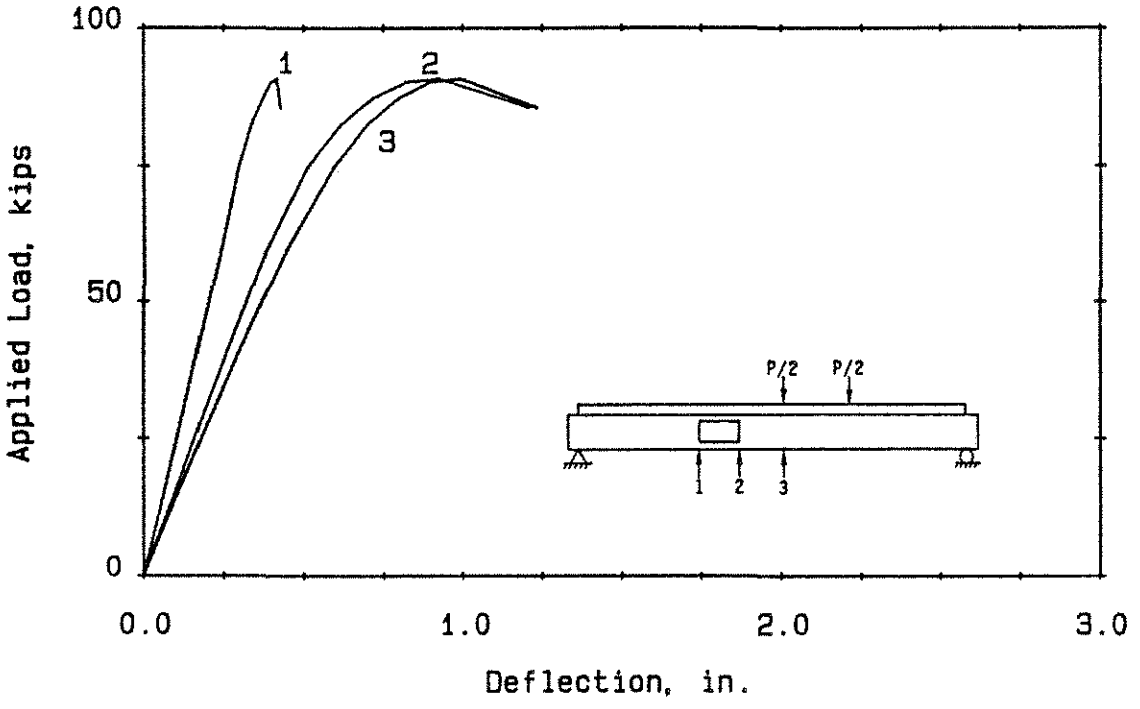

Fig. 3.13 Load-Deflection Curves for Test 7B.

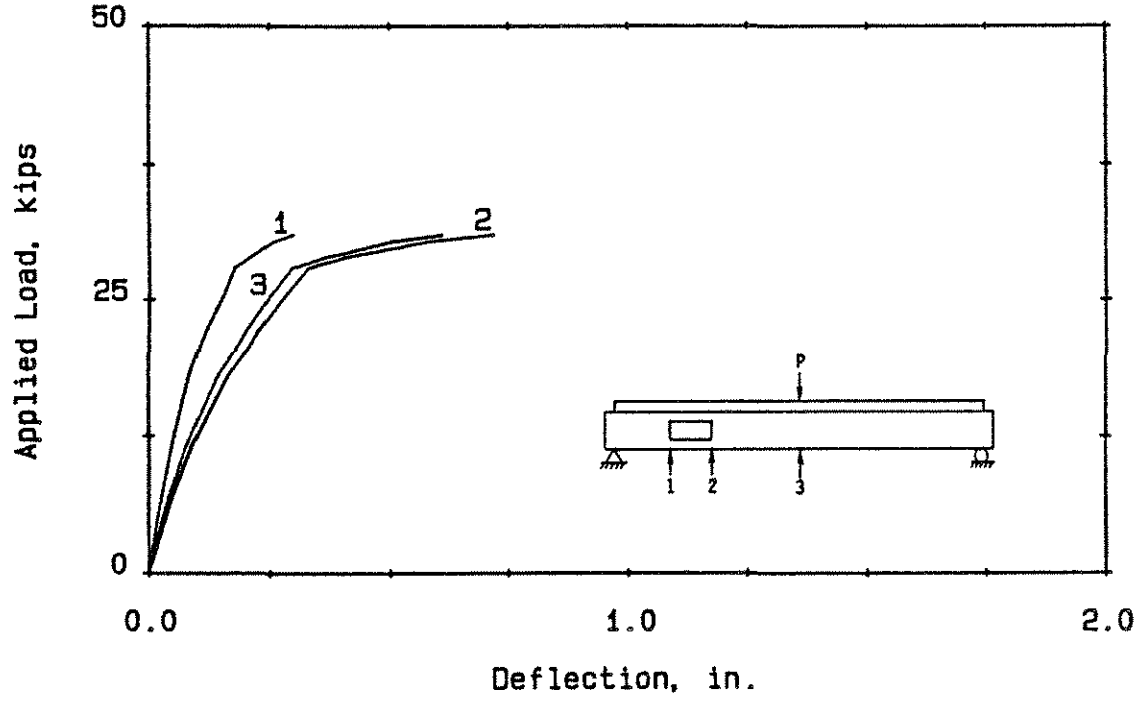

Fig. 3.14 Load-Deflection Curves for Test 8A.

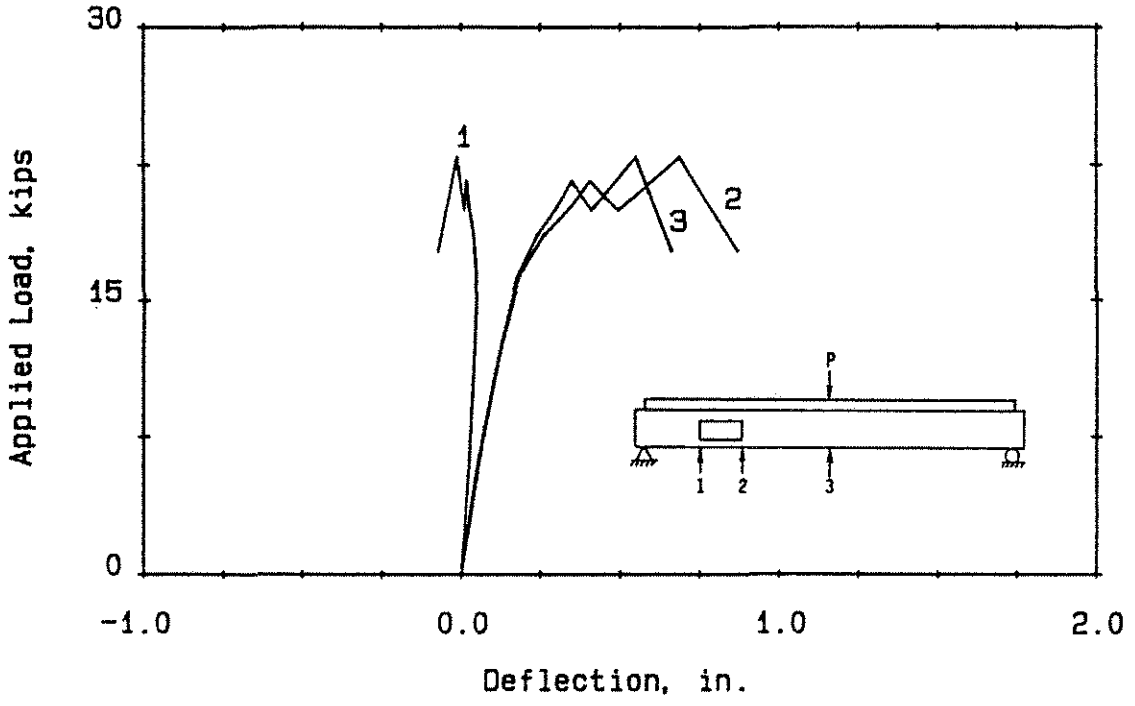

Fig. 3.15 Load-Deflection Curves for Test 8B.

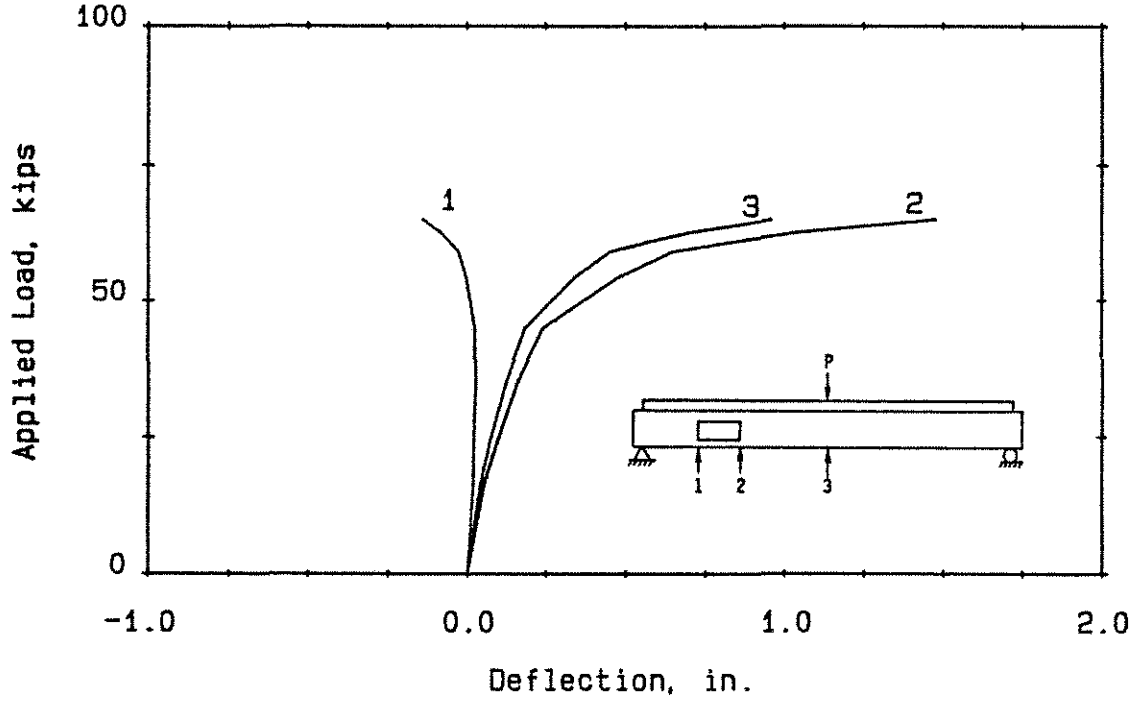

Fig. 3.16 Load-Deflection Curves for Test 9A.

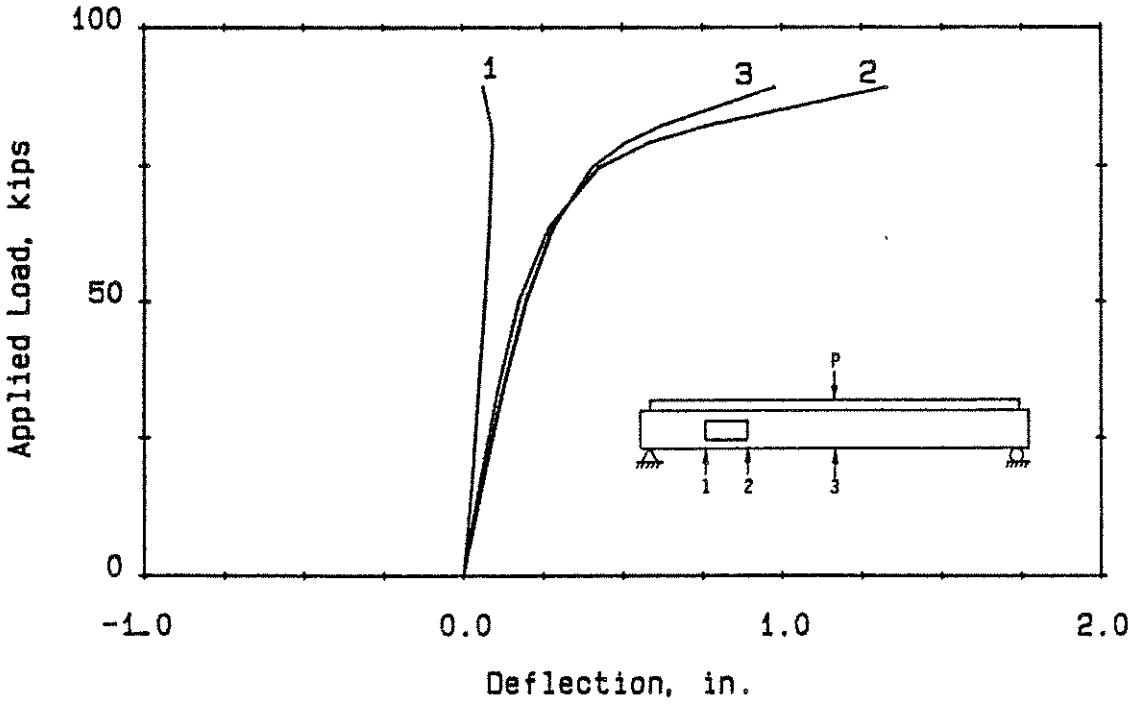

Fig. 3.17 Load-Deflection Curves for Test 9B.

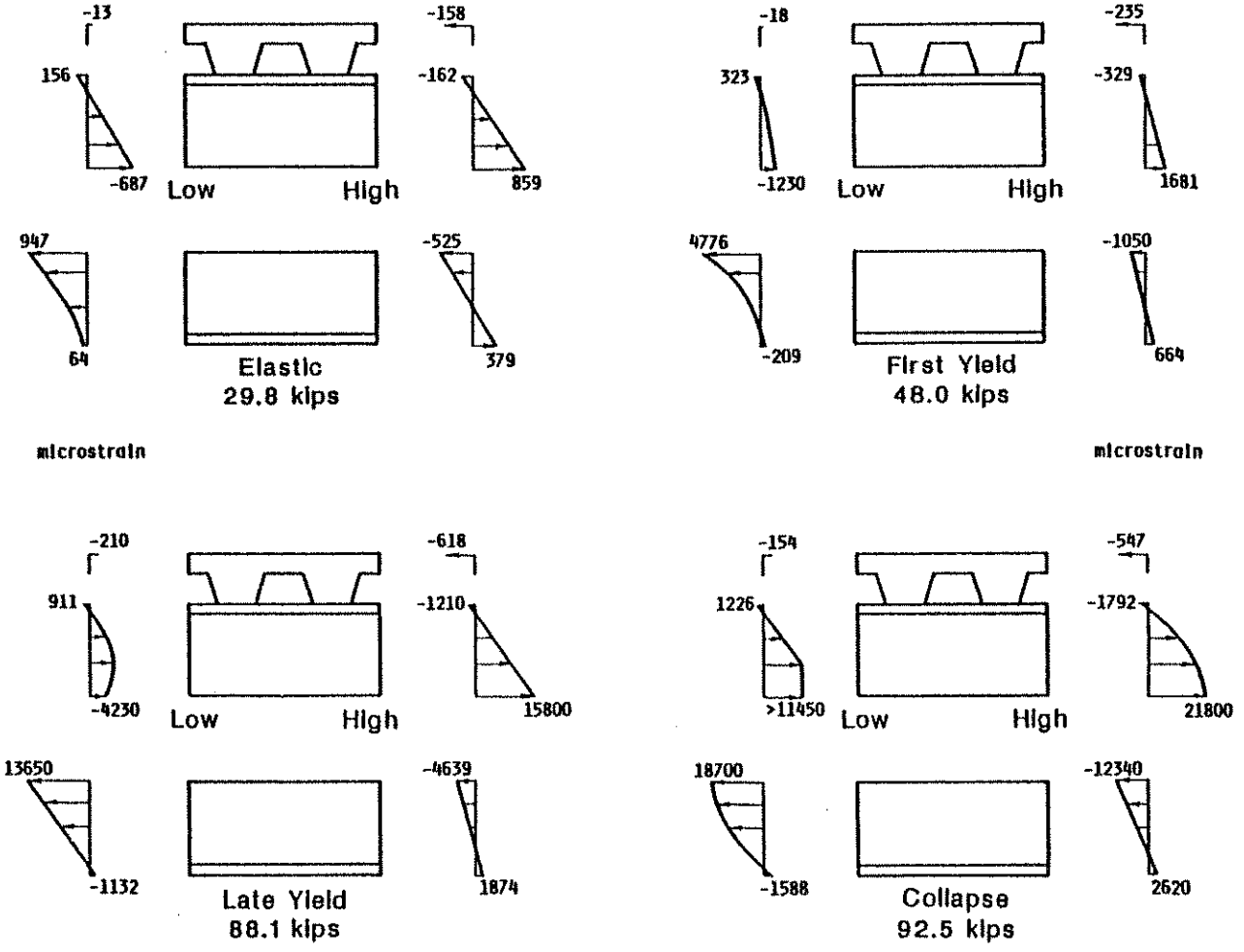

Fig. 3.18 Strain Distributions at the Opening for Test 1.

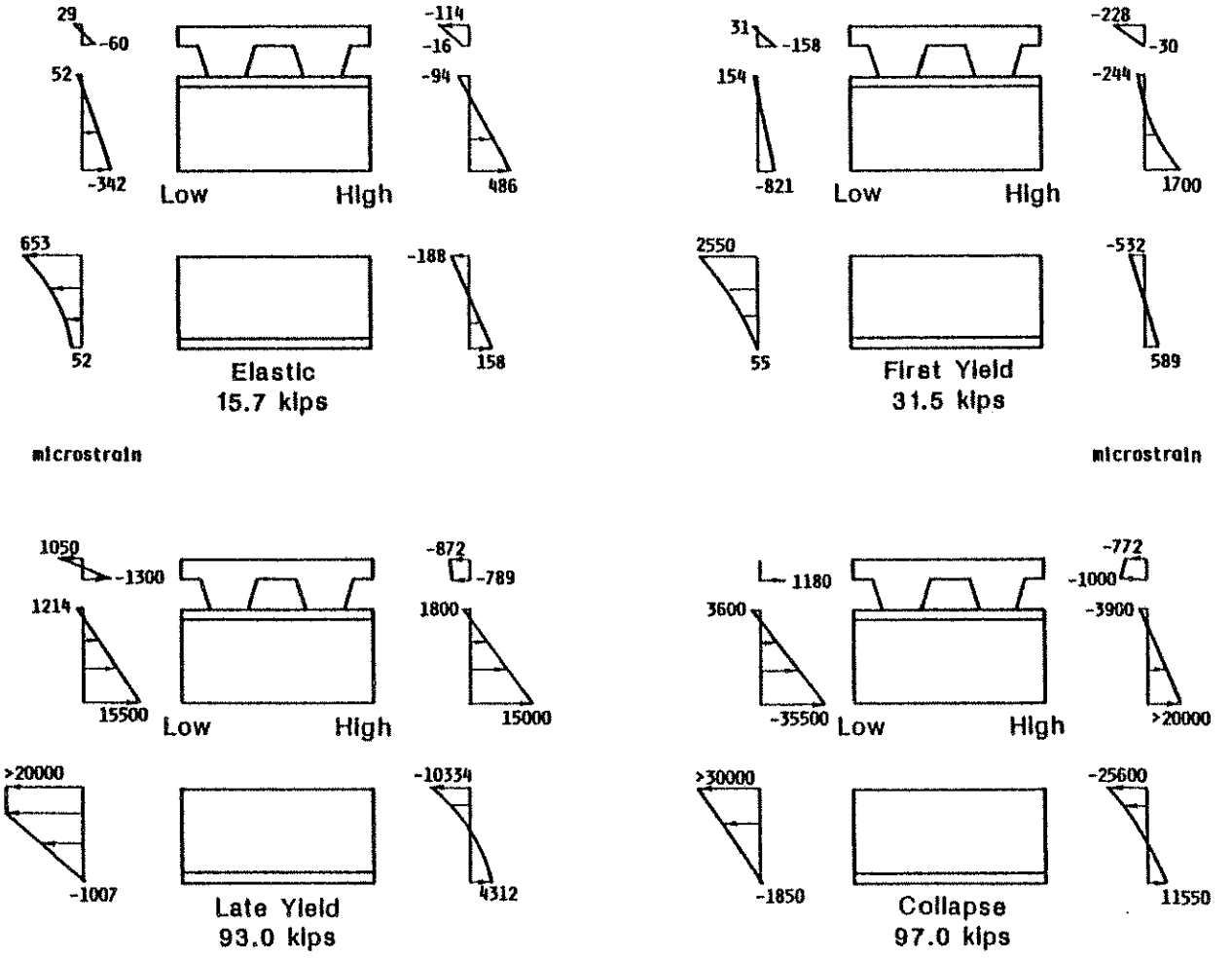

Fig. 3.19 Strain Distributions at the Opening for Test 2.

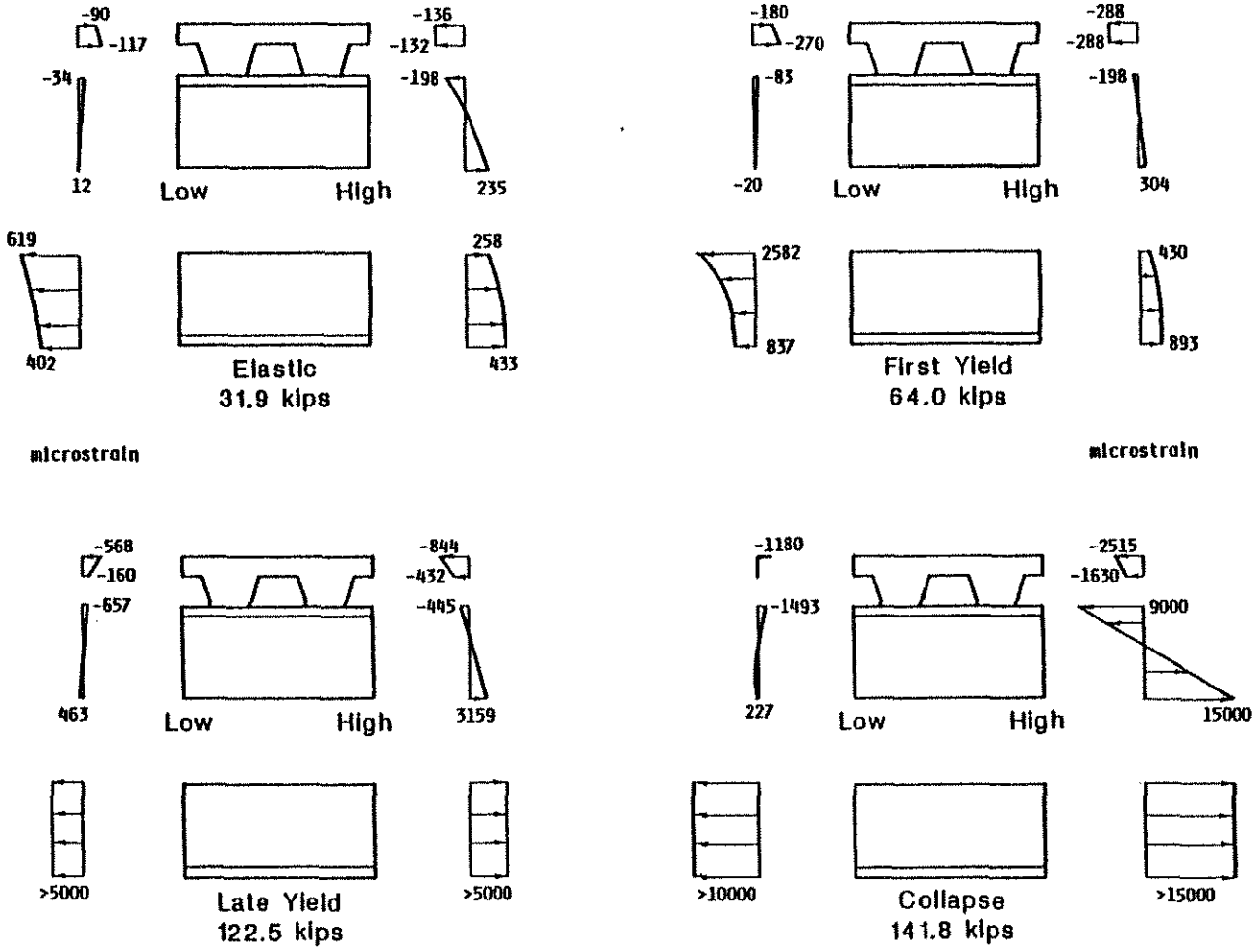

Fig. 3.20 Strain Distributions at the Opening for Test 3.

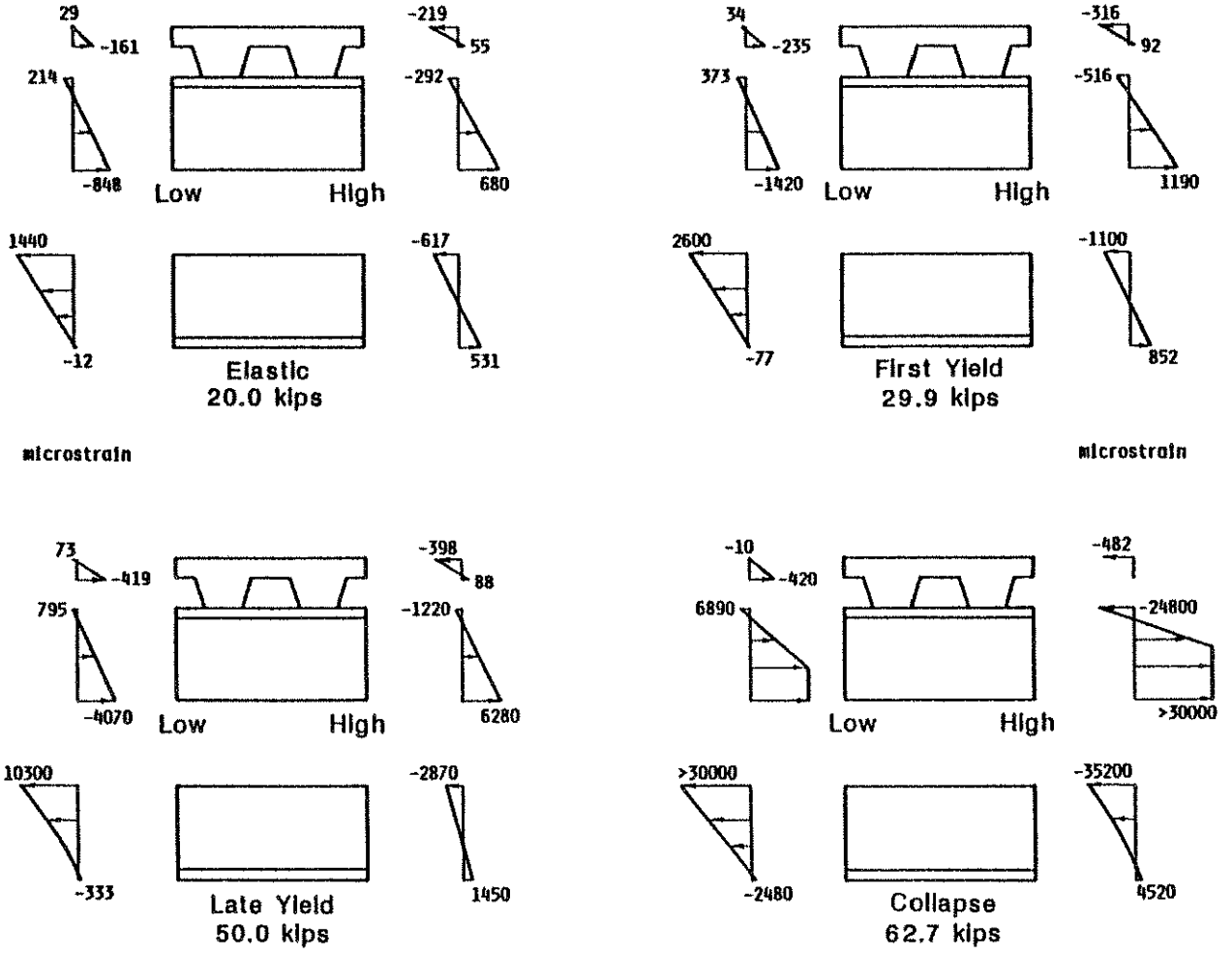

Fig. 3.21 Strain Distributions at the Opening for Test 4A.

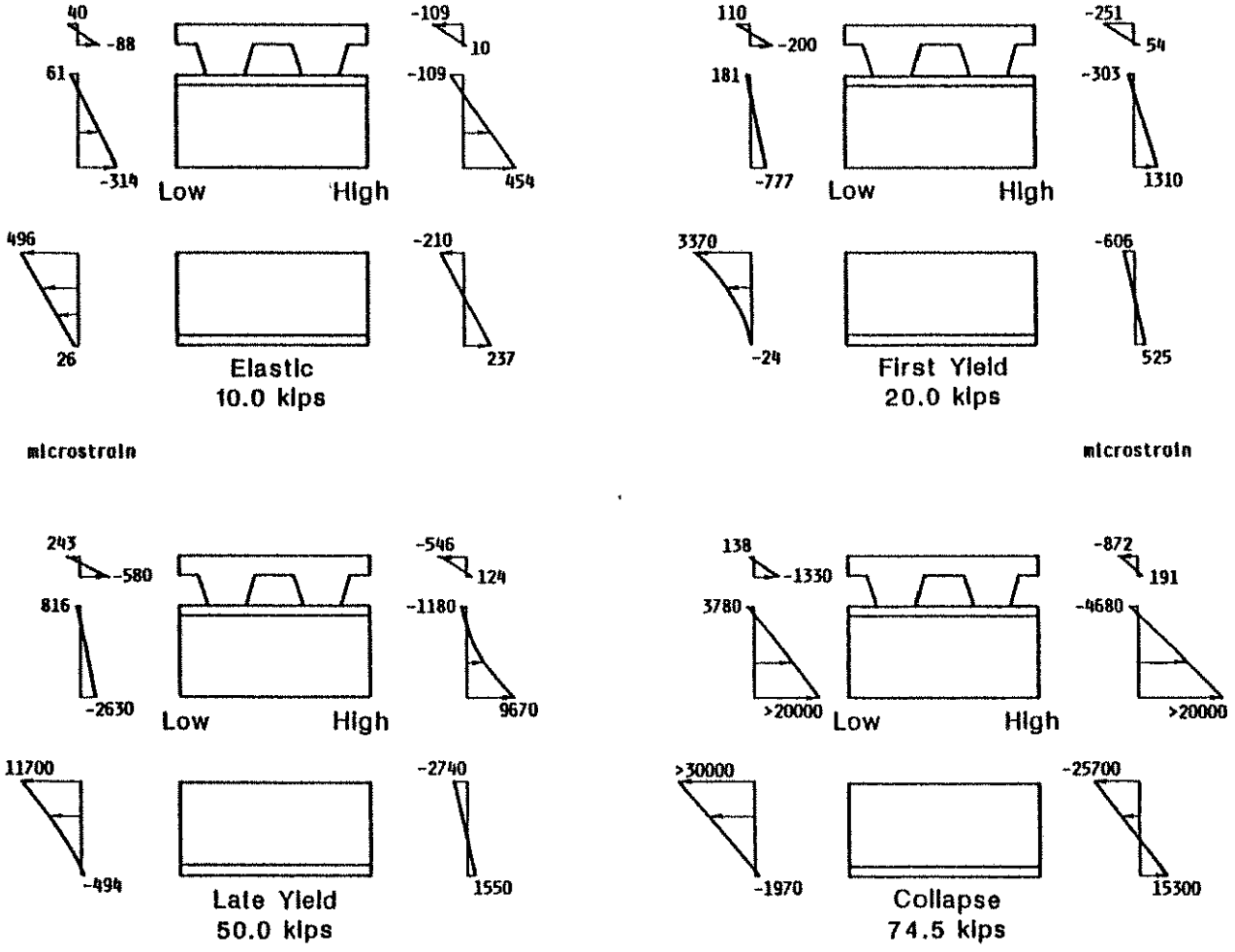

Fig. 3.22 Strain Distributions at the Opening for Test 4B.

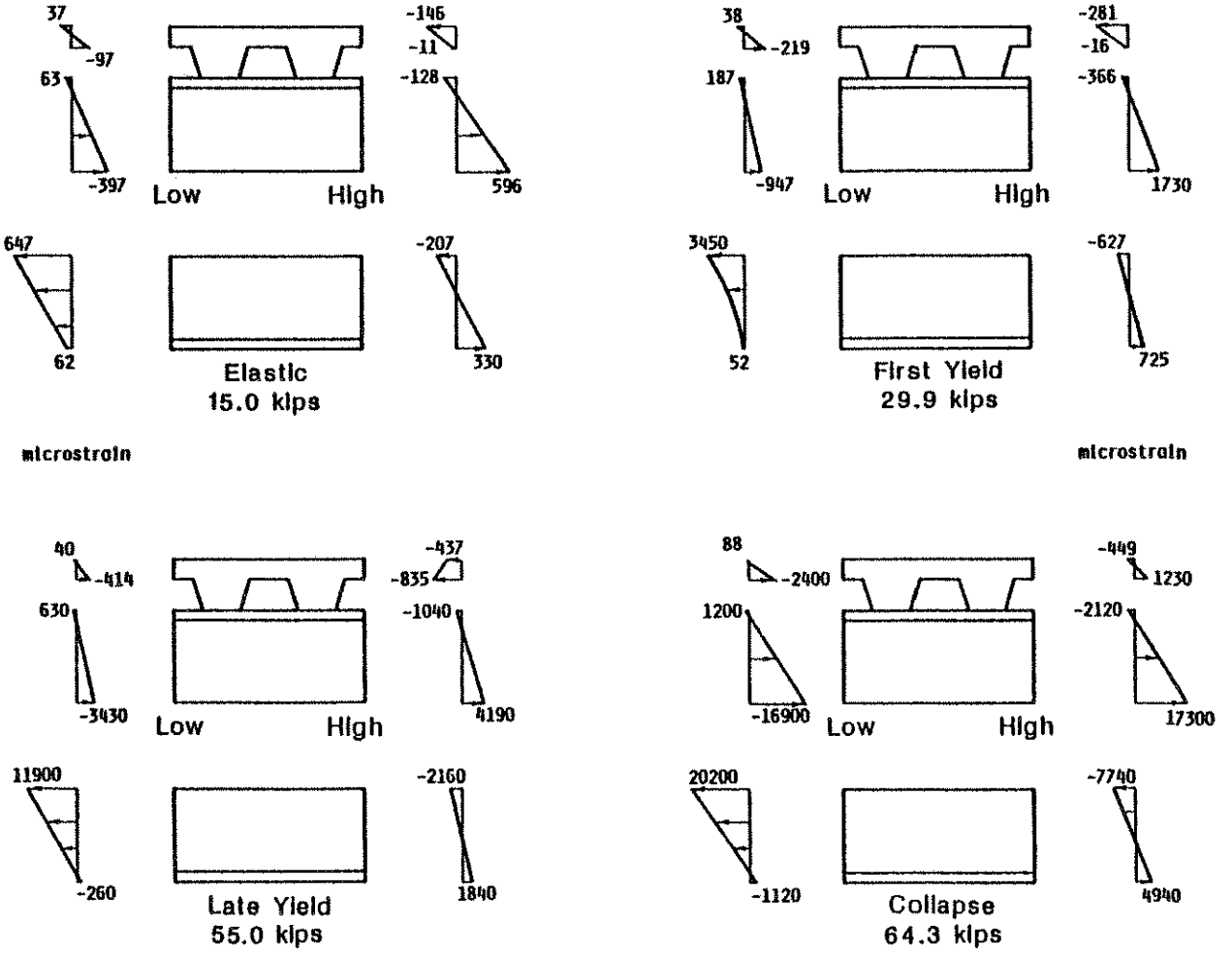

Fig. 3.23 Strain Distributions at the Opening for Test 5A.

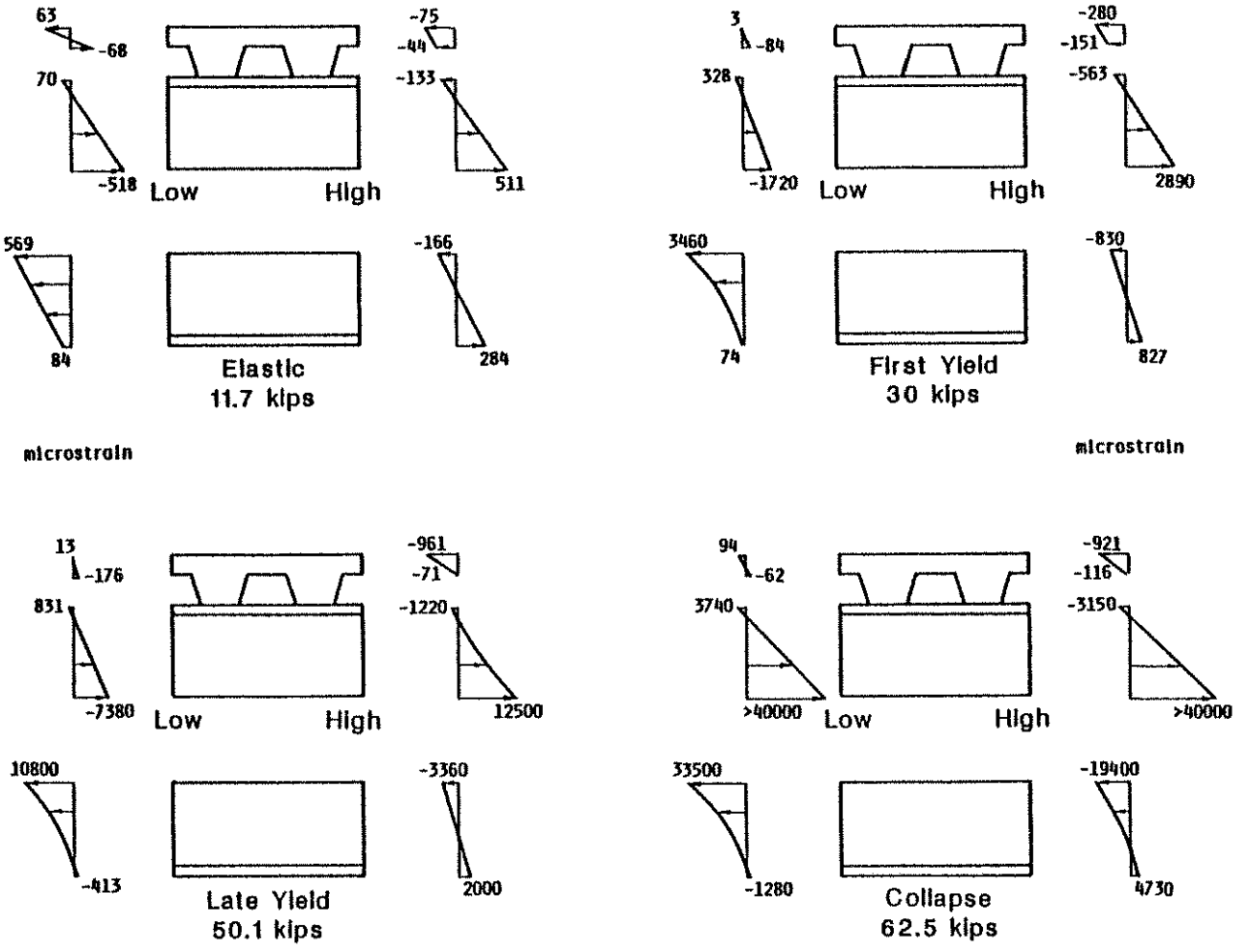

Fig. 3.24 Strain Distributions at the Opening for Test 5B.

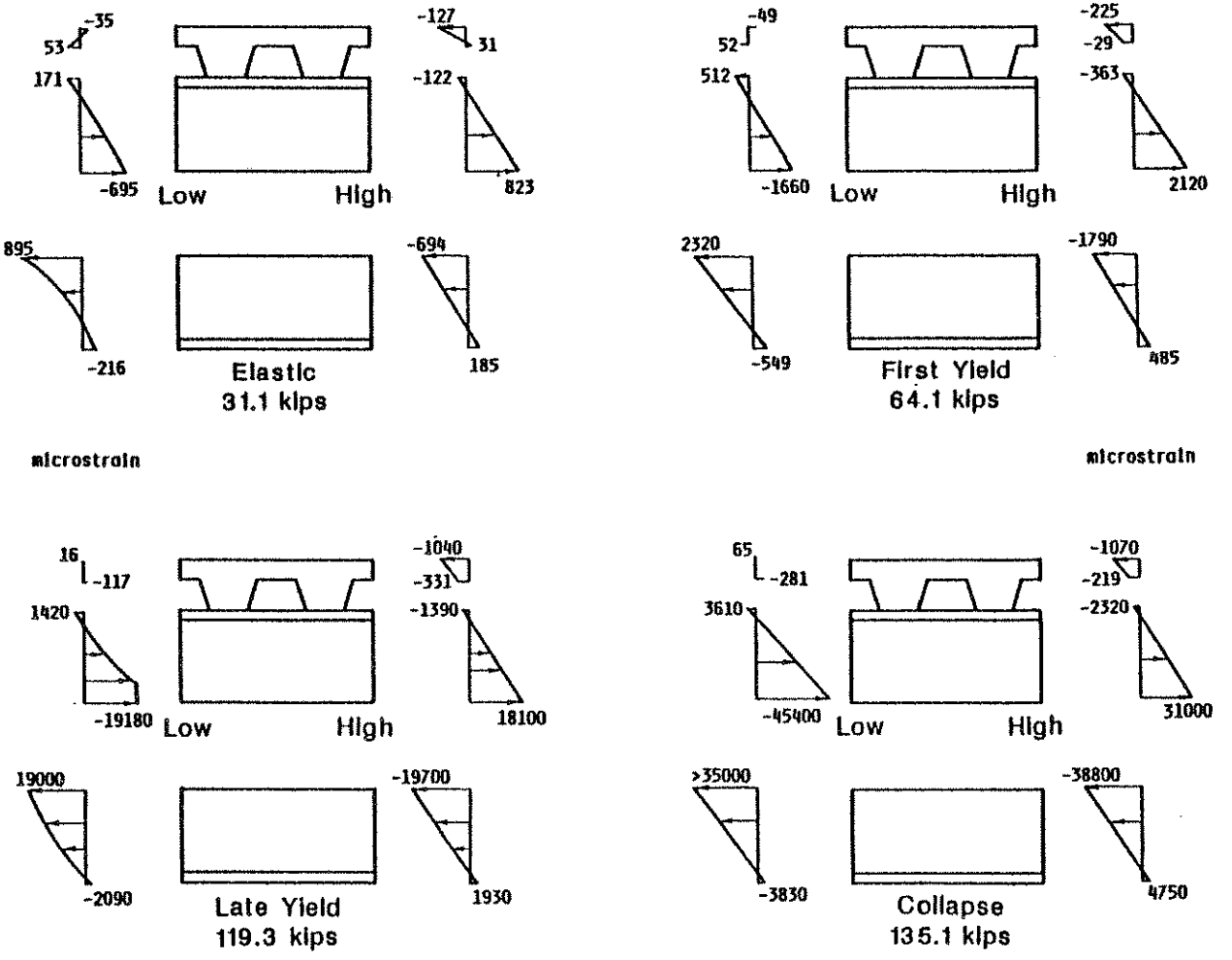

Fig. 3.25 Strain Distributions at the Opening for Test 6A.

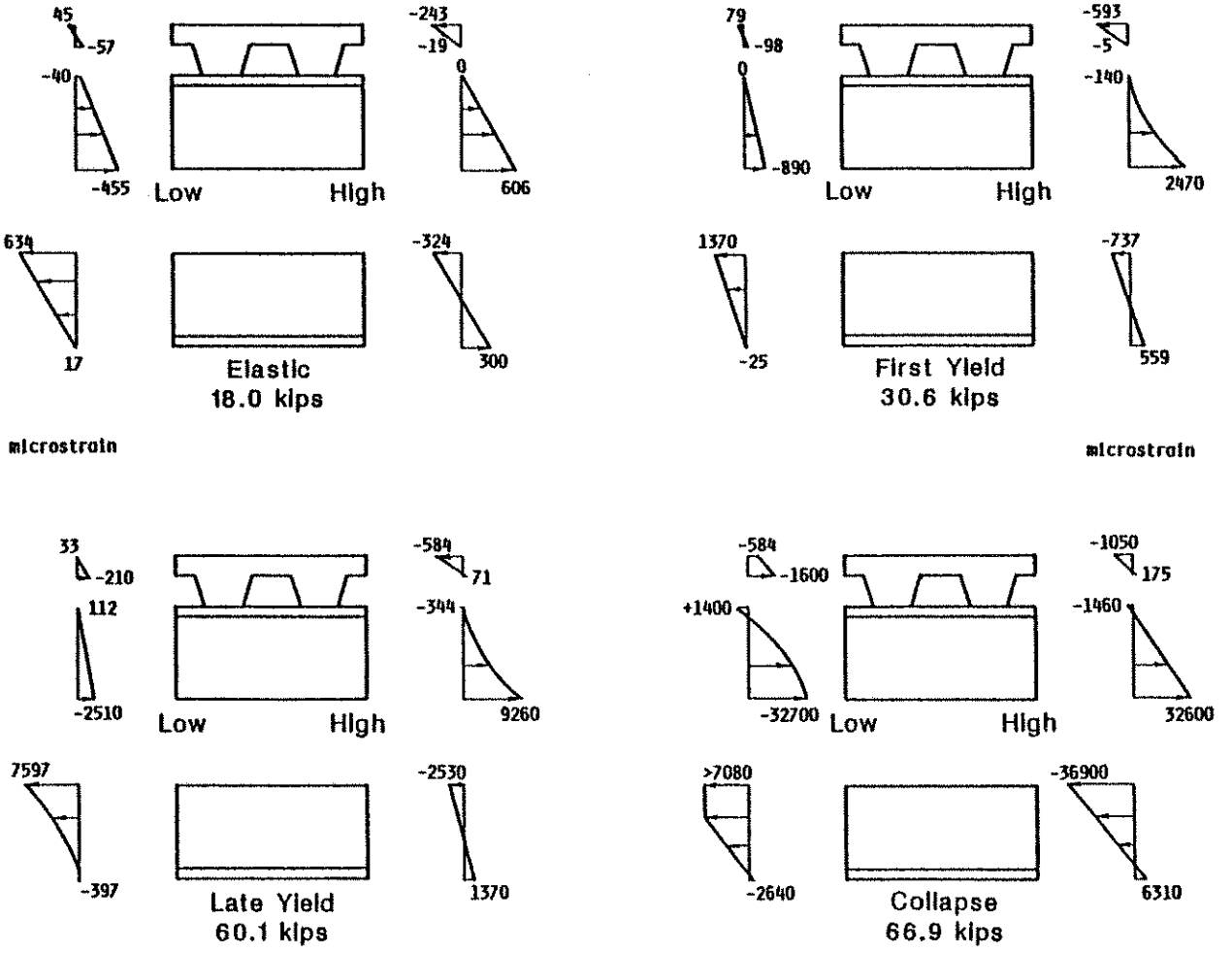

Fig. 3.26 Strain Distributions at the Opening for Test 6B.

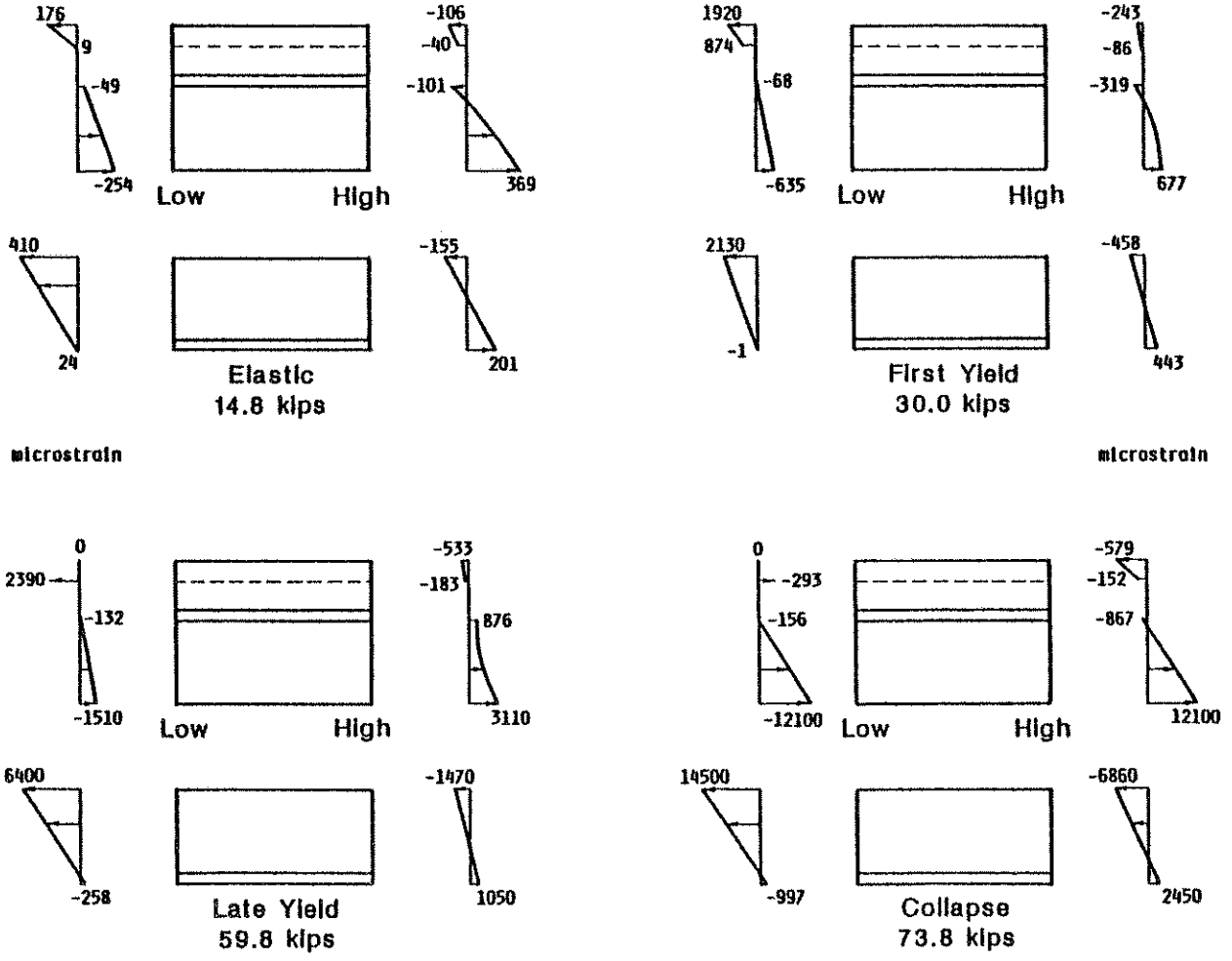

Fig. 3.27 Strain Distributions at the Opening for Test 7A.

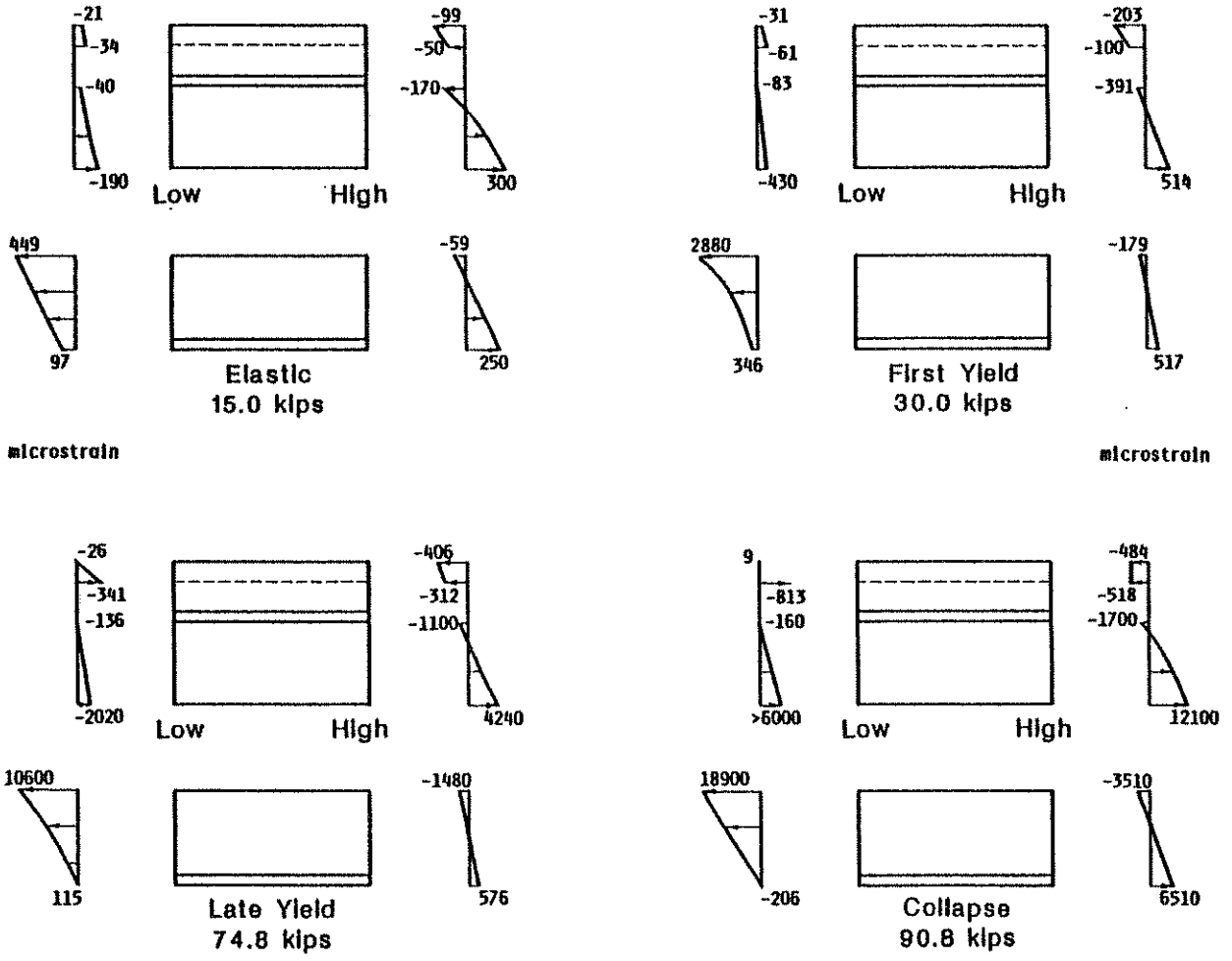

Fig. 3.28 Strain Distributions at the Opening for Test 7B.

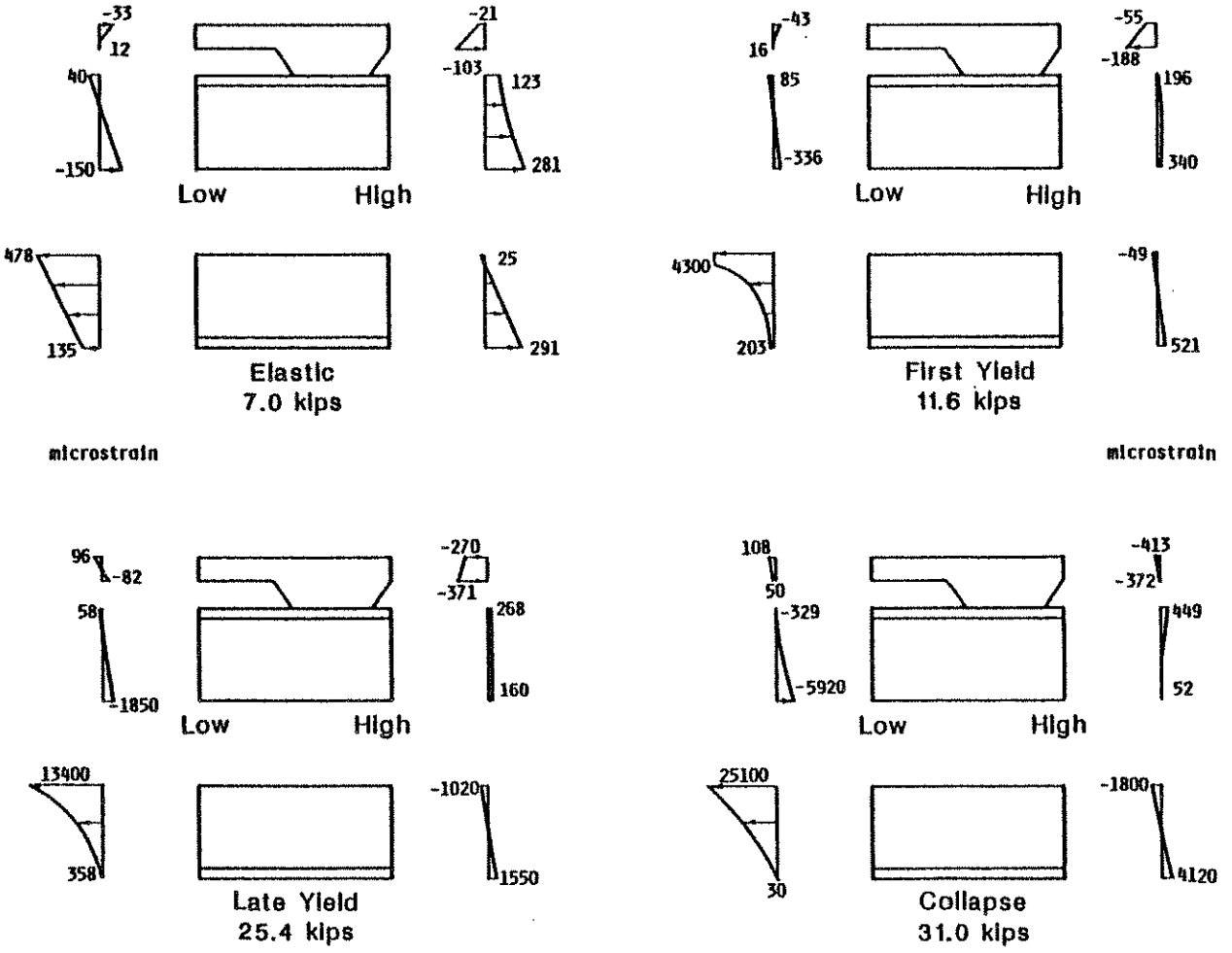

Fig. 3.29 Strain Distributions at the Opening for Test 8A.

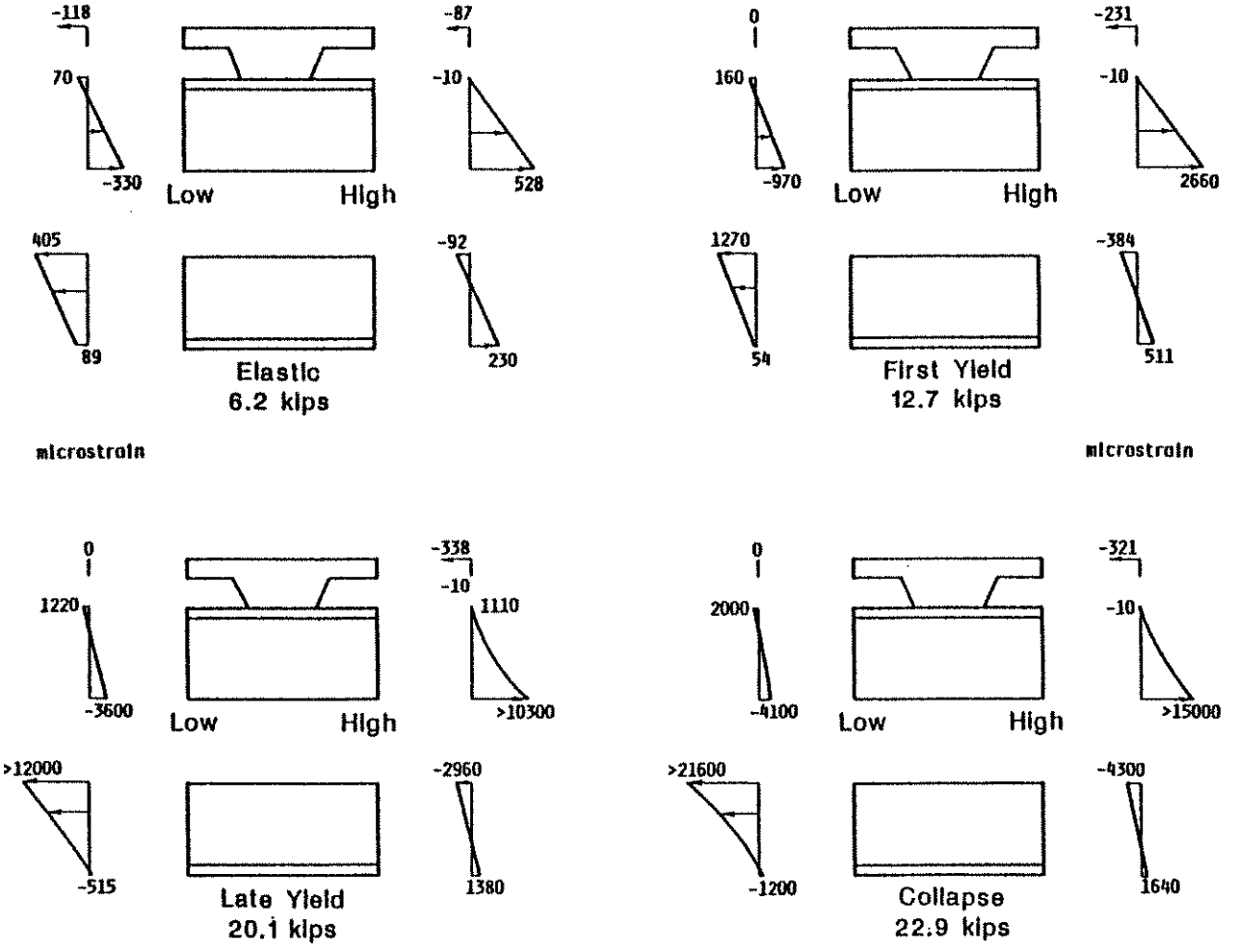

Fig. 3.30 Strain Distributions at the Opening for Test 8B.

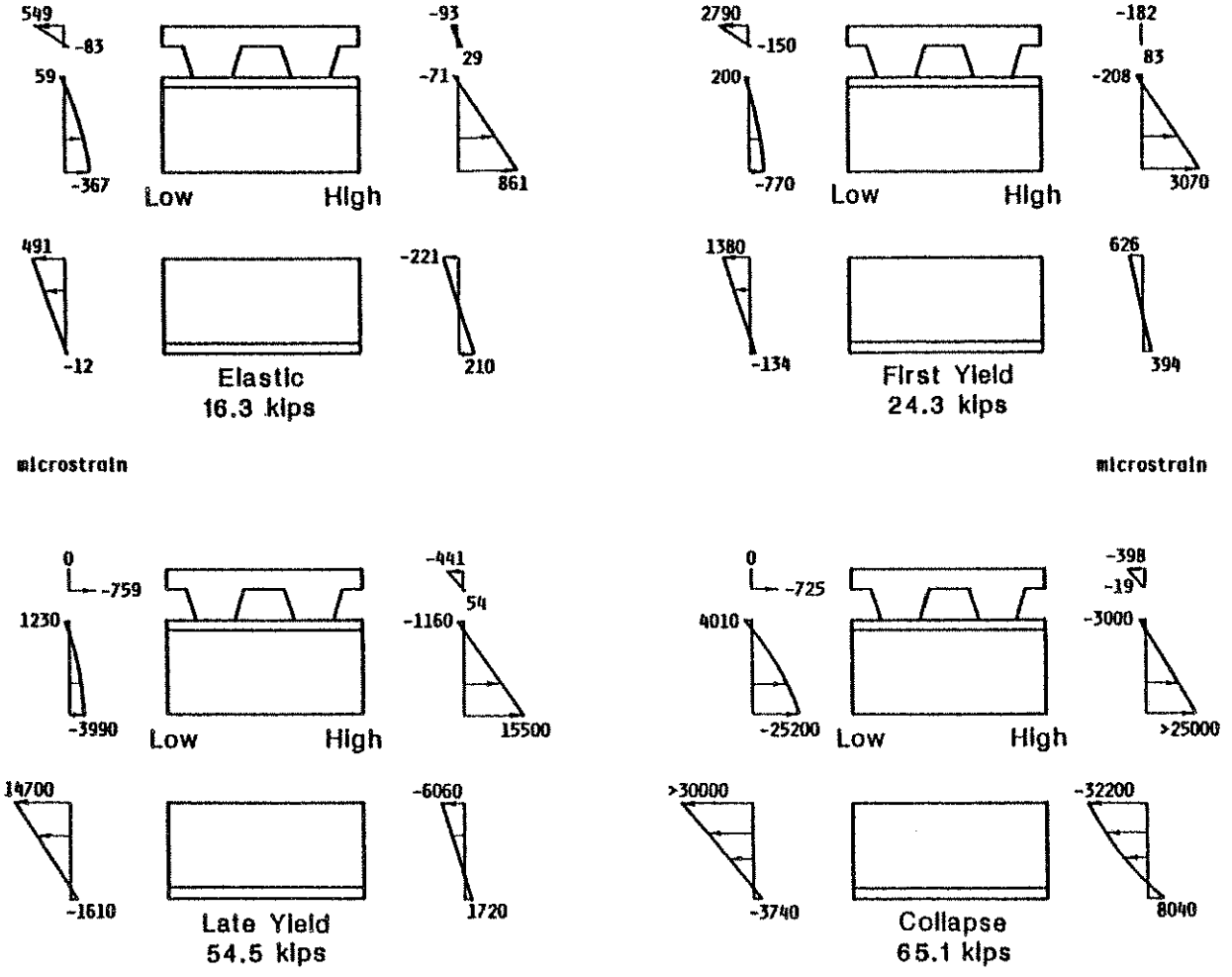

Fig. 3.31 Strain Distributions at the Opening for Test 9A.

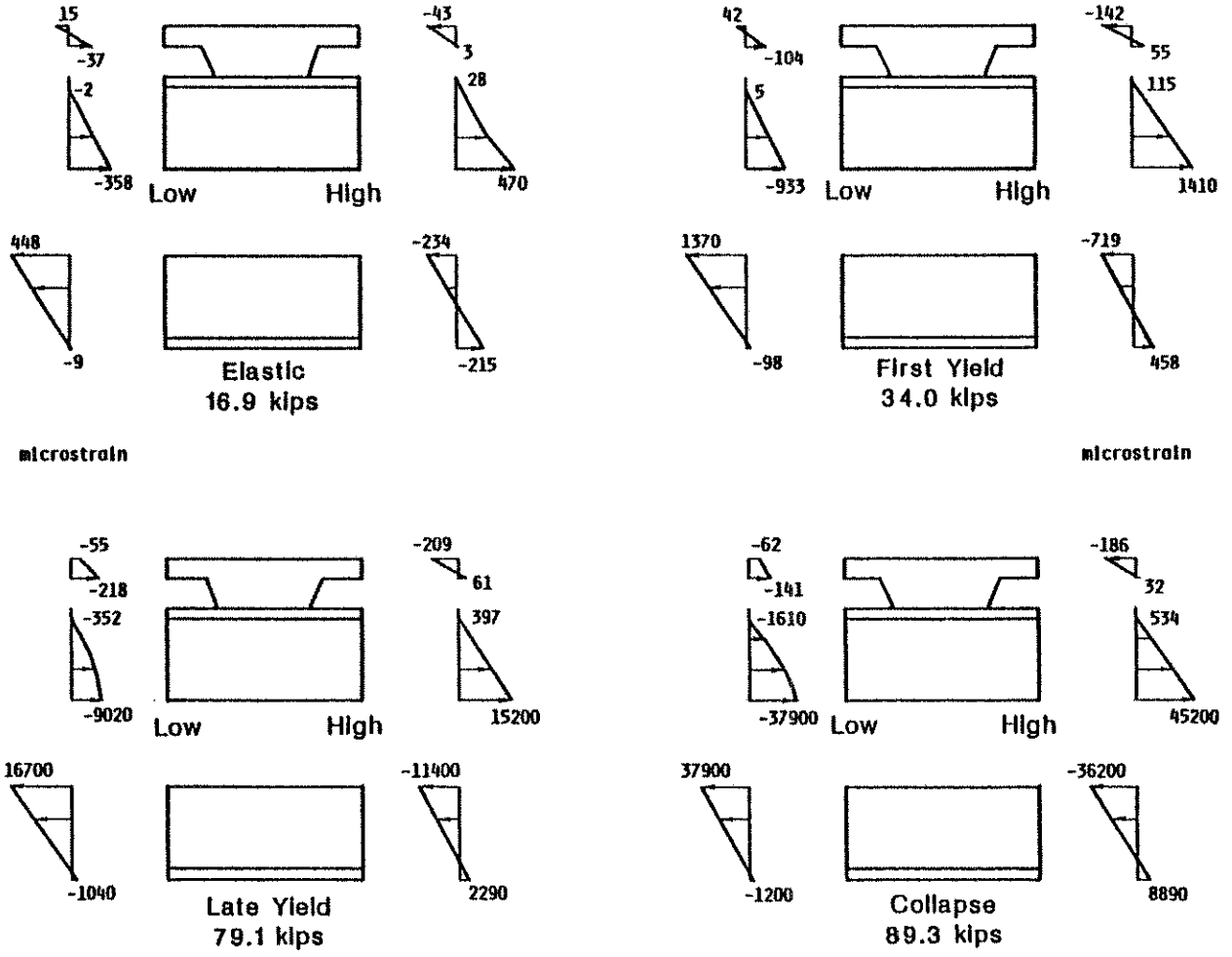

Fig. 3.32 Strain Distributions at the Opening for Test 9B.

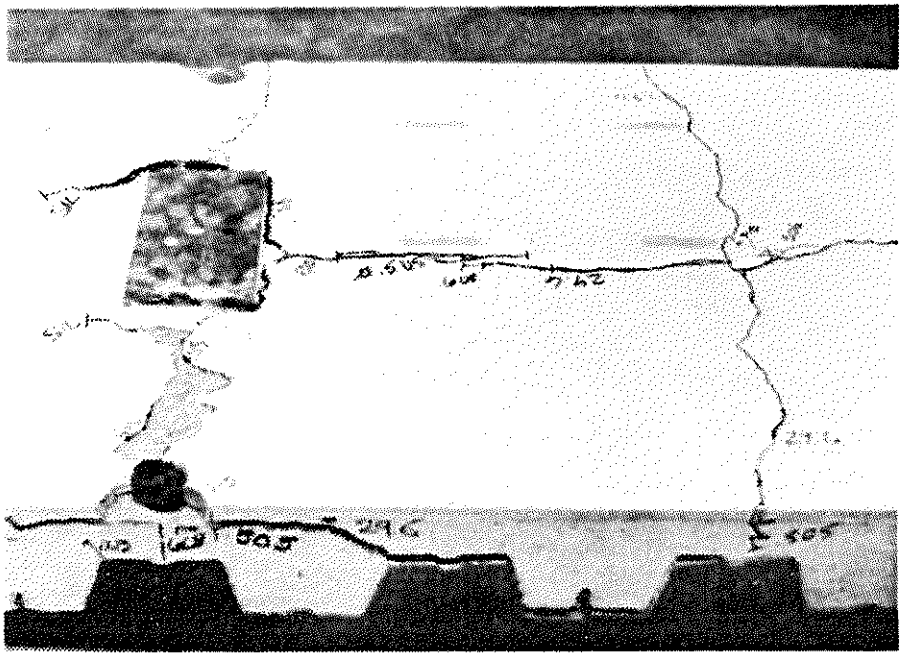

Fig. 3.33 Cracking in the Slab Above the Opening.

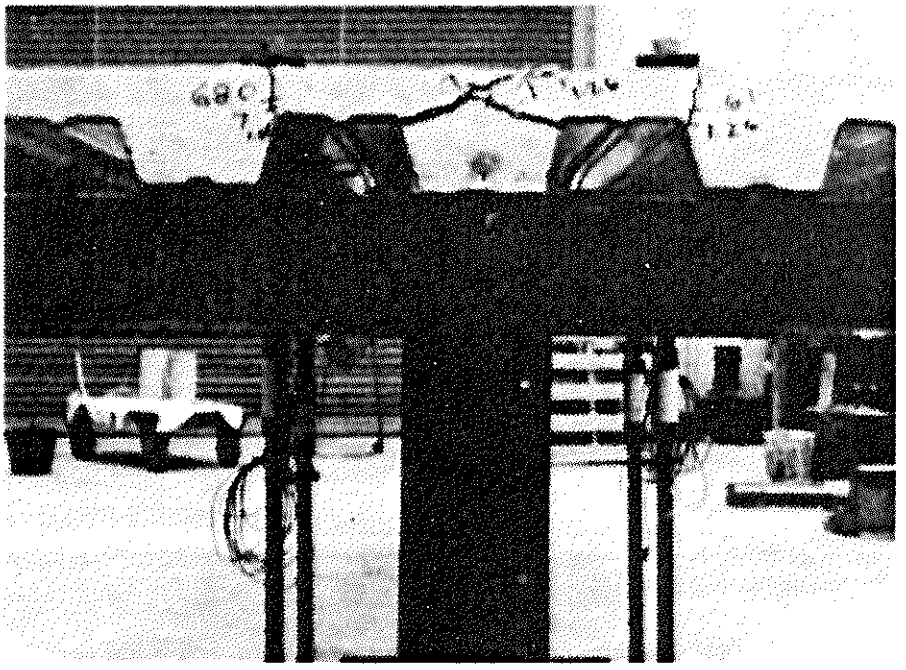

Fig. 3.34 Longitudinal Rib Failure.

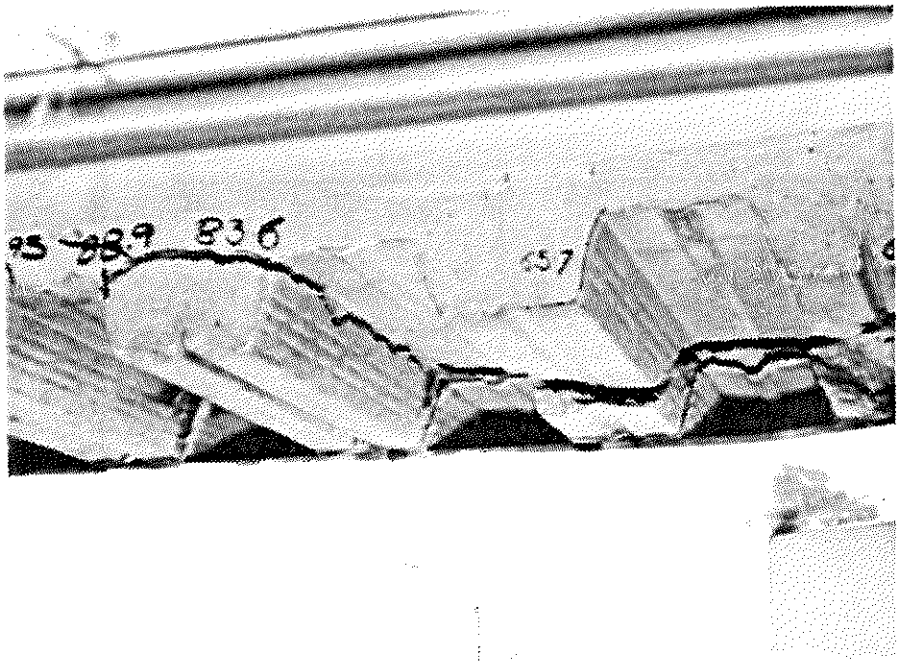

Fig. 3.35 Rib Failure in Slab with Transverse Ribs.

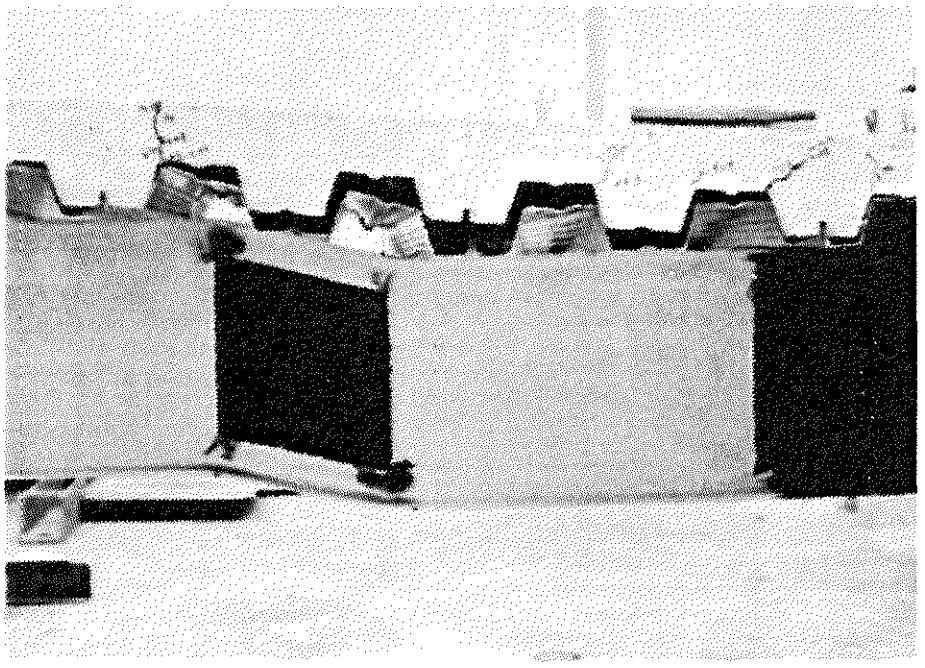

Fig. 3.36 Bridging of Slab at Opening.

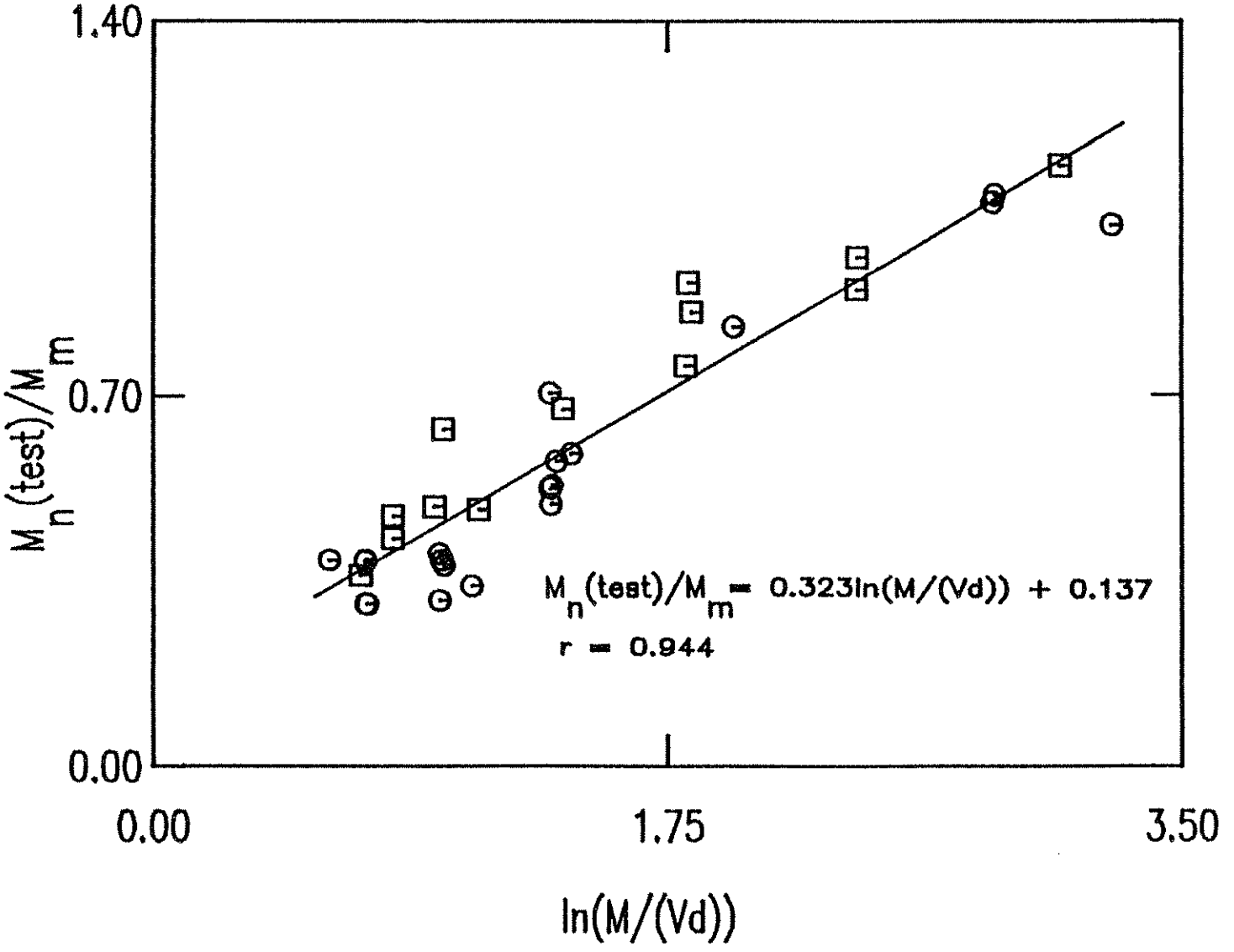

Fig. 3.37 $M_n(test)/M_m$ versus ln(M/Vd) for the Current Tests and for Previous Investigations (8, 9, 11, 19, 32, 34, and 36)

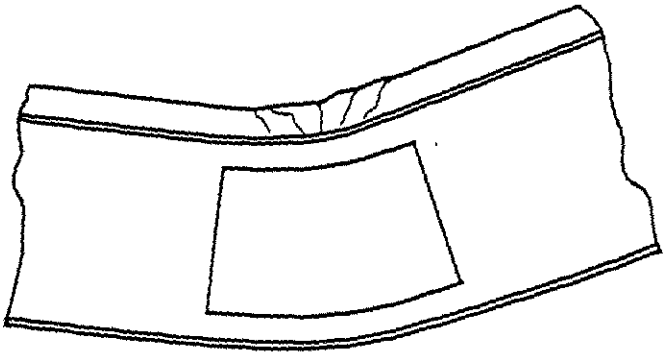

Fig. 4.1 Pure Bending Failure at Opening (10, 11).

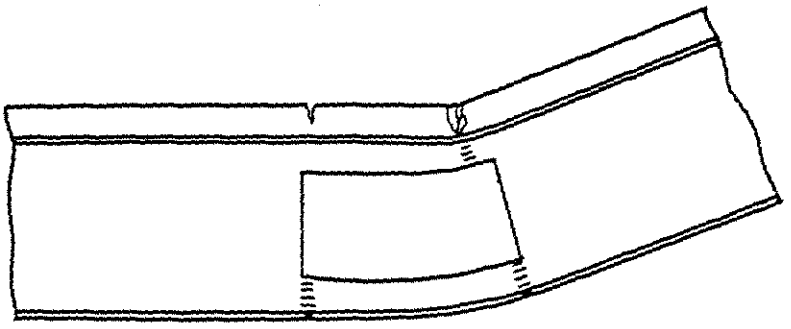

Fig. 4.2 "Mechanism" Failure with Combined Moment and Shear (10, 11).

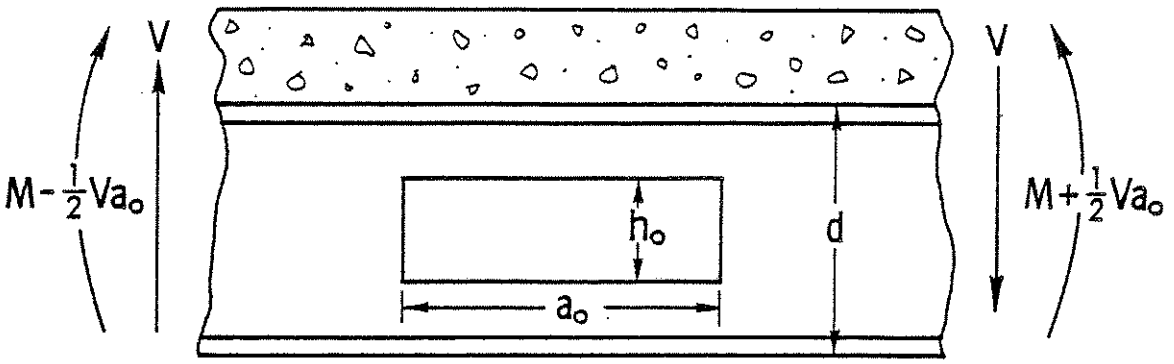

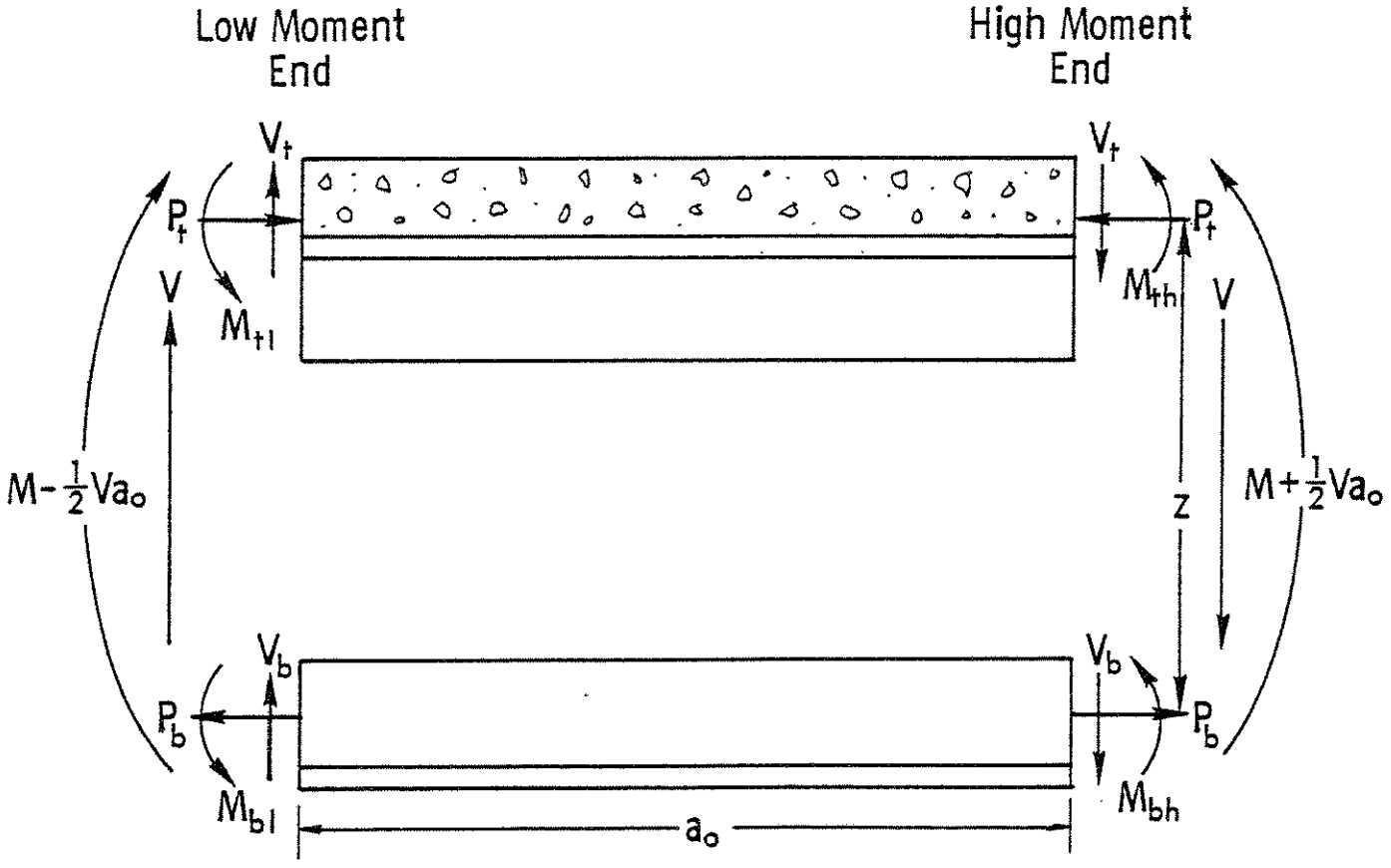

Fig. 4.3 Forces Acting at Web Opening (10, 11).

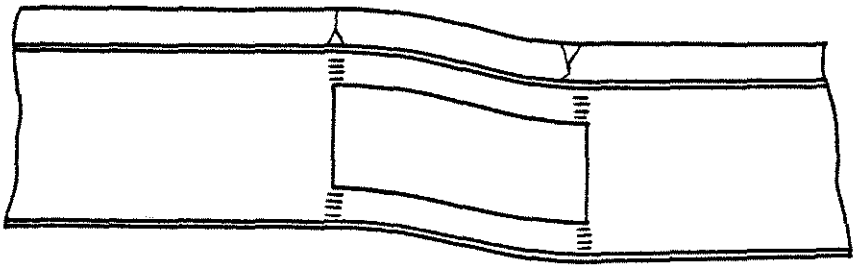

Fig. 4.4 "Mechanism" Failure in Pure Shear (10, 11).

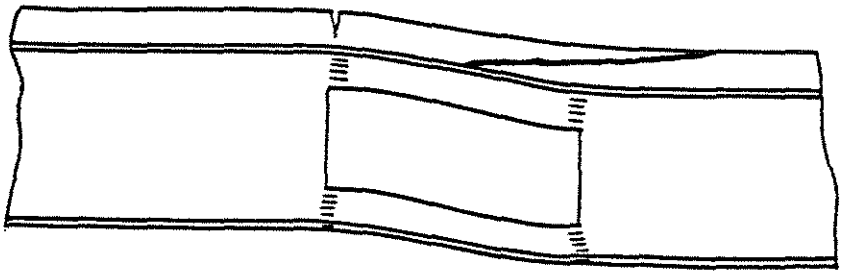

Fig. 4.5 "Shear" Failure in Top Tee (14).

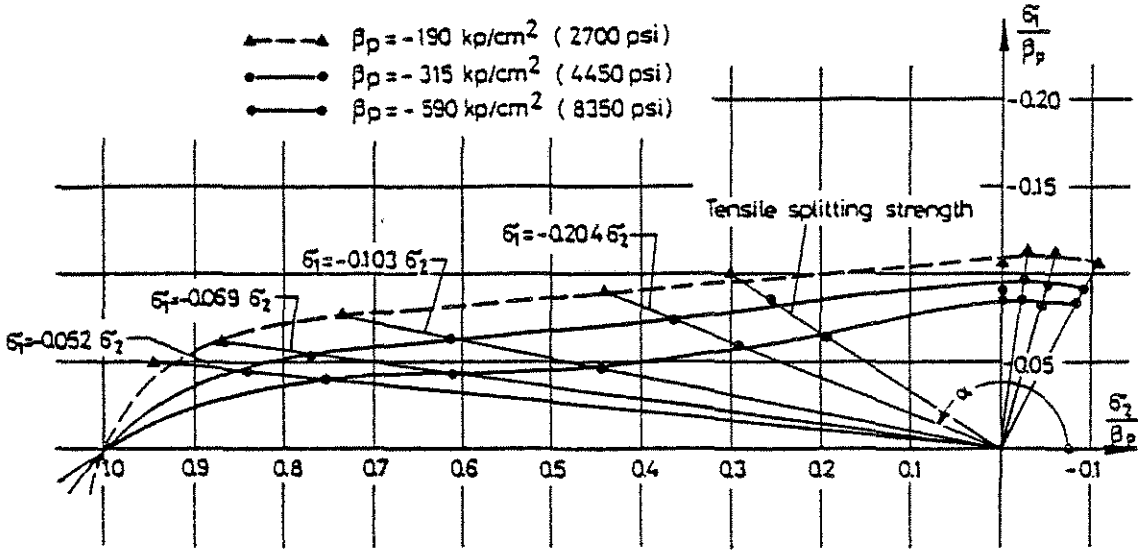

Fig. 4.6 Experimental Results for the Strength of Concrete Under Combined Tension and Compression (23).

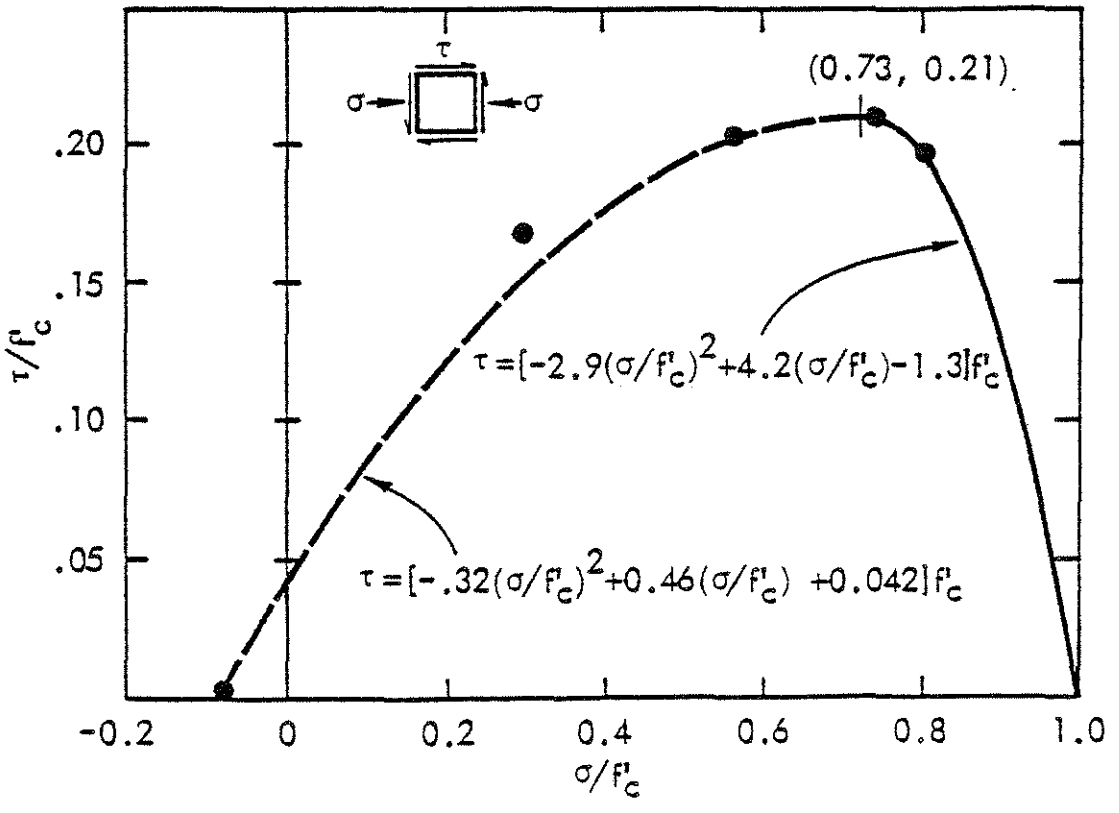

Fig. 4.7 Concrete Strength Under Combined Shear and Normal Stress (10, 11).

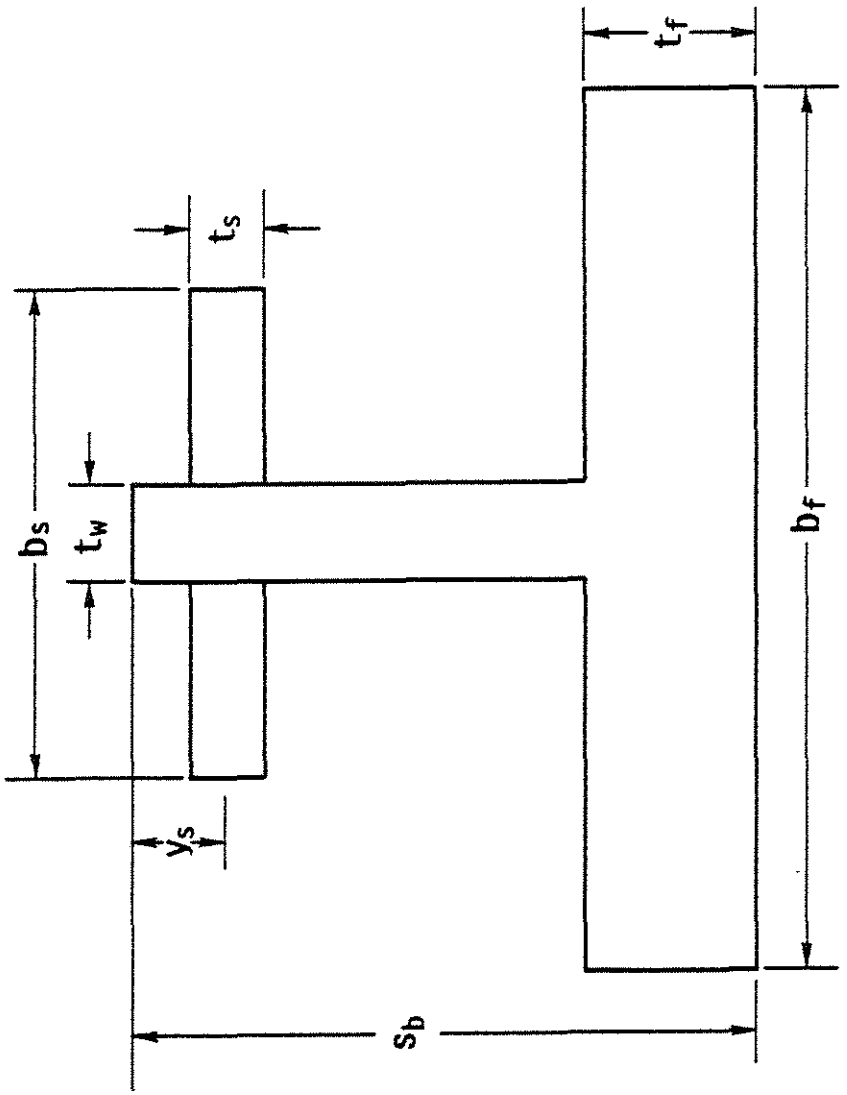

Fig. 4.8 Bottom Tee Cross Section.

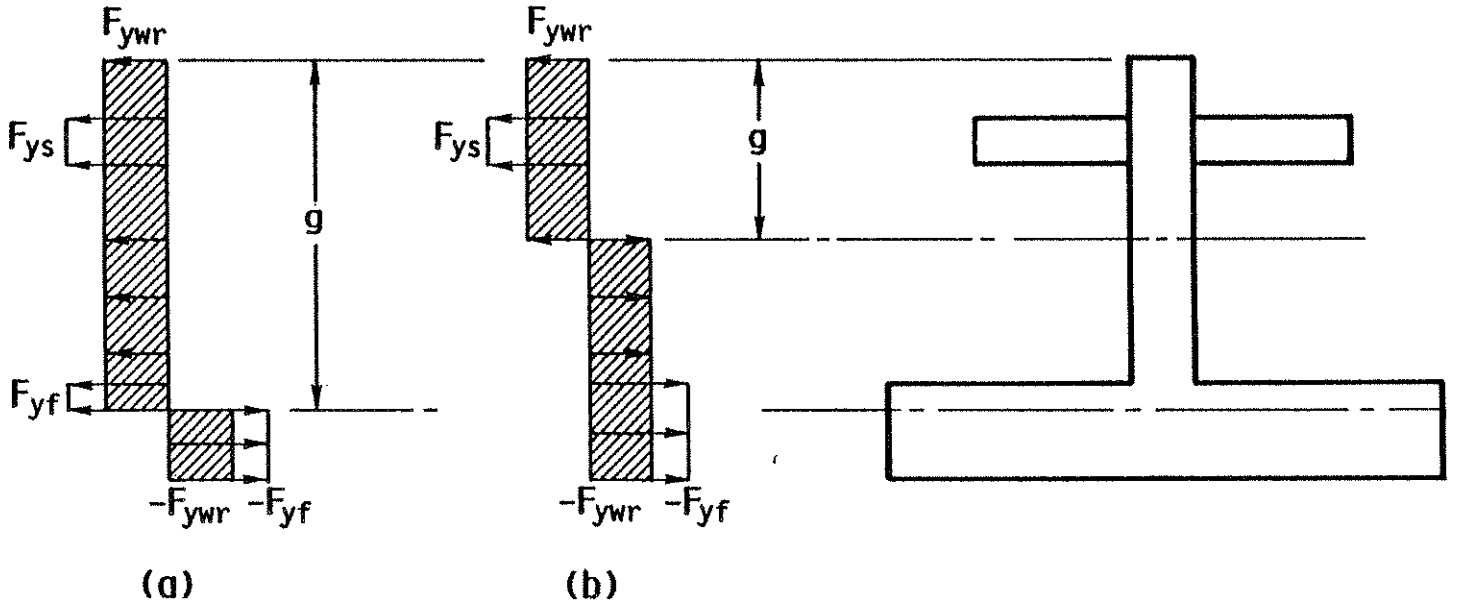

Fig. 4.9 Stress Distributions for Low Moment End of Bottom Tee.
(a) Neutral Axis in Flange. (b) Neutral Axis in Web.

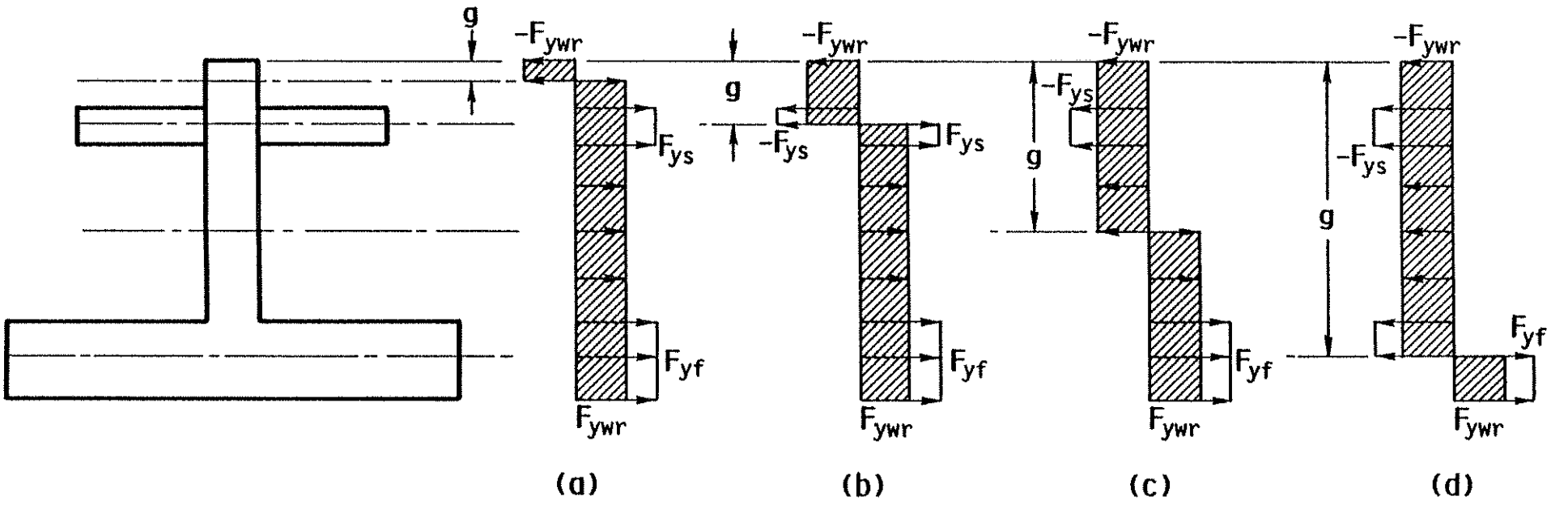

Fig. 4.10 Stress Distributions for High Moment End of Bottom Tee. (a) Neutral Axis in Web Above Stiffener. (b) Neutral Axis in Stiffener. (c) Neutral Axis in Web Below Stiffener. (d) Neutral Axis in Flange.

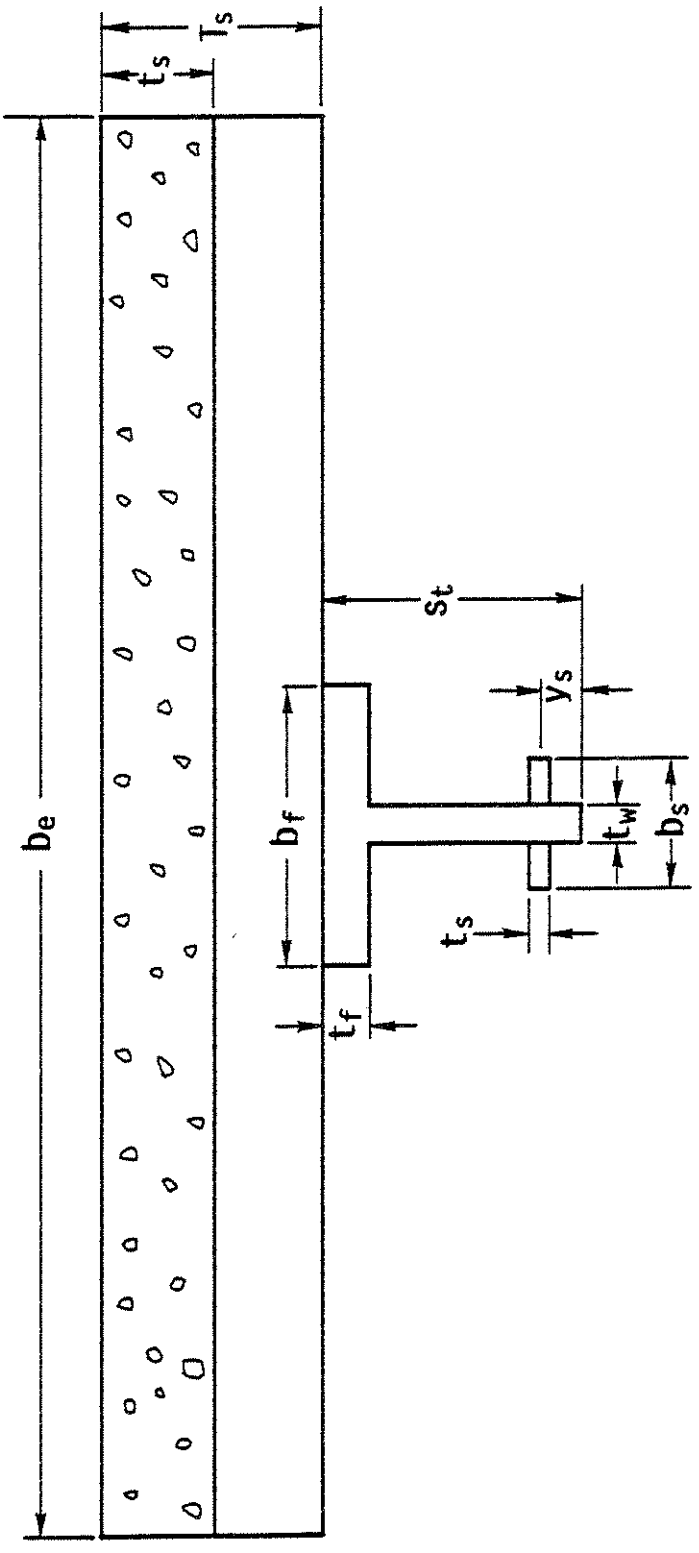

Fig. 4.11 Top Tee Cross Section.

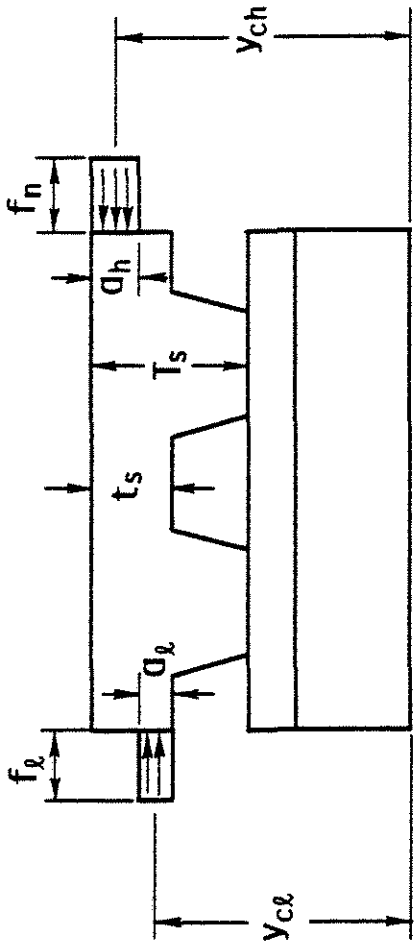

Fig. 4.12 Locations of Forces in Slab.

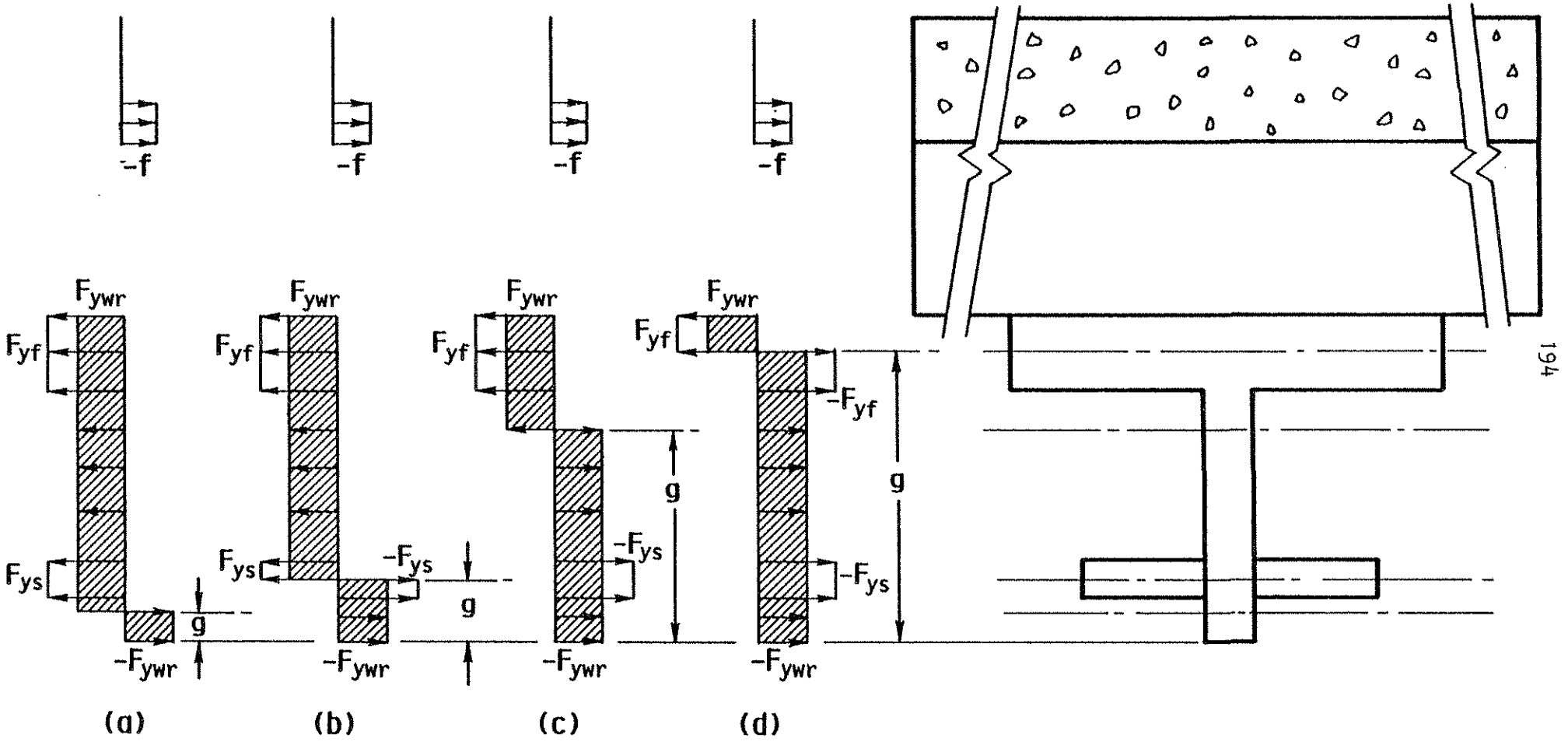

Fig. 4.13 Stress Distributions for Low Moment End of Top Tee. (a) Neutral Axis in Web Below Stiffener. (b) Neutral Axis in Stiffener. (c) Neutral Axis in Web Above Stiffener. (d) Neutral Axis in Flange.

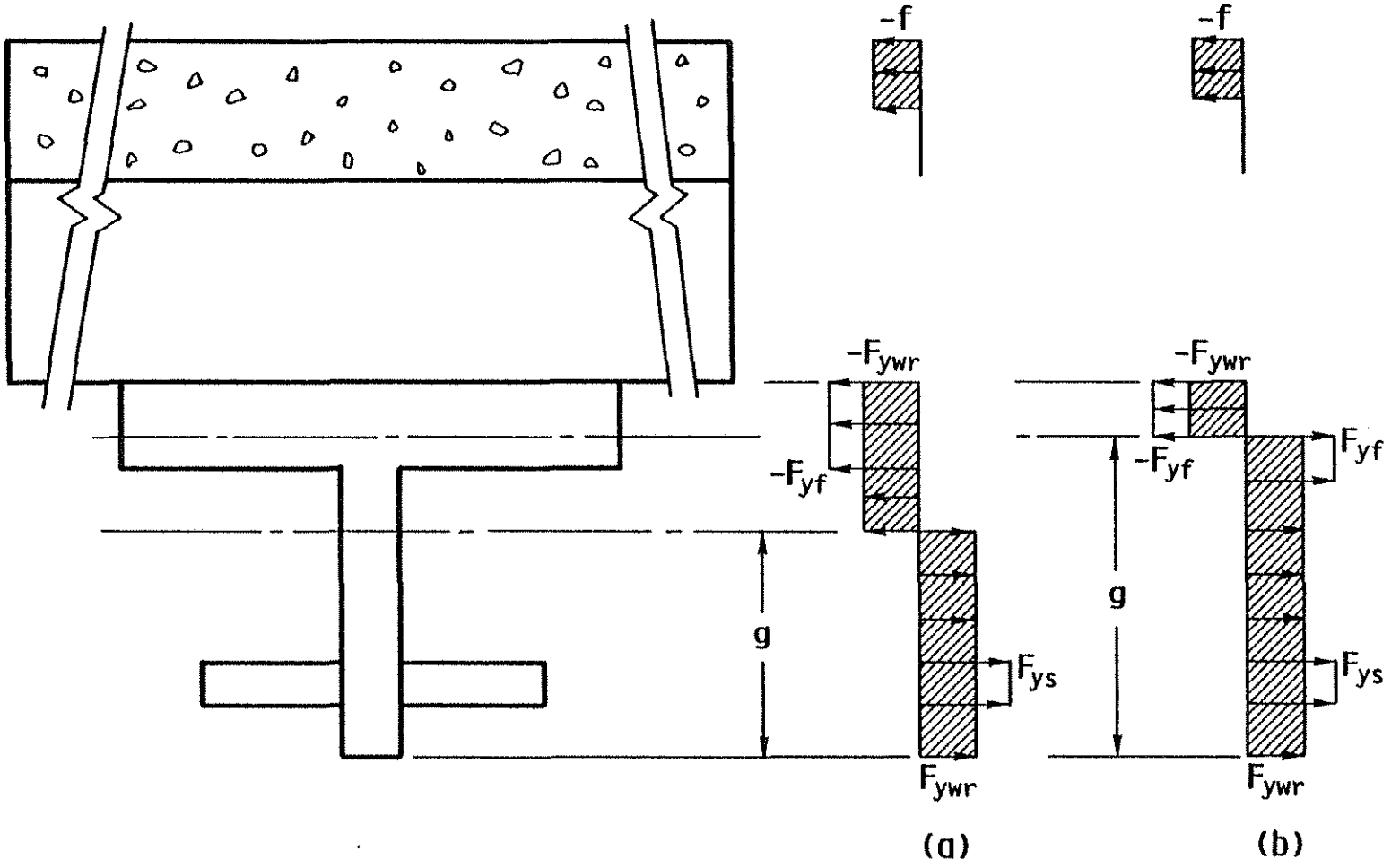

Fig. 4.14 Stress Distributions at High Moment End of Top Tee. (a) Neutral Axis in Web Above Stiffener. (b) Neutral Axis in Flange.

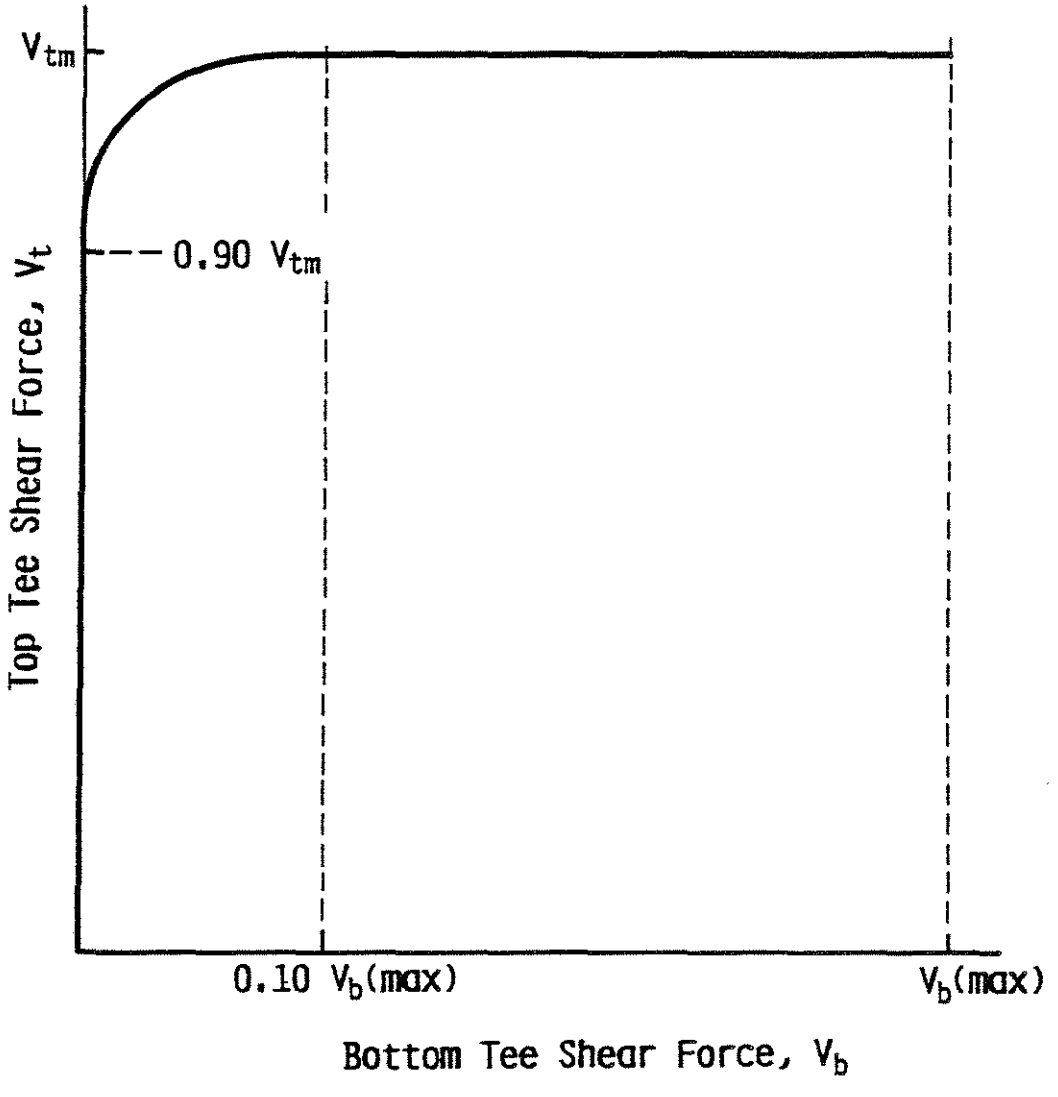

Fig. 4.15 Shear Force Distribution to Top and Bottom Tees.

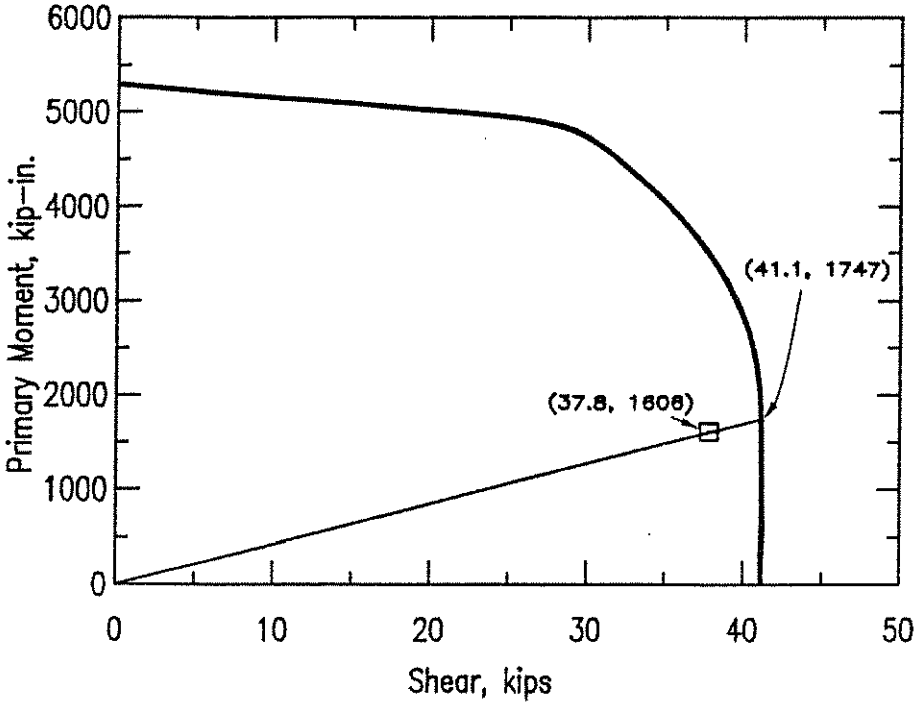

Fig. 4.16 Moment-Shear Interaction Curve for Test 1.

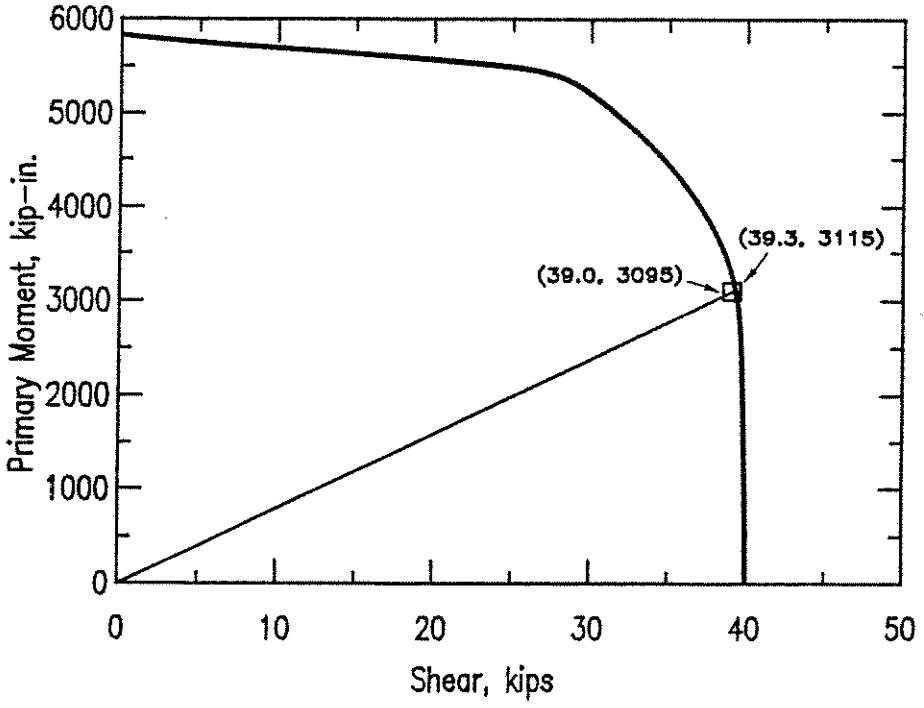

Fig. 4.17 Moment-Shear Interaction Curve for Test 2.

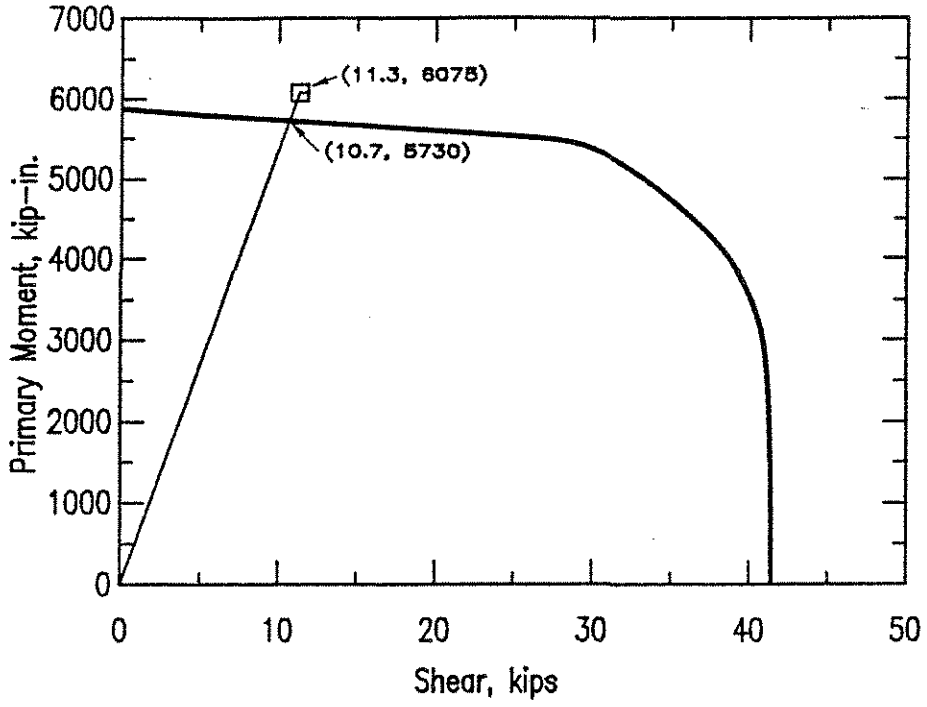

Fig. 4.18 Moment-Shear Interaction Curve for Test 3.

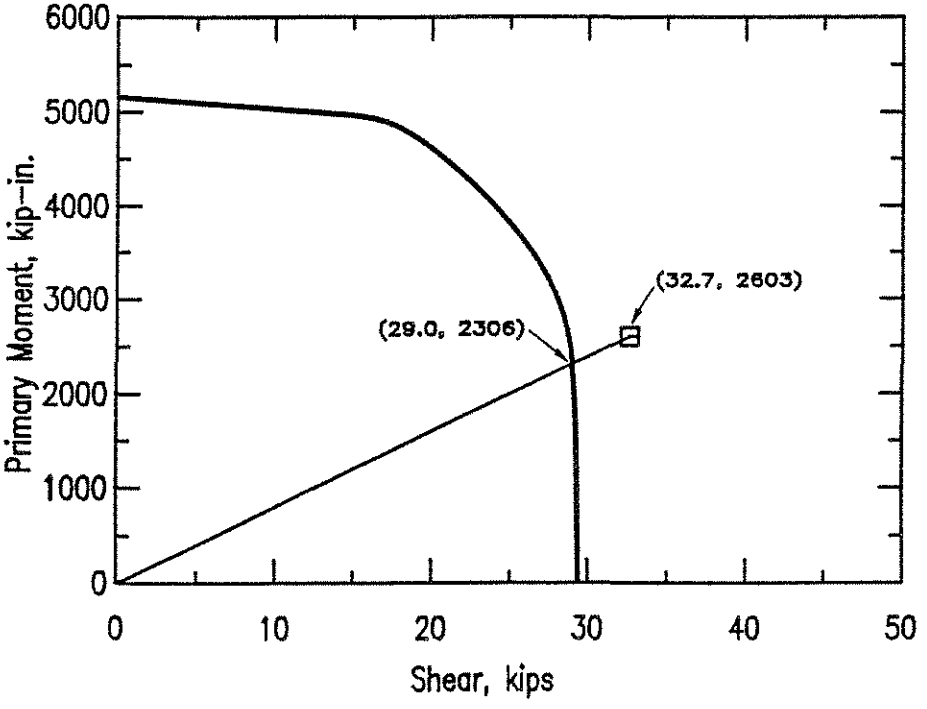

Fig. 4.19 Moment-Shear Interaction Curve for Test 4A.

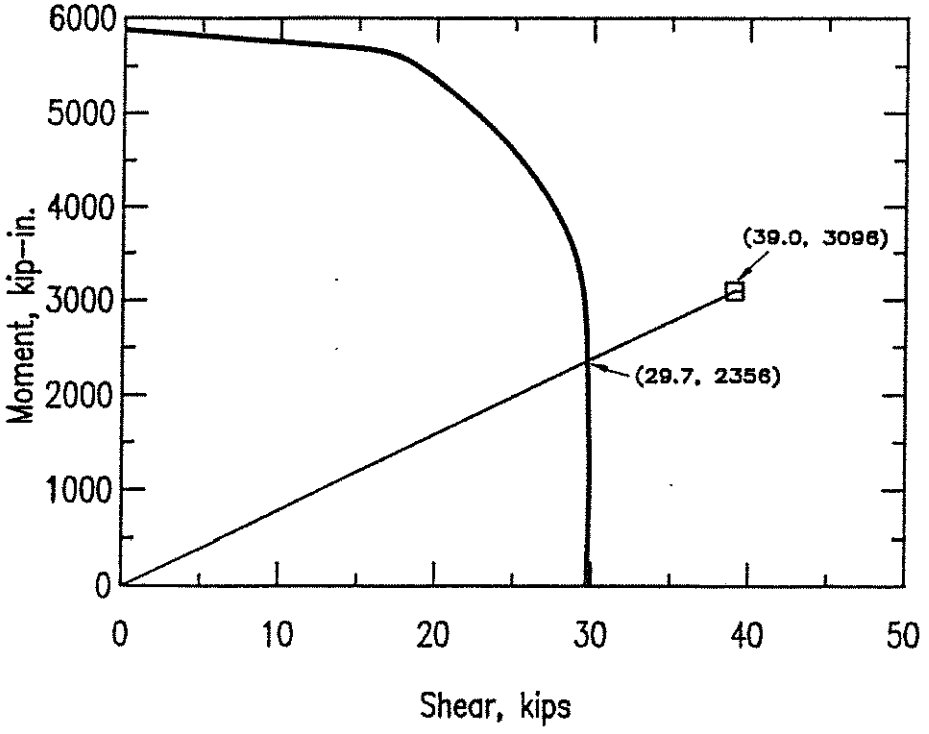

Fig. 4.20 Moment-Shear Interaction Curve for Test 4B.

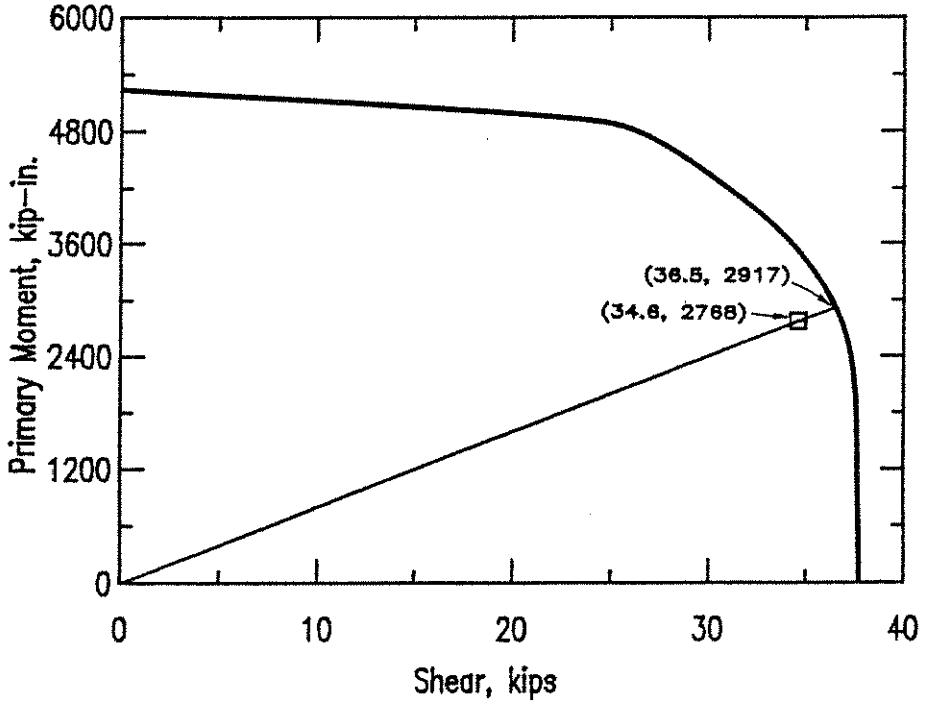

Fig. 4.21 Moment-Shear Interaction Curve for Test 5A.

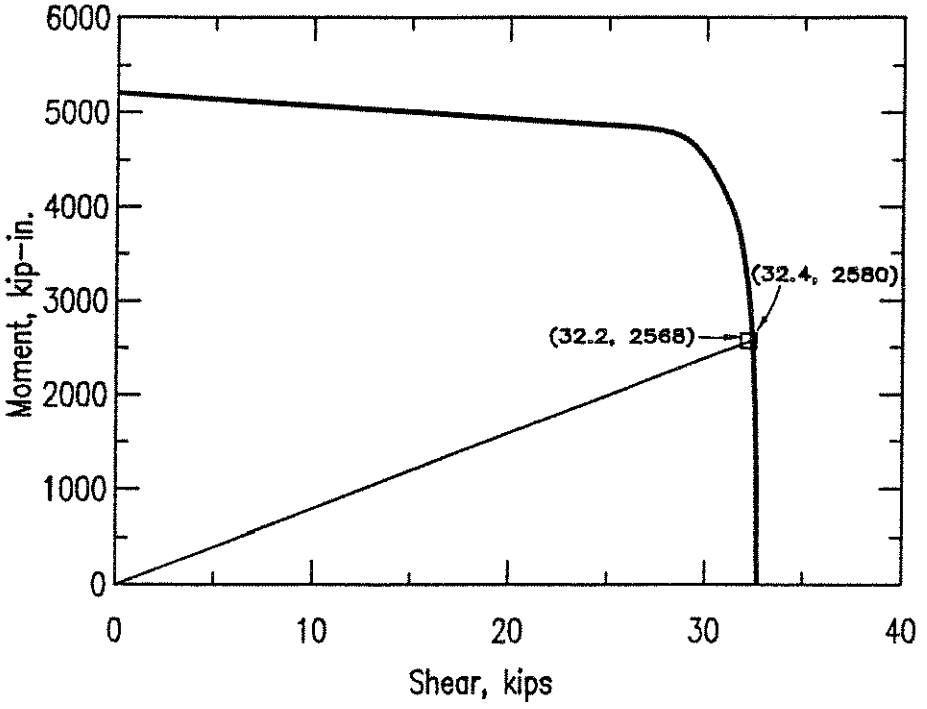

Fig. 4.22 Moment-Shear Interaction Curve for Test 5B.

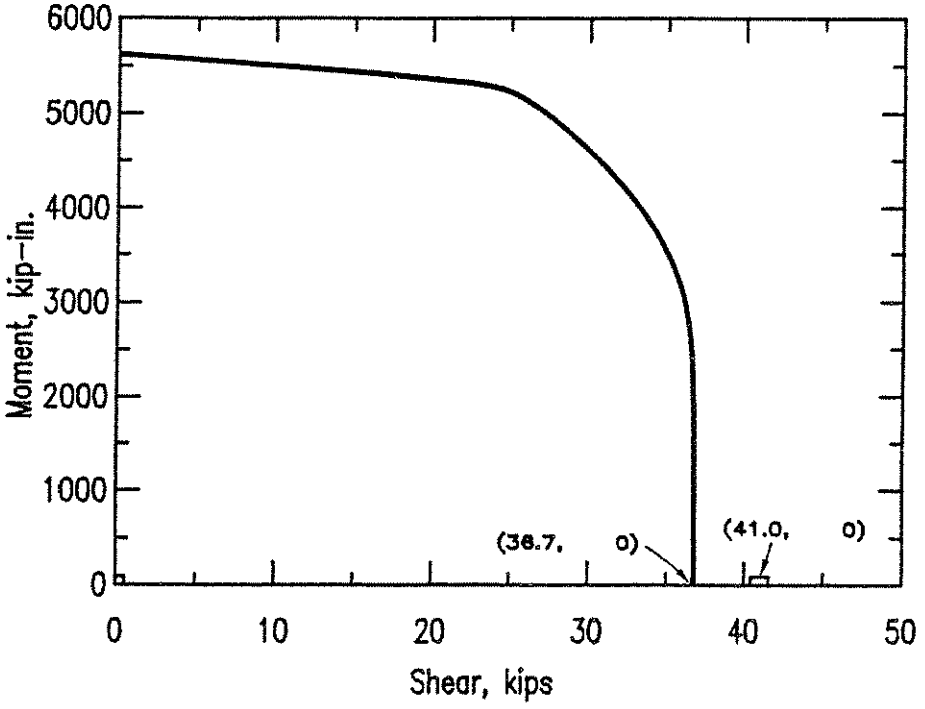

Fig. 4.23 Moment-Shear Interaction Curve for Test 6A.

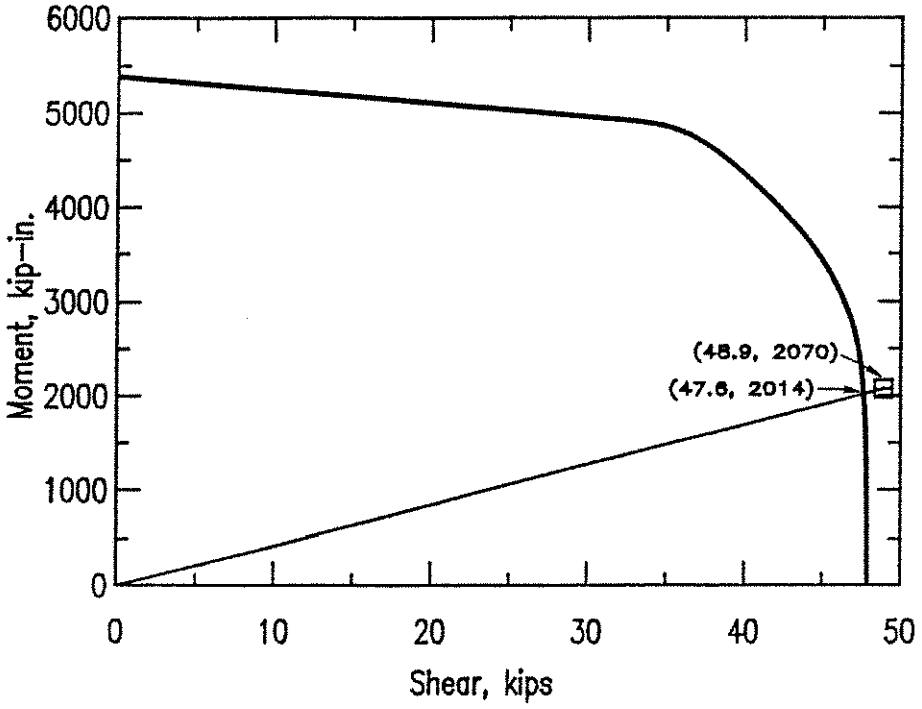

Fig. 4.24 Moment-Shear Interaction Curve for Test 6B.

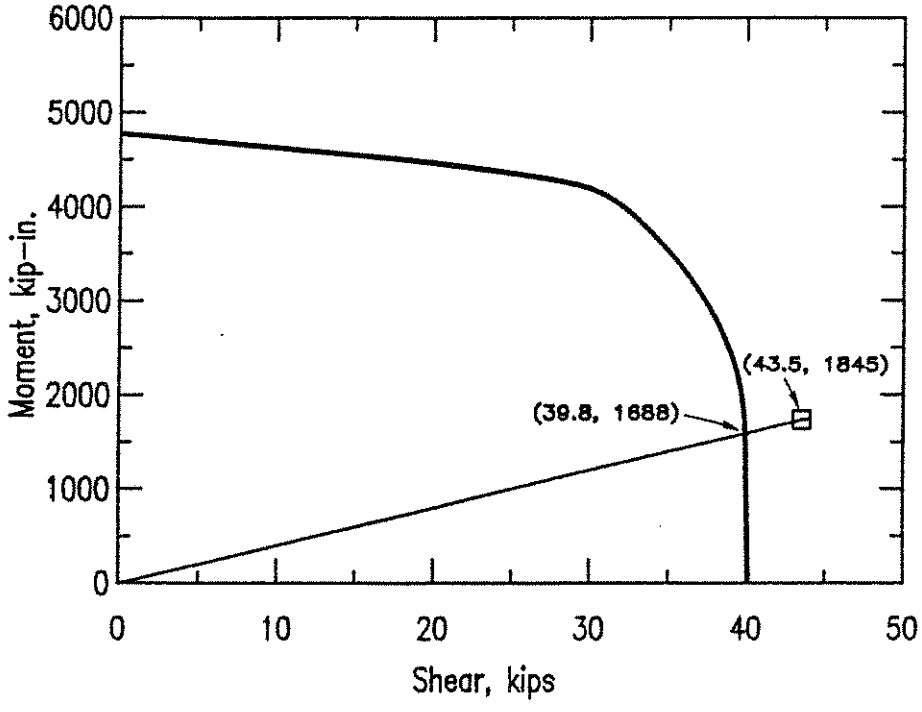

Fig. 4.25 Moment-Shear Interaction Curve for Test 7A.

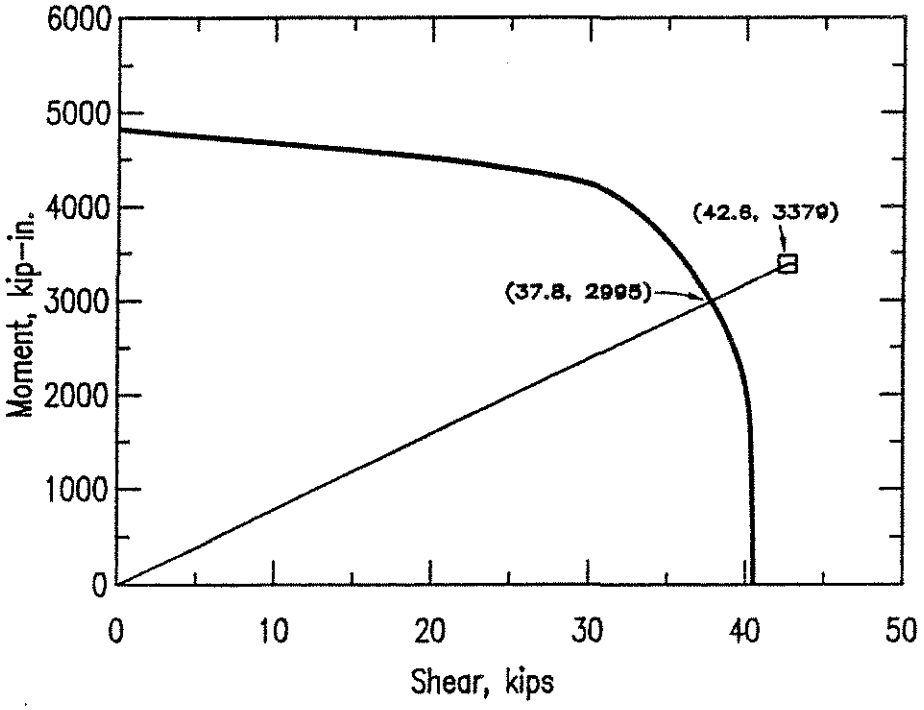

Fig. 4.26 Moment-Shear Interaction Curve for Test 7B.

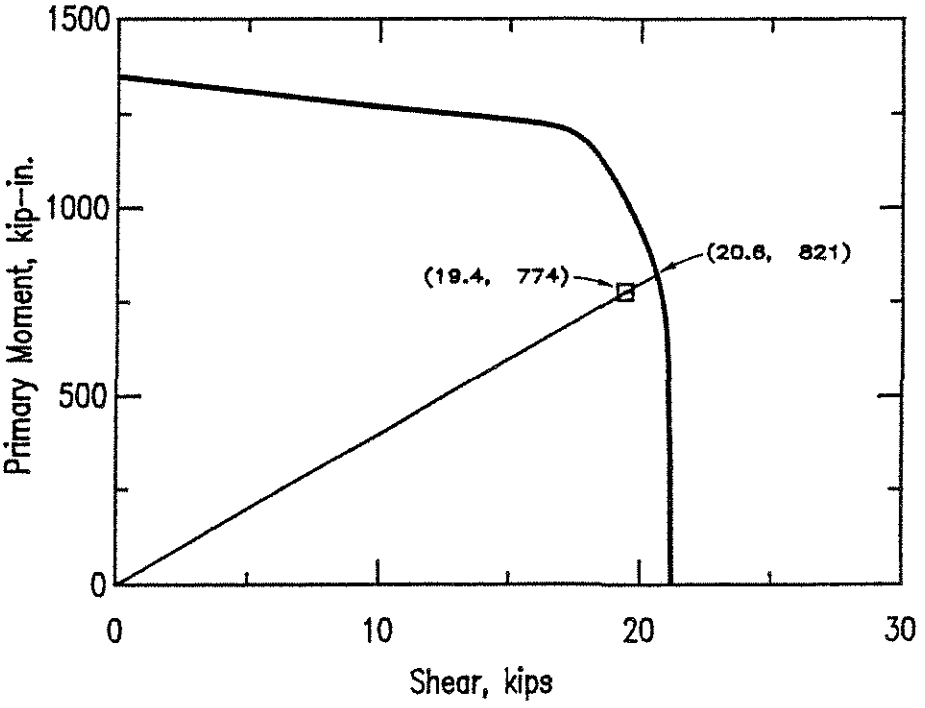

Fig. 4.27 Moment-Shear Interaction Curve for Test 8A.

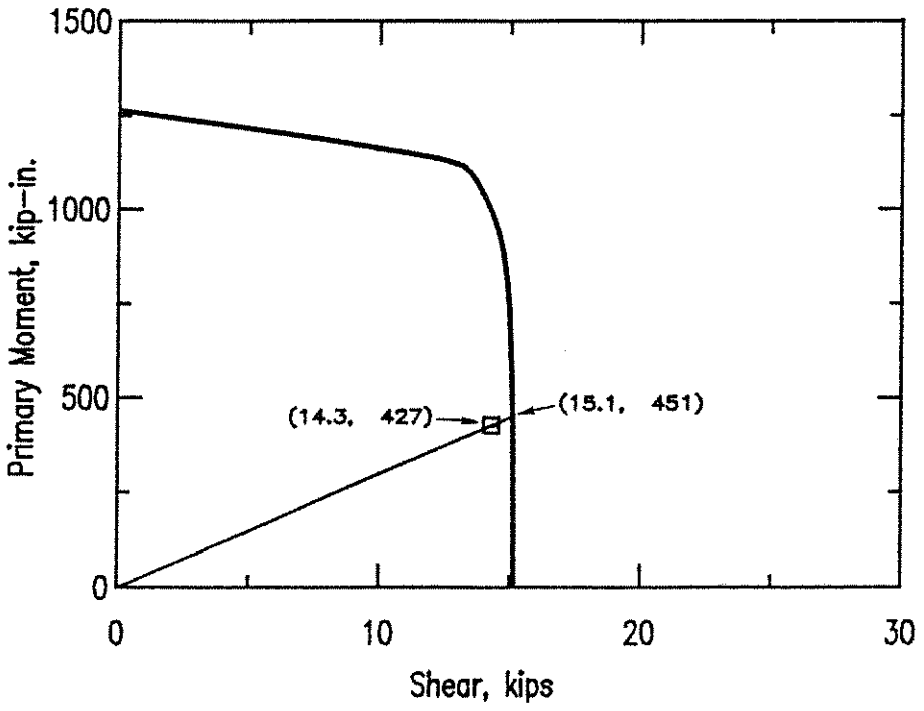

Fig. 4.28 Moment-Shear Interaction Curve for Test 8B.

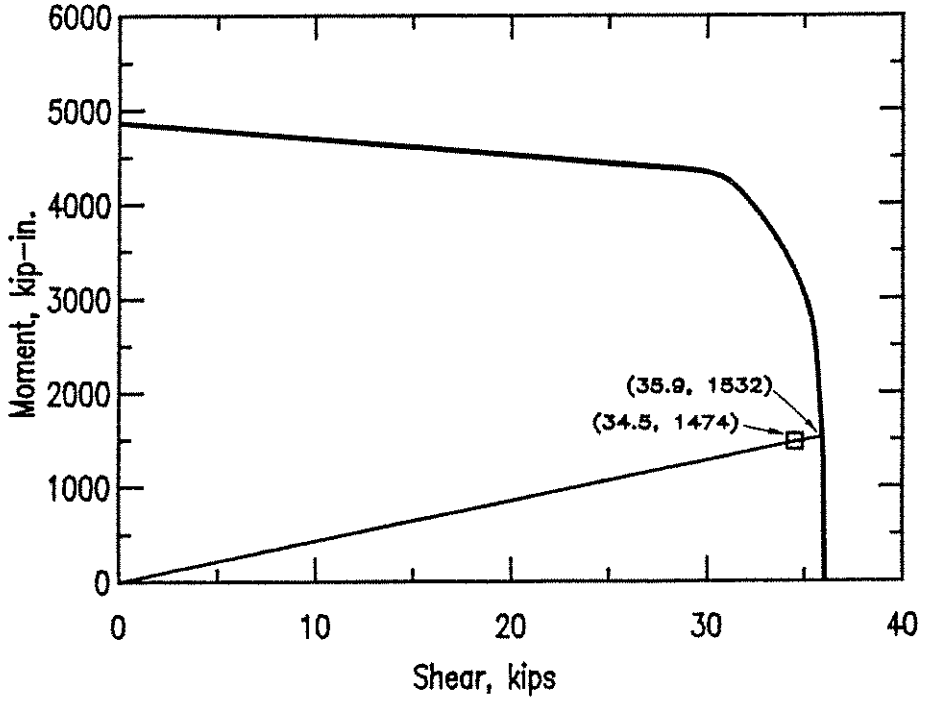

Fig. 4.29 Moment-Shear Interaction Curve for Test 9A.

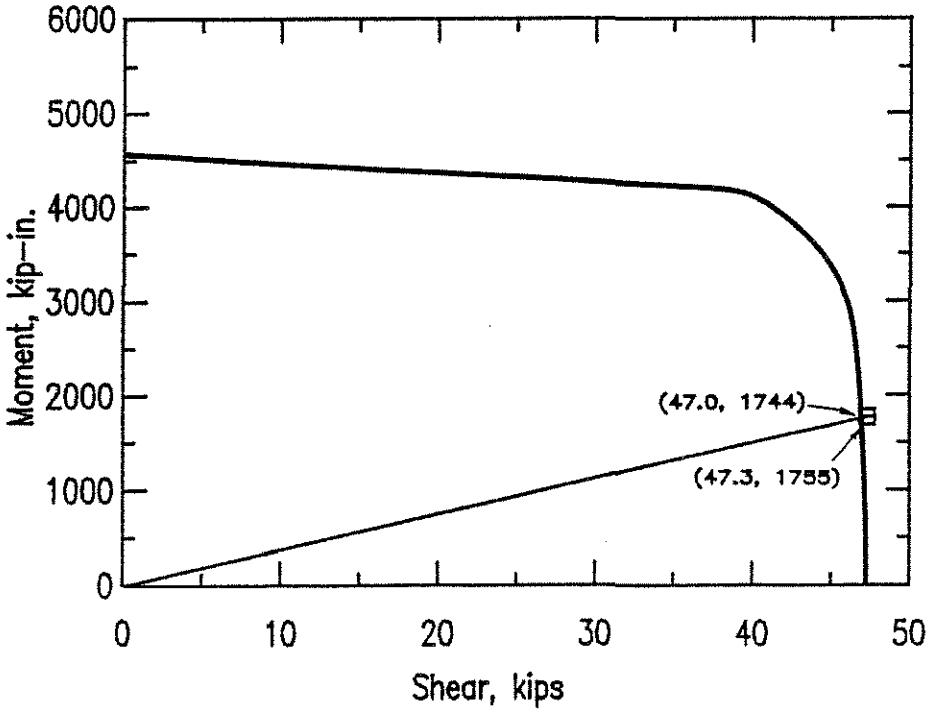

Fig. 4.30 Moment-Shear Interaction Curve for Test 9B.

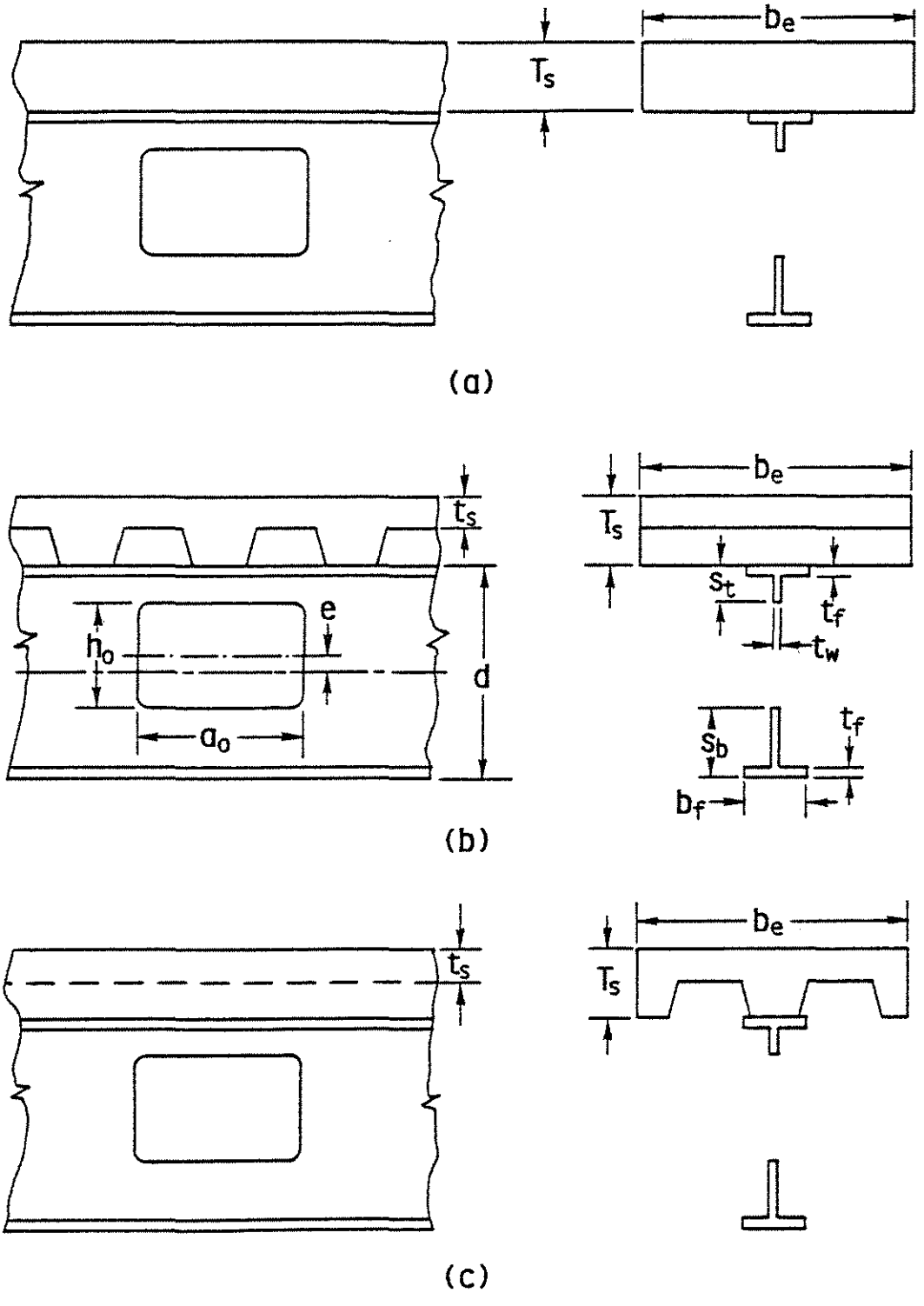

Fig. 5.1 Beam and Opening Configurations. (a) Solid Slab. (b) Ribbed Slab with Transverse Ribs. (c) Ribbed Slab with Longitudinal Ribs.

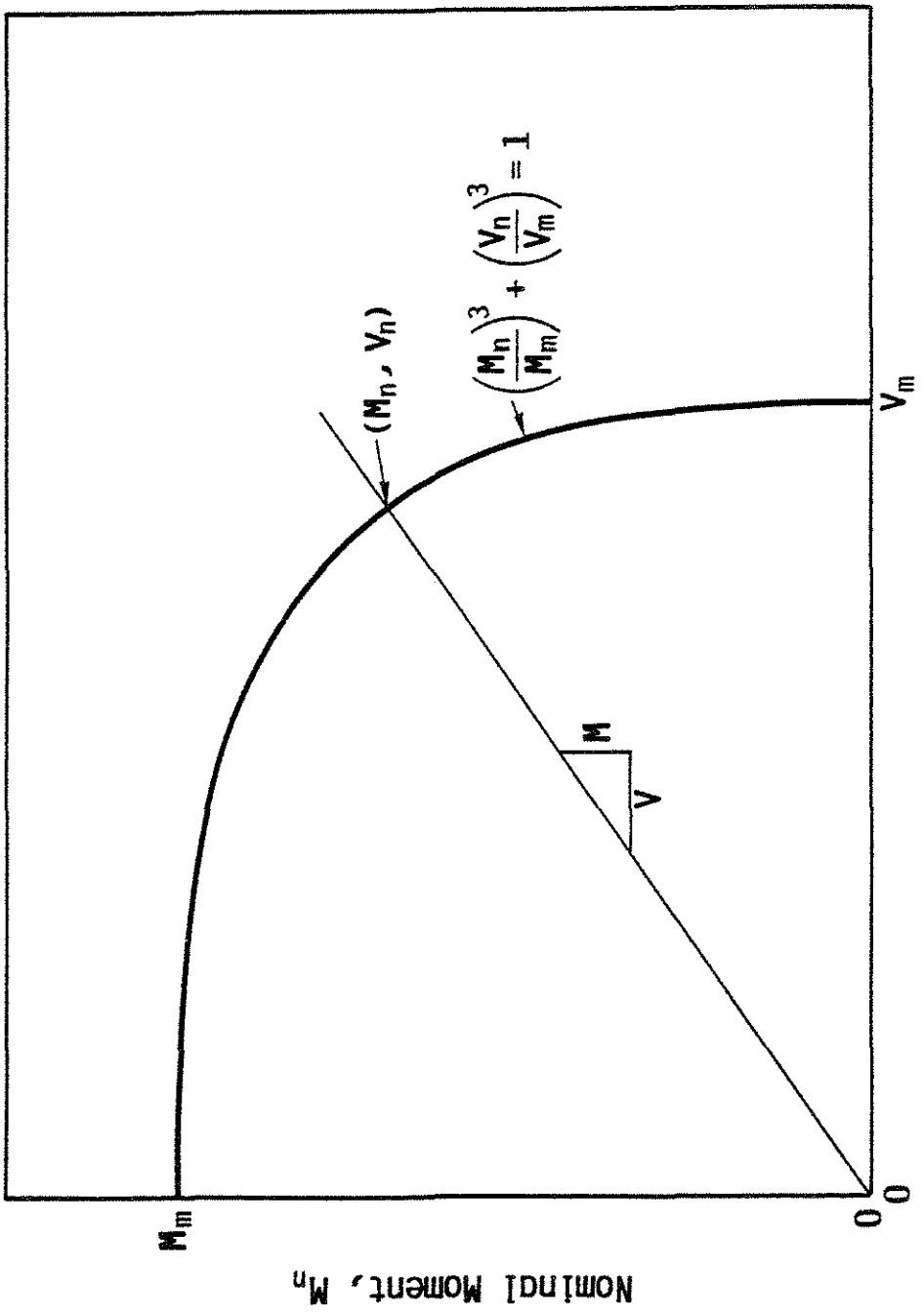

Fig. 5.2 Design Interaction Curve.

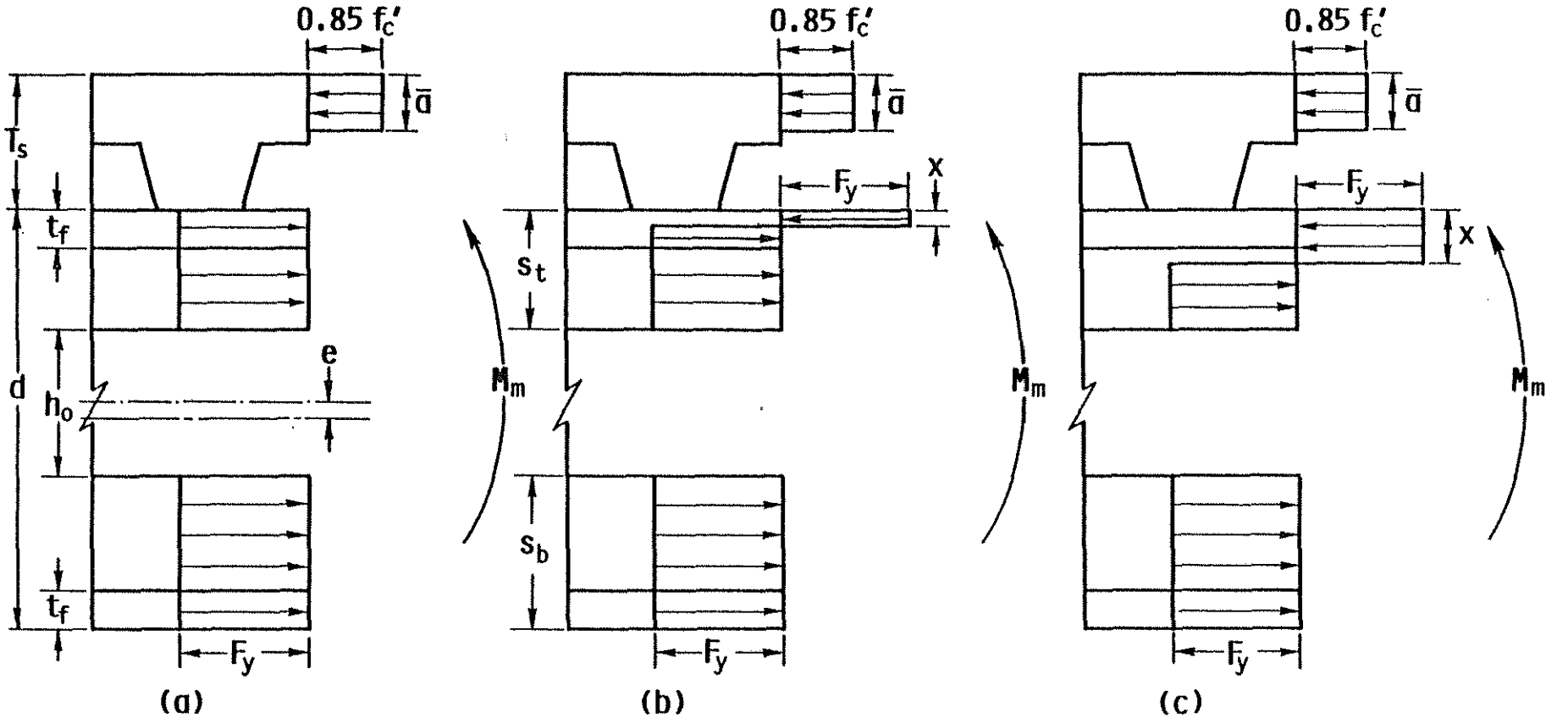

Fig. 5.3 Stress Diagrams at Maximum Moment. (a) Neutral Axis in Slab. (b) Neutral Axis in Flange. (c) Neutral Axis in Web.

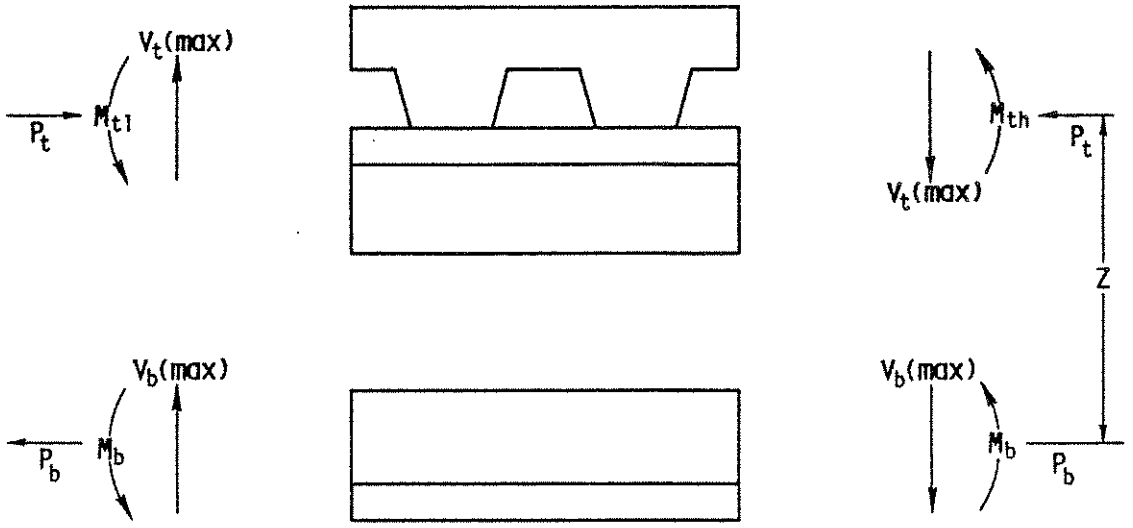

Fig. 5.4 Forces Acting at Web Opening.

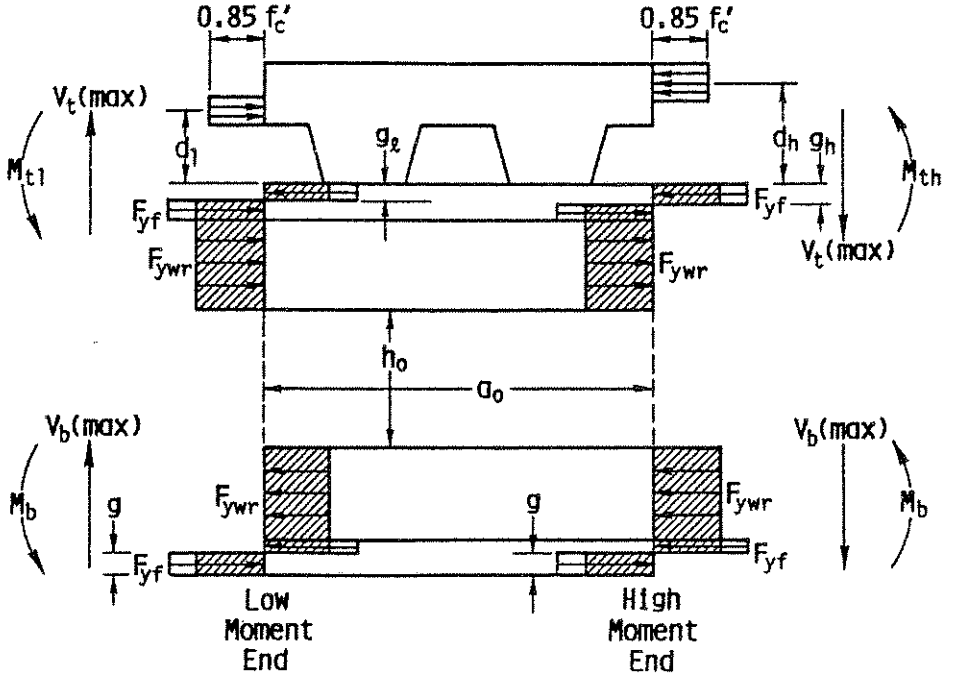

Fig. 5.5 Stress Distributions for Design Method I.

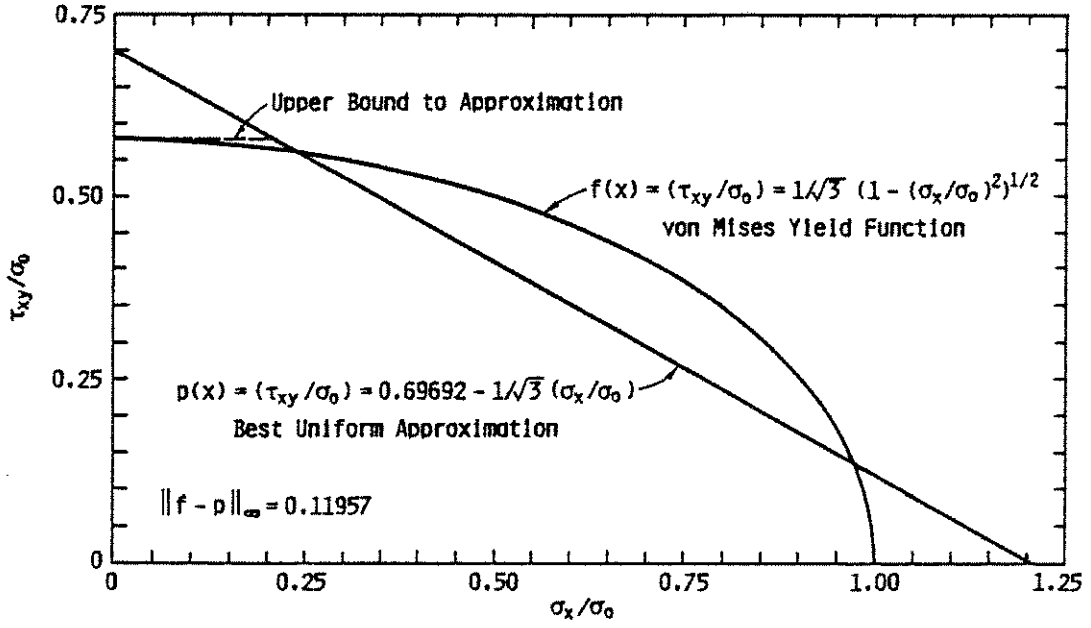

Fig. 5.6 Best Uniform Approximation of the von Mises Yield Function for Plane Stress.

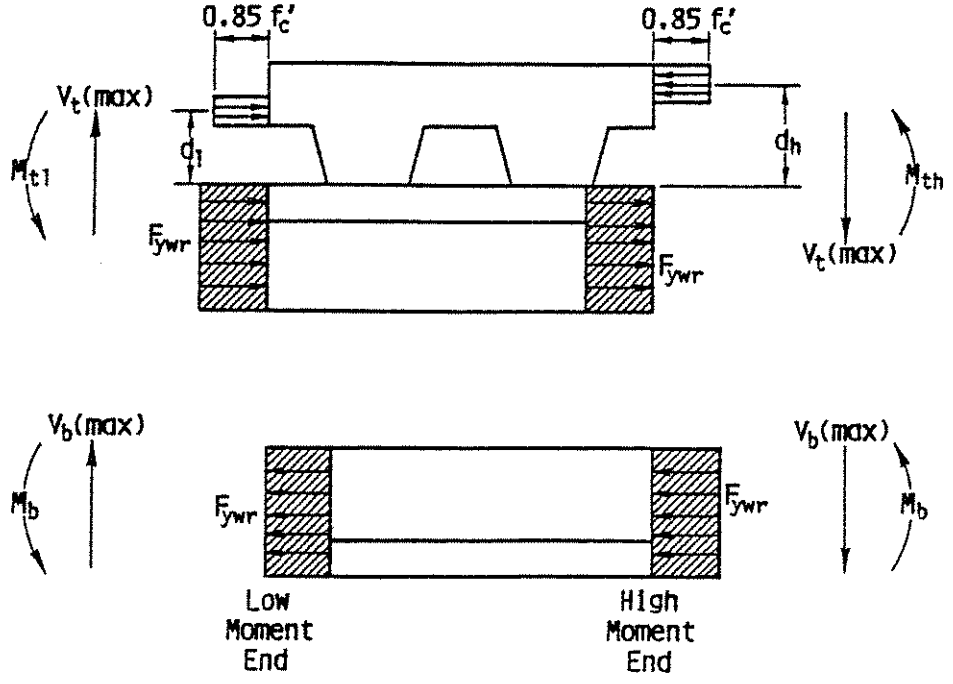

Fig. 5.7 Stress Distributions for Design Methods II and III.

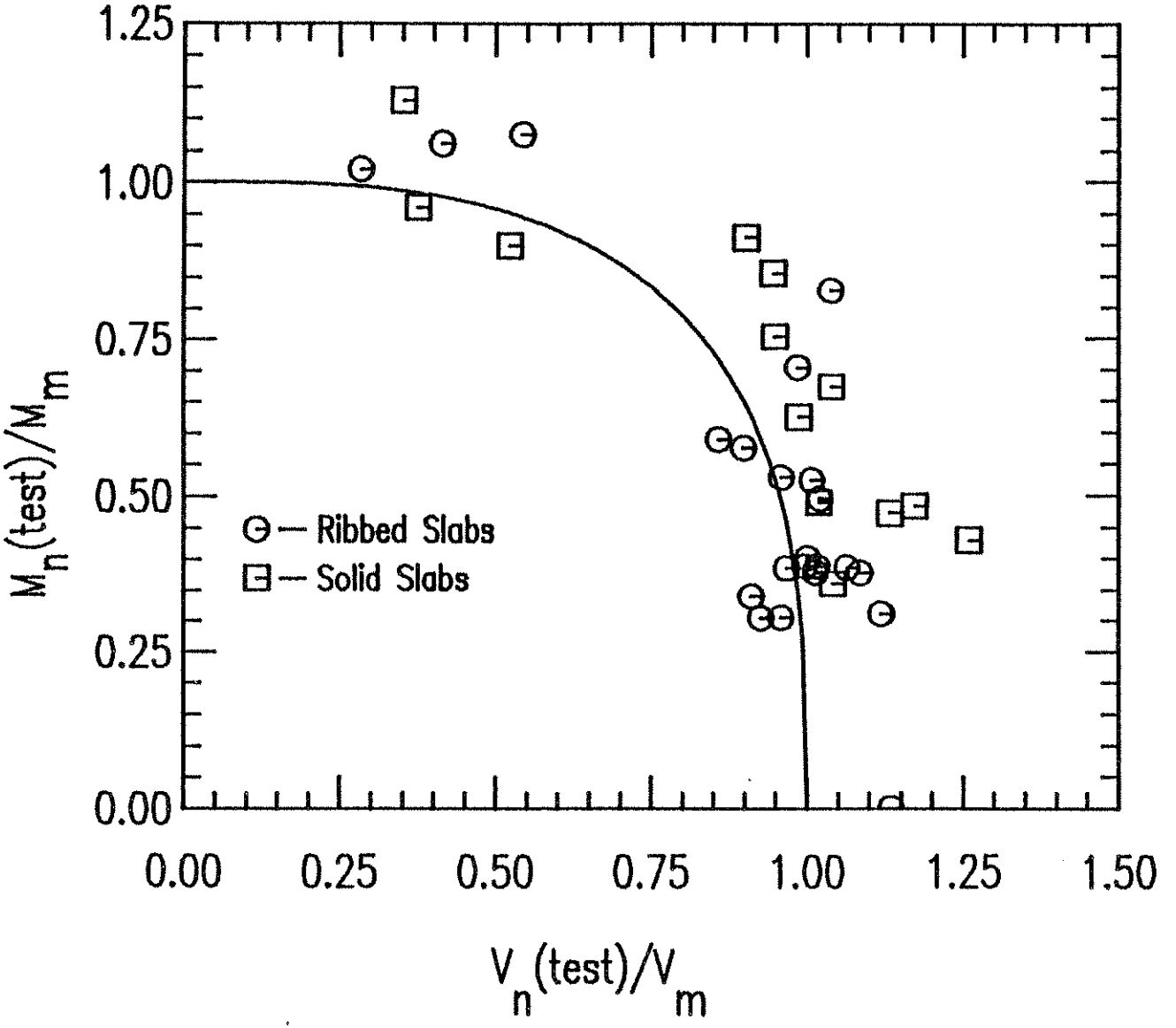

Fig. 5.8 Comparison of Design Method I with Test Results.

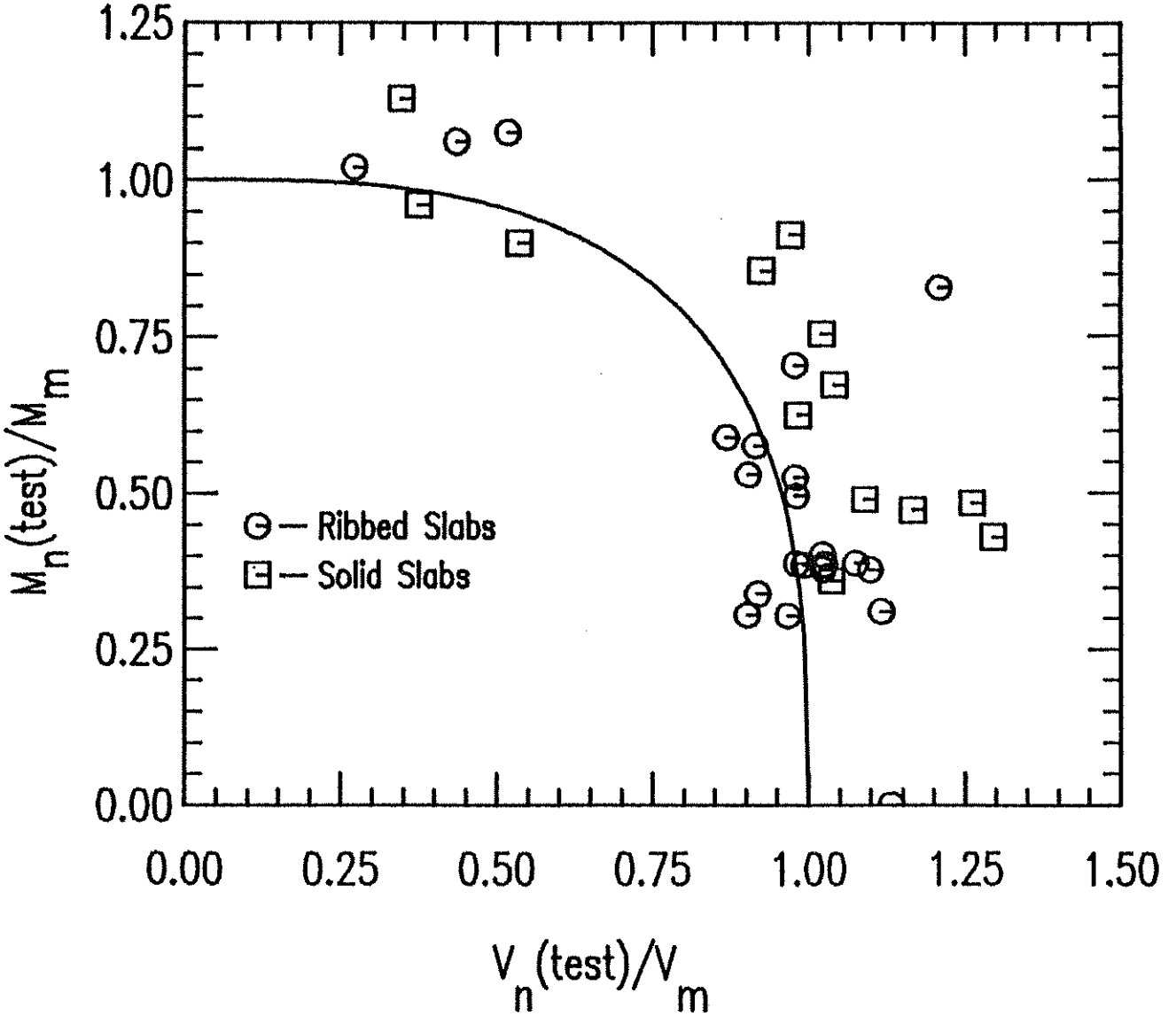

Fig. 5.9 Comparison of Design Method II with Test Results.

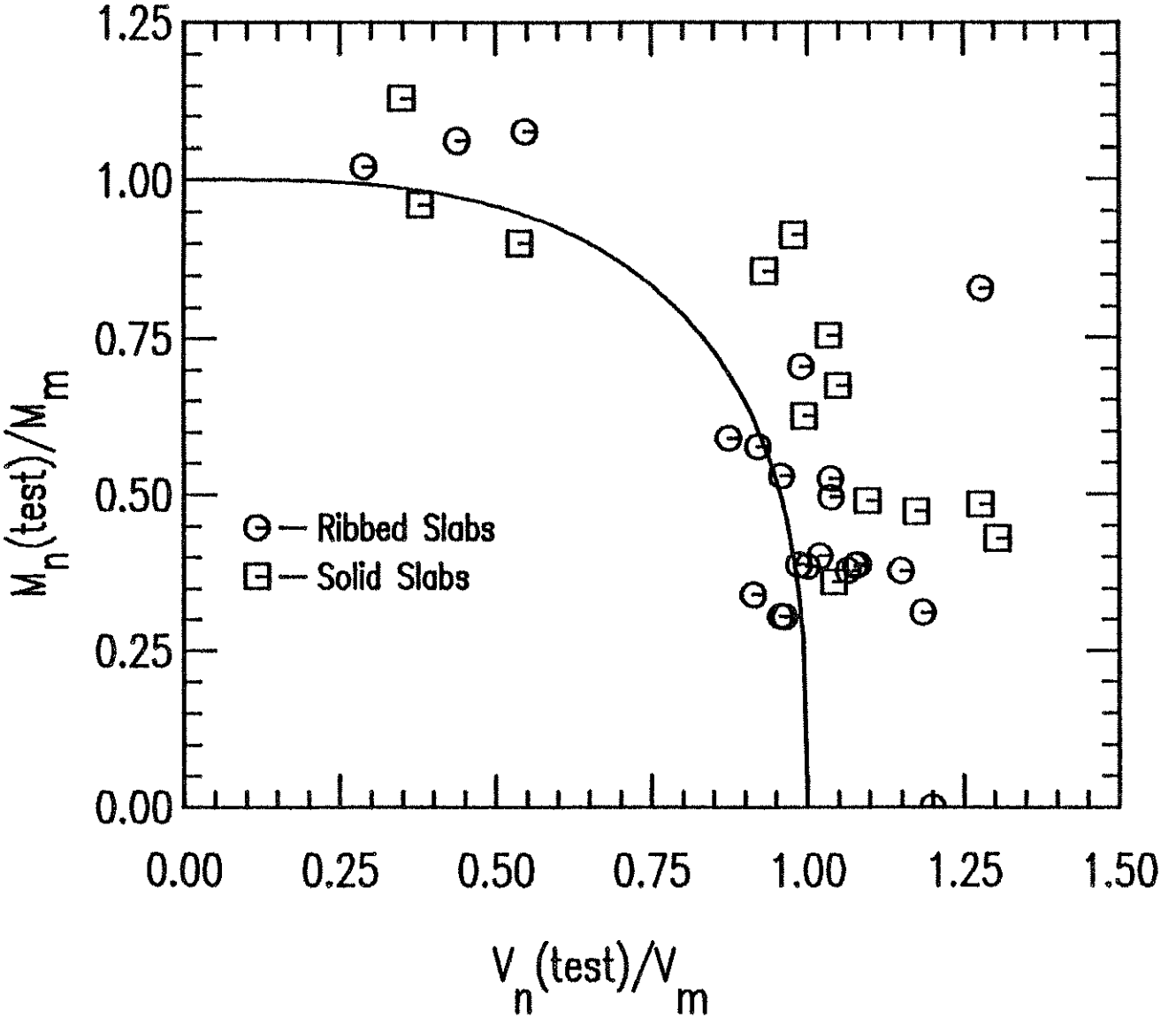

Fig. 5.10 Comparison of Design Method III with Test Results.

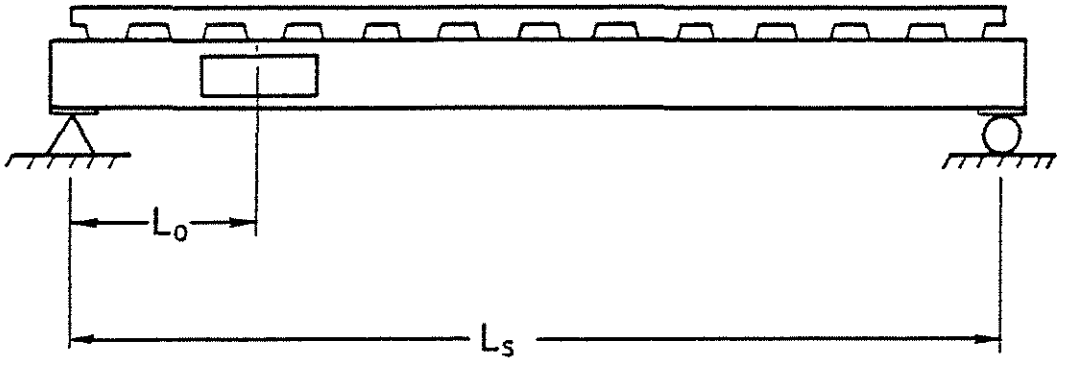

(a)

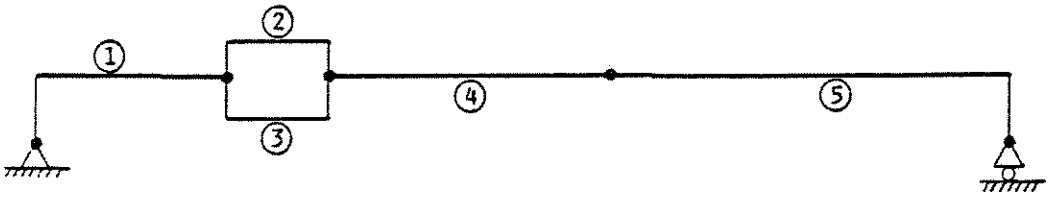

(b)

Fig. 6.1 Composite Beam with Web Opening. (a) Schematic. (b) Deflection Model.

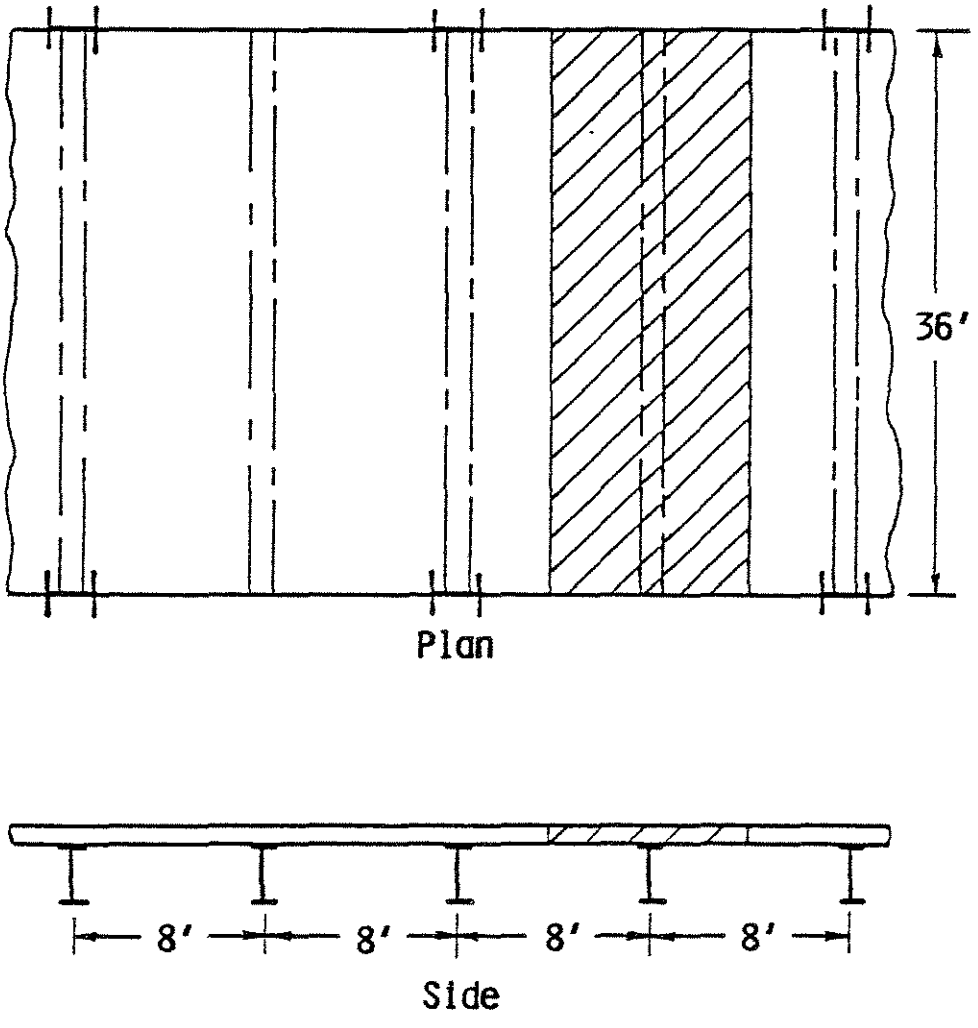

Fig. 6.2 Composite Beam in Floor System.

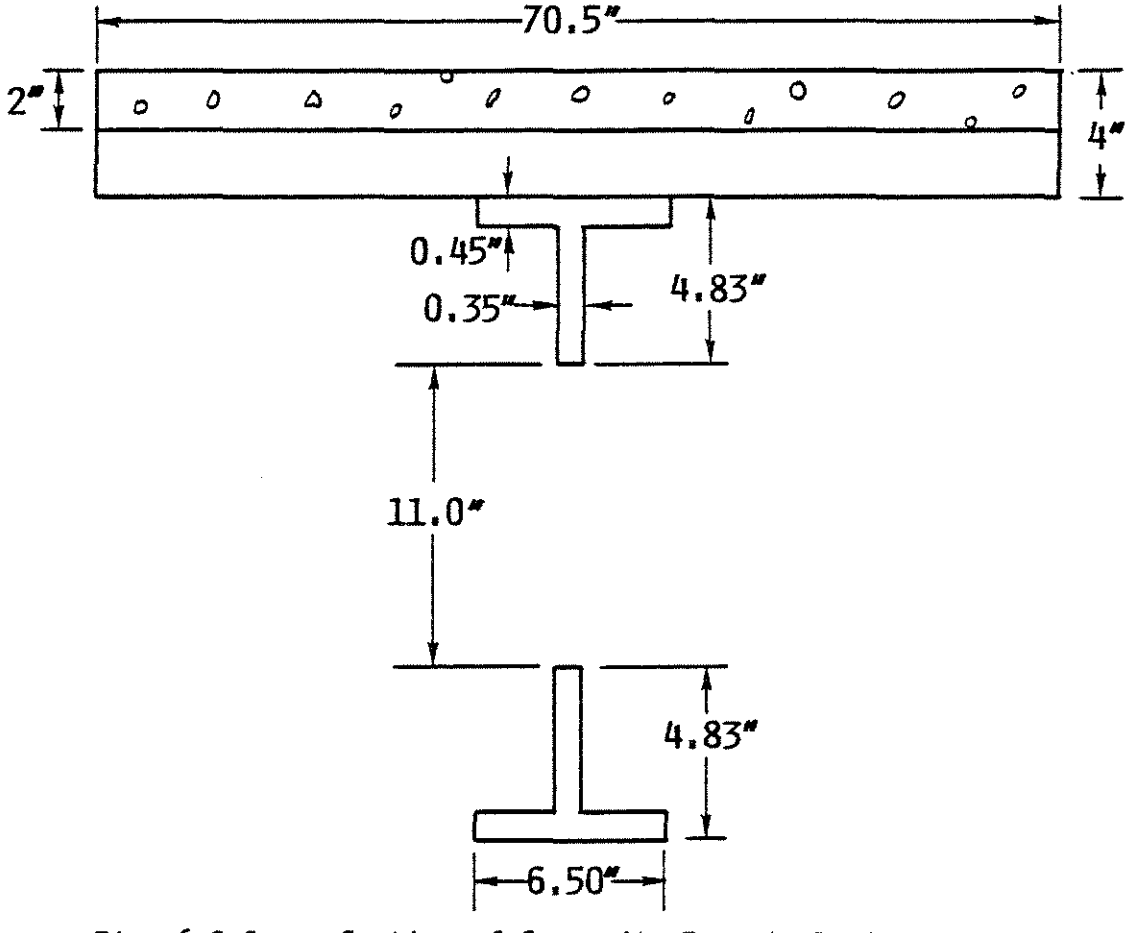

Fig. 6.3 Cross-Section of Composite Beam in Design Example.

APPENDIX A

NOTATION

$\bar{a}$	depth of the stress block in the concrete calculated using a concrete stress of $0.85f'_c$
a_h	depth of the stress block in the slab at the high moment end of the opening
a_l	depth of the stress block in the slab at the low moment end of the opening
a_o	opening length
A_b	effective area for axial stress in the bottom tee
A_{cv}	effective area for shear stress in the slab
A_f	flange area
A_r	area of reinforcing steel suggested to control crack size in the slab above the opening
A_s	stiffener area
A_t	effective area for axial stress in the top tee
A_w	web area
A_y	effective area for shear stress in a beam away from a web opening
A_{yt}	effective area for shear stress in the top tee
A_{yb}	effective area for shear stress in the bottom tee
b_{conc}	total width of slab on test beam
b_e	effective width of slab
b_f	flange width
b_s	total stiffener width, including web thickness
c_h	distance from the neutral axis to the extreme compressive fiber in the slab at the high moment end of the opening

c_l	distance from the neutral axis to the extreme compressive fiber in the slab at the low moment end of the opening
C'	compressive force in the steel section
C_{ai}, i=1-4	constants in the bottom tee moment-axial force equations for the case when the neutral axis is in the web above the stiffener
C_{fi}, i=1-4	constants in the bottom tee moment-axial force equations for the case when the neutral axis is in the flange
C_{si}, i=1-4	constants in the bottom tee moment-axial force equations for the case when the neutral axis is in the stiffener
C_{wi}, i=1-4	constants in the bottom tee moment-axial force equations for the case when the neutral axis is in the web below the stiffener
C_v	coefficient of variation
d	steel section depth
d_h	distance from the top of the flange of the top tee to the centroid of the concrete force at the high moment end of the opening
d_l	distance from the top of the flange of the top tee to the centroid of the concrete force at the low moment end of the opening
D	dead load
e	opening eccentricity
e_{xi}, i=1-2	local x eccentricities at node i for a beam element with two rigid links
e_{yi}, i=1-2	local y eccentricities at node i for a beam element with two rigid links
E	modulus of elasticity
E_c	modulus of elasticity for concrete
f	normal stress in concrete
f'_c	concrete strength

F_u	tensile strength of shear connector
F_y	yield strength of the steel section
F_{yf}	yield strength of the flange in uniaxial tension
F_{ys}	yield strength of the stiffener in uniaxial tension
F_{yw}	yield strength of the web in uniaxial tension
F_{ywr}	the reduced longitudinal yield strength in the web due to shear
g	distance to the neutral axis in the top or bottom tee
g_h	distance to the neutral axis in the top tee at the high moment end of the opening
g_l	distance to the neutral axis in the top tee at the low moment end of the opening
G	shear modulus
h_o	opening height
h_r	rib height
H_s	stud height after welding
I_{eff}	effective moment of inertia for the gross section
I_s	moment of inertia of a steel beam
I_{tr}	moment of inertia of the transformed composite section
$[K_e]$	element stiffness matrix for tee
$[K_g]$	global stiffness matrix for tee
$[K_g]_{wo}$	global stiffness matrix for web opening element
K_{ij}	elements of global stiffness matrix for web opening element
l_b	length of rigid links connecting beam element to the bottom tee element
l_t	length of rigid links connecting beam elements to the top tee element

L	live load or length of a uniform beam element
L_o	distance from a beam support to the centerline of a web opening
L_s	beam span
M	primary moment at the opening centerline
M_b	secondary moment at each end of the bottom tee
M_{bh}	secondary moment in the bottom tee at the high moment end of the opening
M_{bl}	secondary moment in the bottom tee at the low moment end of the opening
M_m	maximum moment capacity
M_n	nominal moment capacity at a web opening
$M_n(test)$	total moment at failure for test opening
$M_{primary}$	primary moment at the opening centerline
M_{th}	secondary moment in the top tee at the high moment end of the opening
M_{tl}	secondary moment in the top tee at the low moment end of the opening
M_u	factored moment at the opening centerline
n	squash load ratio
n^f_{xh}	squash load ratio at crossover of the neutral axis from the web to the flange the high moment end of the bottom tee
n^s_{xh}	squash load ratio at crossover of the neutral axis from the stiffener to the web below the stiffener at the high moment end of the bottom tee
n^w_{xh}	squash load ratio at crossover of the neutral axis from the web above the stiffener to the stiffener at the high moment end of the bottom tee
n^f_{xl}	squash load ratio at crossover of the neutral axis from the flange to the web at the low moment end of the bottom tee

N	number of studs between the high moment end of the opening and the support
N_o	number of stud shear connectors above the web opening
N_r	number of studs per rib
P	axial force in tee
P_b	bottom tee axial force
P_{bl}	bottom tee axial force at low moment end of opening
P_{bh}	bottom tee axial force at high moment end of opening
P_c	crushing capacity of slab
P_{ch}	concrete force at high moment end of web opening
P_{cl}	concrete force at low moment end of web opening
P_{sh}	steel force at high moment end of web opening
P_{smax}	maximum capacity of top tee steel
P_{sl}	steel force at low moment end of opening
P_t	top tee axial force
P_{th}	top tee axial force at high moment end of opening
P_{tl}	top tee axial force at low moment end of opening
P_{wb}	normal force in the bottom tee web
P_{wt}	normal force in the top tee web
P^f_{xh}	normal force in the steel tee at crossover of the neutral axis from the web to the flange at high moment end of opening
P^f_{xl}	normal force in steel tee at crossover of the neutral axis from the web to the flange at low moment end of opening
P^s_{xl}	normal force in steel tee at crossover of the neutral axis from the web below the stiffener to the stiffener at low moment end of opening

P^{w}_{xl}	normal force in steel tee at crossover of the neutral axis from the stiffener to the web above the stiffener at low moment end of opening
q	percentage of maximum top tee shear capacity applied to top tee
q'	parameter for distribution of shear between top and bottom tees
Q_n	nominal strength of one stud shear connector embedded in a solid slab
r	coefficient of correlation
R	reduction factor for studs in ribbed slabs
s_b	web stub depth for bottom tee
s_t	web stub depth for top tee
t_e	effective slab thickness for shear stress
t_f	flange thickness
t_s	minimum slab thickness
t_w	web thickness
T'	yield capacity of net steel section at web opening
T_s	maximum slab thickness
u_{gi}, i=1-2	global degree of freedom in the x direction at node i
$u_{\ell i}$, i=1-2	local degree of freedom in the x direction at node i
$\{U_g\}$	global degrees of freedom for beam element
$\{U_\ell\}$	local degrees of freedom for beam element
v_{gi}, i=1-2	global degree of freedom in the y direction at node i
$v_{\ell i}$, i=1-2	local degree of freedom in the y direction at node i
V	shear force acting at opening centerline
V_b	shear assigned to the bottom tee
V_b(max)	maximum shear capacity of bottom tee

V_h	smaller of the tensile yield capacity of the gross steel section or the crushing strength of the concrete slab
V_h'	sum of shear stud capacities between the point of maximum moment and the nearest point of zero moment
V_m	maximum shear capacity at web opening
V_n	nominal shear capacity at web opening
V_{pb}	plastic shear capacity of the bottom tee web
V_{pt}	plastic shear capacity of the top tee web
$V_t(sh)$	"pure shear" capacity for the top tee
$V_t(max)$	"mechanism" shear capacity of top tee
V_{tc}	shear due to secondary moment from the concrete
V_{tm}	top tee shear strength, smaller of $V_t(max)$ and $V_t(sh)$
$V_n(test)$	total shear at failure for web opening test
w	uniform load applied to beam
w_r	average rib width
x	neutral axis location in the top tee
x_g	global coordinate x axis
x_b	local coordinate x axis for bottom tee
x_t	local coordinate x axis for top tee
y_{ch}	distance from bottom of top tee to centroid of concrete force at high moment end of opening
y_{cl}	distance from bottom of top tee to centroid of concrete force at low moment end of opening
y_s	distance from bottom of top tee to centroid of stiffener
z	distance between the axial forces in the top and bottom tees
α, β, γ	parameters for maximum shear capacity calculation

α_b	parameter for bottom tee maximum shear capacity calculation
β_b, η_b	element stiffness matrix parameters for the bottom tee
β_t, η_t	element stiffness matrix parameter for the top tee
$\bar{\delta}$	normalized opening deflection at failure
$[\bar{\delta}]$	eccentricity transformation matrix
δ_o	deflection across web opening at failure
δ_m	deflection at point of maximum moment at failure
Δ_b	calculated deflection considering bending only
Δ_s	calculated deflection considering shear only
θ_{gi}, i=1-2	global degree of freedom for rotation at node i
$\theta_{\ell i}$, i=1-2	local degree of freedom for rotation at node i
λ	coefficient in linear approximation to von Mises criterion
μ, ν	factors for maximum shear capacity of top tee
σ_o	yield stress obtained from uniaxial tension test
σ_x	normal stress, reduced for shear
τ	shear stress in the slab
τ_b	shear stress in the bottom tee web
τ_t	shear stress in the top tee web
τ_{xy}	shear stress
ϕ_b	flexural strength reduction factor
ϕ_v	shear strength reduction factor

APPENDIX B

SUMMARY OF PREVIOUS EXPERIMENTAL WORK

A number of experimental investigations of composite beams with rectangular web openings have been conducted (8, 9, 11, 19, 32, 34, 37, 41). Granade (19), Clawson and Darwin (9, 11), and Cho (8) tested composite beams with solid, or flat-soffit slab construction. Redwood and others at McGill University (32, 34, 46) tested composite beams with ribbed slab construction with the ribs oriented transverse to the steel section. Prototype tests were conducted in Illinois (37) and Australia (41). The test configurations used in previous investigations are summarized in Tables B.1 - B.3. The test results for the previous investigations are summarized in Table B.4. The two prototype tests are not included in the tables. The beam tested by Wiss, Janney, and Elstner Associates (37) failed by longitudinal shearing of the slab near a support, and the failure was not related to the web opening. The test conducted by Thompson and Ainsworth (41) was not continued to failure.

Table B.1 Material Strengths for Previous Investigations

	Yield Strengths, ksi					
Test*	Top Flange	Bottom Flange	Web	Stiffener	F_u** ksi	f'_c psi
G1	43.8	43.8	47.9	---	N.A.	3970
G2	43.8	43.8	47.9	---		3990
C1	39.4	40.4	38.5	---	N.A.	7000
C2	39.3	39.9	42.4	---		4200
C3	39.3	39.9	42.4	---		4930
C4	46.4	44.9	52.0	---		4460
C5	43.9	45.1	44.2	---		4680
C6	42.9	43.5	49.8	---		4020
CHO3	44.1	43.4	50.8	---	60.3	3270
CHO4	54.0	50.7	64.6	---	60.3	3040
CHO5	54.0	50.7	64.6	---	60.3	3270
CHO6	44.1	43.4	50.8	50.8	60.3	3270
CHO7	54.0	50.7	64.6	50.8	60.3	3170
R0	50.6	50.6	56.1	---	N.A.	3830
R1	40.1	40.1	45.1	---		3190
R2	43.8	43.8	47.3	---		2830
R3	42.2	42.2	47.2	---		4290
R4	43.7	43.7	48.1	---		3960
R5	40.1	40.1	45.1	---		3190
R6	43.7	43.7	47.2	---		2610
R7	43.7	43.7	47.2	---		2610
R8	44.1	44.1	44.0	---		2480

* G - Granade (19)
C - Clawson and Darwin (9, 11)
CHO - Cho (8)
R - McGill Tests (32, 34)

** Stud tensile strength
N.A. indicates data not available

Table B.2 Section and Opening Dimensions for Previous Investigations, in.

Test[t]	d	b_f(Top)	t_f(Top)	t_w	s_t	s_b
G1	8.00	6.54	0.463	0.285	1.630	1.630
G2	8.00	6.54	0.463	0.285	1.630	1.630
C1	14.00	6.75	0.453	0.287	3.003	3.003
C2	17.88	7.50	0.475	0.356	3.475	3.770
C3		7.50	0.475	0.356	3.605	3.650
C4		7.50	0.485	0.343	3.485	3.555
C5	18.13	6.00	0.623	0.380	3.683	3.745
C6	14.00	6.69	0.475	0.296	2.855	2.803
CHO3	7.87	5.91	0.354	0.236	1.500	1.500
CHO4	11.81	5.91	0.354	0.256	2.360	2.400
CHO5	11.81	5.91	0.354	0.256	2.400	2.320
CHO6	7.87	5.91	0.354	0.236	1.540	1.500
CHO7	11.81	5.91	0.354	0.256	2.360	2.360
R0	9.98	4.02	0.256	0.228	2.039	2.039
R1	14.01	6.87	0.448	0.293	2.810	2.810
R2	14.05	6.74	0.441	0.309	2.830	2.830
R3	14.03	6.74	0.444	0.313	2.820	2.820
R4	14.04	6.86	0.436	0.313	2.835	2.835
R5	14.01	6.87	0.448	0.293	1.410	4.210
R6	14.05	6.75	0.437	0.305	2.835	2.835
R7	14.05	6.75	0.437	0.305	2.835	2.835
R8	13.98	6.69	0.450	0.292	2.795	2.795

Test[t]	b_f(Bot)	t_f(Bot)	b_{conc}	b_e*	t_s	T_s	Opening Size
G1	6.54	0.463	24.0	24.0	3.6	3.6	4.80 x 7.20
G2	6.54	0.463	24.0	24.0	3.6	3.6	4.80 x 7.20
C1	6.75	0.453	48.0	48.0	4.0	4.0	8.00 x 16.00
C2	7.50	0.520	48.0	48.0	4.0	4.0	10.81 x 21.63
C3	7.50	0.520	48.0	48.0	4.0	4.0	10.81 x 21.63
C4	7.50	0.495	48.0	45.0	4.0	4.0	10.81 x 21.63
C5	6.00	0.615	48.0	48.0	4.0	4.0	10.81 x 21.63
C6	6.69	0.423	48.0	45.0	4.0	4.0	8.00 x 16.00
CHO3	5.91	0.354	21.6	21.6	5.3	5.3	4.72 x 7.28
CHO4	5.91	0.354	23.8	23.8	5.4	5.4	7.05 x 10.63
CHO5	5.91	0.354	23.8	23.8	5.3	5.3	7.09 x 10.63
CHO6+	5.91	0.354	23.8	23.8	5.3	5.3	4.61 x 7.13
CHO7+	5.91	0.354	23.8	23.8	5.3	5.3	7.09 x 14.37
R0	4.02	0.256	39.4	39.4	2.6	5.6	5.91 x 11.81
R1	6.87	0.448	47.2	39.4	2.6	5.6	8.39 x 16.77
R2**	6.74	0.441	47.2	47.2	2.6	5.6	8.39 x 16.77
R3**	6.74	0.444	47.2	47.2	2.6	5.6	8.39 x 16.75
R4**	6.86	0.436	47.2	47.2	2.6	5.6	8.39 x 16.75
R5	6.87	0.448	47.2	39.4	2.6	5.6	8.39 x 16.77
R6	6.75	0.437	39.4	39.4	2.6	5.6	8.39 x 16.75
R7	6.75	0.437	39.4	39.4	2.6	5.6	8.39 x 16.75
R8	6.69	0.450	39.4	39.4	2.6	5.6	8.39 x 16.75

t G = Granade (19), C - Clawson and Darwin (9, 11)
CHO - Cho (8), R - McGill Tests (32, 34)

* b_e = effective slab width (as per Reference 2)

\+ stiffeners on top and bottom tees: $t_s = 0.236$, $b_s = 4.170$, $y_s = 0.374$

** cover plates of unknown thickness and width were welded to the bottom flange away from the opening.

Table B.3 Stud and Rib Properties for Previous Investigations.

Test	Stud Diameter in.	H_s + in.	h_r t in.	w_r tt in.	N_o *	N **
G1	5/8	2.5	---	---	2	10
G2					2	16
C1	3/4	3.0	---	---	4	14
C2					2	16
C3					2	16
C4					4	10
C5					4	16
C6					4	10
CHO3	1/2	3.94	---	---	4	12
CHO4					4	18
CHO5					4	20
CHO6					4	12
CHO7					4	20
RO	3/4	4.84	3.0	6.0	1*1	4*1
R1					1*1	4*1
R2					1*2	9*2
R3					2*2	11*2
R4					1*0	5*1
R5					1*1	4*1
R6					2*0	2*2
R7					2*2	4*2
R8					2*2	4*2

+ H_s = stud height after welding

t h_r = rib height

tt w_r = average rib width

* N_o = no. of studs over opening -- For ribbed slabs = no. of ribs * no. of studs/rib

** N = no. of studs between high moment end of opening and support -- For ribbed slabs = no. of ribs * no. of studs/rib

Table B.4 Test Results for Previous Investigations.

Test*	Applied Load $\frac{M}{V}$ at Opening (ft)	Total Load $\frac{M}{Vd}$ at opening	Reported Maximum Load at Opening M (in.-kips)	V (kips)
G1	2.00	3.02	791	32.7
G2	4.00	6.11	1296	26.5
C1	7.00	6.17	2886	33.4
C2	9.00	6.24	4107	36.8
C3	33.00	21.84	5468	14.0
C4	3.00	2.02	1723	47.6
C5	6.00	4.03	3511	48.1
C6	3.00	2.60	1471	40.4
CHO3	1.48	2.26	634	35.7
CHO4	2.63	2.68	1477	46.7
CHO5	10.83	10.97	2319	17.9
CHO6	1.48	2.26	721	40.6
CHO7	10.83	11.95	2664	20.6
R0	3.28	4.14	752	18.2
R1	3.10	2.69	978	26.0
R2	8.20	7.20	2904	28.7
R3	19.68	17.36	3995	16.4
R4	19.68	17.49	3217	13.1
R5	3.10	2.68	1037	27.6
R6	3.10	2.65	788	21.2
R7	3.10	2.64	1133	30.5
R8	3.10	2.66	1075	28.9

* G - Granade (19)
  C - Clawson and Darwin (9, 11)
  CHO - Cho (8)
  R - McGill Tests (32, 34)

APPENDIX C

DETERMINATION OF NEUTRAL AXES LOCATIONS IN THE BOTTOM TEE

In the bottom tee, the neutral axis may be located within one of two regions at the low moment end and within one of four regions at the high moment end. The following procedure is used to establish the neutral axis location at each end of the opening.

The moment-axial force equations for the bottom tee are given below. The neutral axis at the low moment end of the opening is initially assumed to be in the flange. The four possible neutral axis locations at the high moment end of the opening are then checked for a valid solution. If no solution is obtained, the neutral axis at the low moment end of the opening is assumed to be in the web. The four possible locations at the high moment end are then checked for a valid solution.

C.1 NEUTRAL AXIS IN THE FLANGE AT THE LOW MOMENT END

When the neutral axis is above the stiffener at the high moment end of the opening, moment equilibrium requires that

$$V_b a_o = M_{bl} + M_{bh}$$

$$= (C_{f1}^2 C_{f3} + C_{a1}^2 C_{a3}) n^2 + 2(C_{f1} C_{f2} C_{f3} - C_{a1} C_{a2} C_{a3}) n + C_{f2}^2 C_{f3} + C_{a2}^2 C_{a3} + C_{f4} + C_{a4} \qquad (C.1)$$

in which C_{f1}, C_{f2}, C_{f3}, and C_{f4} are given by Eq. (4.11a)-(4.11e) and C_{a1}, C_{a2}, C_{a3}, and C_{a4} are given by Eq. (4.19a)-(4.19e).

The crossover shear at the high moment end, V_{xh}, is obtained by substituting n^s_{xh} (Eq. (4.23)) for n in Eq. (C.1). The crossover shear at the low moment end, V_{xl}, is obtained by substituting n^f_{xl} (Eq. (4.17)) for n in Eq. (C.1). If $V_b \leq V_{xh}$ and $V_b \leq V_{xl}$, Eq. (C.1) is valid for V_b and is solved for n.

When the neutral axis is in the stiffener at the high moment end, moment equilibrium requires that

$$V_b a_o = M_{bl} + M_{bh}$$

$$= (C_{f1}^2 C_{f3} + C_{s1}^2 C_{s3})n^2 + 2(C_{f1}C_{f2}C_{f3} - C_{s1}C_{s2}C_{s3})n + C_{f2}^2 C_{f3} + C_{s2}^2 C_{s3} + C_{f4} + C_{s4} \qquad (C.2)$$

in which C_{s1}, C_{s2}, C_{s3}, and C_{s4} are given by Eq. (4.21a)-(4.21e).

V_{xh} is obtained by substituting n^w_{xh} (Eq. (4.25)) for n in Eq. (C.2), while V_{xl} is obtained by substituting n^f_{xl} (Eq. (4.17)) for n in Eq. (C.2). If $V_b \leq V_{xh}$ and $V_b \leq V_{xl}$, Eq. (C.2) is valid for V_b and is solved for n.

When the neutral axis is in the web at the high moment end, moment equilibrium requires that

$$V_b a_o = M_{bl} + M_{bh}$$

$$= (C_{f1}^2 C_{f3} + C_{w1}^2 C_{w3})n^2 + 2(C_{f1}C_{f2}C_{f3} - C_{w1}C_{w2}C_{w3})n + C_{f2}^2 C_{f3} + C_{w2}^2 C_{w3} + C_{f4} + C_{w4} \qquad (C.3)$$

in which C_{w1}, C_{w2}, C_{w3}, and C_{w4} are given by Eq. (4.15a)-(4.15e).

V_{xh} is obtained by substituting n_{xh}^f (Eq. (4.27)) for n in Eq. (C.3), while V_{xl} is obtained by substituting n_{xl}^f (Eq. (4.17)) for n in Eq. (C.3). If $V_b \leq V_{xh}$ and $V_b \leq V_{xl}$, Eq. (C.3) is valid for V_b and is solved for n.

When the neutral axis is in the flange at the high moment end, moment equilibrium requires that

$$V_b a_o = M_{bl} + M_{bh}$$

$$= 2(C_{f1}^2 C_{f3})n^2 + 2(C_{f2}^2 C_{f3} + C_{f4}) \qquad (C.4)$$

V_{xl} is obtained by substituting n_{xl}^f for n in Eq. (C.4). If $V_b \leq V_{xl}$, Eq. (C.4) is valid for V_b and is solved for n.

C.2 NEUTRAL AXIS IN THE WEB AT THE LOW MOMENT END

When the neutral axis is above the stiffener at the high moment end of the opening, moment equilibrium requires that

$$V_b a_o = M_{bl} + M_{bh}$$

$$= (C_{w1}^2 C_{w3} + C_{a1}^2 C_{a3})n^2 + 2(C_{w1}C_{w2}C_{w3} - C_{a1}C_{a2}C_{a3})n + C_{w2}^2 C_{w3} + C_{a2}^2 C_{a3} + C_{w4} + C_{a4} \qquad (C.5)$$

V_{xh} is obtained by substituting n_{xh}^s (Eq. (4.23)) for n in Eq. (C.5). If $V_b \leq V_{xh}$, Eq. (C.5) is valid for V_b and is solved for n.

When the neutral axis is in the stiffener at the high moment end, moment equilibrium requires that

$$V_b a_o = M_{bl} + M_{bh}$$

$$= (C_{w1}^2 C_{w3} + C_{s1}^2 C_{s3})n^2 + 2(C_{w1}C_{w2}C_{w3} - C_{s1}C_{s2}C_{s3})n + C_{w2}^2 C_{w3} + C_{s2}^2 C_{s3} + C_{w4} + C_{s4} \qquad (C.6)$$

V_{xh} is obtained by substituting n_{xh}^w (Eq. (4.25)) for n in Eq. (C.6). If $V_b \leq V_{xh}$, Eq. (C.6) is valid for V_b and is solved for n.

When the neutral axis is in the web at the high moment end, moment equilibrium requires that

$$V_b a_o = M_{bl} + M_{bh}$$

$$= 2(C_{w1}^2 C_{w3})n^2 + 2(C_{w2}^2 C_{w3} + C_{w4}) \qquad (C.7)$$

V_{xh} is obtained by substituting n^f_{xh} (Eq. (4.27)) for n in Eq. (C.7). If $V_b \leq V_{xh}$, Eq. (C.7) is valid for V_b and is solved for n.

When the neutral axis is in the flange at the high moment end, V_{xh} is obtained by substituting n^f_{xh} (Eq. (4.27)) for n in Eq. (C.3). If $V_b \leq V_{xh}$, Eq. (C.3) is valid for V_b and is solved for n.

APPENDIX D

MECHANISM SHEAR CAPACITIES OF TOP AND BOTTOM TEES FOR COMPARISON WITH TEST DATA

For comparison with test data, the bottom and top tee shear capacities are calculated using separate values for the web and flange yield strengths, as follows:

BOTTOM TEE

$$V_b(max) = \frac{\beta - \sqrt{\beta^2 - 4\alpha\gamma}}{2\alpha} \qquad (D.1)$$

in which $\alpha = 3 + 2\sqrt{3}\,\frac{a_o}{s_b}$

$$\beta = 2\sqrt{3}\,\frac{F_{yf}(b_f - t_w)}{s_b}\,(s_b^2 - s_b t_f + t_f^2)$$

$$+ 2\sqrt{3}\,\lambda\,F_{yw}t_w s_b + 2a_o\left(F_{yf}(b_f - t_w) + \lambda F_{yw}t_w\right)$$

$$\gamma = F_{yf}^2(b_f - t_w)^2 t_f^2 + 2\lambda F_{yw}F_{yf}t_w(s_b^2 - s_b t_f + t_f^2)$$

and $\lambda = 1.207.$

F_{yf} = flange yield strength and F_{yw} = web yield strength for the bottom tee.

TOP TEE

$$V_t(\max) = \frac{\beta - \sqrt{\beta^2 - 4\alpha\gamma}}{2\alpha} \qquad (D.2)$$

in which $\alpha = 3 + 2\sqrt{3}\,\frac{a_o}{s_t}$

$$\beta = 2\sqrt{3}\,\frac{F_{yf}(b_f - t_w)}{s_t}\,(s_t^2 - s_t t_f + t_f^2) + 2\sqrt{3}\,\lambda F_{yw} t_w s_t$$

$$+ 2a_o\left(F_{yf}(b_f - t_w) + \lambda F_{yw} t_w\right) + \frac{2\sqrt{3}}{s_t}(P_{ch} d_h - P_{cl} d_l)$$

$$+ \sqrt{3}(P_{ch} - P_{cl})$$

$$\gamma = F_{yf}^2 (b_f - t_w)^2 t_f^2 + \lambda^2 F_{yw}^2 t_w^2 s_t^2$$

$$+ 2\lambda F_{yw} F_{yf} t_w (s_t^2 - s_t t_f + t_f^2)$$

$$+ 2\left((b_f - t_w) + \lambda t_w\right)(P_{ch} d_h - P_{cl} d_l)$$

$$- \frac{(P_{ch}^2 + P_{cl}^2)}{2} + \left((b_f - t_w) t_f + \lambda t_w s_t\right)(P_{ch} - P_{cl})$$

F_{yf} = flange yield strength and F_{yw} = web yield strength for the top tee.

APPENDIX E

DEFLECTIONS

E.1 GENERAL

The introduction of a web opening in a composite beam can have a significant affect on the beam deflection. The reduced stiffness at the opening will cause both an increased maximum deflection and a differential deflection across the opening. In some cases, these increased deflections may be unacceptable. Thus, there is a need for an analysis procedure which predicts the total and local deformations due to web openings.

Deflection analysis procedures that consider the effects of web openings in steel and in composite beams have been proposed (16, 17, 26, 27, 38). While one of these procedures (16) has been shown to provide reasonable agreement with data for steel beams, no comparisons have been made with data for composite beams. Procedures do exist for obtaining the deflection of composite sections without openings (19, 34).

The deflection analysis procedures for steel beams with web openings (16, 17, 26, 27, 38) require that the deflected shape of the unperforated section be calculated. Deflections due to the web opening are then added to those found for the unperforated section.

The Subcommittee on Beams with Web Openings of the Task Committee on Flexural Members of the Structural Division of the ASCE (38) has proposed an approximate procedure which models the portions

of the beam above and below the web opening as cantilevered tees with the low moment end fixed. One half of the shear at the opening is applied as a concentrated load to the free end of each tee. The deflection of the beam from the high moment end of the opening to the support is found by enforcing compatibility of vertical displacement and rotation at the high moment end of the opening. The deflection of the beam from the low moment end of the opening to the other support is ignored. Only the bending deflection of the tees is considered. Also, no consideration is made for slope compatibility at the low moment end of the opening or for axial deformation of the tees. While no comparisons with test results have been published, the subcommittee reports that the procedure is conservative.

McCormick has proposed an approximate procedure in which points of contraflexure are assumed to be at the opening centerline (26, 27). Bending and shear deformations of the tees are considered, but compatibility at the opening ends is not enforced. McCormick suggests that no composite action should be considered at the web opening in composite beams. No comparisons with experimental results are made.

Dougherty considers the bending and shear deformation of the tees and enforces compatibility of vertical displacement and slope at ends of the opening (16, 17). Axial deformation of the tees is neglected. Dougherty also proposes an empirical procedure for finding the inelastic deformation of steel beams with openings.

Both McCormick and Dougherty assign shear to the tees in proportion to their relative flexural and shear stiffnesses. Dougherty's procedures give good results when compared with experimental work (16).

Granade (19) and Redwood and Wong (34) compare calculated deflections of unperforated composite beams with measured deflections of composite beams with web openings. Granade considers only bending of the gross section, while Redwood and Wong consider both bending and shear deformations. In both cases, the analyses are too stiff, and the predicted total deflections are slightly low.

Obviously, the introduction of a web opening will have an effect on the stiffness of a beam. A web opening will reduce the beam stiffness by:

1) Lowering the gross moment of inertia at the opening,
2) Eliminating strain compatibility between the tees at the opening, and
3) Reducing the amount of material available to transfer shear at the opening.

While the first reduction will result in increased curvature at openings subjected to bending, the second and third reductions will result in Vierendeel (differential) deflections across openings subjected to shear.

To correctly calculate the deflection of a beam, equilibrium, compatibility, and material properties must be satisfied throughout the span. A complete analysis will consider both bending and shear

deformation. Although classical methods incorporating all of these requirements can be developed, it is possible to obtain equivalent results (within the accuracy of any assumptions) using matrix methods. The matrix approach is particularly attractive since it can automatically enforce compatibility of displacement and rotation at the ends of an opening.

In the following sections, the stiffness method of matrix analysis is applied to beams with web openings. Experimental data are used in a parametric study to determine the importance of including shear deformation in the analysis. Recommendations for the practical application of the procedure are made.

E.2 ANALYSIS PROCEDURE

Fig. E.1 illustrates a web opening in a composite beam. The opening is of length a_o and depth h_o. The beam span and the opening location are L_s and L_o, respectively. Section dimensions at the opening are as shown (Fig. E.1b). The web adjacent to an isolated opening is considered to be infinitely rigid. If the portions of the beam above and below the opening, the top and bottom tees, are modeled as uniform beam elements, a web opening element consisting of two beam elements connected by rigid links can be developed.

A web opening element (Fig. E.2) is constructed using four rigid links and two beam elements. The nodes of the web opening element are connected to the ends of the top and bottom tee elements by rigid links of length l_t and l_b, respectively.

Nodes 1 and 2 of the web opening element are located so that the positive global coordinate x axis, x_g, passes through the nodes. The local coordinate x axes for the tee elements, x_t and x_b, pass through the centroids of the respective tees. The web opening element stiffness matrix is developed using an eccentricity transformation (13).

A beam element with two rigid links, representing a top tee, is shown in Fig. E.3. The local and global x axes are parallel, and eccentricities in both x and y directions exist at each node (Fig. E.3a). The local degrees of freedom for the beam element, $\{U_\ell\}$, are given by

$$\{U_\ell\}^T = \{u_{\ell 1}, v_{\ell 1}, \theta_{\ell 1}, u_{\ell 2}, v_{\ell 2}, \theta_{\ell 2}\} \qquad (E.1)$$

and the global degrees of freedom for nodes 1 and 2, $\{U_g\}$, are given by

$$\{U_g\}^T = \{u_{g1}, v_{g1}, \theta_{g1}, u_{g2}, v_{g2}, \theta_{g2}\} \qquad (E.1a)$$

as shown in Fig. E.3b.

An eccentricity transformation matrix, $[\bar{\delta}]$, relates the local element degrees of freedom and global degrees of freedom of nodes 1 and 2.

$$\{U_\ell\} = [\bar{\delta}]\{U_g\} \qquad (E.2)$$

$$[\bar{\delta}] = \begin{bmatrix} 1 & 0 & -e_{y1} & 0 & 0 & 0 \\ 0 & 1 & e_{x1} & 0 & 0 & 0 \\ 0 & 0 & 1 & 0 & 0 & 0 \\ 0 & 0 & 0 & 1 & 0 & -e_{y2} \\ 0 & 0 & 0 & 0 & 1 & e_{x2} \\ 0 & 0 & 0 & 0 & 0 & 1 \end{bmatrix} \qquad (E.3)$$

in which e_{y1} and e_{y2} are the local y eccentricities and e_{x1} and e_{x2} are the local x eccentricities for nodes 1 and 2, respectively (Fig. E. 3a).

For the web opening element, $e_{x1} = e_{x2} = 0$ for each tee. $e_{y1} = e_{y2} = l_t$ for the top tee, while $e_{y1} = e_{y2} = - l_b$ for the bottom tee (Fig. E.2).

The global stiffness matrix for each tee is

$$[K_g] = [\bar{\delta}]^T [K_e][\bar{\delta}] \qquad (E.4)$$

in which $[K_e]$ is the element stiffness matrix for a tee. The global stiffness matrix for the web opening element, $[K_g]_{wo}$, is the sum of the global stiffness matrices for the top and bottom tee elements, $[K_g]$.

$[K_e]$, the stiffness matrix for a uniform beam element incorporating both shear and axial deformation, is (13)

$$[K_e] = E\beta/L \begin{bmatrix} A/\beta & 0 & 0 & -A/\beta & 0 & 0 \\ & 1 & L/2 & 0 & -1 & L/2 \\ & & (L^2/3 + \eta) & 0 & -L/2 & (L^2/6 - \eta) \\ & & & A/\beta & 0 & 0 \\ & \text{SYM.} & & & 1 & -L/2 \\ & & & & & (L^2/3 + \eta) \end{bmatrix} \quad (E.5)$$

in which E = the modulus of elasticity, $\beta = I/(L^2/12 + \eta)$, $\eta = EI/(A_y G)$, A_y = the effective shear area, A = the gross transformed area for axial deformation, L = the element length, and I = the moment of inertia for the transformed section.

The tee elements in the web opening element are of length a_o. Therefore, substituting for L and adding the global stiffness matrices for the top and bottom tee elements gives $[K_g]_{wo}$.

$$[K_g]_{wo} = E/a_o \begin{bmatrix} K_{11} & K_{12} & K_{13} & K_{14} & K_{15} & K_{16} \\ & K_{22} & K_{23} & K_{24} & K_{25} & K_{26} \\ & & K_{33} & K_{34} & K_{35} & K_{36} \\ & & & K_{44} & K_{45} & K_{46} \\ & \text{SYM.} & & & K_{55} & K_{56} \\ & & & & & K_{66} \end{bmatrix} \quad (E.6)$$

Away from the opening, the web of the steel section carries all of the shear. Thus,

$$A_y = dt_w \qquad (E.8)$$

in which d = the steel section depth and t_w = the web thickness (Fig. E.1b).

Moments of inertia for the individual tees at the opening are calculated considering the steel tees only. The concrete is not considered to be effective for the top tee moment of inertia. Web openings subjected to moderate or high amounts of shear display cracking of the concrete over the opening at relatively low loads. Also, it is likely that only limited composite action develops over the opening at service loads (low slip). The concrete slab will, therefore, add only a small amount to the bending stiffness of the top tee.

The effective area of the top tee, A_t, is calculated using the area of the top tee steel plus the transformed area of the concrete at the opening. Thus, the centroid of the top tee element is the centroid of the transformed section of the top tee.

At the opening, the webs of the steel tees carry the shear. Thus,

$$A_{yt} = s_t t_w \qquad (E.9a)$$

and

$$A_{yb} = s_b t_w \qquad \text{(E.9b)}$$

in which s_t = the top tee stub depth and s_b = the bottom tee stub depth (Fig. E.1b).

Steel sections are modeled using E = 29,000 ksi and G = 11,150 ksi. Concrete is modeled using $E = 57\sqrt{f'_c}$ ksi; f'_c in psi.

E.4 PARAMETRIC STUDY

E.4.1 General

In this section, the proposed deflection analysis procedures are compared with the results of twenty-five tests. The calculated deflections are compared with measured deflections at 30 and 60 percent of the ultimate load. The analyses are made using POLO-FINITE (24).

To study the importance of shear deformation on beam deflection, the beam deflections are calculated either 1) considering shear deformations throughout the span (V) or 2) ignoring shear deformations throughout the span (NV).

As a preliminary step in the study, the analysis procedure was tested for its sensitivity to the number of elements used to model a beam. A single beam was analyzed using 5, 9, and 11 elements, representing models with 3 gross section and 2 web opening elements; 7 gross section and 2 web opening elements; and 7 gross section and 4 web opening elements, respectively (Fig. E.4). The maximum variation

in deflection at the maximum moment location was 0.2%. Because the analyses were not sensitive to the number of elements, most models use 5 elements. The single exception is Test 6A from the current study, which requires 6 elements.

The test beams are modeled using rigid links at the supports in addition to the rigid links at the web opening (Fig. E.4). The links at the supports connect the node at the bottom flange of the beam to the centroid of the transformed section. All openings are modeled with two eccentric beam elements (Fig. E.4a), with one element for each tee. This combination is equivalent to the single web opening element defined in Eq. (E.6).

The deflection data used in the parametric study include 13 tests from the current study, 6 tests by Clawson and Darwin (9, 11), 2 tests by Granade (19), and 4 tests by Redwood and Wong (34). Two of the beams tested by Redwood and Wong had cover plates. The width and thickness of these plates was not published; a cover plate of the same thickness and width as the beam flange is assumed. The data for 4 tests conducted at McGill and for Cho's tests were not published in a useable form. Two openings in the current study (Beams 4A and 4B) and the fourth opening tested by Redwood and Wong had no studs over the opening and are excluded from the parametric study.

The comparisons that follow should be prefaced by a comment on a built-in bias of the test results. The tests were designed primarily to obtain data on the strength at web openings; the beams were relatively short and opening locations in high shear regions

predominated. For this reason, the relative importance of shear deformation and deflection through the opening will be greater than for longer beams in which flexural deformation plays a greater role.

E.4.2 Comparison with Test Data

The following comparisons are based on deflections under applied load (i.e., dead load deflections are not considered). Calculated and measured deflections at the point of maximum moment and through the opening are compared for the two models (V and NV) in Fig. E.5-E.8. The measured and calculated deflections for each test are also presented in Tables E.1 and E.2, along with the ratios of calculated to measured deflection for the models. The tables include the mean ratios of the calculated to measured deflection, along with the standard deviation and the coefficient of variation for the two models. The deflections across the opening are compared with the total deflections, both for the test and calculated results, in Table E.3.

Overall, both models provide reasonable agreement with test results for total deflections at the point of maximum moment. The models provide somewhat poorer agreement with test results for deflections through the opening. In most cases, model V provides better agreement with test results for total deflections, while model NV provides better agreement with test results for deflections across the opening. The ratios of calculated to measured deflection

decrease as the load is increased from 30 to 60 percent of the applied load at ultimate, reflecting the relatively early onset of yield at the openings (Chapter 3).

At both 30 and 60 percent of the ultimate load, on the average model V provides good agreement with test results for total deflections, while model NV is too stiff (Fig. E.5 and E.6 and Tables E.1 and E.2). However, some individual tests deviate appreciably from the calculated deflections. At 30 percent of ultimate load, the average ratios of calculated to measured deflection for models V and NV are 1.155 (coefficient of variation, C_v = 26.1 percent) and 0.996 (C_v = 26.6 percent), respectively. At 60 percent of ultimate load, the average ratios of calculated to measured deflection are 1.025 (C_v = 20.8 percent) and 0.882 (C_v = 21.3 percent), respectively.

For total deflections, model V is stiff when compared with test results for openings with high shear-span to depth ratios, M/Vd. At 30 percent of ultimate load, the ratios of calculated to measured deflection are 0.951, 0.741, and 0.991, for Tests 3 (M/Vd = 26.30), R3 (M/Vd = 16.83), and C3 (M/Vd = 22.14), respectively. These represent the lowest ratios of calculated to measured deflection for each of the respective test series. However, model V is very flexible when compared with test results for openings with relatively stiff slabs and low M/Vd ratios. Tests 8A, 8B, 9A, and 9B had relatively stiff slabs as compared to the steel tees at the opening. The ratios of calculated to measured deflection for the four tests are 1.652, 1.713, 2.069, and 1.624.

Both models exhibit large scatter when compared with the deflection across the opening (Fig. E.7 and E.8). At 30 percent of ultimate load, both models are too flexible when compared with most test data (Table E.1). At 60 percent of ultimate load, the models are better, but on the average are still flexible when compared with test results (Table E.2). Six of the tests were considerably stiffer than the models (8B, 9A, 9B, R0, C1, and C4). Tests 8A-9B had relatively stiff slabs as compared to the steel tees at the opening. Tests R0, C1, and C4 had very small measured deflections across the openings (less than 0.062 in. at 60 percent of ultimate load), although they had relatively low M/Vd ratios. Low deflections tend to amplify the effects of other factors, such as measurement errors and seating errors in the beam. These six tests tend to skew the data, resulting in mean ratios of calculated to measured relative deflection that indicate a flexible model.

These comparisons with test results suggest that in some cases the models may be improved by the addition of partial composite action at the opening. However, sizeable improvement will likely require the consideration of non-linear material response.

The relative importance of the deflection across the opening to the total deflection is considered in Table E.3. Ratios of the deflection across the opening to the total deflection are summarized for the measured deflections at 30 and 60 percent of ultimate load and for the calculated deflections. In most cases, the ratios for measured deflection are relatively constant as the load increases

from 30 to 60 percent of ultimate, while the ratios obtained for the two models compare well with each other. Also, in most cases, the ratios for the calculated deflections agree with the ratios for the measured deflections. Noteable exceptions are Tests 8B, 9B, and C4, three tests for which the models greatly overestimate the deflection across the opening.

As would be expected, the relative importance of the deflection across the opening tends to decrease with increasing M/Vd ratio. Tests 3, R3, and C3 have the highest M/Vd ratios for their respective test groups and have the lowest ratios of deflection across the opening to total deflection.

E.4.3 Case Study

The deflection analysis procedures generally provide good agreement with test results for total beam deflection. However, the test results were obtained from beams which were not typical of beams used in buildings. Most of the test beams had relatively short spans and all of the test beams were loaded using point loads.

A limited study of composite beams with uniform loads is conducted to determine the effects of web openings on uniformly loaded beams. W21 x 44 steel beams with a 6 in. composite ribbed deck (3 in. ribs) are modeled. The beams are spaced at 8 ft and are loaded with a uniform load of 1.52 kips/ft (equivalent to a live load of 0.128 kips/ft^2 and a dead load of 0.062 kips/ft^2). Two spans, 40 ft and 20 ft, are considered. The beams are modeled assuming E = 29,000

ksi, G = 11,150 ksi, A_y = 7.32 $in.^2$, and I_{eff} = 2936 $in.^3$ A 12-3/8 x 24-3/4 in. opening is placed in the beam. The distance of the opening centerline from the support, L_o, is varied from 4 to 20 ft for the beams with span length L_s = 40 ft and is varied from 4 to 10 ft for the beams with L_s = 20 ft (Fig. E.1a). Shear deflections through the span are considered and ignored in separate analyses. Similar beams with no openings are also modeled.

The results of the analyses are summarized in Table E.4. As the table indicates, the effect of the opening on the centerline deflection is relatively small for the beams with 40 ft spans, but is somewhat higher for the beams with 20 ft spans. The greater relative effect of the openings on the shorter beams is due to the fact that the opening represents a greater portion of the span.

For the beams with 40 ft spans, the ratio of the centerline deflection with an opening to the centerline deflection without an opening decreases from 1.054 to 1.044 (model V) as the opening is moved from 4 ft from the support to midspan. In this case, the effect of shear deformation through the span is nearly independent of opening location. The ratio of the centerline deflection considering shear to the centerline deflection ignoring shear varies from 1.048 to 1.043 as the opening moves from 4 ft from the support to midspan, while the calculated ratio for the beam without an opening is 1.046.

For the beams with 20 ft spans, the ratio of the centerline deflection with an opening to the centerline deflection without an opening decreases from 1.286 to 1.058 (model V) as the opening is

moved from 4 ft from the support to midspan. The ratio of centerline deflection considering shear to the centerline deflection ignoring shear drops from 1.179 to 1.164 as the opening moves from 4 ft from the support to midspan, while the ratio for the beam without an opening is 1.203.

The maximum deflection for the beams with a 40 ft span is 1.136 in. and occurs when the opening is 4 ft from the support. This deflection is equivalent to $L_s/423$ and is well within the limit set by the Uniform Building Code (43) for live load plus dead load deflection ($L_s/240$). Since the beams are over-designed for the 20 ft span, the deflections are so small under the given loads as to be of no consequence.

Using classical beam theory for a uniformly loaded beam, the ratio of maximum deflection considering bending and shear to the maximum deflection considering only bending, $(\Delta_b + \Delta_s)/\Delta_b$, can be shown to be

$$\frac{\Delta_b + \Delta_s}{\Delta_b} = 1 + \frac{48EI_{eff}}{5A_y G L_s^2} \qquad (E.10)$$

This ratio is 1.044 and 1.174 for the beams with 40 and 20 ft spans, respectively. The ratios compare well with the results obtained from the matrix analysis, suggesting a practical alternative to model V; to include the effect of shear deflection, the total deflection of

beams with web openings can be obtained by multiplying the deflections obtained with model NV by Eq. (E.10). The ratios also show that the error caused by ignoring shear deflection is about the same, with or without a web opening.

One more comparison is in order. That is a comparison of an accurate estimate of true total deflection (model V) with the deflection obtained by ignoring both the opening and the effects of shear deflection. The latter case is, of course, the standard used in building design.

In the case of the 40 ft span, the ratio of the V model deflection with an opening to the NV model deflection without an opening ranges between 1.09 and 1.10. For the 20 ft span, the ratio ranges from 1.28 to 1.55. For long spans, the contribution of the two effects still represents only a small portion of the total deflection. However, for shorter spans or long spans with multiple openings, these effects can be significant and should be included in the analysis.

This comparison suggests some useful future research: The development of a design aid with factors, based on opening size and location, that would be applied to the bending deflection of a beam without an opening to obtain an accurate estimate of total deflection with an opening.

E.5 RECOMMENDATIONS

Model V provides reasonable results when compared with the test results for total deflection, while model NV is about 12 percent too stiff when compared to total deflections at 60 percent of ultimate. Neither model provides a good correlation with test results for the deflection across the opening. However, both models are, on the average, more flexible through the opening than the test specimens and are therefore conservative for design applications.

The case study indicates that a web opening has an increasing effect on deflection as both the shear at the opening and the relative size of the opening are increased. The case study also indicates that the deflections obtained with model NV can be modified to include shear effects by multiplying by Eq. (E.10).

Based on this limited study, a number of practical alternatives for estimating total deflection exist. The most accurate estimates can be obtained with the model V. Similar results, with little loss in accuracy, can be obtained by multiplying the deflections obtained with model NV by Eq. (E.10). Ignoring both shear deflections and the opening can lead to significant errors in estimates of total deflections.

Table E.1 Measured and calculated deflections at 30 percent of ultimate load.

		Deflection at Point of Maximum Moment					Deflection across Opening				
		Deflection, in.			Calculated-Measured Ratio		Deflection, in.			Calculated-Measured Ratio	
			Calculated					Calculated			
Test	M/Vd*	Measured	V	NV	V	NV	Measured	V	NV	V	NV
1	2.04	0.116	0.128	0.110	1.106	0.945	0.065	0.071	0.064	1.098	0.987
2	3.78	0.137	0.137	0.117	0.997	0.853	0.060	0.066	0.058	1.103	0.966
3	26.30	0.211	0.201	0.175	0.951	0.829	0.052	0.027	0.025	0.517	0.477
5A	3.78	0.111	0.132	0.116	1.193	1.044	0.052	0.059	0.052	1.134	0.995
5B	3.78	0.128	0.132	0.115	1.034	0.897	0.081	0.084	0.073	1.034	0.907
6A	0.00	0.048	0.049	0.035	1.013	0.733	0.047	0.052	0.046	1.101	0.968
6B	2.04	0.108	0.123	0.104	1.140	0.967	0.066	0.083	0.073	1.254	1.106
7A	2.04	0.147	0.174	0.154	1.182	1.049	0.061	0.089	0.081	1.458	1.323
7B	3.78	0.199	0.211	0.189	1.060	0.951	0.061	0.084	0.076	1.374	1.238
8A	3.89	0.062	0.102	0.087	1.652	1.402	0.033	0.046	0.038	1.379	1.160
8B	2.90	0.064	0.110	0.097	1.713	1.519	0.028	0.101	0.094	3.621	3.362
9A	2.04	0.057	0.118	0.101	2.069	1.779	0.055	0.115	0.106	2.088	1.918
9B	1.75	0.100	0.162	0.141	1.624	1.407	0.046	0.159	0.146	3.463	3.171
R0	3.94	0.153	0.144	0.124	0.940	0.811	0.031	0.053	0.048	1.702	1.535
R1	2.66	0.100	0.081	0.066	0.807	0.662	0.038	0.050	0.043	1.307	1.143
R2	7.00	0.233	0.173	0.157	0.741	0.675	0.047	0.039	0.034	0.836	0.726
R3	16.83	0.272	0.279	0.252	1.027	0.928	0.017	0.024	0.020	1.400	1.156
C1	6.00	0.329	0.344	0.319	1.047	0.968	0.051	0.070	0.062	1.379	1.217
C2	6.04	0.274	0.276	0.252	1.008	0.921	0.060	0.068	0.061	1.138	1.017
C3	22.15	0.285	0.282	0.256	0.991	0.897	0.028	0.036	0.034	1.293	1.219
C4	2.01	0.091	0.112	0.092	1.228	1.012	0.023	0.081	0.070	3.508	3.058
C5	3.97	0.186	0.209	0.186	1.123	1.001	0.059	0.079	0.069	1.333	1.175
C6	2.57	0.124	0.148	0.124	1.193	1.001	0.048	0.072	0.062	1.509	1.293
G1	3.00	0.108	0.107	0.086	0.987	0.795	Mean			1.566	1.292
G2	6.00	0.128	0.136	0.110	1.059	0.857	Std. Dev.			0.833	0.763
Mean					1.155	0.996	Coeff. of Variation			53.2%	59.1%
Std. Dev.					0.302	0.265					
Coeff. of Variation					26.1%	26.6%					

* Based on applied load

Table E.2 Measured and calculated deflections at 60 percent of ultimate load.

		Deflection at Point of Maximum Moment					Deflection across Opening				
		Deflection, in.			Calculated-Measured Ratio		Deflection, in.			Calculated-Measured Ratio	
			Calculated					Calculated			
Test	M/Vd*	Measured	V	NV	V	NV	Measured	V	NV	V	NV
1	2.04	0.256	0.257	0.219	1.002	0.857	0.170	0.142	0.127	0.834	0.748
2	3.78	0.305	0.272	0.233	0.892	0.763	0.161	0.132	0.116	0.822	0.720
3	26.30	0.447	0.400	0.350	0.896	0.782	0.088	0.053	0.049	0.600	0.553
5A	3.78	0.244	0.264	0.231	1.081	0.945	0.127	0.118	0.103	0.929	0.815
5B	3.78	0.303	0.264	0.229	0.871	0.755	0.214	0.167	0.146	0.778	0.682
6A	0.00	0.107	0.096	0.070	0.899	0.657	0.149	0.103	0.090	0.694	0.895
6B	2.04	0.246	0.245	0.208	0.997	0.845	0.162	0.166	0.145	1.022	0.453
7A	2.04	0.321	0.348	0.308	1.083	0.960	0.150	0.177	0.160	1.179	1.069
7B	3.78	0.409	0.421	0.378	1.029	0.923	0.130	0.167	0.150	1.281	1.154
8A	3.89	0.159	0.192	0.160	1.210	1.008	0.090	0.087	0.077	0.966	0.851
8B	2.90	0.146	0.218	0.193	1.495	1.325	0.102	0.202	0.187	1.978	1.836
9A	2.04	0.152	0.236	0.203	1.552	1.334	0.174	0.230	0.210	1.320	1.207
9B	1.75	0.223	0.325	0.280	1.457	1.257	0.130	0.319	0.292	2.451	2.244
R0	3.94	0.272	0.287	0.248	1.053	0.913	0.062	0.104	0.093	1.685	1.502
R1	2.66	0.230	0.161	0.131	0.702	0.571	0.115	0.098	0.085	0.855	0.738
R2	7.00	0.453	0.344	0.313	0.760	0.692	0.096	0.078	0.068	0.808	0.711
R3	16.83	0.585	0.558	0.504	0.953	0.861	0.033	0.048	0.039	1.442	1.191
C1	6.00	0.836	0.689	0.637	0.824	0.762	0.034	0.140	0.124	4.108	3.651
C2	6.04	0.643	0.552	0.504	0.859	0.784	0.154	0.137	0.122	0.887	0.793
C3	22.15	0.679	0.564	0.511	0.830	0.753	0.073	0.072	0.067	0.992	0.921
C4	2.01	0.216	0.223	0.183	1.034	0.848	0.058	0.161	0.141	2.782	2.426
C5	3.97	0.403	0.417	0.371	1.034	0.922	0.139	0.157	0.139	1.131	0.997
C6	2.57	0.277	0.295	0.248	1.064	0.896	0.116	0.145	0.124	1.249	1.070
G1	3.00	0.216	0.213	0.171	0.987	0.790	Mean			1.339	1.189
G2	6.00	0.255	0.270	0.218	1.059	0.856	Std. Dev.			0.816	0.729
Mean					1.025	0.882	Coeff. of Variation			60.9%	61.3%
Std. Dev.					0.213	0.188					
Coeff. of Variation					20.8%	21.3%					

* Based on applied load

Table E.3 Ratios of Deflection across the Opening to to Deflection at the Point of Maximum Moment.

Test	M/Vd*	Ratios for Measured Deflection 30%	Ratios for Measured Deflection 60%	Ratios for Calculated Deflection V	Ratios for Calculated Deflection NV
1	2.04	0.560	0.664	0.555	0.582
2	3.78	0.438	0.528	0.482	0.496
3	26.30	0.246	0.197	0.134	0.143
5A	3.78	0.468	0.520	0.447	0.448
5B	3.78	0.633	0.706	0.636	0.635
6A	0.00	0.979	1.393	1.061	1.314
6B	2.04	0.611	0.659	0.675	0.701
7A	2.04	0.415	0.467	0.511	0.526
7B	3.78	0.307	0.318	0.398	0.402
8A	3.89	0.532	0.566	0.451	0.437
8B	2.90	0.438	0.699	0.918	0.969
9A	2.04	0.965	1.145	0.975	1.050
9B	1.75	0.460	0.583	0.981	1.035
R0	3.94	0.203	0.228	0.368	0.387
R1	2.66	0.380	0.500	0.617	0.652
R2	7.00	0.202	0.212	0.225	0.217
R3	16.83	0.063	0.056	0.086	0.079
C1	6.00	0.155	0.041	0.203	0.194
C2	6.04	0.219	0.240	0.246	0.242
C3	22.15	0.098	0.108	0.128	0.133
C4	2.01	0.253	0.269	0.723	0.761
C5	3.97	0.317	0.345	0.378	0.371
C6	2.57	0.387	0.419	0.486	0.500

* Based on applied load

Table E.4 Effect of a 12-3/8 x 24-3/4 in. Web Opening on the Deflection of a W21 x 44 Composite Beam.

40 ft Span

		Centerline			Across Opening	
Opening Location	Model	Deflection in.	V-NV Ratio	Opening-No Opening Ratio	Deflection in.	V-NV Ratio
4	V	1.136	1.048	1.054	0.271	1.063
4	NV	1.084		1.051	0.255	
6.5	V	1.133	1.047	1.051	0.240	1.062
6.5	NV	1.082		1.049	0.226	
9	V	1.131	1.045	1.049	0.204	1.068
9	NV	1.082		1.049	0.191	
14	V	1.132	1.044	1.050	0.117	1.054
14	NV	1.084		1.051	0.111	
20	V	1.125	1.043	1.044	0.000	--
20	NV	1.079		1.047	0.000	
No Opening	V	1.078	1.046	--		
No Opening	NV	1.031		--		

20 ft Span

		Centerline			Across Opening	
Opening Location	Model	Deflection in.	V-NV Ratio	Opening-No Opening Ratio	Deflection in.	V-NV Ratio
4	V	0.099	1.179	1.286	0.056	1.120
4	NV	0.084		1.313	0.050	
10	V	0.082	1.164	1.058	0.000	--
10	NV	0.070		1.094	0.000	
No Opening	V	0.077	1.203	--		
No Opening	NV	0.064		--		

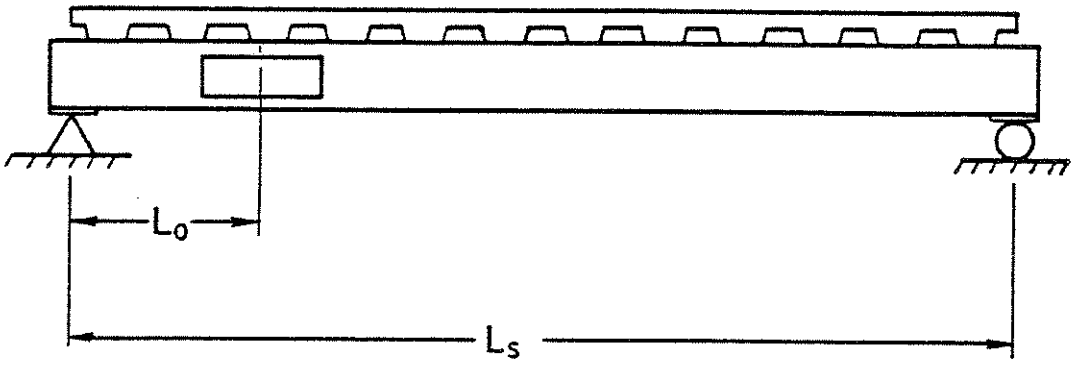

(a)

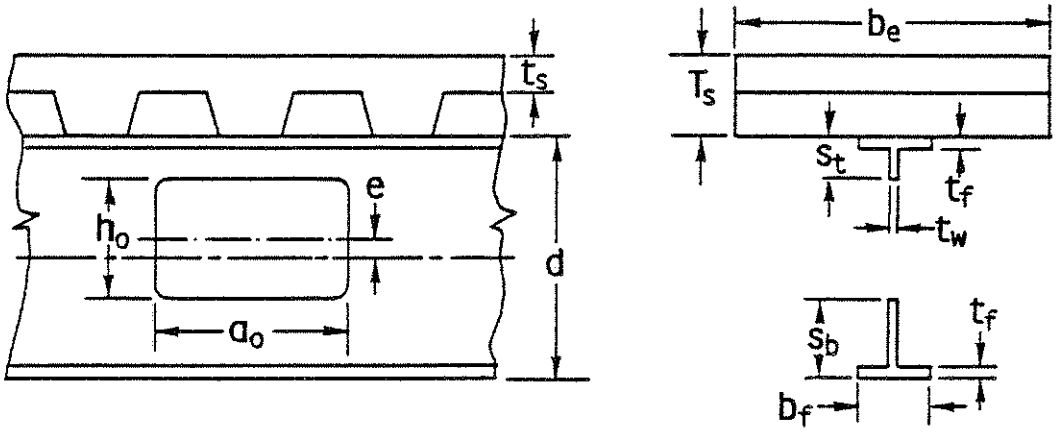

(b)

Fig. E.1 Composite Beam with Web Opening. (a) Schematic of Beam. (b) Detail of Opening.

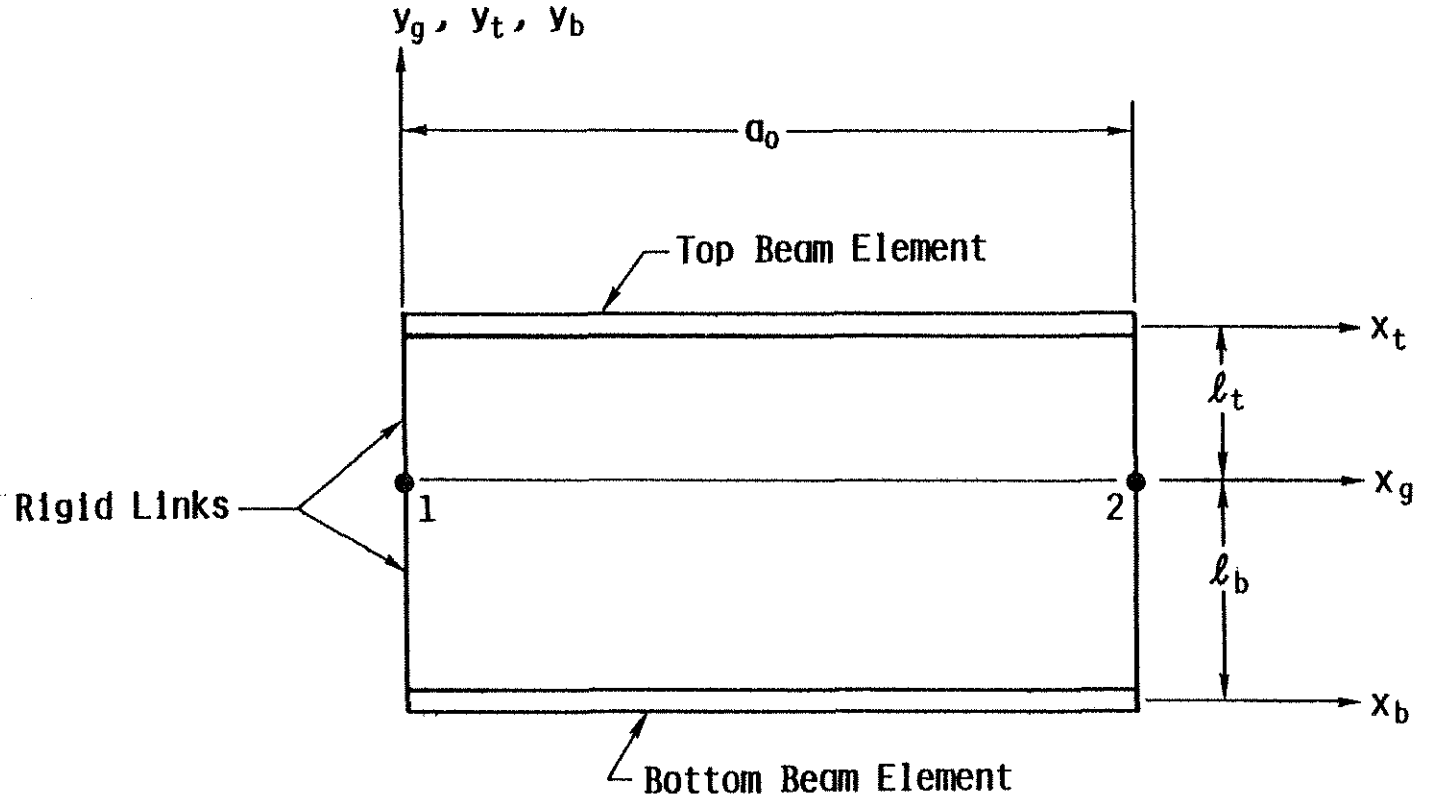

Fig. E.2 Web Opening Element Geometry and Axes Orientations.

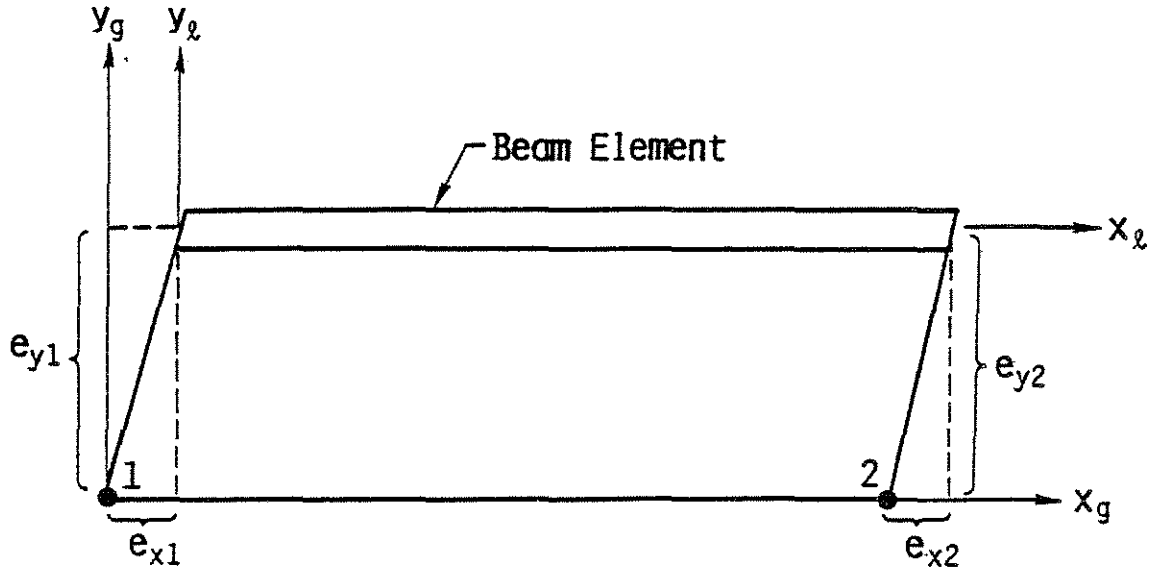

(a)

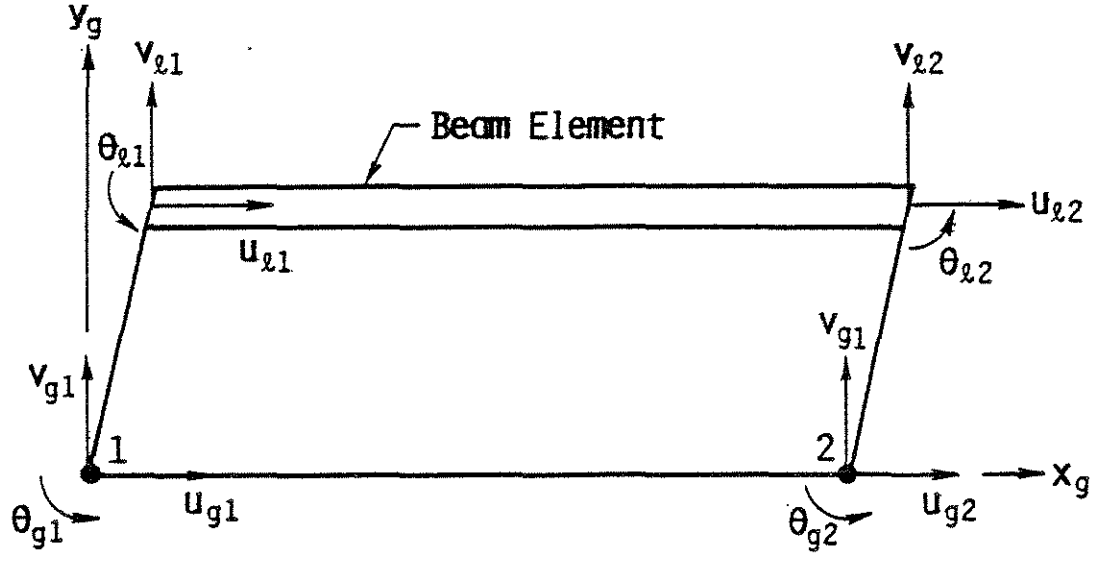

(b)

Fig. E.3 Beam Element with Two Rigid Links. (a) Global and Local Axes. (b) Global and Local Degrees of Freedom.

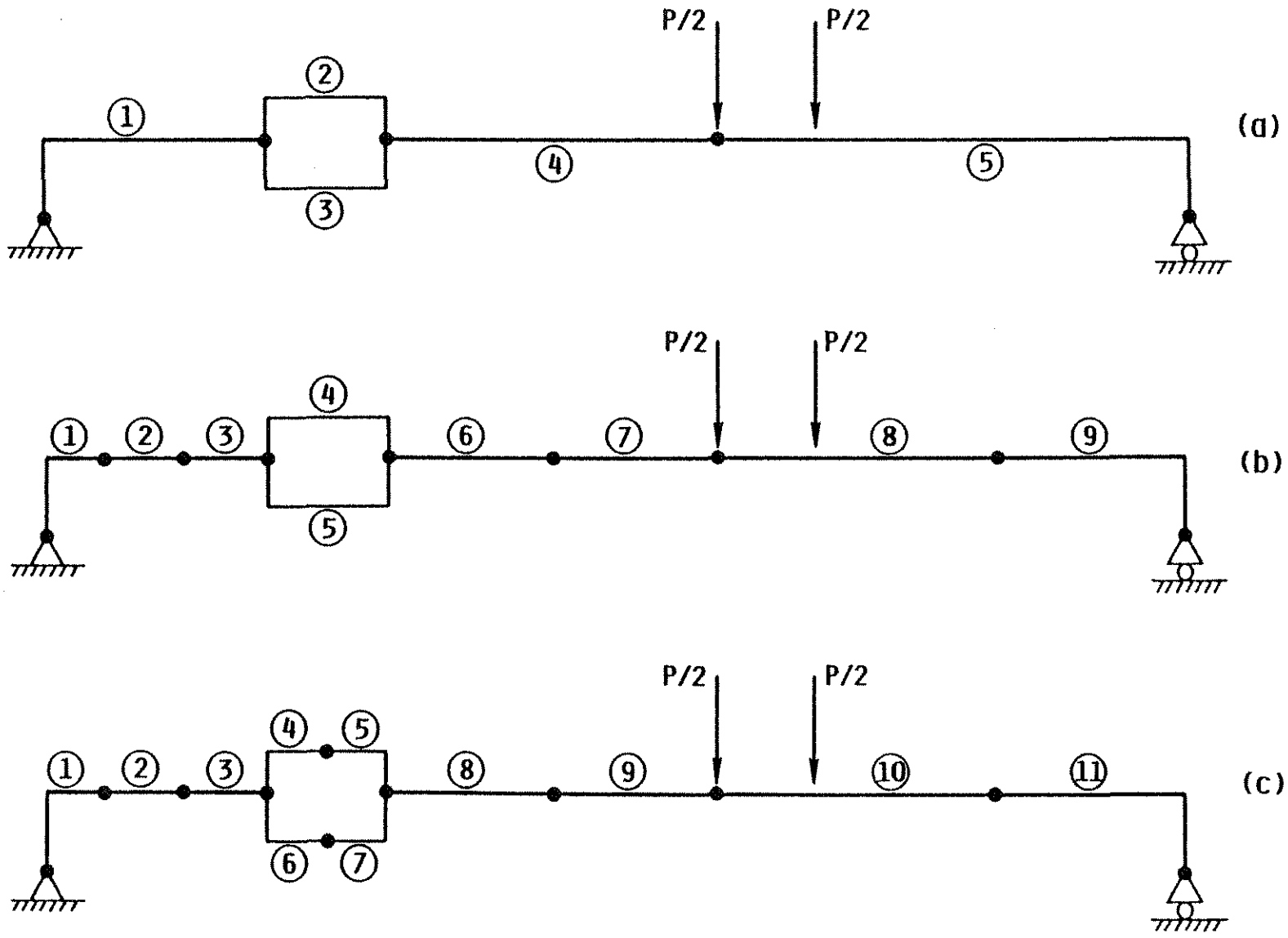

Fig. E.4 Deflection Analysis Model for Beam with Web Opening. (a) 5 Element Model. (b) 9 Element Model. (c) 11 Element Model.

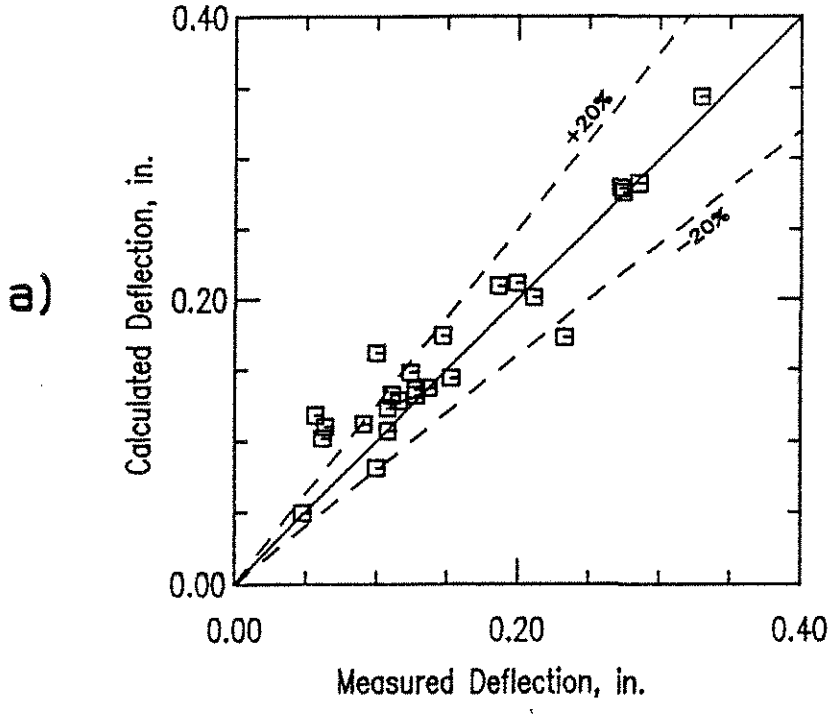

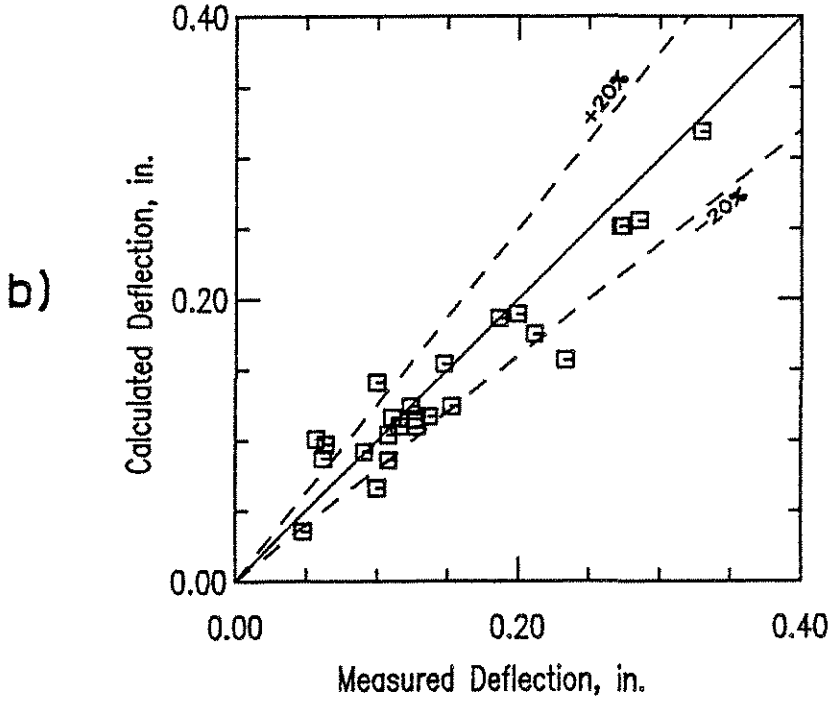

Fig. E.5 Calculated versus Measured Total Deflection at 30 Percent of Ultimate Load. (a) Model V. (b) Model NV.

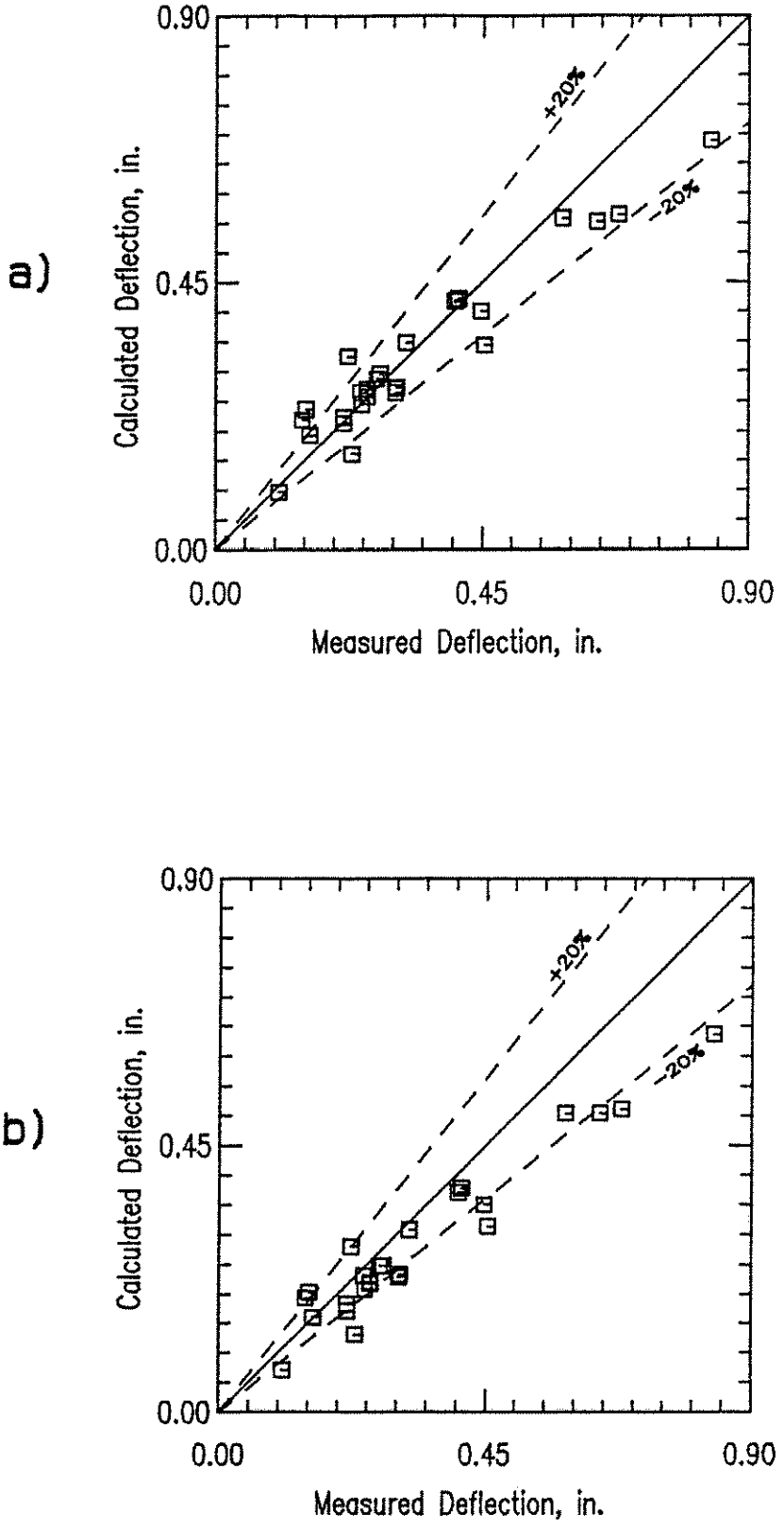

Fig. E.6 Calculated versus Measured Total Deflection at 60 Percent of Ultimate Load. (a) Model V. (b) Model NV.

a)

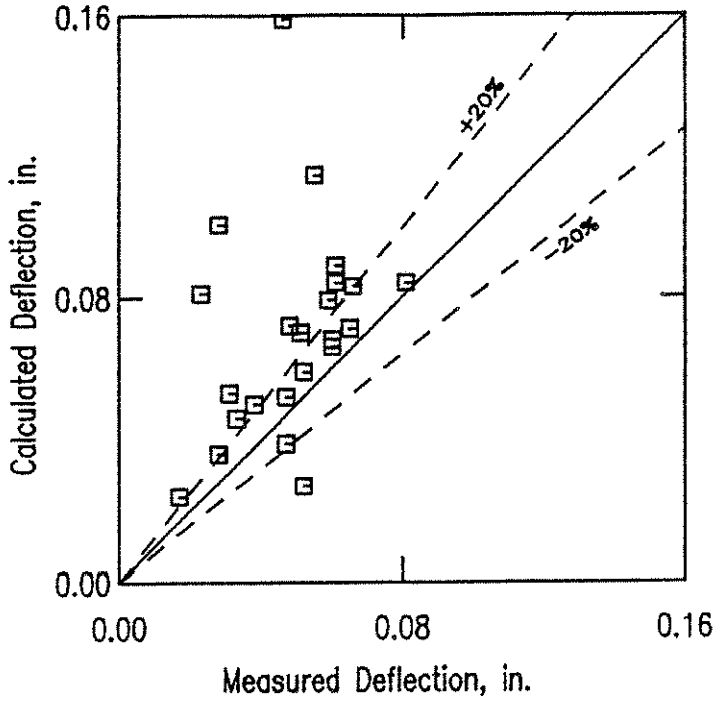

b)

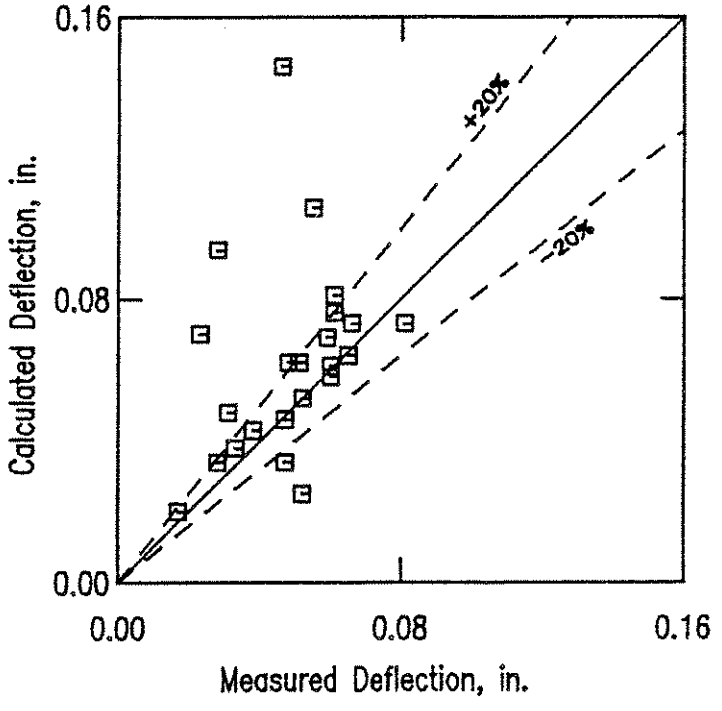

Fig. E.7 Calculated versus Measured Deflection across the Opening at 30 Percent of Ultimate Load. (a) Model V. (b) Model NV.

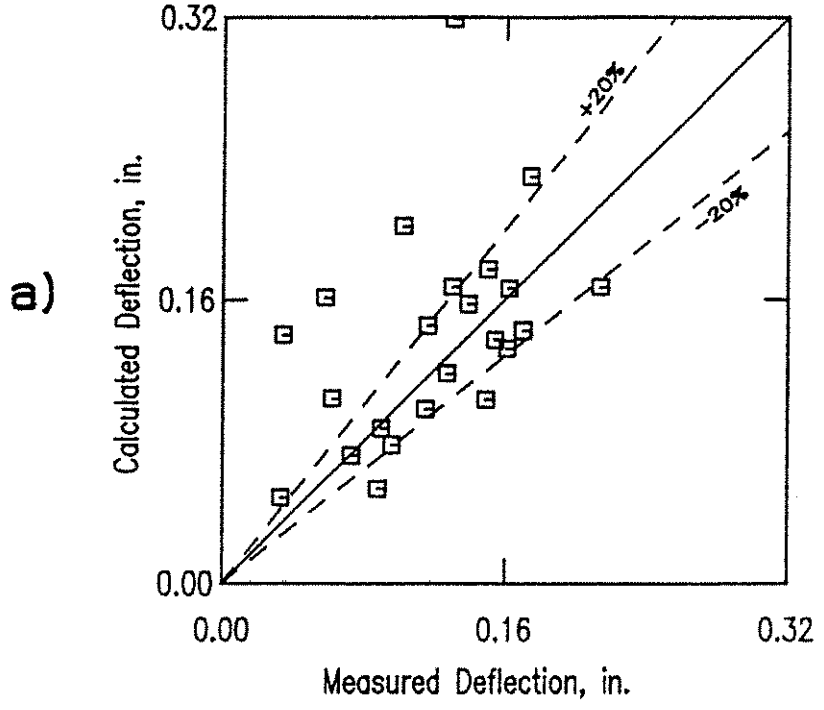

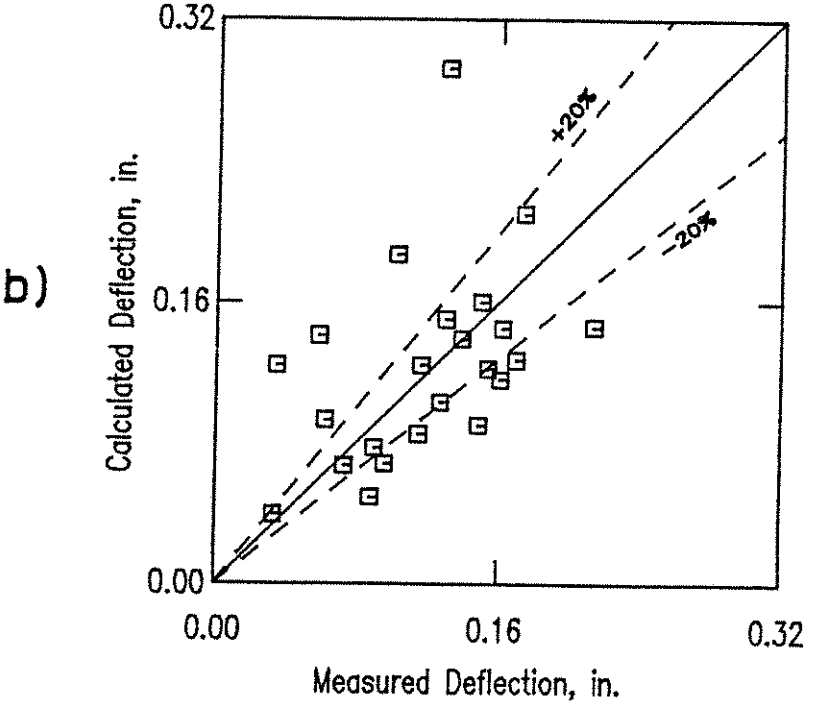

Fig. E.8 Calculated versus Measured Deflection across the Opening at 60 Percent of Ultimate Load. (a) Model V. (b) Model NV.